

**INTRACELLULAR PROCESSING OF COBALAMINS IN  
MAMMALIAN CELLS**

A dissertation submitted  
to Kent State University in collaboration  
with the Lerner Research Institute, Cleveland Clinic in partial  
fulfillment of the requirements for the  
degree of Doctor in Philosophy

By

Luciana Hannibal  
August, 2009

Dissertation written by  
Luciana Hannibal  
B.S., Universidad de la República, Montevideo, Uruguay, 2004  
Ph.D., Kent State University, 2009

Approved by

\_\_\_\_\_, Chair, Doctoral Dissertation Committee  
Donald W. Jacobsen, Ph.D.

\_\_\_\_\_, Co-Advisor, Doctoral Dissertation Committee  
Nicola E. Brasch, Ph.D.

\_\_\_\_\_, Member, Doctoral Dissertation Committee  
Soumitra Basu, Ph.D.

\_\_\_\_\_, Member, Doctoral Dissertation Committee  
Thomas M. McIntyre, Ph.D.

\_\_\_\_\_, Member, Doctoral Dissertation Committee  
Dennis J. Stuehr, Ph.D.

Accepted by

\_\_\_\_\_, Chair, School of Biomedical Sciences  
Robert V. Dorman, Ph.D.

\_\_\_\_\_, Dean, College of Arts and Sciences  
John R.D. Stalvey, Ph.D.

## Table of Contents

	<b>Page</b>
List of Figures .....	viii
List of Tables .....	xiv
List of Schemes .....	xvii
List of Abbreviations .....	xviii
Dedication .....	xxii
Acknowledgments .....	xxiii
Preface .....	xxv
<b>CHAPTER 1 Introduction and Background .....</b>	<b>1</b>
1.1 The discovery of cobalamin .....	1
1.2 The structure of cobalamin .....	2
1.3 Cobalamin metabolism in mammals .....	5
1.4 Scope of this dissertation .....	9
<b>CHAPTER 2 Chemistry of cobalamin forms with potential biological activity .....</b>	<b>10</b>
2.1 Project 1: Synthesis and characterization of nitroxylcobalamin (NOCbl) and nitrocobalamin (NO <sub>2</sub> Cbl) .....	10
INTRODUCTION .....	10
RESULTS AND DISCUSSION .....	11
A. Development of a method of synthesis of NOCbl .....	11

B. X-ray analysis of NOCbl .....	16
C. Reaction of aquacobalamin with nitric oxide donors .....	23
SUMMARY .....	38
MATERIALS AND METHODS .....	40
2.2 Project 2: Synthesis and characterization of imidazolylcobalamin (ImCbl) and histidinylcobalamin (HisCbl) .....	49
INTRODUCTION .....	49
RESULTS AND DISCUSSION .....	50
A. Synthesis and characterization of ImCbl and HisCbl .....	50
B. X-ray analysis of ImCbl and HisCbl .....	53
SUMMARY .....	58
MATERIALS AND METHODS .....	59
2.3 Project 3: Synthesis and characterization of the MeCbl analogs ethyl-, propyl-, butyl-, pentyl-, and hexyl-cobalamin .....	63
INTRODUCTION .....	63
RESULTS AND DISCUSSION .....	64
A. Synthesis and characterization of alkylcobalamins .....	64
B. X-ray analysis of EtCbl and BuCbl .....	67
C. Separation of alkylcobalamins by HPLC .....	78
SUMMARY .....	79
MATERIALS AND METHODS .....	79
<b>CHAPTER 3 Mechanisms of cobalamin processing in cells .....</b>	<b>85</b>
3.1 Project 1: Development of a method for the accurate assessment	

of intracellular cobalamins .....	85
INTRODUCTION .....	85
RESULTS AND DISCUSSION .....	86
A. Extraction of Cbls from cultured cells .....	86
B. Development of an HPLC method for the separation of Cbls .....	87
C. Accurate assessment of intracellular Cbls: cold-trapping .....	90
SUMMARY .....	93
MATERIALS AND METHODS .....	99
3.2 Project 2: Processing of alkylcobalamins in mammalian cells: a role for the MMACHC ( <i>cblC</i> ) gene product .....	104
INTRODUCTION .....	105
RESULTS AND DISCUSSION .....	105
A. Cbl uptake and cofactor biosynthesis by BAEC .....	105
B. Cytotoxicity of xenobiotic alkylcobalamins .....	107
C. Dealkylation of xenobiotic alkylcobalamins by BAEC .....	108
D. Genetic background, biochemical characterization and ability of <i>cblC</i> cell lines to perform decyanation of [ <sup>57</sup> Co]-CNCbl .....	111
E. Dealkylation of xenobiotic alkylcobalamins by normal and <i>cblC</i> mutant fibroblasts .....	113
SUMMARY .....	115
MATERIALS AND METHODS .....	121
3.3 Project 3: Dealkylation of alkylcobalamins by the MMACHC ( <i>cblC</i> ) gene product: <i>in vitro</i> studies .....	125

INTRODUCTION .....	125
RESULTS AND DISCUSSION .....	126
A. Dealkylation of MeCbl and AdoCbl <i>in vitro</i> .....	126
B. Binding of the <i>cblC</i> protein to MeCbl analogues .....	128
C. Dealkylation of MeCbl analogs by <i>cblC</i> and GSH .....	129
D. Identification of reaction products by mass spectrometry .....	133
SUMMARY .....	135
MATERIALS AND METHODS .....	137
<b>CHAPTER 4 Biochemistry of the <i>cblC</i> disorder and cobalamin</b>	
<b>deficiency in humans</b> .....	142
4.1 Project 1: Metabolic profile of human fibroblasts carrying the	
<i>cblC</i> mutation .....	142
INTRODUCTION .....	142
RESULTS AND DISCUSSION .....	143
A. Production of Hcy and MMA .....	143
B. Cbl uptake and cofactor biosynthesis .....	143
C. Cell morphology .....	146
D. Intracellular levels of Cbl and folates .....	149
SUMMARY .....	150
MATERIALS AND METHODS .....	151
4.2 Project 2: Assessment of the human proteome of patients with a	
defective MMACHC ( <i>cblC</i> ) gene by 2D-DIGE .....	154

INTRODUCTION .....	154
RESULTS AND DISCUSSION .....	155
A. Cy-dye labeling of the normal and <i>cb1C</i> proteome .....	156
B. Decyder® analysis of differentially expressed protein .....	157
C. Identification of proteins by LC/MS and validation assays .....	162
SUMMARY .....	183
MATERIALS AND METHODS .....	185
4.3 Project 3: Bioinformatic analysis of the pathways perturbed in the <i>cb1C</i> disorder/cobalamin deficiency .....	192
INTRODUCTION .....	192
RESULTS AND DISCUSSION .....	193
A. Analysis of the normal and <i>cb1C</i> proteomes in the absence of exogenous HOCbl .....	193
B. Analysis of the normal and <i>cb1C</i> proteomes supplemented with HOCbl .....	199
SUMMARY .....	205
MATERIALS AND METHODS .....	205
<b>CONCLUDING REMARKS .....</b>	<b>207</b>
<b>REFERENCES .....</b>	<b>209</b>

## List of Figures

	<b>Page</b>
<b>CHAPTER 1 Introduction and Background</b> .....	1
Figure 1.1. Chemical structure of Cbls with atom numbering.....	4
Figure 1.2. Cellular transport and metabolism of Cbl .....	7
<b>CHAPTER 2 Chemistry of cobalamin forms with potential biological activity</b> .....	10
Figure 2.1 Spectroscopic characterization of NOCbl .....	13
Figure 2.2 Reaction of NOCbl with atmospheric oxygen .....	14
Figure 2.3 UV-visible spectra of $\text{H}_2\text{OCbl}^+$ , $\text{NO}_2\text{Cbl}$ and NOCbl .....	15
Figure 2.4 Crystallization of NOCbl .....	16
Figure 2.5 Thermal ellipsoid plot of $\text{NOCbl}\cdot 15\text{H}_2\text{O}$ .....	18
Figure 2.6 XAS spectrum of a $\text{NOCbl}\cdot 15\text{H}_2\text{O}$ crystal before and after irradiation .....	21
Figure 2.7 UV-vis spectra of the reaction between $\text{HOCbl}$ and DEA- NONOate at pH 9.80 .....	24
Figure 2.8 $^1\text{H}$ NMR spectra of pure DEA, DEA-NO and DEA- NONOate .....	29
Figure 2.9 Analysis of non-cobalamin products.....	30
Figure 2.10 Formation of a second reaction product .....	31
Figure 2.11 $^1\text{H}$ NMR spectroscopy time course of the reaction	

between HOCbl and DEA-NONOate .....	33
Figure 2.12 Reaction of NOCbl with NO <sub>(g)</sub> .....	34
Figure 2.13 Reaction of HOCbl with Angeli's salt .....	37
Figure 2.14 Experimental set-up for the reaction between NOCbl and authentic NO .....	48
Figure 2.15 UV-visible spectra of HOCbl, ImCbl and HisCbl .....	50
Figure 2.16 <sup>1</sup> H NMR spectra of ImCbl and HisCbl .....	51
Figure 2.17 Molecular structure of ImCbl and HisCbl .....	57
Figure 2.18 Superposition of HisCbl with one of the HisCbl moieties present in the monoclinic structure of bovine transcobalamin .....	58
Figure 2.19 Thermal ellipsoid plots for EtCbl and BuCbl .....	69
Figure 2.20 Scatter plot of the corrin fold angle (ϕ) versus the axial Co-N3B distance for Co-C bonded cobalamins .....	72
Figure 2.21 Surface maps for EtCbl and BuCbl .....	73
Figure 2.22 Superposition of the structures of MeCbl and EtCbl .....	75
Figure 2.23 Plot of axial Co-C against Co-N3B for Co-C bonded cobalamins .....	77
Figure 2.24 HPLC chromatogram of a mixture of alkylcobalamins ...	78
<b>CHAPTER 3 Mechanisms of cobalamin processing in cells .....</b>	<b>85</b>
Figure 3.1 HPLC of a mixture of seven Cbls .....	88
Figure 3.2 Profile of [ <sup>57</sup> Co]-Cbls in cultured BAECs in the absence of excess H <sub>2</sub> OCbl <sup>+</sup> .....	89
Figure 3.3 Formation of [ <sup>57</sup> Co]-Cbls as a result of β-axial ligand	

exchange .....	89
Figure 3.4 Profile of [ <sup>57</sup> Co]-CbIs in cultured BAEC extracted in the presence of excess H <sub>2</sub> OCbl <sup>+</sup> (“cold-trapping”) .....	90
Figure 3.5 Reactions of aquacobalamin with relevant biological ligands .....	95
Figure 3.6 Processing of [ <sup>57</sup> Co]-CNCbl in BAEC .....	106
Figure 3.7 Processing of [ <sup>57</sup> Co]-HOCbl and [ <sup>57</sup> Co]-HOCbl by BAEC .....	107
Figure 3.8 Cytotoxicity of xenobiotic alkylcobalamins .....	108
Figure 3.9 Processing of [ <sup>57</sup> Co]-PrCbl in BAEC .....	109
Figure 3.10 Processing of [ <sup>57</sup> Co]-MeCbl by human normal and <i>cbIC</i> mutant fibroblasts .....	114
Figure 3.11 Processing of [ <sup>57</sup> Co]-PrCbl by human normal and <i>cbIC</i> mutant fibroblasts .....	115
Figure 3.12 Possible mechanisms for the dealkylation of alkylcobalamins mediated by the <i>cbIC</i> protein .....	120
Figure 3.13 Dealkylation of MeCbl by <i>cbIC</i> in the presence of GSH .....	126
Figure 3.14 Dealkylation of AdoCbl by <i>cbIC</i> in the presence of GSH .....	127
Figure 3.15 Binding of MeCbl analogues to the <i>cbIC</i> protein .....	129
Figure 3.16 Dealkylation of EtCbl by <i>cbIC</i> in the presence of GSH .....	130
Figure 3.17 Dealkylation of HxCbl by <i>cbIC</i> in the presence of GSH .....	131
Figure 3.18 Dealkylation rates of alkylcobalamins by the <i>cbIC</i> /GSH system .....	132
Figure 3.19 Identification of Me-SG as the dealkylation product by .....	

mass spectrometry .....	134
Figure 3.20 A mechanism for the biological dealkylation of alkylcobalamins .....	135
<b>CHAPTER 4 Biochemistry of the <i>cb1C</i> disorder and cobalamin deficiency in humans .....</b>	<b>142</b>
Figure 4.1 Determination of Hcy and MMA in the conditioned cultured medium of normal and <i>cb1C</i> fibroblasts .....	144
Figure 4.2 Uptake of [ <sup>57</sup> Co]-HOCbl by normal and <i>cb1C</i> fibroblasts...	145
Figure 4.3 Morphology of normal and <i>cb1C</i> fibroblasts .....	148
Figure 4.4 DNA laddering assay .....	148
Figure 4.5 β-galactosidase staining of normal and <i>cb1C</i> fibroblasts ...	148
Figure 4.6 Fluorescence scans of Cy-dye labeled proteins of normal and <i>cb1C</i> (patient WG1801) cells without exogenous HOCbl.....	158
Figure 4.7 Fluorescence scans of Cy-dye labeled proteins of normal and <i>cb1C</i> (patient WG1801) cells supplemented with HOCbl .....	159
Figure 4.8 A representative scheme for 2D-DIGE image analysis .....	160
Figure 4.9 Differential expression of proteins in three <i>cb1C</i> mutants compared to normal fibroblasts grown without exogenous HOCbl.....	162
Figure 4.10 Western blots of PDI, CLIC4 and UCHL1 .....	164
Figure 4.11 Differential expression of proteins in three <i>cb1C</i> mutants compared to normal fibroblasts supplemented with HOCbl .....	164
Figure 4.12 Vimentin: immunocytochemistry of normal and <i>cb1C</i> fibroblasts	169
Figure 4.13 Western blot for vimentin .....	170

Figure 4.14 GST and Annexin V determinations .....	171
Figure 4.15 Cell cycle, gene expression and drug metabolism network of differentially expressed proteins from <i>cb1C</i> cell lines grown in the absence of exogenous HOCbl .....	194
Figure 4.16 Genetic disorders, skeletal and muscular disorders and lipid disorders network of differentially expressed proteins from <i>cb1C</i> cell lines grown in the absence of exogenous HOCbl .....	195
Figure 4.17 Top ranked associations for diseases and disorders derived from IPA® analysis of the <i>cb1C</i> proteome in the absence of exogenous HOCbl ...	197
Figure 4.18 Top ranked associations for physiological systems development and functions derived from IPA® analysis of the <i>cb1C</i> proteome in the absence of exogenous HOCbl .....	198
Figure 4.19 Cancer, post-translational modification and protein folding network of differentially expressed proteins from <i>cb1C</i> cell lines grown with HOCbl supplementation .....	199
Figure 4.20 Genetic disorders, skeletal and muscular disorders and cancer network of differentially expressed proteins from <i>cb1C</i> cell lines grown with HOCbl supplementation .....	200
Figure 4.21 Cellular assembly and organization, small molecule biochemistry and molecular transport network of differentially expressed proteins from <i>cb1C</i> cell lines grown with HOCbl supplementation .....	201

Figure 4.22 Top ranked associations for diseases and disorders derived from IPA® analysis of the <i>cb1C</i> proteome in the absence of exogenous HOCbl ...	203
Figure 4.23 Top ranked associations for physiological systems development and functions derived from IPA® analysis of the <i>cb1C</i> proteome supplemented with HOCbl .....	204

## List of Tables

	<b>Page</b>
<b>CHAPTER 2 Chemistry of cobalamin forms with potential biological activity</b> .....	10
Table 2.1 Data collection and refinement statistics for NOCbl•15H <sub>2</sub> O .....	17
Table 2.2 Comparison of the coordination sphere in NOCbl and NO <sub>2</sub> Cbl structures .....	19
Table 2.3 <sup>1</sup> H NMR spectroscopy chemical shifts of pure DEA, DEA-NO and DEA-NONOate .....	29
Table 2.4 <sup>1</sup> H NMR spectroscopy assignments of the protons of the upper axial ligand in ImCbl and HisCbl .....	52
Table 2.5 Crystallographic data for ImCbl and HisCbl.....	54
Table 2.6 UV-visible and <sup>1</sup> H NMR spectroscopy data for alkylcobalamins .....	66
Table 2.7 Refinement parameters for EtCbl and BuCbl .....	68
Table 2.8 Comparison of the Co coordination sphere in EtCbl, BuCbl and selected alkylcobalamins .....	71
<b>CHAPTER 3 Mechanisms of cobalamin processing in cells</b> .....	85
Table 3.1 Total Cbl uptake, intracellular distribution of [ <sup>57</sup> Co]-Cbls and total GSH in BAEC, HFF and HepG2 .....	92

Table 3.2 Activity of the Cbl-dependent enzymes in different cell types .....	97
Table 3.3 Uptake and processing of [ <sup>57</sup> Co]-CNCbl by BAEC .....	105
Table 3.4 Processing of natural and xenobiotic Cbls by BAEC .....	110
Table 3.5 Genetic and biochemical background of the <i>cbIC</i> patient cell lines used in this study .....	112
Table 3.6 Processing of [ <sup>57</sup> Co]-MeCbl by human normal and <i>cbIC</i> mutant fibroblasts .....	113
Table 3.7 Dealkylation rates of alkylcobalamins by the <i>cbIC</i> /GSH system .....	132
<b>CHAPTER 4 Biochemistry of the <i>cbIC</i> disorder and cobalamin deficiency in humans .....</b>	<b>142</b>
Table 4.1 Processing of [ <sup>57</sup> Co]-HOCbl by normal and <i>cbIC</i> fibroblasts .....	146
Table 4.2 Intracellular levels of Cbl and folates in normal and <i>cbIC</i> fibroblasts .....	149
Table 4.3 Gel set up for 2D-DIGE experiments .....	157
Table 4.4 Differentially expressed proteins in normal versus <i>cbIC</i> fibroblasts without exogenous HOCbl .....	163
Table 4.5 Differentially expressed proteins in normal versus <i>cbIC</i> fibroblasts supplemented with HOCbl .....	166

Table 4.6 Genes directly and indirectly associated with the <i>cb1C</i> phenotype without exogenous HOCbl, linked to functions by IPA® ...	196
Table 4.7 Genes directly and indirectly associated with the <i>cb1C</i> phenotype supplemented with HOCbl, linked to functions by IPA® ...	202

## List of Schemes

	<b>Page</b>
<b>CHAPTER 2 Chemistry of cobalamin forms with potential biological activity</b> .....	<b>10</b>
Scheme 2.1. Synthesis of NOCbl from HOCbl•HCl and DEA- NONOate .....	12
Scheme 2.2. Nitric oxide donors utilized in this study .....	23
Scheme 2.3. Reaction of HOCbl with DEA-NONOate .....	35
Scheme 2.4. Reaction of HOCbl with Angeli's salt .....	37
Scheme 2.5. Labeling scheme for the $\beta$ -axial ligand of ImCbl, HisCbl and N-MeImCbl .....	52
Scheme 2.6. Reaction of Cbl(I) with alkyl halides .....	65
<b>CHAPTER 3 Mechanisms of cobalamin processing in cells</b> .....	<b>85</b>
Scheme 3.1 Flow-diagram of the extraction procedure for Cbls.....	87

## List of Abbreviations

AdoCbl	Adenosylcobalamin
Ado-SG	S-Adenosylglutathione
Angeli's salt	$\alpha$ -Oxyhyponitrite
BAEC	Bovine aortic endothelial cells
BuCbl	Butylcobalamin
CAPS	3-(Cyclohexylamino)-1-propanesulfonic acid
Cbl	Cobalamin
Cbl(I)	Cob(I)alamin (2e reduced)
Cbl(II)	Cob(II)alamin (1e reduced)
<i>cblC</i>	Cobalamin complementation group C
CHES	2-(Cyclohexylamino)ethanesulfonic acid
CNCbl	Cyanocobalamin
DEA	Diethylamine
DEA-NO	Nitrosodiethylamine
DEA-NONOate	2-(N,N-Diethylamino)-diazene 2-oxide
DMEM	Dulbecco's minimum essential medium
EtCbl	Ethylcobalamin
GSCbl	Glutathionylcobalamin
GSH	Reduced glutathione

GSSG	Oxidized glutathione
HC	Haptocorrin
Hcy	Homocysteine
HEPES	4-(2-Hydroxyethyl)piperazine-1-ethanesulfonic acid, N-(2-Hydroxyethyl)piperazine-N'-(2-ethanesulfonic acid)
HepG2	Human hepatoma cell line G2
HFF	Human foreskin fibroblasts
HOcbl, H <sub>2</sub> OCbl <sup>+</sup>	Hydroxycobalamin, hydroxocobalamin, aquacobalamin
HPLC	High performance liquid chromatography
HxCbl	Hexylcobalamin
IF	Intrinsic factor
IPA®	Ingenuity pathways analysis
LC/MS	Liquid chromatography/mass spectrometry
MeCbl	Methylcobalamin
Me-SG	S-Methylglutathione
MM	Methylmalonyl-CoA mutase
MMA	Methylmalonic acid

MMACHC	Methylmalonic aciduria combined with homocystinuria type C
MS	Methionine synthase
NMR	Nuclear magnetic resonance
NO	$\cdot\text{NO}$ , $\text{NO}^+$ , $\text{NO}^-$
$\text{NO}_2\text{Cbl}$	Nitrocobalamin
$\text{NOcbl}$	Nitroxylcobalamin, nitrosylcobalamin
PBS	Phosphate buffered saline
$\text{PnCbl}$	Pentylcobalamin
$\text{PrCbl}$	Propylcobalamin
$\text{SO}_3\text{Cbl}$	Sulfitocobalamin
Sulfo-NONOate	Hydroxydiazenesulfonic acid 1-oxide
TAPS	N-[Tris(hydroxymethyl)methyl]-3- aminopropanesulfonic acid, [(2-Hydroxy-1,1- bis(hydroxymethyl)ethyl)amino]-1- propanesulfonic acid
TC	Transcobalamin
UV-vis	Ultraviolet and visible
Vitamin B <sub>12</sub>	Cyanocobalamin
XAS	X-ray absorption spectrum
XCbl	Unknown cobalamin, X: undefined upper axial ligand

$\delta$

NMR Chemical shifts

2D-DIGE

Two dimensional differential gel  
electrophoresis

## **DEDICATION**

*A Mamá y Papá*

*(To Mom and Dad)*

## ACKNOWLEDGEMENTS

First, I would like to thank my Advisors Dr. Brasch and Dr. Jacobsen for their guidance and support during the past 3.75 years. It was an exciting and enriching experience to be introduced to the field of Vitamin B<sub>12</sub> under your expertise.

I would like to specifically thank Dr. Jacobsen for providing me with opportunities not ordinarily offered to graduate students. Whether managing students in the lab, writing grants, exchanging scientific ideas and material directly with his collaborators, or handling the day to day running of a research laboratory, the experience I have gained during these years will continue to serve me well in the future. Thank you for believing in me and treating me as a coworker.

I am extremely grateful to Drs. Soumitra Basu, Thomas McIntyre and Dennis Stuehr for taking time out of their busy schedules to serve in my Ph.D. committee, and to Dr. Robert Dorman for volunteering to serve as the Graduate Faculty Representative. Thanks for your invaluable professional guidance and support.

I would like to thank my coworkers in the laboratory. I have learned something truly meaningful from each one of you. Special thanks go to Armend, for his constant support and encouragement in moments where the path to success looked overpopulated with stones.

A number of collaborators made the work described in this dissertation more colorful and complete. I would like to express my gratitude to Drs. Ruma Banerjee, Michael Kinter, Edward Quadros, David Rosenblatt, Clyde Smith, Sihe Wang, David Watkins and Belinda Willard.

This project would not have been completed without the moral support of my husband Gabriel, my parents Marta and Jorge, my sister Erika, my dearest friend Verónica, and a number of great coworkers from my undergraduate experience in Uruguay. They made me feel that 5,467 miles is not a long distance. Thanks Gabriel, for showing me that slow could sometimes be better than fast, that silence could be fulfilling, and that limit is just a word. You have been a great friend throughout the years. Mamá and Papá, I could not have had better parents than you. I have not enough words to thank you for your love and support throughout life. The best lectures that I have ever taken have come from both of you. Thanks for raising me as free-thinking child, and for making my dreams entirely yours.

## PREFACE

Vitamin B<sub>12</sub> (Cobalamin, Cbl) is an essential micronutrient required by all cells in the body. The primary clinical consequences of Cbl deficiency are megaloblastic anemia and neuropathies (Carmel 2001). The causes of Cbl deficiency are multi-factorial and involve both genetic components (Rosenblatt and Fenton 2001) and acquired conditions (Stabler and Allen 2004). Insufficient dietary intake, malabsorption, or defective intracellular processing of Cbl results in a partial or total failure to synthesize either or both of the biologically active Cbl forms: adenosylcobalamin (AdoCbl) and methylcobalamin (MeCbl), which serve as cofactors for the enzymes methylmalonyl-CoA mutase (EC 5.4.99.2) (Banerjee and Chowdhury 1999) and methionine synthase (EC 2.1.1.13) (Olteanu and Banerjee 2001), respectively. The synthesis of AdoCbl and MeCbl from other Cbl forms is dependent on the MMACHC gene product (GeneID: 25974), which defines the *cb1C* complementation group (Lerner-Ellis et al. 2006). The *cb1C* type is the most common inborn error of Cbl metabolism in humans, and therefore the principal cause of combined homocystinuria and methylmalonic aciduria.

Cobalamin processing, coenzyme formation and the manifestations of Cbl deficiency at the cellular level is a neglected area of research. The focus of my PhD research was to gain insight on: 1) The chemistry of cobalamin derivatives with potential biological activity; 2) the mechanisms of cobalamin processing within cells, and 3) the biochemistry of the *cb1C* disorder and cobalamin deficiency in humans.

# CHAPTER 1

## INTRODUCTION AND BACKGROUND

### 1.1 THE DISCOVERY OF COBALAMIN

More than fifty years ago, in 1949, Folkers and coworkers isolated a red crystalline compound (Rickes et al. 1949), that had been previously found to improve the hematological response of patients with Addisonian pernicious anemia (West 1948) and to be required to support the growth of the microorganism *Lactobacillus lactus* Dorner (Shorb 1948). The compound was named “vitamin B<sub>12</sub>” (Rickes et al. 1949).

The isolation of crystalline vitamin B<sub>12</sub> promoted active research in several laboratories to further elucidate its chemical structure and potential biological properties. The first elemental analysis of vitamin B<sub>12</sub> was carried out by Brink and coworkers in 1949 (Brink et al. 1954). The result indicated a compound with a general composition C<sub>61-64</sub>H<sub>86-92</sub>N<sub>14</sub>O<sub>13</sub>PCo, which was remarkably close to the currently known composition: C<sub>63</sub>H<sub>88</sub>O<sub>14</sub>N<sub>14</sub>PCo. In 1956, the X-ray crystal structure of vitamin B<sub>12</sub> was determined by the laboratory of Dorothy Hodgkin (Hodgkin et al. 1956). This was the largest structure to be determined by crystallographic analysis at that time, thus meriting Dorothy Hodgkin’s Nobel Prize in 1965. The analysis revealed the presence of the unique corrin ring containing four reduced pyrrole rings, and a cyanide ion coordinated at the β-axial position. The first evidence for the existence of a naturally-occurring organometallic compound was presented by Lenhert and Hodgkin in 1961, with the elucidation of the structure of AdoCbl by X-ray crystallography (Lenhert and Hodgkin 1961). The analysis revealed the presence of a Co-C

bond linking the 5'-deoxyadenosyl moiety with the cobalt center of cobalamin. In 1985, the X-ray crystal structure of MeCbl was reported, showing once again the presence of a Co-C bond (Rossi et al. 1985).

Since then, understanding the intricate mechanisms by which cobalamin complexes attain their roles *in vivo* has become one of the most interesting challenges for scientists and physicians.

## 1.2 THE STRUCTURE OF COBALAMIN

Cobalamins are cobalt complexes coordinated by four equatorial nitrogens from a corrin ring macrocycle. The corrin ring incorporates a total of seven amide side chains - 3 acetamides and 4 propinamides (**Figure 1.1**). In addition, the Co center is coordinated to a nitrogen atom from a biologically unusual 5,6-dimethylbenzimidazole (DMB) moiety at the lower ( $\alpha$ ) axial position, which is referred to as “base-on” conformation. Surprisingly, the two crystal structures of Cbl-dependent methionine synthase (EC 2.1.1.13) (Olteanu and Banerjee 2001) and methylmalonyl-CoA mutase (EC 5.4.99.2) (Banerjee and Chowdhury 1999) revealed that the two enzymes bind Cbl in a base-off conformation, where the DMB moiety is displaced by a protein-derived imidazole nitrogen. On the other hand, crystallographic analysis of the Cbl transport protein transcobalamin (TC), and the molecular modeling of haptocorrin (HC) and intrinsic factor (IF) showed that these proteins bind Cbl in their base-on conformation (Wuerger et al. 2007). Therefore, both the base-on and base-off conformations of Cbl are relevant *in vivo*. The upper ( $\beta$ ) axial position can be occupied by a range of ligands including alkyl groups such as methyl and 5'-deoxyadenosyl, giving rise to

the naturally occurring organometallic corrinoids methylcobalamin (MeCbl) and adenosylcobalamin (AdoCbl), respectively. Most of the biologically relevant Cbl reactions occur via substitution, displacement or elimination of the upper ligand (Brown 2005). In addition, the Co center can exist in three oxidation states, giving rise to cob(I)alamin, cob(II)alamin and cob(III)alamin forms. All three oxidation states are thought to occur *in vivo*; in fact, the three species have been observed in *in vitro* enzymatic assays with methionine synthase and methylmalonyl-CoA mutase (Banerjee, Chen, and Gulati 1997; Banerjee and Chowdhury 1999).

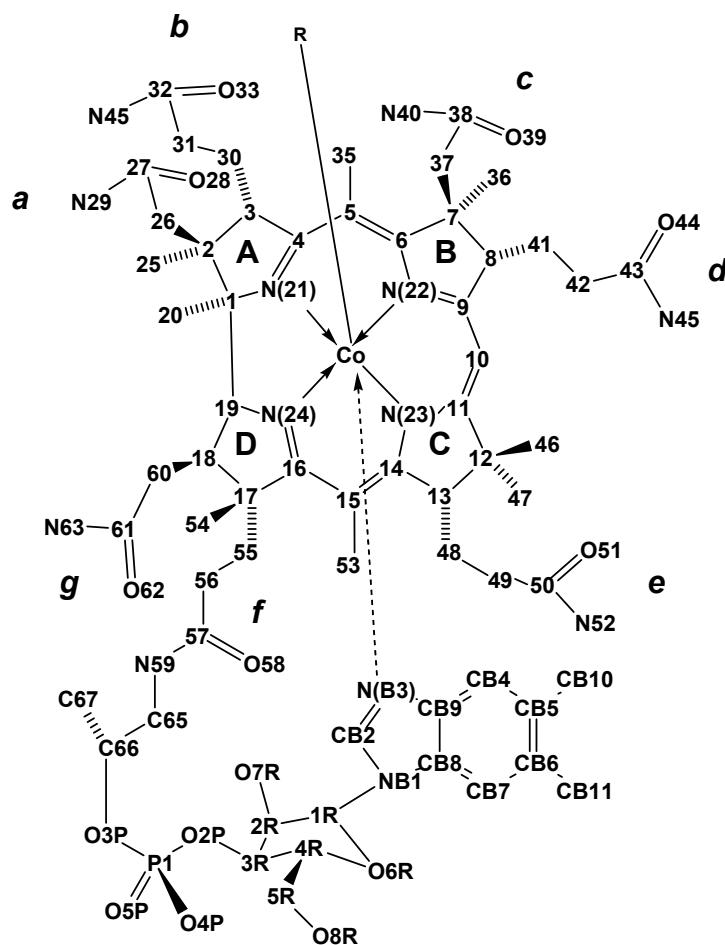


**Figure 1.1 Chemical structure of cobalamins with atom numbering.** X= H<sub>2</sub>O, aquacobalamin; X=CN<sup>-</sup>, cyanocobalamin (vitamin B<sub>12</sub>); X=5'-deoxyadenosyl, adenosylcobalamin; X=CH<sub>3</sub>, methylcobalamin, etc. The pyrrole rings are labeled as A, B, C, and D. Rings B and C are connected through a methylene carbon (C<sub>10</sub>). Side chains are indicated as *a*, *b*, *c*, *d*, *e*, *f* and *g*.

### 1.3 COBALAMIN METABOLISM IN MAMMALS

Cobalamins are dietary micronutrients that serve as coenzymes for cytoplasmic methionine synthase (Olteanu and Banerjee 2001) and mitochondrial methylmalonyl-CoA mutase (Banerjee and Chowdhury 1999). Thus, Cbl are essential cofactors for one-carbon metabolism, propionic acid metabolism, and cell division (Fenton, Gravel, and Rosenblatt 2001; Chanarin 1979; Finkelstein 1990). The clinical consequences of Cbl deficiency include hyperhomocysteinemia, methylmalonicacidemia, megaloblastic anemia and neurological disease (Healton et al. 1991; Cooper and Rosenblatt 1987; Mollin 1960; Beck 1991; Metz 1993; Allen et al. 1990). Hyperhomocysteinemia is associated with cardiovascular disease, complications of pregnancy, cognitive dysfunction including Alzheimer's disease, and osteoporosis (McCully 1969; McCully and Ragsdale 1970; Brattström and Lindgren 1992; Green and Jacobsen 1995; Regland et al. 1995; Diaz-Arrastia 1998; Morris 2003; Shinawi 2007). Three soluble Cbl-binding proteins are known to be involved in the uptake and transport of Cbls in humans: haptocorrin (HC) (Alpers and Russell-Jones 1999), intrinsic factor (IF) (Mathews et al. 2007), and transcobalamin (TC) (Wuerges et al. 2006). These proteins ensure that Cbl reaches its two target enzymes- methionine synthase and methylmalonyl-CoA mutase. The transcobalamin receptor (TCblR), which was recently cloned and characterized by Quadros et al. (Quadros, Nakayama, and Sequeira 2008), captures circulating holo-TC by TCblR-mediated absorptive endocytosis as shown in **Figure 1.2**.

Mutations in the genes that encode the enzymes or proteins involved in Cbl processing, trafficking and biosynthesis are defined as Cbl complementation groups (*cblA-*

*cblG* and *mut<sup>0</sup>*) (Rosenblatt 2001; Rosenblatt and Fenton 2001; Rosenblatt and Whitehead 1999) (**Figure 1.2**). The intracellular processing of dietary cobalamin for the synthesis of AdoCbl and MeCbl is dependent on *MMACHC*, the product of the *MMACHC* (*cblC*) locus (Gene ID: 25974), which is defective in patients with cobalamin disorders belonging to the *cblC* complementation group (Lerner-Ellis et al. 2006). The first patient with the *cblC* defect was described 4 decades ago by Harvey Mudd and colleagues (Mudd, Levy, and Abeles 1969). The absence of MeCbl results in increased concentrations of Hcy in blood as well as decreased blood levels of methionine. In the absence of AdoCbl, MM is unable to convert methylmalonyl-CoA into succinyl-CoA, resulting in increased levels of methylmalonic acid in blood and urine. The *cblC* complementation group represents the most common inborn error of cobalamin metabolism in humans (MIM 277400), and therefore the principal cause of combined homocystinuria and methylmalonic aciduria (Lerner-Ellis et al. 2006).

Despite its importance, little information is available on the intracellular events that occur after internalization of TC-Cbl. These events probably include (**Figure 1.2**): 1) dissociation of TC-XCbl from TCblR in acidic endosomes; 2) recycling of TCblR back to the cell surface (Jacobsen, Amagasaki, and Green 1990); 3) fusion of TC-XCbl-containing endosomes with lysosomes; 4) proteolytic degradation of TC and transport of cobalamin (XCbl) to the cytoplasm; 5) XCbl processing; and, 6) intracellular trafficking of Cbl to its target enzymes.

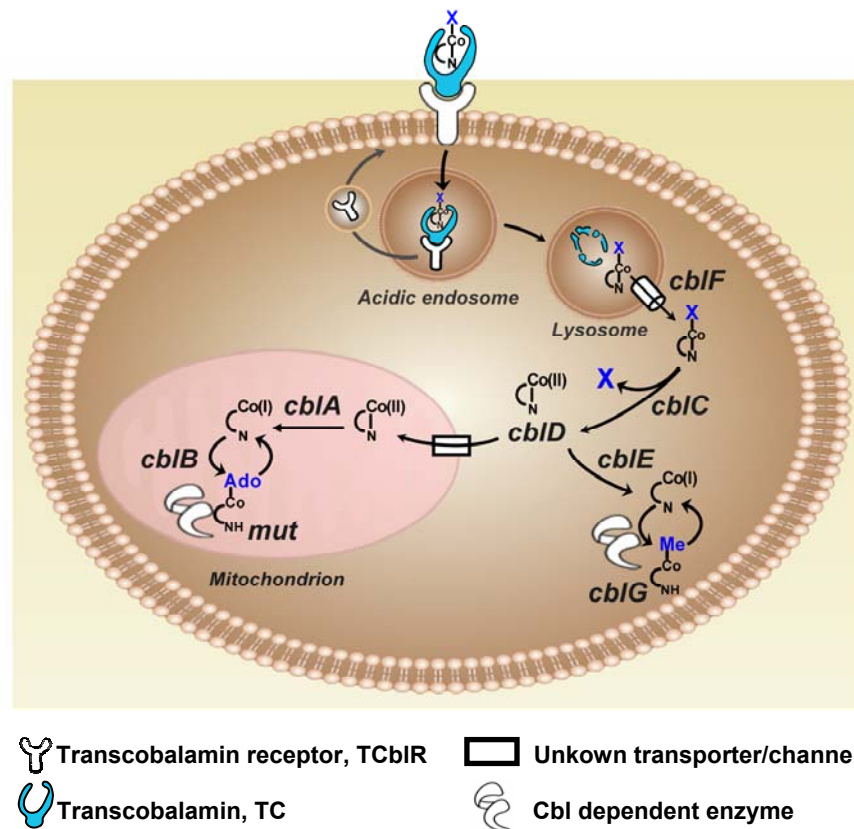


**Figure 1.2. Transport and metabolism of cobalamin (Cbl).** Mammalian cells express receptors for transcobalamin (TC), a serum Cbl-binding protein that delivers the vitamin throughout the body. The transcobalamin receptor (TCbIR) captures holo-TC (TC•XCbl) from circulation and internalizes the complex by absorptive endocytosis. Holo-TC dissociates from the receptor in acidic endosomes, and TCbIR is recycled back to the cell surface. Holo-TC is degraded in lysosomal vesicles by proteolysis and the XCbl is exported to the cytosol via the lysosomal transporter *cbIF*, where it then binds to the *cbIC* (*MMACHC*) chaperone. The  $\beta$ -axial ligand “X-group” is eliminated by the *cbIC* (*MMACHC*) chaperone. The *cbID* gene product is thought to direct *cbIC*-bound Cbl to the mitochondria for AdoCbl synthesis (via *cbIA* and *cbIB*), or to cytosolic methionine synthase for MeCbl synthesis (via *cbIE* and *cbIG*).

Previous studies performed in our laboratory showed that *cbIC* fibroblasts displayed reduced Cbl reductase and  $\beta$ -ligand transferase activities compared to normal fibroblasts (Pezacka 1993). This finding led us to hypothesize that the *MMACHC* gene may encode a putative decyanase/reductase protein product (Pezacka 1993). A more recent study showed that *cbIC* cell lines displayed reduced rate of methionine formation, decreased MS and MM activities, diminished Cbl uptake, and very low amounts of intracellular MeCbl and AdoCbl

compared to normal fibroblasts (Suormala et al. 2004). Both the synthesis of methionine and the enzyme activities of MS and MM were only partially restored by addition of HOCbl to the culture medium (Suormala et al. 2004).

The sequence of the *MMACHC* gene was recently reported by Lerner-Ellis et al. (Lerner-Ellis et al. 2006). According to the gene sequence, the *MMACHC* protein is not a member of any previously identified gene family (Lerner-Ellis et al. 2006). Although it is well conserved among mammals, its C-terminal end does not seem to be conserved in eukaryotes outside mammalia, and no homologous are found in prokaryotes. The *MMACHC* protein has two motifs that are similar to motifs present in bacterial genes with Cbl-related functions: a) a Cbl-binding motif 52% identical to the corresponding motif of MM of *Streptomyces avermitilis*, and b) a TonB motif ~40-50% identical to various TonB proteins from Gram negative bacteria (Lerner-Ellis et al. 2006). The *MMACHC* gene appeared to be expressed in most tissues. High mRNA levels were detected in fetal liver, lower levels were detected in spleen, lymph node, thymus and bone marrow, and no message was detected in peripheral blood leukocytes. In addition, the cellular *cbiC* phenotype was complemented in two immortalized *cbiC* fibroblast cell lines infected with wild-type *MMACHC* cDNA. Function of both MS and MM was restored to control levels, or above, in infected *cbiC* fibroblasts. Moreover, the conversion of CNCbl into AdoCbl and MeCbl was more effective in the complemented cell lines (Lerner-Ellis et al. 2006).

The mystery of how decyanation of CNCbl occurs was recently solved by the *in vitro* studies of Kim et al. (Kim, Gherasim, and Banerjee 2008). The reductive decyanation of CNCbl is catalyzed by the *MMACHC* chaperone in the presence of a flavoprotein reductase and NADPH (Kim, Gherasim, and Banerjee 2008). The *cbiC* protein was able to bind both

MeCbl and AdoCbl inducing their base-off conformation (Kim, Gherasim, and Banerjee 2008); however, the protein did not catalyze the dealkylation of MeCbl and AdoCbl, the two major dietary forms of Cbl. This intriguing and somewhat unexpected finding was re-examined in collaboration with the research group of Dr. Ruma Banerjee (University of Michigan, Ann Arbor, MI), and as a result, a new function was uncovered for the *cbIC* protein. These results will be described in Chapter 3 of this dissertation.

#### 1.4 SCOPE OF THIS DISSERTATION

The intracellular events that occur after internalization of Cbl remain largely unknown. Decyanation/reduction of Cbl is the key step preceding cofactor biosynthesis. Patients carrying mutations in the *cbIC* gene fail to synthesize both AdoCbl and MeCbl, which results in combined methylmalonic aciduria and homocystinuria (Lerner-Ellis et al. 2006).

The present thesis provides insightful data on: **a)** the chemistry of cobalamin forms with potential biological activity (**Chapter 2**), **b)** the mechanisms of intracellular processing of Cbl (**Chapter 3**), and **c)** the biochemistry of the *cbIC* disorder and cobalamin deficiency in humans (**Chapter 4**).

**CHAPTER 2**  
**CHEMISTRY OF COBALAMIN FORMS WITH POTENTIAL BIOLOGICAL**  
**ACTIVITY**

**2.1 Project 1: Synthesis and characterization of nitroxylcobalamin (NOCbl) and  
nitrocobalamin (NO<sub>2</sub>Cbl).**

**INTRODUCTION**

Both methionine synthase and MMA-CoA mutase are inhibited by nitric oxide under *in vivo* and *in vitro* conditions (Nicolaou et al. 1996; Kambo et al. 2005). It has been proposed that inhibition occurs through formation of nitrosylcobalamin (NOCbl) at the active site of the enzymes, leading to their inactivation (Nicolaou et al. 1996; Kambo et al. 2005). It has also been observed that hydroxycobalamin suppresses or reverses certain actions of NO *in vivo*, such as relaxation of smooth muscle (Schubert et al. 2004), vasodilation (Jiang, Li, and Rand 1997), inhibition of cell proliferation and neural tube defects (Brouwer et al. 1996). The structural characterization of NOCbl has been difficult due to the extreme oxygen sensitivity of the molecule (Randaccio et al. 2006). NOCbl itself has been associated with considerable controversy in the literature, not withstanding its existence (Firth et al. 1969), and, more recently, whether or not aquacobalamin reacts directly with NO to form NOCbl (it is now well established that this is not the case (Wolak et al. 2000; Zheng and Birke 2001)). Indeed, NOCbl was referred to as "elusive" in a recent comprehensive review of B<sub>12</sub> structures (Randaccio et al. 2006), in which the absence of structural information on NOCbl was noted. This has led to speculation on the geometry, bond distances and bond angles of

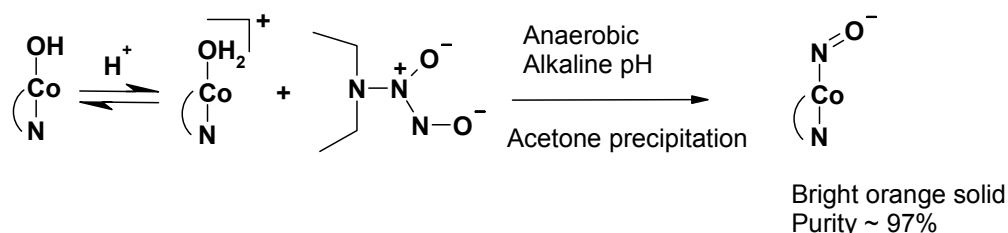
NOCbl (Randaccio et al. 2006; Selcuki, Van Eldik, and Clark 2004). The oxidation state of the Co center of NOCbl is also of considerable interest (Zheng and Birke 2001; Zheng, Yan, and Birke 2002; Wolak et al. 2000; Wolak et al. 2001; Wolak, Stochel, and van Eldik 2006). *Project 1* describes the development of a simple method for the synthesis of NOCbl (and of its oxidation product, NO<sub>2</sub>Cbl), the X-ray structural characterization of NOCbl by X-ray diffraction, and a kinetic study of the unprecedented reaction between hydroxycobalamin and diazeniumdiolates to form NOCbl. Part of this work has been published (Hannibal, Smith et al. 2007; Hassanin, Hannibal, Jacobsen, Brown et al. 2009; Suarez-Moreira et al. 2006; Hassanin, Hannibal, Jacobsen, El-Shahat et al. 2009).

## **RESULTS AND DISCUSSION**

### **A. Development of a method of synthesis of NOCbl**

Prior to this work, there was substantial controversy in the literature regarding the synthesis and the chemical properties of NOCbl (Wolak et al. 2000; Zheng and Birke 2001). NOCbl can be synthesized by bubbling NO(g) into a solution of Cbl(II) (Wolak et al. 2001) or GSCbl (Zheng and Birke 2002) under strictly anaerobic conditions. Although both methods yield highly pure NOCbl (>95%), the reactions require the use of reducing agents (ascorbate, NaBH<sub>4</sub>, Zn amalgam) and/or resulted in the formation of byproducts (such as GS<sup>-</sup>, GS<sup>•</sup>, GSSG), respectively, that might be hard to remove from the aqueous synthesis

mixture. I designed a simple method for the synthesis of solid, highly pure NOCbl from the reaction between hydroxycobalamin and the nitric oxide donor DEA-NONOate, under strictly anaerobic, alkaline conditions (pH 8.9) (**Scheme 2.1**) (Hannibal, Bunge et al. 2007). Isolation of the bulk material by precipitation with acetone gave a bright orange product in 85% yield that was ~97% pure.



**Scheme 2.1.** Synthesis of NOCbl from HOCbl•HCl and diethylamine-NONOate.

UV-visible and  $^1\text{H}$  NMR spectroscopic data are presented in **Figure 2.1**. Our spectroscopic characterization is in excellent agreement with literature values (Wolak et al. 2001; Zheng and Birke 2001; Zheng and Birke 2002). Solid NOCbl was found to be relatively stable even in the presence of air, in the absence of moisture. Exposure of NOCbl in aqueous solution to oxygen results in its rapid decomposition to form  $\text{NO}_2\text{Cbl}$  (Hannibal, Bunge et al. 2007), as shown in **Figure 2.2**. Our synthesis procedure represents a novel and simpler approach compared with the previous attempts to synthesize NOCbl.

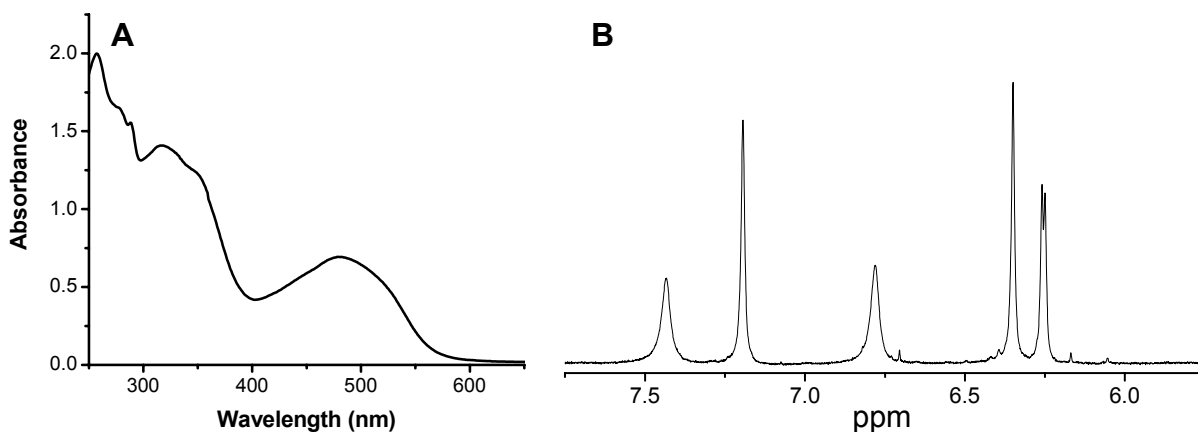


**Figure 2.1. Spectroscopic characterization of NOCbl.** A. UV-visible spectrum of nitrosylcobalamin ( $1.00 \times 10^{-4}$  M) in anaerobic 0.10 M TES buffer, pH 7.4, 25 °C. Wavelength maxima occur at 257, 318, 350 (shoulder) and 479 nm. B.  $^1\text{H}$  NMR spectrum of the aromatic region of NOCbl ( $\sim 1.04 \times 10^{-2}$  M) re-dissolved in anaerobic TES buffer (0.010 M, pD 7.4) in  $\text{D}_2\text{O}$ :  $\delta = 7.44, 7.19, 6.78, 6.35$  and  $6.26$  ppm, in agreement with literature values (Wolak et al. 2001; Zheng and Birke 2002). Small signals ( $\sim 2\%$ ) arising from impurities in the reactant  $\text{HOcbl}\cdot\text{HCl}$  are present at 6.71, 6.17 and 6.06 ppm (Hannibal, Smith et al. 2007).

The ability to isolate large amounts of highly pure NOCbl enabled me to perform a comprehensive characterization of this so far elusive cobalamin complex.

I initially attempted the synthesis of NOCbl using another family of NO donors, namely, nitrosothiols. In addition to the desired product, NOCbl (yield:  $\sim 85\text{-}90\%$ ), this reaction gave rise to the corresponding thiolatocobalamin derivative (yield:  $\sim 10\text{-}15\%$ ). The mechanism of this interesting reaction was published during the development of this project by the research group of Prof. Dr. Rudi van Eldik (Wolak, Stochel, and van Eldik 2006).

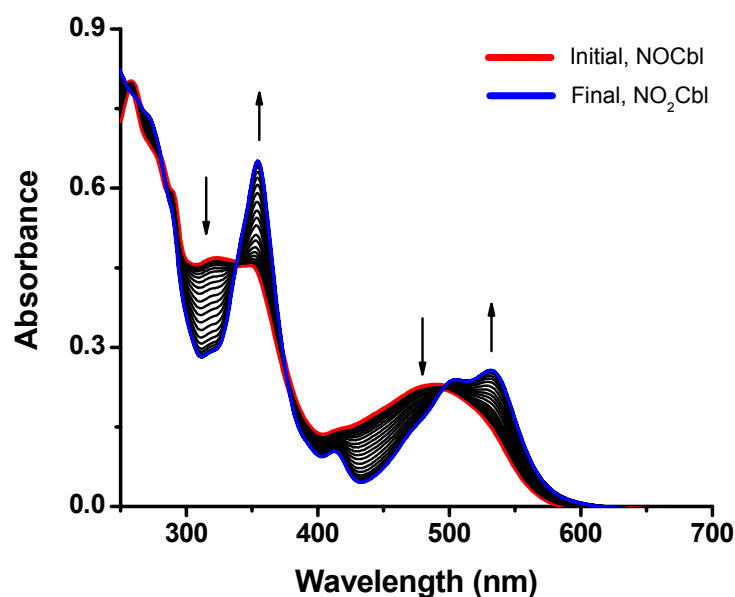


**Figure 2.2. Reaction of NOCbl ( $3.0 \times 10^{-5}$  M) with atmospheric oxygen.** The reaction was initiated by exposure of an anaerobic solution of NOCbl to air. The experiment was performed with constant stirring, at  $T = 25^\circ\text{C}$ . Spectra were recorded every 1 min. Isosbestic points: 338 and 497 nm (Hannibal, Smith et al. 2007)

A simple procedure for the synthesis of  $\text{NO}_2\text{Cbl}$  was also developed (Suarez-Moreira et al. 2006).  $\text{NO}_2\text{Cbl}$  was obtained in high yield and purity (yield  $\sim 92\%$ ; purity  $\sim 99\%$ ) from the reaction of  $\text{HOCbl}\cdot\text{HCl}$  with 1.2 equivalents of sodium nitrite, at room temperature. The product was precipitated by drop-wise addition into cold acetone, vacuum dried and characterized by UV-vis and  $^1\text{H}$  NMR spectroscopies. The UV-visible spectrum of  $\text{NO}_2\text{Cbl}$  is remarkably similar to that of  $\text{H}_2\text{OCbl}^+/\text{HOCbl}$ , but clearly distinct from that of NOCbl (**Figure 2.3**). Three different X-ray crystal structures of  $\text{NO}_2\text{Cbl}$  have been reported by other research groups, and will be considered later in this chapter.

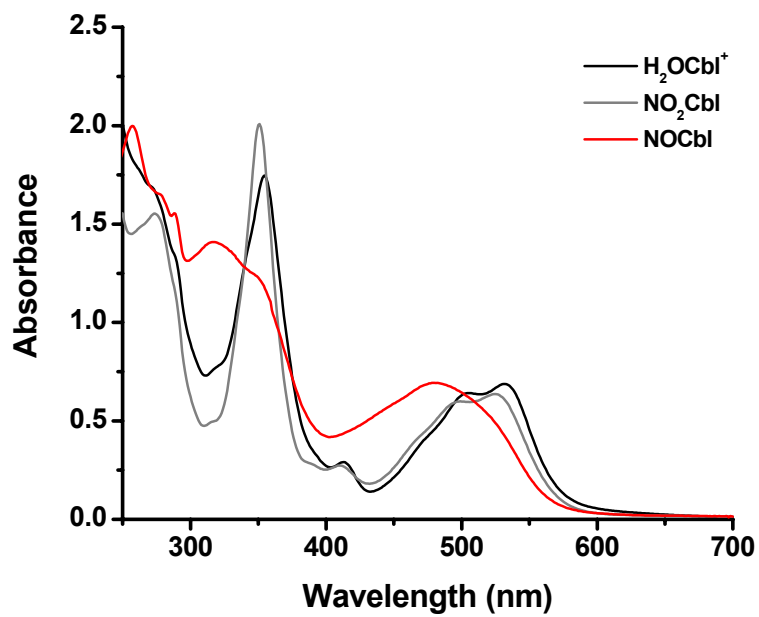


**Figure 2.3.** UV-visible spectra of  $\text{H}_2\text{OCbl}^+$ ,  $\text{NO}_2\text{Cbl}$  and  $\text{NOCbl}$ . Cobalamins were dissolved in 0.100 M MES, pH 6.00, at 25 °C.

## B. X-ray analysis of NOCbl

Crystals of NOCbl suitable for X-ray analysis were obtained, and therefore, the structure of the complex finally revealed (Hannibal, Smith et al. 2007). A photograph of NOCbl crystals grown in aqueous acetone is given in **Figure 2.4**. A crystal of NOCbl ( $\sim 0.1 \times 0.1 \times 0.3$  mm), obtained from aqueous acetone, was mounted under paraffin oil in a nylon loop in a glove box and flash frozen in liquid nitrogen. Diffraction experiments were carried out at the Stanford Synchrotron Radiation Laboratory.

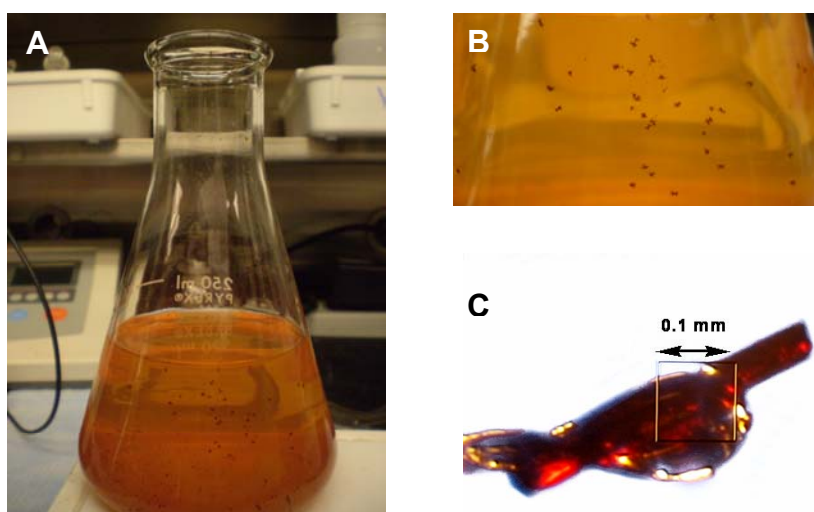


**Figure 2.4 Crystallization of NOCbl.** **A.** Crystals grown on the walls of an Erlenmeyer flask from a solution of  $\sim 80\%$  acetone/ $20\% \text{H}_2\text{O}$ . **B.** Close-up view of a population of crystals. **C.** A crystal of NOCbl as mounted prior to X-ray analysis (courtesy of Dr. Clyde A. Smith).

$\text{NOCbl} \cdot 15\text{H}_2\text{O}$  crystallizes in the orthorhombic space group  $\text{P2}_12_12_1$  with one molecule per asymmetric unit. The crystallographic data is summarized in **Table 2.1**, and a thermal ellipsoid plot is given in **Figure 2.5**. The solvent structure in  $\text{NOCbl} \cdot 15\text{H}_2\text{O}$  has been modelled as 15 water molecules, all of which are involved in hydrogen bonding

interactions with either oxygen or nitrogen atoms on the cobalamin moiety. The cobalamin is in the "base-on" conformation and the NO ligand is seen in three different orientations, such

**Table 2.1 Data Collection and Refinement Statistics for NOCbl•15H<sub>2</sub>O**

Empirical formula	C <sub>62</sub> H <sub>89</sub> N <sub>14</sub> O <sub>15</sub> PCo
FW	1359 g/mol
Temperature	100 K
Wavelength	0.82653 Å
Space group	P2 <sub>1</sub> 2 <sub>1</sub> 2 <sub>1</sub>
Unit cell dimensions	$a = 15.930$ $b = 21.390$ $c = 24.066$
Volume	8200.3(1) Å <sup>3</sup>
Z	4
Absorption coefficient	0.29 mm <sup>-1</sup>
F(000)	3912
Limiting indices	$-18 \leq h \leq 18, -26 \leq k \leq 26, -29 \leq l \leq 29$
Reflections collected/unique	39700/17159
R <sub>merge</sub> and R <sub>sym</sub>	0.035, 0.041
Refinement method	Full-matrix least squares on F <sup>2</sup>
Data/restraints/parameters	15872/0/1036
GOF on F <sup>2</sup>	0.975
R factors (I > 4σ <sub>I</sub> )	R1 = 0.0964, wR2 = 0.2786
R factor (all data)	R1 = 0.1061
Largest difference peak and hole	+0.53 and -0.46 e/Å <sup>3</sup>

that three positions for the oxygen atom are observed. Rotational disorder is common for NO ligands (Bultitude et al. 1984). The Co-N-O angle provides important information on the oxidation state of the Co center, since the Co-N-O group of low spin nitroxyl-Co(III) complexes is bent (~120°) as a consequence of the lone pair on the N atom of nitroxyl (NO<sup>-</sup>) (Holleman-Wiberg.), while Co-N-O is essentially linear for nitrosyl complexes (Holleman-Wiberg.). The Co-N-O angle in NOCbl•15H<sub>2</sub>O ranged from 117.4-121.4° (Table 1); hence NOCbl is best described as “nitroxylcob(III)alamin” in both the solid and solution states (Zheng and Birke 2001; Wolak et al. 2001). As expected, the NO ligand is bound to the

cobalt through a N atom, with a Co-N bond distance of 1.93 Å (**Table 2.2**). The bond distance is similar to the Co-N bond length found in the three reported structures of NO<sub>2</sub>Cbl (1.91 - 1.94 Å, **Table 2.2**) and is also consistent with Co-N bond lengths observed in nitroxyl and nitro complexes of Co porphyrin complexes (**Table 2.2**).

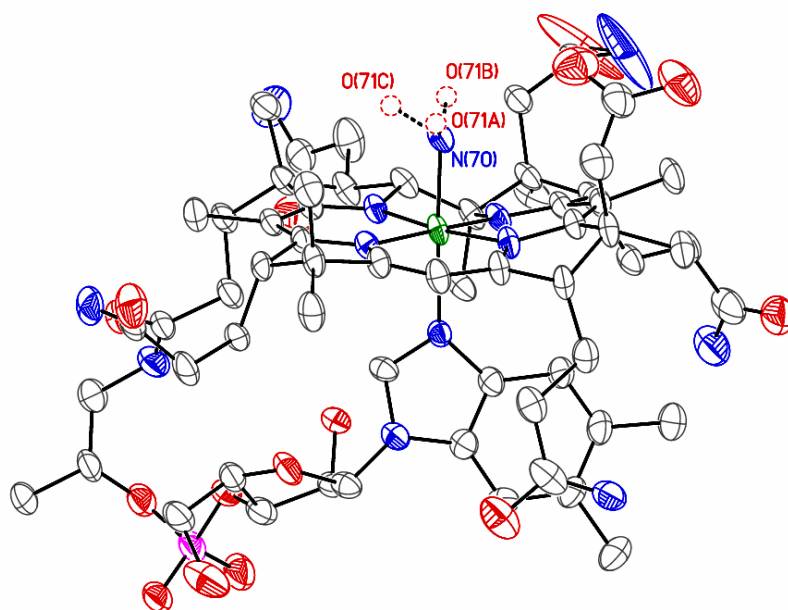


**Figure 2.5.** Thermal ellipsoid plot (30%) of NOCbl•15H<sub>2</sub>O. View of the entire cobalamin complex. The NO ligand is bound to the Co through the nitrogen atom (Co-N distance = 1.927(6) Å). Water solvent molecules are not shown for clarity. Inset: A close-up view of the Co coordination sphere.

**Table 2.2. Comparison of the Co coordination sphere in NOCbl and NO<sub>2</sub>Cbl structures.**

	NOCbl <sup>[a]</sup>	NO <sub>2</sub> Cbl•2LiCl <sup>[b]</sup>	NO <sub>2</sub> Cbl•NaCl <sup>[b]</sup>	NO <sub>2</sub> Cbl <sup>[c]</sup>
Co-N	1.927(6)	1.942(6)	1.912(5)	1.941(5)
Co-N3B	2.126(5)	1.992(6)	2.014(5)	2.008(4)
Co-N21	1.858(4)	1.873(5)	1.868(5)	1.888(4)
Co-N22	1.908(5)	1.920(4)	1.902(5)	1.917(4)
Co-N23	1.915(4)	1.919(5)	1.900(5)	1.922(4)
Co-N24	1.887(5)	1.894(5)	1.870(5)	1.906(4)

<sup>[a]</sup> This work. <sup>[b]</sup> Reference (Garau et al. 2003). <sup>[c]</sup> Reference (Perry et al. 2003).

Evidence for the presence of a NO<sup>-</sup> group as opposed to the oxidized form NO<sub>2</sub><sup>-</sup> comes from comparison of the N-O bond distances with other structures. The N-O distances for the three orientations of NOCbl range from 1.14 to 1.20 Å and are entirely consistent with a N=O double bond as reported for the nitroxyl complexes of tetraphenylporphyrin (TPP) (Scheidt and Hoard 1973; Richter-Addo et al. 1996), octylethylporphyrin (OEP) (Ellison and Scheidt 1998), and two tropocoronand ligands (TC-3,3 and TC-4,4) (Table 1) (Franz et al. 2001). Nitro ligands, on the other hand, typically show two distinct N-O bond distances (N-O1 and N-O2, **Table 2.2**), and the N-O/N=O bond distances for the three reported NO<sub>2</sub>Cbl structures are in the range 1.22-1.32 Å. Importantly, further support for the presence of nitroxyl compared to NO<sub>2</sub><sup>-</sup> comes from a comparison of the Co-N  $\alpha$  (lower) axial bond distance, Co-N3B, in NOCbl, with those found in the three NO<sub>2</sub>Cbl structures (2.13 versus 1.99 – 2.01 Å, respectively; **Table 2.2**). The nitroxyl anion is a moderate  $\pi$  acceptor in addition to being a strong  $\sigma$  donor ligand (Bultitude et al. 1984), and therefore exhibits a stronger *trans* weakening effect compared with NO<sub>2</sub><sup>-</sup>, resulting in a longer Co-N3B bond

distance. Indeed, the Co-N3B bond length is similar to that reported for the strong donor ligands  $\text{SO}_3^{2-}$  (Co-NB3 = 2.13 Å) and Me (Co-NB3 = 2.16 Å) (Randaccio et al. 2006). The final piece of evidence for NOCbl rather than  $\text{NO}_2\text{Cbl}$  is more qualitative and relates to the observed color of the crystals. As noted above, the crystals and the solution from which they grew were bright orange in color. The crystal chosen for X-ray diffraction studies remained orange throughout data collection. Subsequently, the vial containing the remaining crystals was opened to the air and the solution present immediately turned deep red, as expected for  $\text{NO}_2\text{Cbl}$ . The aerobic decomposition of NOCbl to  $\text{NO}_2\text{Cbl}$  has been previously reported (Wolak et al. 2001; Wolak, Stochel, and van Eldik 2006). The crystals in the vial slowly changed from orange to deep red over the course of several days.

Numerous crystal structures of cobalamins have been described, with the majority of structures crystallizing in the  $\text{P}2_12_12_1$  space group (Randaccio et al. 2006); NOCbl is no exception.  $\text{NOCbl}\cdot 15\text{H}_2\text{O}$  belongs to cluster type I (Randaccio et al. 2006), with  $c/a$  and  $b/a$  ratios of 1.511 and 1.343, respectively. The cobalamin molecules are oriented such that the plane of the corrin ring is roughly parallel to the  $ab$  plane of the unit cell, with the axial base and the NO ligand extending out into solvent pockets. All potential hydrogen bonding donors and acceptors are involved in at least one hydrogen bond, with the exception of O2P, the oxygen atom bridging the ribose and phosphate groups. There are significant intermolecular contacts in the crystal lattice, including six direct hydrogen bonds linking neighbouring cobalamin molecules (O28–N45', N29–N52', N34–O5P', N34–O3P, N45–N52', and O51–N63'), with the other interactions involving water-mediated hydrogen bonds. Although the final R-factor of 9.64% is typical of cobalamin structures, this might be

explained by the presence of disorder in the solvent structure and the relative lack of direct hydrogen bonding contacts versus water-mediated interactions.

The cobalt absorption spectrum of cobalamin crystals can provide information on the degree of irradiation damage incurred on the crystal during X-ray diffraction data collection. The cobalt absorption spectrum for the NOCbl crystal used for X-ray diffraction data collection (irradiated NOCbl) and for a fresh crystal (unirradiated NOCbl) between 7650 and 7850 eV are shown in **Figure 2.6**. The overall shape of the spectra are similar to the spectra reported for other cobalamins (Champloy et al. 2000).

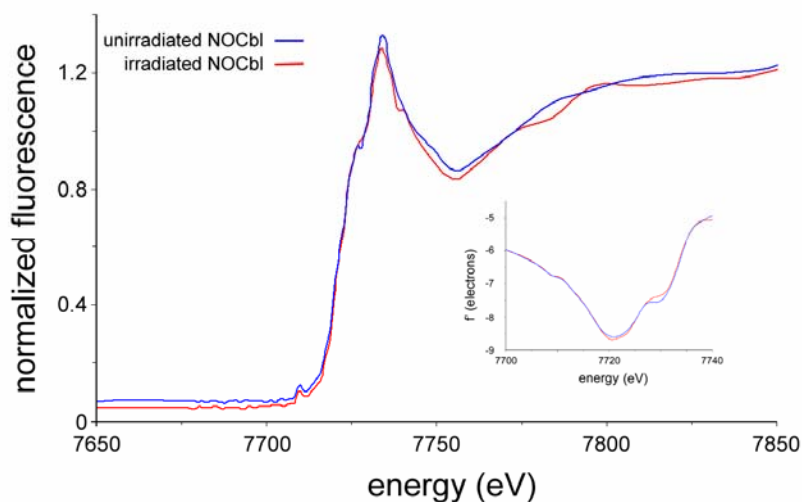


**Figure 2.6.** XAS spectrum of a NOCbl·15H<sub>2</sub>O crystal before and after irradiation.

The intensity and position of the absorption peak as calculated from the second derivative (not shown) is unchanged (7734.1 eV,  $f'' = 5.46$  for the unirradiated sample and 7733.7 eV,  $f'' = 5.38$  for the irradiated sample), and the overall shape of the XANES and low energy EXAFS regions are very similar. Therefore there appears to be only minor differences

following prolonged irradiation, and hence practically no evidence of radiation damage, in contrast to the recently reported study on N-acetylcysteinylcobalamin ( $\text{Na}^+$  salt), where the spectrum of unirradiated versus irradiated NACCbl showed a significant drop in peak intensity in addition to differences in some of the XANES and near-EXAFS features (Suarez-Moreira et al. 2006). It is not clear why susceptibility to radiation damage should differ between cobalamin complexes.

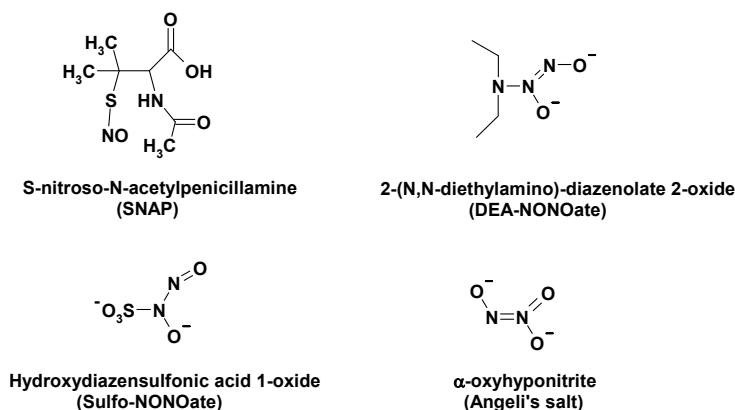
The inflection point or threshold energy of the absorption edge, calculated from the first derivative of the edge spectrum (see inset to **Figure 2.6**) using the Kramers-Kronig algorithm implemented in AUTOCHOOCH, is 7720.8 eV for the unirradiated NOCbl (corresponding to a dispersive component of the cobalt anomalous scatter ( $f''$ ) of -8.60 electrons) and 7720.6 eV for the irradiated sample. It has previously been suggested that the threshold energy is correlated with the oxidation state of the cobalt, and even though the energy of the NOCbl complex is only slightly lower than the threshold energy reported for other Co(III)Cbl systems where the measured values range from 7721.0 to 7723.5 eV (Scheuring, Sagi, and Chance 1994; Chance 1999), the position of the inflection point is apparently not a very reliable indicator of the oxidation state since the values obtained for Cbl(I) (7721.0 eV) and Cbl(II) (7722.0 eV) also fall within this range of energies. A similar conclusion was recently reached for N-acetylcysteinylcobalamin (Suarez-Moreira et al. 2006).

### C. Reaction of aquacobalamin with nitric oxide donors.

## RESULTS AND DISCUSSION

### Reaction of aquacobalamin with SNAP.

The reactions of  $\text{H}_2\text{OCbl}^+$  and  $\text{Cbl(II)}$  with the nitrosothiol SNAP were investigated by UV-vis and  $^1\text{H}$  NMR spectroscopy.  $\text{H}_2\text{OCbl}^+$  reacted with 2.5, 5.0 and 7.5 equiv. SNAP to produce  $\text{NOCbl}$  and the corresponding thiolatocobalamin in a  $\sim 85\%:15\%$  ratio. Conversely,  $\text{Cbl(II)}$  reacted with SNAP to produce very pure  $\text{NOCbl}$ ;  $\sim 96\%$  by  $^1\text{H}$  NMR spectroscopy. While we were investigating these reactions, Prof. Dr. Rudi van Eldik's research group published a comprehensive article covering the mechanisms of these reactions (Wolak, Stochel, and van Eldik 2006). Our results were in excellent agreement with their report (Wolak, Stochel, and van Eldik 2006). We therefore decided to redirect our research towards the use of a different class of nitric oxide donors, namely, diazeniumdiolates, which do not contain a thiol functionality. **Scheme 2.3** shows the nitric oxide donors selected for the study.



**Scheme 2.2.** Nitric oxide donors utilized in the present study.

### Reaction of aquacobalamin/hydroxycobalamin with DEA-NONOate.

The reaction of aquacobalamin with DEA-NONOate was studied by both UV-visible and  $^1\text{H-NMR}$  spectroscopy. UV-visible measurements evidenced the occurrence of a single step reaction between the two species, yielding authentic NOCbl as the final cobalamin product. To our knowledge, this is the first report of a reaction between aquacobalamin/hydroxycobalamin and a diazeniumdiolate. Since decomposition of the nitric oxide donor is acid-catalyzed (Maragos et al. 1991), the reactions were carried out under strictly alkaline conditions. **Figure 2.7** panel **A**, shows UV-vis spectra for the reaction of aquacobalamin with 5 equivalents of DEA-NONOate, at pH 9.80. Three isosbestic points were identified at 341, 370 and 498 nm.

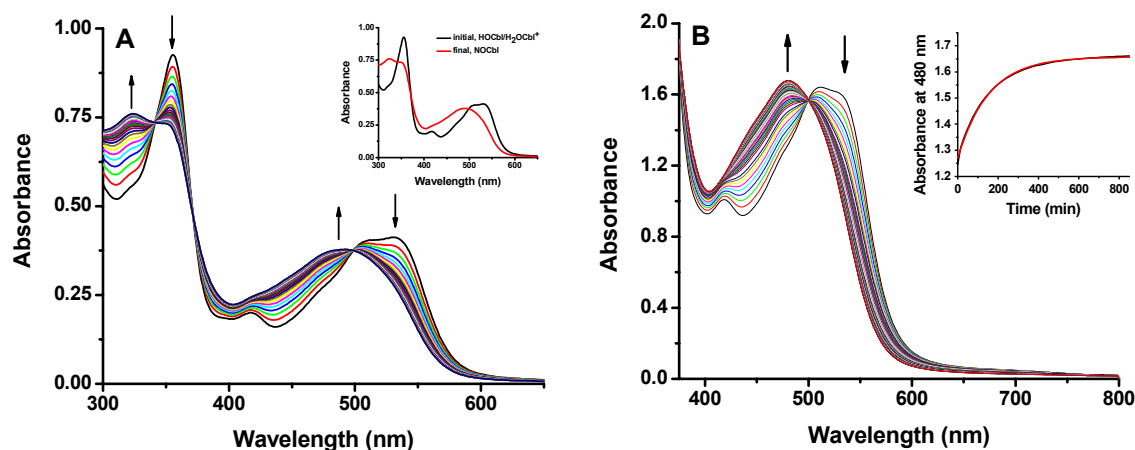


**Figure 2.7.** UV-vis spectra of the reaction between HOCbl and DEA-NONOate at pH 9.80 (0.100 M CHES,  $I = 1.0$  M, KCl), at  $T = 25.0$  °C. **A.**  $[\text{HOCbl}] = 0.050$  mM,  $[\text{DEA-NONOate}] = 0.25$  mM. Inset: overall spectral change after 16 h after mixing of the reactants. The final product is NOCbl. Isosbestic points occur at: 341, 370 and 498 nm. **B.**  $[\text{HOCbl}] = 0.25$  mM,  $[\text{DEA-NONOate}] = 2.5$  mM. Inset: fit of the absorbance data at 480 nm versus time to a first-order reaction, giving  $k_{\text{obs}} = 0.0640$   $\text{min}^{-1}$ . Scan rate: 1 spec/15 min.

Birke and co-workers have reported practically identical isosbestic points for the reaction between aquacobalamin and pure  $\text{NO}$  in a photolysis experiment with excitation at 514.5 nm (isosbestic points: 340, 370, 497 nm) (Zheng and Birke 2001). This further suggests that only two absorbing species (HOCbl and NOCbl) are present in detectable amounts in our system. Increasing the concentration of DEA-NONOate resulted in faster formation of NOCbl. Spontaneous decomposition of DEA-NONOate is a first-order process and hence independent of DEA-NONOate concentration (Maragos et al. 1991). **Figure 2.7** panel **B**, presents the UV-vis spectra for the reaction between hydroxycobalamin and 5 equiv. DEA-NONOate, at pH 9.80. The inset shows the time course at 480 nm and the corresponding best fit to a first-order exponential equation. A  $k_{\text{obs}}$  value of  $6.40 \times 10^{-2} \text{ min}^{-1}$  was obtained for this reaction.

In addition,  $^1\text{H}$  NMR experiments confirmed that hydroxycobalamin and NOCbl are the only detectable cobalamin species that occur during the reaction performed under our experimental conditions. The spontaneous decomposition of DEA-NONOate was also studied, simultaneously. Decomposition of DEA-NONOate followed first-order kinetics, in agreement with the literature (Maragos et al. 1991).  $k_{\text{obs}}$  for the spontaneous decomposition of DEA-NONOate at pH 9.80 was found to be  $4.62 \times 10^{-4} \text{ min}^{-1}$ , more than two orders of magnitude slower than reaction of DEA-NONOate with HOCbl. Hence, decomposition of DEA-NONOate is not a prerequisite for the reaction to occur. Taken together, these data supports the notion of a *direct reaction* between hydroxycobalamin and DEA-NONOate.

We found that the reaction rate was strongly affected by pH. Whereas the formation of NOCbl occurs more rapidly at lower pH, a second reaction also occurs, that leads to the

subsequent formation of a second Cbl product. More details on this reaction will be provided in the next sections.

### **Dependence of the reaction rate on [DEA-NONOate], [HOCbl] and pH.**

Concentration- dependence studies were carried out at alkaline pH conditions only since formation of a second product was observed at low pH. In addition, decomposition of the nitric oxide donor generates diethylamine ( $pK_a = 11.1$ ) (Maragos et al. 1991), which affected the pH of the reaction mixture, especially at high concentration of the nitric oxide donor. Preliminary experiments showed that the reaction becomes slower with increasing pH. One possible interpretation for this result is that the higher the pH, the smaller the fraction of aquacobalamin available to react with DEA-NONOate ( $\text{HOCbl} + \text{H}^+ \leftrightarrow \text{H}_2\text{OCbl}^+$ ,  $pK_a = 8.1$ , at  $I = 1.00 \text{ M}$ ,  $\text{KCl}$ ,  $T = 25^\circ\text{C}$ ) (Reenstra and Jencks 1979). The effect of varying the concentration of hydroxycobalamin was also studied. Experiments using fixed concentrations of Cbl of 0.025 mM and 0.25 mM, with varying [DEA-NONOate], were also performed. As a result, the observed rate constants,  $k_{\text{obs}}$ , were 0.0098 and 0.0103  $\text{min}^{-1}$ , respectively ([DEA-NONOate] = 4.68 mM, 0.300 M CHES, pH 9.80,  $I = 1.00 \text{ M}$ ,  $\text{KCl}$ ,  $T = 25^\circ\text{C}$ ). This shows that varying [Cbl] by one order of magnitude did not significantly affect the rate of the reaction.

### **Stoichiometry of the reaction between aquacobalamin and DEA-NONOate.**

The stoichiometry of the reaction was assessed by reacting aquacobalamin with 0.55, 1.1 and 2.5 equivalents of DEA-NONOate, under strictly alkaline conditions (0.100 M CAPS, pH 10.8; to prevent spontaneous decomposition of DEA-NONOate). We found that a

minimum of 1.1-1.2 equivalents of DEA-NONOate are required for the reaction to proceed to completion. This suggests that only one out of the two nitric oxide moieties present in the parent diazeniumdiolate reacts with the cobalamin to form NOCbl. Reaction with 0.55 equivalents yielded approximately 40% NOCbl, and 60% unreacted starting material (HOCbl).

**Analysis of the reaction products from the reaction between  $\text{H}_2\text{OCbl}^+/\text{HOCbl}$  and DEA-NONOate.**

**a) Identification of DEA-NO.**

Analysis of the non-cobalamin products formed upon reaction of DEA-NONOate with hydroxycobalamin was carried out in order to gain a better understanding of the mechanism of this interesting reaction.

As mentioned earlier, DEA-NONOate decomposes spontaneously to give up to 2 moles of  $\cdot\text{NO}$  and 1 mole of DEA per mole of parent compound. However, we have gathered evidence for a direct reaction between HOCbl and DEA-NONOate (the intact diazeniumdiolate), and therefore, the product/s of this unprecedented reaction should be identified. In addition, others (Wolak et al. 2000) and we have demonstrated that no reaction occurs between aquacobalamin and  $\cdot\text{NO}$ . Furthermore, we have also shown that no reaction occurs between aquacobalamin and DEA.

Therefore, a  $^1\text{H-NMR}$  spectroscopy experiment was performed with the two following precautions:

- a) The reaction was performed under alkaline conditions (pH 10.8) to prevent spontaneous decomposition of DEA-NONOate.

b) The reaction was performed in the presence of a slight excess (1.2 equiv.) of DEA-NONOate, to identify the reaction product from the reaction with aquacobalamin, rather than the products of potential side reactions. In addition, this experimental set-up allowed us to confirm the stoichiometry of the reaction.

First, the chemical shifts of pure DEA, DEA-NO and DEA-NONOate were determined at pD10.9 (0.100 M Na<sub>2</sub>CO<sub>3</sub>). The spectra and a summary of chemical shifts are presented in **Figure 2.8** and **Table 2.3**, respectively. **Figure 2.9** shows the <sup>1</sup>H NMR spectrum for the reaction of hydroxycobalamin with 1.2 equivalents DEA-NONOate at pD 10.9.

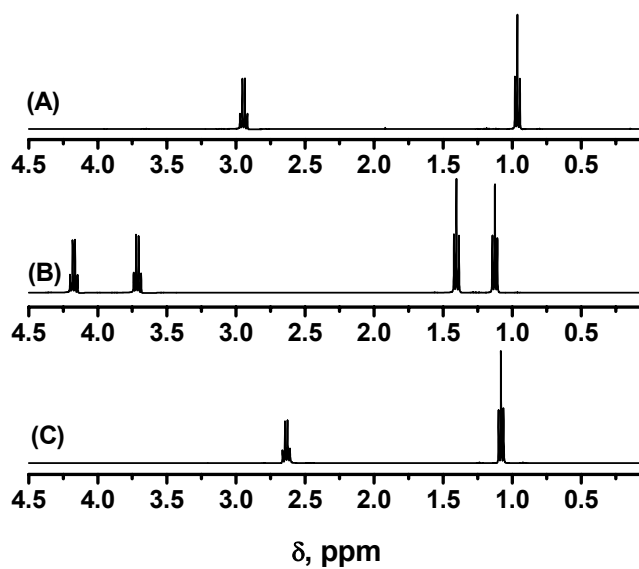


**Figure 2.8.**  $^1\text{H}$  NMR spectra of pure DEA (A), DEA-NO (B) and DEA-NONOate (C) in 0.100 M  $\text{Na}_2\text{CO}_3$ , pD 10.9. Reference: TSP.

Species	Chemical shifts (ppm)
DEA	2.664, 2.646, 2.627, 2.609 1.100, 1.082, 1.064
DEA-NO	4.201, 4.182, 4.164, 4.146 3.741, 3.723, 3.704, 3.686 1.422, 1.404, 1.386 1.144, 1.126, 1.108
DEA-NONOate	2.971, 2.953, 2.935, 2.917 0.981, 0.963, 0.945

**Table 2.3.**  $^1\text{H}$  NMR chemical shifts of pure DEA, DEA-NO and DEA-NONOate in 0.100 M  $\text{Na}_2\text{CO}_3$ , pD 10.9. Reference: TSP.

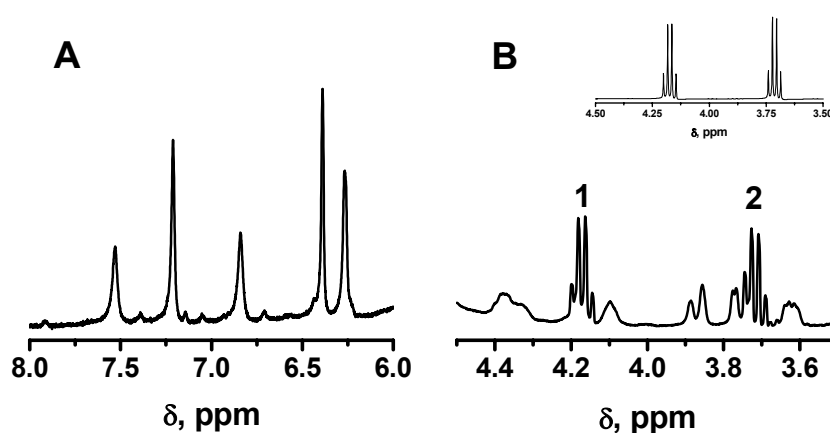


**Figure 2.9.** Analysis of the non-cobalamin products from the reaction between aquacobalamin and 1.2 equiv. DEA-NONOate at pD 10.9 (0.100 M Na<sub>2</sub>CO<sub>3</sub>). **A.** Aromatic region of the <sup>1</sup>H NMR spectrum, showing the five characteristic signals of the final product, NOCbl: 7.53, 7.21, 6.84, 6.39 and 6.27 ppm. **B.** Signals corresponding to DEA-NO, (1) 4.20, 4.18, 4.16 and 4.15 ppm and (2) 3.75, 3.73, 3.71 and 3.69 ppm. **Inset:** <sup>1</sup>H NMR spectrum of pure DEA-NO, between 4.5 and 3.5 ppm, at pD 10.9. Chemical shifts for the pure standard are: 4.20, 4.18, 4.16 and 4.15; and 3.74, 3.72, 3.70 and 3.67 ppm.

As presented in **Figure 2.9**, panel **A**, the cobalamin product is NOCbl. **Figure 2.9**, panel **B**, shows that the major non-cobalamin product of this reaction is DEA-NO (note: other peaks present correspond to Cbl aliphatic signals). Importantly, the signals attributed to DEA-NO were not present in the <sup>1</sup>H NMR spectrum of the pure starting material, HOCbl•HCl. The **inset** to **Figure 2.9**, panel **B**, shows the <sup>1</sup>H NMR spectrum of pure DEA-NO, in 0.100 M Na<sub>2</sub>CO<sub>3</sub>, pD 10.9. Signals corresponding to unreacted DEA-NONOate (which account for 15% according to the integration of the <sup>1</sup>H NMR signals), were also observed (not shown).

### Determination of NO<sub>2</sub><sup>-</sup>.

Formation of nitrite as a possible reaction product was determined by the Griess assay (Green et al. 1982; Griess 1879). No significant amounts of nitrite were found in the synthesis mixture. However, when the reaction mixture was exposed to the air, a positive

reaction for nitrite developed. This was probably due to oxidation of excess  $\cdot\text{NO}$  in solution with atmospheric oxygen. Nitrite was also formed in reaction mixtures where high concentrations of DEA-NONOate and/or low pH were used.

### b) Identification of a second reaction product: $\text{NO}_2\text{Cbl}$ .

As mentioned previously, a second reaction was observed in the presence of excess DEA-NONOate (**Figure 2.10**).

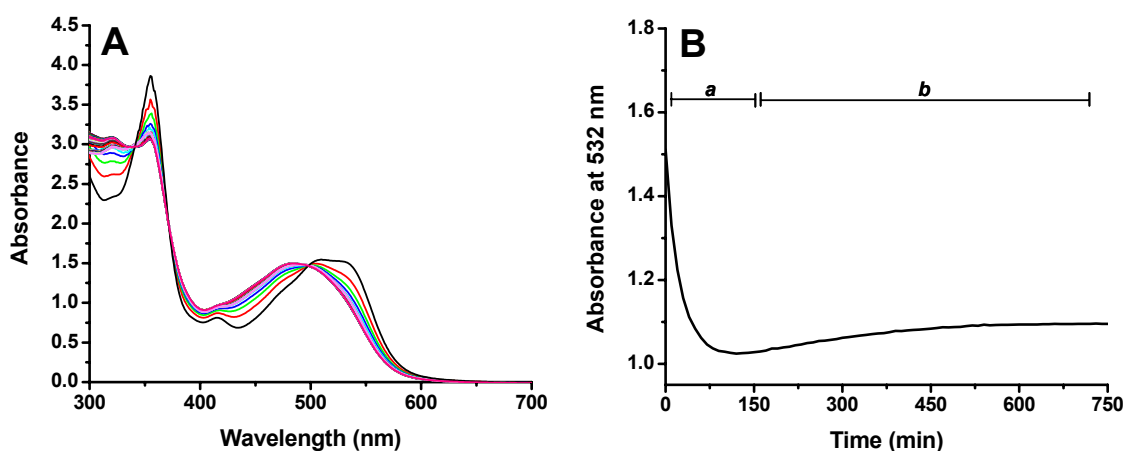


**Figure 2.10. Formation of a second reaction product:  $\text{NO}_2\text{Cbl}$**  **A.** UV-vis spectra of the reaction between aquacobalamin and DEA-NONOate at pD 8.80 (0.100 M TAPS,  $I=1.0$  KCl).  $[\text{Cbl}] = 0.25$  mM;  $[\text{DEA-NONOate}] = 2.5$  mM. **B.** Time course of the reaction between aquacobalamin and DEA-NONOate at pD 8.80 (0.100 M TAPS,  $I=1.0$  KCl).  $[\text{Cbl}] = 0.25$  mM;  $[\text{DEA-NONOate}] = 2.5$  mM. The first part of the time course, *a*, leads to the formation of  $\text{NO}\text{Cbl}$ , with the characteristic spectral changes and isobestic points. The reaction is allowed to proceed for longer periods of time, *b*, and the formation of a second Cbl product is observed.

In order to identify the product of the second reaction, the reaction between aquacobalamin and DEA-NONOate was studied at pH 8.80. Formation of NOCbl occurred rapidly, and the spectral shifts (**Figure 2.10** panel **A**) suggested either decomposition of NOCbl to give the starting material, aquacobalamin/hydroxycobalamin, or, formation of NO<sub>2</sub>Cbl, whose UV-vis spectrum is extremely similar to that of aquacobalamin (see **Figure 2.3** in this chapter) (Suarez-Moreira et al. 2006). The isosbestic points for the conversion of NOCbl into NO<sub>2</sub>Cbl by addition of oxygen (**Figure 2.2**) were 338 and 497 nm, which are practically identical to those of the reaction of aquacobalamin with DEA-NONOate to produce NOCbl (337 and 499 nm). Therefore, a <sup>1</sup>H NMR spectroscopy study was conducted to investigate the second reaction further and identify the cobalamin product/s. **Figure 2.11** shows a kinetic <sup>1</sup>H NMR spectroscopy experiment performed at pD 8.70 (0.500 M TAPS). The experiment shows that after rapid mixing of the reactants, a mixture of NOCbl and NO<sub>2</sub>Cbl is obtained, as identified by the corresponding chemical shifts. The half-life for the conversion of NOCbl to NO<sub>2</sub>Cbl was found to be ~ 45 min. No other cobalamin intermediates were observed in this reaction. We found that the same reaction occurs under alkaline conditions (although it is substantially slower) in the presence of a large excess of DEA-NONOate (20-100-fold excess).

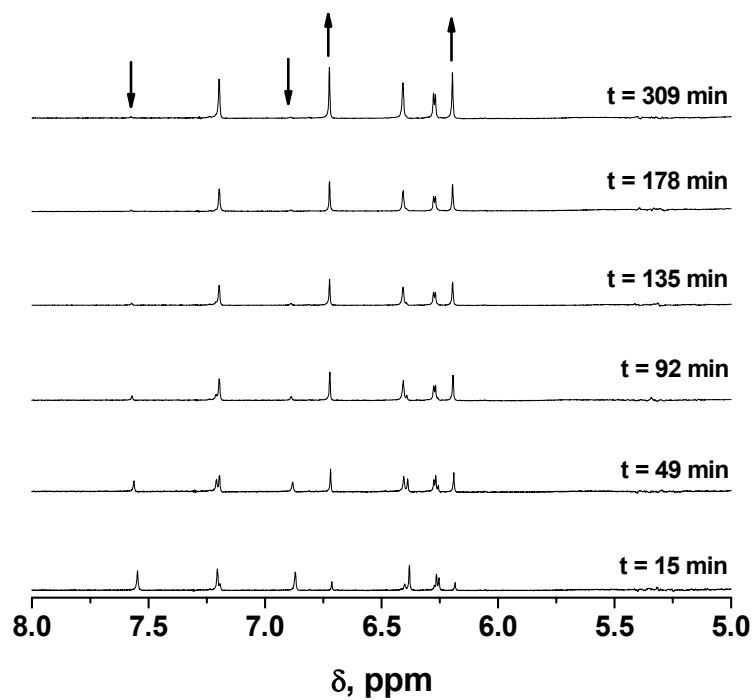


**Figure 2.11.**  $^1\text{H-NMR}$  spectroscopy time course of the reaction between hydroxycobalamin and DEA-NONOate at pD 8.70 (0.500 M TAPS,  $I=1.0$  KCl).  $[\text{Cbl}] = 0.25$  mM;  $[\text{DEA-NONOate}] = 2.5$  mM. Arrows indicate disappearance of signals corresponding to NOCbl ( $\downarrow$ ) or appearance of the characteristic signals of NO<sub>2</sub>Cbl ( $\uparrow$ ). Time,  $t$ , denote time elapsed after mixing of HOCbl with DEA-NONOate.

### Reaction of NOCbl with NO gas.

To investigate whether the formation of  $\text{NO}_2\text{Cbl}$  was due to the reaction of NOCbl with NO, the reaction between NOCbl and NO was studied by UV-vis spectroscopy. NOCbl was synthesized by the reaction of cob(II)alamin (generated from photolysis of MeCbl) with NO gas. NO(g) was then bubbled through the NOCbl solution for up to 120 min, and the UV-vis spectra were recorded. **Figure 2.12** shows the gradual conversion of NOCbl to  $\text{NO}_2\text{Cbl}$  upon exposing the solution to NO(g) at pH 8.46. These results demonstrate that the reaction of NOCbl with excess NO generates  $\text{NO}_2\text{Cbl}$ .

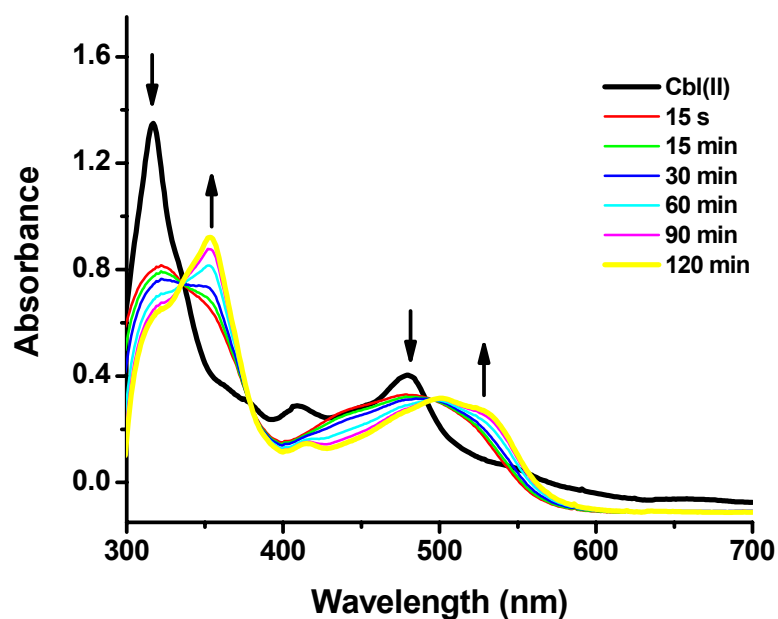


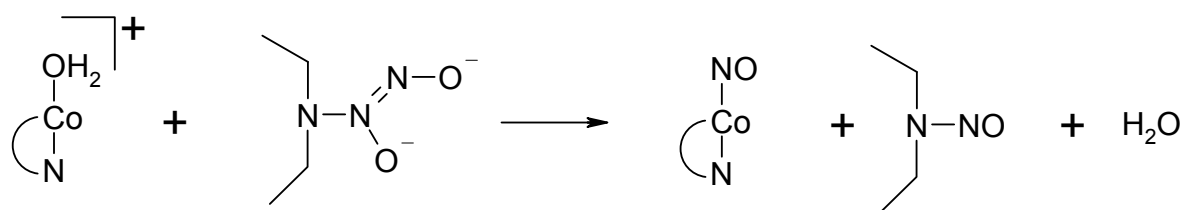
**Figure 2.12.** Reaction of NOCbl with NO(g) at pH 8.46 (0.10 M TAPS). NOCbl was synthesized by the reaction of Cbl(II) with NO(g). NOCbl was bubbled through with NO(g) for up to 120 min. Spectra were collected at the indicated times.

### Reaction of aquacobalamin with DEA-NO and DEA.

We hypothesized that DEA-NO could potentially react with  $\text{H}_2\text{OCbl}^+/\text{HOCbl}$  to form  $\text{NOcbl}$ , as observed with DEA-NONOate. However, no reaction was observed between the species, even in the presence of a large excess of DEA-NO (up to 200 equiv.) in 0.10 M TAPS, pH 8.80. This suggests that the diazeniumdiolate moiety itself is important for the reactivity toward  $\text{HOCbl}$ . In order to investigate whether the presence/accumulation of DEA may play a role in this reaction, we assessed its direct reaction with aquacobalamin, under the same conditions used for the reactions with DEA-NONOate. No reaction was observed upon addition of excess DEA (up to 200 equiv.), after 24 h. Addition of DEA did not have an effect on the rate of the reaction between aquacobalamin and DEA-NONOate.

**Effect of  $\text{NO}_2^-$ .** To investigate whether  $\text{NO}_2^-$  could act as a catalyst in the reaction as it has been reported for the reaction of cobalt porphyrins with  $\text{NO}$  (Roncaroli et al. 2006), kinetic experiments were carried out in the absence or in the presence of  $1 \mu\text{M NO}_2^-$ , at pH 9.80. No effect was observed on either the reaction rate or in the isosbestic points.

In conclusion, the reaction between aquacobalamin and DEA-NONOate can be described as follows (**Scheme 2.3**):



**Scheme 2.3.** Reaction of  $\text{H}_2\text{OCbl}^+$  with DEA-NONOate.

## Reaction of aquacobalamin with other NONOates.

### Reaction of aquacobalamin with Angeli's salt

Preliminary experiments on the reaction of aquacobalamin with Angeli's salt were also carried out. Angeli's salt is regarded as a classical nitroxyl ( $\text{NO}^-$ ) donor, but under certain conditions evolution of  $\cdot\text{NO}$  is also observed (Keefer et al. 1996; Maragos et al. 1991). Angeli's salt spontaneously dissociates in a pH-dependent, first-order process with a half-life of 2.3 min at 37°C (pH 7.4) to liberate 0.54 moles of NO per mole of parent compound (Keefer et al. 1996; Maragos et al. 1991). The reaction of  $\text{H}_2\text{OCbl}^+$  with 1.1 equiv. Angeli's salt at pH 7.4 produced approximately equimolar amounts of  $\text{NOCbl}$  and  $\text{NO}_2\text{Cbl}$ . Since decomposition of Angeli's salt is acid-catalyzed, its reaction with aquacobalamin was also investigated under alkaline conditions. Reaction of aquacobalamin with 7.5 equivalents of Angeli's salt at pH 8.5 (TAPS, 0.100 M,  $I = 1.00$  M, KCl), produced pure  $\text{NOCbl}$  as shown by UV-vis spectroscopy (**Figure 2.13**). The reaction had a half-life of  $\sim 2$  min, whereas the spontaneous decomposition of Angeli's salt had a half-life of  $\sim 50$  min.

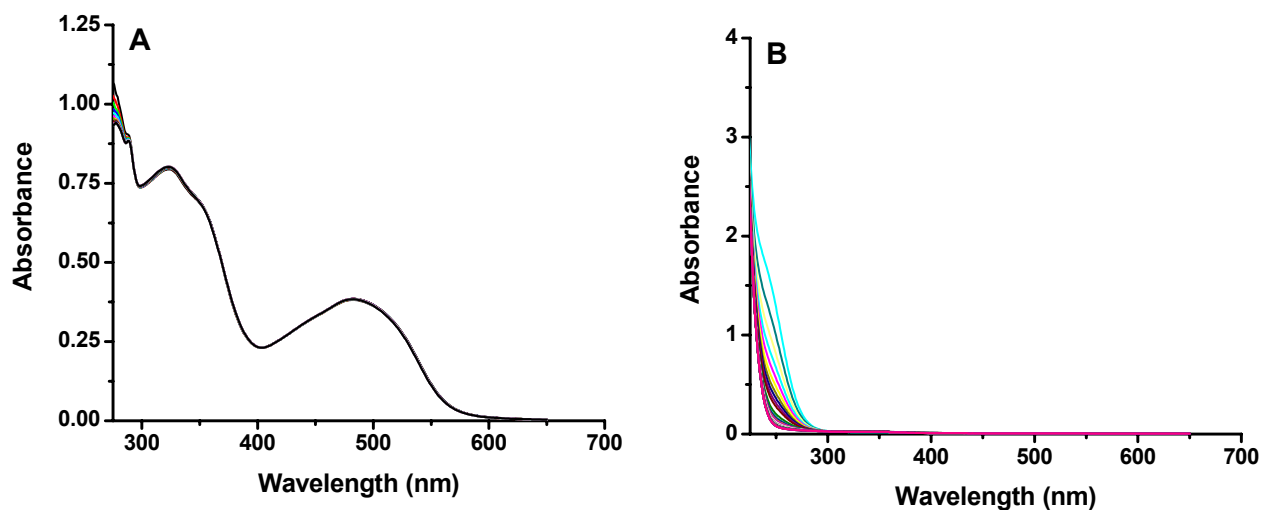
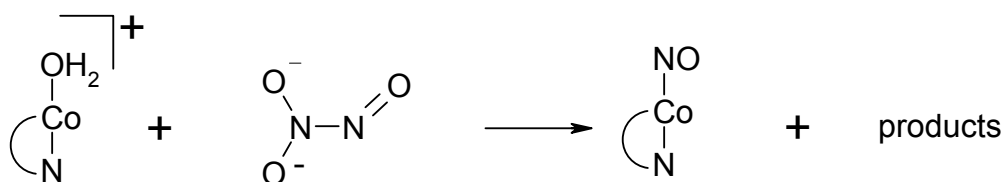


**Figure 2.13. Reaction of aquacobalamin with Angeli's salt.** **A.** Reaction of aquacobalamin ( $5 \times 10^{-5}$  M) with 7.5 equivalents of Angeli's salt (0.100 M TAPS, pH 8.5, I = 1.00 M, KCl). The half-life for this reaction was < 2 min. **B.** Spontaneous decomposition of Angeli's salt in 0.100 M TAPS, pH 8.50, I = 1.00 M, KCl. The half-life for this reaction was ~50 min.

Our preliminary data suggests that as observed in the case of DEA-NONOate, a *direct* reaction between aquacobalamin and the diazeniumdiolate Angeli's salt does occur, to form NOCbI (Scheme 2.4).



**Scheme 2.4. Reaction of  $\text{H}_2\text{OCbI}^+$  with Angeli's salt.**

### **Reaction of aquacobalamin with sulfo-NONOate**

Sulfo-NONOate undergoes spontaneous first-order decomposition to give sulfate and nitrous oxide in a pH-dependent manner (Maragos et al. 1991). Hence, unlike the other two diazeniumdiolates investigated herein, sulfo-NONOate decomposes to form nitrous oxide but not nitric oxide (NO) at physiological pH (Maragos et al. 1991). Therefore it may be used as a negative control as a reagent that does not release NO (Maragos et al. 1991). The reaction of  $\text{H}_2\text{OCbl}^+$  with 1.1 and 7.5 equiv. sulfo-NONOate was studied at pH 8.5. No reaction was observed after 24 h. The half-life for the decomposition of sulfo-NONOate in the presence of Cbl or in the absence of Cbl was  $\sim 45$  min and 51 min, respectively, that is, Cbl does not affect the rate of decomposition of sulfo-NONOate.

### **Reaction of AdoCbl and MeCbl with DEA-NONOate.**

In order to investigate whether DEA-NONOate could react with cobalamins with covalently bound  $\beta$ -axial ligands, the two natural cofactors MeCbl and AdoCbl were chosen. No reaction was observed between AdoCbl or MeCbl (0.25 mM) and DEA-NONOate (2.5 mM) at pH 8.90. The reactions were performed in anaerobic TAPS (0.100 M, pH 8.80) as described before for the other reactions, and no spectral changes were observed after 24 h.

## **SUMMARY**

The synthesis and characterization of NOCbl and its oxidation product,  $\text{NO}_2\text{Cbl}$ , were performed successfully. The determination of the X-ray crystal structure of the extremely air-sensitive NOCbl revealed that the Co atom is in the oxidized form (Co(III)), and that the Co-

NO group exists in a bent conformation, with an angle of  $\sim 121^\circ$ . The reaction of hydroxycobalamin with DEA-NONOate leads to the formation of NOCbl and DEA-NO as the final products. The reaction rate was shown to be affected by both the concentration of DEA-NONOate and the pH. We found that 1.2 equivalents of DEA-NONOate are required for the reaction to proceed to completion under alkaline conditions. No detectable cobalamin intermediates were formed under our experimental conditions.

Decomposition of the diazeniumdiolate was not a prerequisite for the reaction to occur. Hence, taken together, our results provided strong evidence for a *direct reaction* between the species. The reaction of NOCbl with a second molecule of NO (under strictly anaerobic conditions) leads to formation of  $\text{NO}_2\text{Cbl}$ .

Studies on the reaction of aquacobalamin with other model diazeniumdiolates including Angeli's salt and sulfo-NONOate showed that the reaction itself strongly depends on the chemical nature of the diazeniumdiolate under study. No reaction was observed between DEA-NONOate and the alkylcobalamins MeCbl and AdoCbl. It is possible that the reaction of Cbls with diazeniumdiolates only occurs with cobalamins presenting exchangeable upper axial ligands.

Further studies on this complex system were conducted by another student in the laboratory (Ms. Hanaa Hassanin), leading to a joint publication (Hassanin, Hannibal, Jacobsen, El-Shahat et al. 2009).

## MATERIALS AND METHODS

**General procedures and chemicals.** Hydroxycobalamin hydrochloride (HOCbl•HCl; stated purity by manufacturer is  $\geq 96\%$ , was purchased from Fluka BioChemica. The percentage of water in HOCbl•HCl ( $\cdot n\text{H}_2\text{O}$ ) (batch-dependent; typically 10-15%), was taken into account when calculating the amount of HOCbl•HCl used in the reactions, and was determined by converting HOCbl•HCl to dicyanocobalamin,  $(\text{CN})_2\text{Cbl}^-$  (0.10 M KCN, pH 10.0,  $\epsilon_{368} = 3.04 \times 10^4 \text{ M}^{-1} \text{ cm}^{-1}$  (Barker et al. 1960)). 2-(N,N-Diethylamino)-diazonolate 2-oxide (DEA-NONOate,  $\text{Na}^+$  salt, crystalline), N-nitrosodiethylamine (DEA-NO), diethylamine (DEA), sulfo-NONOate, TES buffer ( $\geq 99\%$ ), TAPS buffer ( $\geq 99.5\%$ ), CHES buffer ( $\geq 99\%$ ), CAPS buffer ( $\geq 99\%$ ), KCl ( $\geq 99\%$ ),  $\text{NaBH}_4$  (99%) and acetone were purchased from SIGMA; the former was handled according to manufacturer's recommendations. Angeli's salt and S-Nitroso-N-acetylpenicillamine (SNAP) were purchased from Cayman, Inc. Griess reagent was purchased from SIGMA. All chemicals were used without further purification. Water was purified using a Barnstead Nanopure Diamond water purification system and/or HPLC grade water was used.

All solutions used for the reactions were degassed by at least three freeze-pump-thaw cycles under argon using standard Schlenck techniques. Preparation of stock solutions and mixing of the reactants was carried out in a MBRAUN Labmaster 130 (1250/78) glove box operating under argon atmosphere. pH measurements were made in the glove box at room temperature with a Corning Model 445 pH meter equipped with a Mettler-Toledo Inlab 423 electrode. The electrode was filled with 3 M KCl/saturated AgCl solution, pH 7.0, and standardized with standard BDH buffer solutions at pH 4.01 and 6.98.

UV-visible spectra were recorded on a Cary 5000 spectrophotometer equipped with a thermostatted cell holder, operating with WinUV Bio software (version 3.00).  $^1\text{H}$  NMR spectra were recorded on a Varian Inova 500 MHz spectrometer equipped with a 5 mm thermostatted ( $22.0 \pm 0.5$  °C) probe. Solutions were prepared in  $\text{D}_2\text{O}$  and TSP (3-(trimethylsilyl)propionic-2,2,3,3- $\text{d}_4$  acid,  $\text{Na}^+$  salt) used as an internal reference. J. Young NMR tubes (Wilmad, 535-JY-7) were utilized and samples were allowed to equilibrate for 30 min before recording of spectra commenced.

**Synthesis of NOCbl.** A freshly prepared anaerobic solution of DEA-NONOate ( $\text{Na}^+$  salt, 25.1 mg, 2.5 equiv.) in NaOH (10 mM) was added quickly to an anaerobic solution of  $\text{HOcbl}\cdot\text{HCl}$  (100.6 mg) dissolved in TES buffer (0.10 M, 1 mL, pH 7.4). The resultant pH was 8.9. The product solution was shaken gently to ensure complete mixing and the reaction left to proceed at room temperature for 3 h. Formation of the desired product was checked by UV-vis spectroscopy. The product was precipitated by drop-wise addition to cold acetone (20 mL,  $-20$  °C), filtered and dried under vacuum ( $2 \times 10^{-2}$  mbar) overnight at 25 °C. Both the synthesis and handling of the final product were carried out inside a glove box under an argon atmosphere. Yield (two independent syntheses): 85 and 84%. The purity assessed by  $^1\text{H}$  NMR spectroscopy was  $98 \pm 2$  %. The percentage of non-cobalamin impurities in the product was determined by converting NOCbl to  $(\text{CN})_2\text{Cbl}^-$  (0.10 M KCN, pH 10.0,  $\epsilon_{368} = 3.04 \times 10^4 \text{ M}^{-1} \text{ cm}^{-1}$  (Barker et al. 1960)), and found to be  $5 \pm 3\%$ . Extinction coefficients were also determined for NOCbl (in  $\text{H}_2\text{O}$ , final pH 8.9;  $\epsilon_{259} = 19.9 \text{ mM}^{-1} \text{ cm}^{-1}$ ,  $\epsilon_{314} = 14.4 \text{ mM}^{-1} \text{ cm}^{-1}$  and  $\epsilon_{478} = 6.91 \text{ mM}^{-1} \text{ cm}^{-1}$ ). The solid product is stable for at least 2 months in a

desiccator, but decomposes if stored in the presence of atmospheric moisture. Exposure of 3 mL of a 50  $\mu$ M solution of NOCbI to air resulted in a rapid conversion of NOCbI to NO<sub>2</sub>CbI. UV-visible spectroscopy showed that complete decomposition of NOCbI occurs in less than 5 min.

**Synthesis of NO<sub>2</sub>CbI.** Nitrocobalamin was synthesized by drop-wise addition of a solution of NaNO<sub>2</sub> (61.1 mM, 100  $\mu$ L, 61.1  $\mu$ mol, 1.2 mol equiv.) to a solution of HOCbI·HCl (80.0 mg, 50.9  $\mu$ mol) in MES buffer (pH 6.0, 0.90 ml), and the mixture left to react at 0 °C (ice bath) for 2 h. The product precipitated upon dripping into acetone (5 ml), and was washed with acetone (20ml) and dried overnight under vacuum at 60 °C. Yield: 151 mg (92%). The purity assessed by conversion to dicyanocobalamin (Barker et al. 1960) was 99  $\pm$  2%. <sup>1</sup>H NMR (D<sub>2</sub>O,  $\delta$ , ppm) 6.20 (s C10), 6.28 (d R1), 6.42 (s B4), 6.74 (s B2), 7.20 (s B7). The cobalamin purity assessed by <sup>1</sup>H NMR spectroscopy was 98%. ES-MS analysis, m/z: 1375.7 (calcd for [NO<sub>2</sub>CbI + H]<sup>+</sup>, C<sub>62</sub>H<sub>90</sub>CoN<sub>14</sub>O<sub>16</sub>P = 1376.6); 1398.6 (calcd for [NO<sub>2</sub>CbI + Na]<sup>+</sup>, C<sub>62</sub>H<sub>89</sub>CoN<sub>14</sub>NaO<sub>16</sub>P = 1398.6); 689.0 (calcd for [NO<sub>2</sub>CbI + 2 H]<sup>2+</sup>, C<sub>62</sub>H<sub>91</sub>CoN<sub>14</sub>O<sub>16</sub>P = 688.8); 699.9 (calcd for [NO<sub>2</sub>CbI + Na + H]<sup>2+</sup>, C<sub>62</sub>H<sub>90</sub>CoN<sub>14</sub>NaO<sub>16</sub>P = 699.8).

**X-ray Diffraction Studies.** HOCbI·HCl (100 mg) was reacted with DEA-NONOate (Na<sup>+</sup> salt, 32 mg) in TES buffer (1.00 mL, 0.10 M, pH 7.4) in a 10 mL glass vial under anaerobic conditions. The NOCbI product was precipitated by drop-wise addition to cold (-20 °C) anaerobic acetone, and anaerobic acetone added to the remaining product in the vial.

Small orange crystals of NOCbl grew after 2 days in the vial. The crystals were stored in an argon atmosphere at room temperature until data collection.

A crystal of NOCbl (~0.1 x 0.1 x 0.3 mm) was mounted under paraffin oil in a nylon loop and flash frozen in liquid nitrogen. Diffraction experiments were carried out on beamline BL9-2 at the Stanford Synchrotron Radiation Laboratory (SSRL). Data were collected on a MarMosaic 325 CCD detector using X-rays produced by a 16 pole wiggler insertion device, with a wavelength of 0.8265 Å (15000 eV) from a liquid nitrogen cooled double Si(111) crystal monochromator. A data set was collected consisting of 120 1° images with a crystal to detector distance of 95 mm and an exposure time of 15 s. The data were processed with the program XDS (Kabsch 1993) and scaled together with the program XSCALE (Kabsch 1993). Bijvoet pairs were not merged and no absorption correction was applied. A total of 39700 reflections were measured to a nominal resolution of 0.74 Å, resulting in a final unique dataset of 17159 reflections with a merging R-factor of 0.035.

The structure was solved by Patterson methods to locate the cobalt, phosphorus and sulfur atoms, then the lighter atoms located by difference Fourier synthesis, as implemented in the program SHELXS (Sheldrick and Schneider 1997). The structure was refined by full matrix least-squares methods using the program SHELXL (Sheldrick and Schneider 1997) using data from 100 to 0.8 Å resolution (15872 unique reflections, 94.6% of the expected number of reflections in this range). All non-hydrogen atoms were refined with anisotropic thermal parameters and hydrogen atoms were added in idealized positions and refined in riding positions. A correction for the anomalous scattering from cobalt at 15000 eV was applied during refinement. Additional difference electron density peaks were modeled as water molecules with site occupancies of 1.0. The oxygen atom of the NO ligand was

observed in three distinct positions, and the site occupancies of these atoms were refined. The final crystallographic R factor, R1 was 0.0964 for 13916 reflections with  $F_o > 4\sigma_F$ . Additional data collection and refinement statistics are given in Table 1.

**Measurement of the Co(III) absorption spectrum.** The Co(III) absorption edge for NOCbl was measured on SSRL beamline BL9-2 from the same frozen crystal used for X-ray diffraction data collection (“irradiated NOCbl”). The spectrum was collected in fluorescence mode between 7500 and 7900 eV using a Canberra/Eurisys Si drift detector with a total acquisition time of 440 s. The spectrum was normalized by dividing the sample fluorescence at each point by the sample fluorescence at the inflection point of the first EXAFS peak (7773 eV). The first derivative of the spectrum was calculated using the program AUTOCHOCH (Evans and Pettifer 2001) which is based on the Kramers-Kronig transformation algorithm. The inflection point is taken as the minimum of this transform and is measured in electrons. A similar absorption spectrum was collected from a second freshly mounted crystal which had never been exposed to X-rays (“unirradiated NOCbl”) and treated in an identical manner as the irradiated sample.

### **Kinetic measurements.**

**(a) UV-visible spectroscopy.** All solutions were made up in 0.100 M buffer unless specifically stated otherwise and at total ionic strength of 1.00 M KCl. All the experiments were performed under pseudo-first-order conditions, i.e., at least 10-fold excess of diazeniumdiolate. An excellent fit to a single first-order rate equation was found for all kinetic data for at least 5 half-lives (Microcal Origin, v7.0).

**(b) NMR spectroscopy.** Samples for  $^1\text{H}$  NMR spectroscopy were prepared inside a glove-box operating under argon atmosphere, and transferred to gastight (J Young) NMR tubes. Spectra were recorded on a Bruker Avance 400 MHz spectrometer, at 25 °C. TSP was used as the internal reference. To minimize the delay between mixing of the reactants and data collection in the case of fast reactions, the NMR instrument was tuned using a standard solution of HOCl (reactant) made up in the reaction buffer, before mixing of the reactants of the actual reaction to be studied.

**Preparation of DEA-NONOate, DEA-NO, DEA, sulfo-NONOate and Angeli's salt solutions.** Solutions of these reactants were prepared freshly before measurements by dissolving a weighted amount of the solid (or pipetting the appropriate amount of liquid in the case of DEA) in alkaline buffer, and were protected from exposure to ambient light before and during the experiments. Decomposition of diazeniumdiolates is catalyzed by acids, thus all the reactions were carried out in alkaline buffer. When lower pH conditions were required (for example pH 7.40), a stock solution (10X-50X) of the diazeniumdiolate was prepared in 1.0 mM NaOH, and the reaction was started by mixing an aliquot of the diazeniumdiolate stock solution with the cobalamin previously dissolved in the corresponding buffer.

**Preparation of SNAP solutions.** Decomposition of SNAP is faster at alkaline pH, therefore, 10-50X stock solutions were prepared in 1.0 mM HCl, and the reactions started as described for the diazeniumdiolates.

**Preparation of Cbl(II) solutions.** Reduced cobalamin was prepared via chemical reduction of aquacobalamin with 1.2 equiv. of sodium borohydride. Removal of unreacted sodium borohydride after total conversion of aquacobalamin to Cbl(II) (assessed by UV-visible spectroscopy) was accomplished by addition of 1.2 equiv. acetone.

**Stoichiometry of the reaction.** Reaction of HOCbl with 0.55, 1.1 and 2.2 equivalents of DEA-NONOate was carried out under strictly alkaline conditions (0.100 M CAPS, pH 10.8), where the spontaneous decomposition of DEA-NONOate is negligible. Extent of reaction progress was determined by  $^1\text{H-NMR}$ , by integration of the signals corresponding to the starting material (HOCbl) with respect to those of the product (NOCbl).

**Identification of the reaction products.** Characterization of the reaction products was performed in 0.100 M  $\text{Na}_2\text{CO}_3$  buffer, pD 10.9 ( $\text{pK}_a = 10.5$ ) using 1.2 equivalents of DEA-NONOate (minimal amount of diazeniumdiolate that we found necessary for the reaction to proceed completely to the formation of NOCbl). Cobalamin reaction products were analyzed by both UV-vis and  $^1\text{H-NMR}$  spectroscopy, by comparison with spectroscopic data available from the literature (Suarez-Moreira et al. 2006; Wolak et al. 2001; Zheng and Birke 2001).

DEA-NONOate decomposition products were analyzed by  $^1\text{H-NMR}$ , by comparison with the corresponding spectra of pure commercial standards. The chemical shifts of the possible/expected DEA-NONOate reaction products, DEA-NO and DEA, were determined in the same buffer used for the reaction (0.100 M  $\text{Na}_2\text{CO}_3$ , pD10.9;  $\text{pK}_a = 10.5$ ). Chemical shifts,  $\delta$ , in ppm: DEA-NONOate: 2.971, 2.953, 2.935, 2.917, 0.981, 0.963, 0.945; DEA-NO:

4.198, 4.180, 4.162, 4.144, 1.144, 1.126, 1.108 and 3.741, 3.723, 3.704, 3.686, 1.422, 1.404, 1.386; and DEA: 3.108, 3.090, 3.072, 3.052, 1.301, 1.283, 1.265. As a possible reaction product, formation of nitrite was also investigated and determined using the Griess reagent (Green et al. 1982; Griess 1879).

**Reaction of NOCbl with NO gas.** NOCbl was prepared from the reaction of Cbl(II) with NO gas under strictly anaerobic conditions. Cbl(II) was generated by photolysis of MeCbl. Commercially available NO was passed through two anaerobic traps containing freshly prepared 1.0 N NaOH to remove potential oxidation products, before it reached the reaction cuvette (a picture of the experimental set-up is given in **Figure 2.14**). Formation of NO<sub>2</sub>Cbl was monitored by UV-visible spectroscopy at 15 s, 15, 30, 60, 90 and 120 min after addition of NO. Note: prior to the measurements, the NO gas was replaced by argon (since argon is heavier than NO) to prevent oxidation due to potential leakage of ambient oxygen into the reaction mixture.

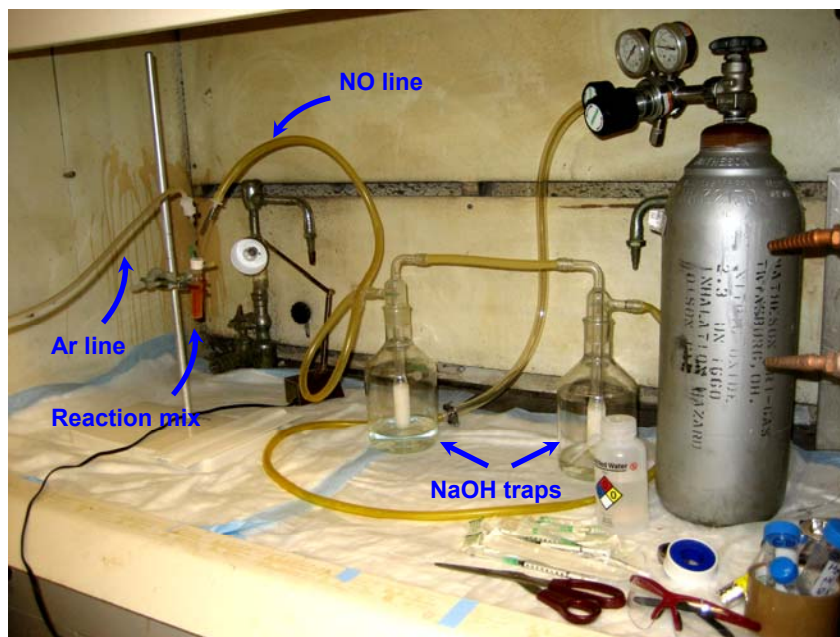


**Figure 2.14.** Experimental set up for the reaction between NOCl with NO gas.

## **2.2 Project 2: Synthesis and characterization of imidazolylcobalamin (ImCbl) and histidinylcobalamin (HisCbl).**

### **INTRODUCTION**

The X-ray crystal structure of both bovine and human TC has been recently reported by Wuerges et al (Wuerges et al. 2006). Bovine and human apoTC were reconstituted with  $\text{H}_2\text{OCbl}^+$  and the analysis of the corresponding crystal structures revealed that the  $\text{H}_2\text{O}$  at the  $\beta$ -axial position of the Cbl is replaced by a nitrogen of the benzimidazole moiety of a His residue from the protein (Wuerges et al. 2006). Replacement of  $\text{H}_2\text{O}$  by a histidinyl residue has also been observed in mutases and methionine synthase, at their  $\alpha$ -axial position. Unfortunately, due to restraints applied during the protein refinement, relevant bond distances within the Cbl structure were only roughly estimated. For instance, the Co-N3B bond distance was confined to 2.15 Å due to the presence of mixed oxidation states of the Co center (Co(III)/Co(II)), probably due to reduction caused by extensive irradiation during X-ray data collection. **Project 2** describes the synthesis and crystallization of HisCbl as a model for Cbl bound to TC to be able to: 1) obtain more accurate structural parameters and 2) compare the structural parameters of free *versus* TC bound HisCbl. This work has been published (Hannibal, Bunge et al. 2007).

## RESULTS AND DISCUSSION

### A. Synthesis and characterization of ImCbl and HisCbl.

ImCbl and HisCbl were synthesized in high yield and purity from the reaction between hydroxycobalamin and imidazole or histidine respectively as the starting materials, at neutral pH (0.10 M TES, pH 7.4) (Hannibal, Bunge et al. 2007). The products were analyzed by UV-visible spectroscopy (**Figure 2.15**),  $^1\text{H}$  NMR spectroscopy (**Figure 2.16** panels **A** and **B**, and **Table 2.4**), 2D-NMR spectroscopy (**Table 2.4**), ES/MS, and X-ray crystallography (Hannibal, Bunge et al. 2007).

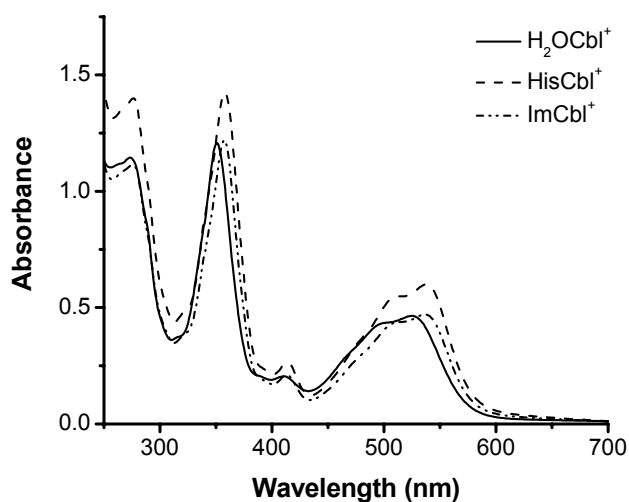


**Figure 2.15.** UV-visible spectra of the starting material ( $\text{H}_2\text{OCbl}^+$ ) and the two cobalamin derivatives, ImCbl and HisCbl. Absorption maxima occurs at: 357, 413, and 536 nm for ImCbl; and 358, 414, and 538 nm for HisCbl (Hannibal, Bunge et al. 2007). These values are in agreement with literature values (Marques et al. 1990).

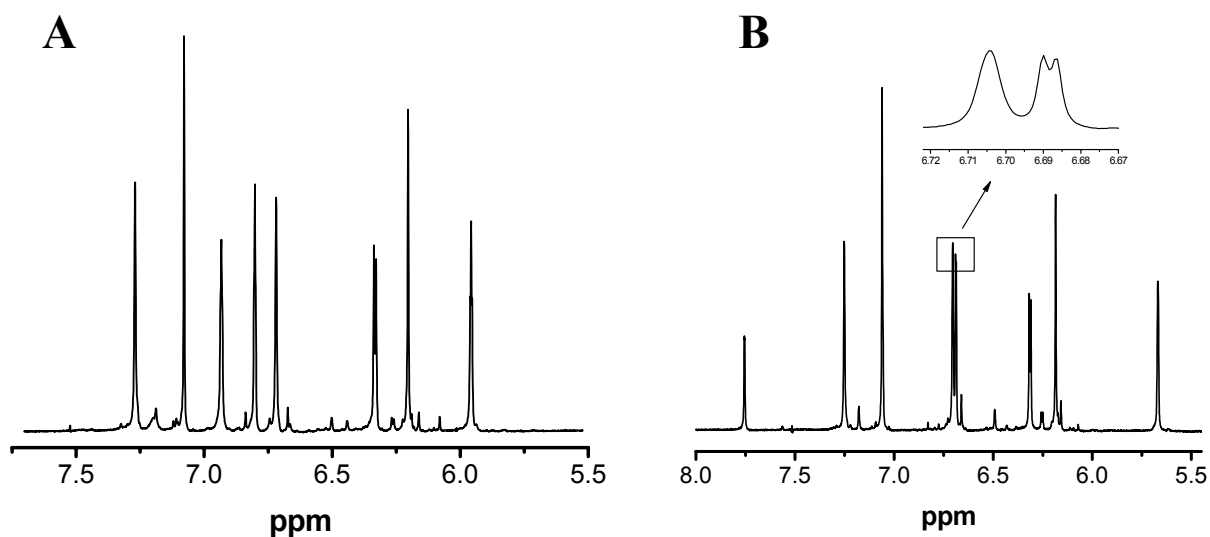


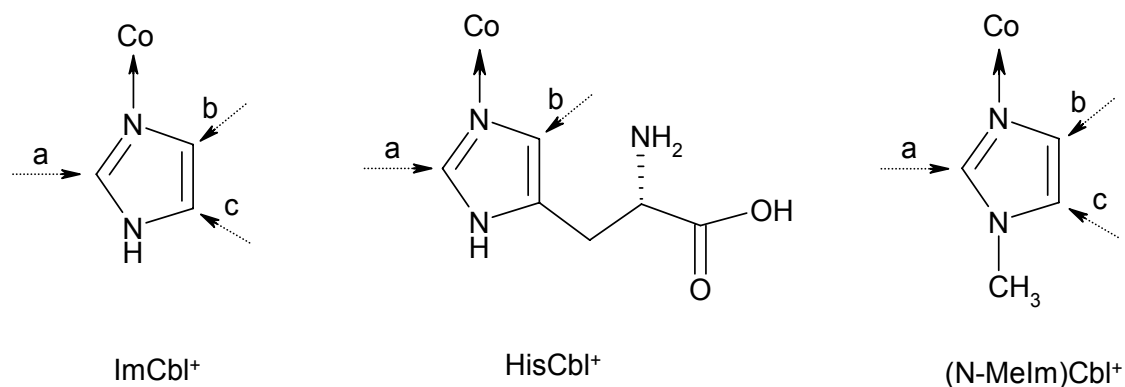
**Figure 2.16.** **A.**  $^1\text{H}$  NMR spectrum of ImCbl in TAPS buffer (0.10 M, pD 8.80). Chemical shifts are  $\delta$  (ppm): 7.27, 7.08, 6.93, 6.80, 6.72, d(3.37,6.33), 6.20 and 5.95. **B.**  $^1\text{H}$  NMR spectrum of HisCbl in TAPS buffer (0.10 M, pD 8.80). Chemical shifts are  $\delta$  (ppm): 7.76, 7.25, 7.06, 6.70, 6.69, d(6.32,6.31), 6.19, and 5.67 (Hannibal, Bunge et al. 2007). Chemical shifts of free histidine: 7.76 and 7.06 ppm.

**Table 2.4** and **Scheme 2.5** show a summary of  $^1\text{H}$  NMR and 2D-NMR spectroscopic assignments for ImCbl, HisCbl (present study) (Hannibal, Bunge et al. 2007) and (N-MeIm)Cbl $^+$  previously published by Cregan et al (Cregan, Brasch, and van Eldik 2001).  $^1\text{H}$  NMR chemical shifts and assignments for signals observed in the aromatic region are given in **Table 2.4**, and are similar to those previously observed for N-MeImCbl $^+$  (Cregan, Brasch, and van Eldik 2001). Signal assignments were possible with the additional information provided by HSQC, HMBC and HMQC –TOCSY experiments.

**Table 2.4.**  $^1\text{H}$  NMR spectroscopy assignments of the protons in the aromatic region for ImCbl, HisCbl and (N-MeIm)Cbl $^+$ . See **Scheme 2.5** for the labeling (a,b,c) of the  $\beta$ -axial ligand (Hannibal, Bunge et al. 2007).

ImCbl $^+$ <sup>a</sup>		HisCbl $^+$ <sup>a</sup>		(N-MeIm)Cbl $^+$ (Cregan, Brasch, and van Eldik 2001), <sup>b</sup>	
Signal (ppm)	Assignment	Signal(ppm)	Assignment	Signal (ppm)	Assignment
5.95	b	5.67	B	5.85	b
6.20	C10	6.19	C10	6.14	C10
6.35(d)	R1	6.32 (d)	R1	6.30 (d)	R1
6.80	a/c	6.69	a or B4	6.43	a
6.72	B4	6.70	a or B4	6.68	B4
6.93	a/c	-	-	6.85	c
7.08	B2	7.06	B2	7.06	B2
7.27	B7	7.25	B7	7.23	B7

<sup>a</sup> pD = 8.80. <sup>b</sup> pD = 8.51.



**Scheme 2.5.** Labeling scheme for the  $\beta$ -axial ligand of ImCbl $^+$ , HisCbl $^+$  and N-MeImCbl $^+$  (Hannibal, Bunge et al. 2007).

## B. X-ray analysis of **ImCbl** and **HisCbl**.

The three dimensional structures of **ImCbl** and **HisCbl** were determined by X-ray crystallography. Crystal data and structural refinement parameters are given in **Table 2.5**. **ImCbl** and **HisCbl** crystallize in the orthorhombic space group  $P2_12_12_1$ , the most common space group observed for cobalamin structures (Gruber et al. 1998; Randaccio et al. 1999). Cobalamin structures have previously been classified into three to four packing types, based on the unit cell ratios  $b/a$  and  $c/a$  (Gruber et al. 1998; Randaccio et al. 1999). Both **ImCbl** and **HisCbl** fall into the range of cluster type II (for **ImCbl**  $b/a$  and  $c/a$  = 1.419 and 1.627, respectively; for **HisCbl**  $b/a$  and  $c/a$  = 1.428 and 1.619, respectively).

Both structures show the Cbl complex in its standard base-on form with imidazole and histidine as the  $\beta$ -axial ligand (**Figure 2.17, panels A and B**). The distances between cobalt and the imino N of the  $\beta$ -ligands are 1.94(1) Å (in **ImCbl**) and 1.951(7) Å (to N $\epsilon$ 2 in **HisCbl**). The Co-N bond distances to the lower  $\alpha$ -5,6-dimethylbenzimidazole (DMB) ligand are 2.01(1) Å and 1.979(8) Å, respectively. Since the  $\alpha$ -DMB is a weaker nucleophile (Fasching et al. 2000) in addition to being more sterically demanding, it is not surprising that the Co-N(Im) and Co-N(His) bond distances are shorter than the Co-N(DMB) in both structures. The Co-N(DMB) bond length of cobalamins can vary from 1.95 to 2.27 Å depending on the  $\sigma$  donor strength of the ligand *trans* to the Co-N(DMB); values of 2.01 and 1.98 Å fall within the range expected for weak  $\sigma$  donor ligands such as imidazole and histidine (Randaccio et al. 1999).

In both structures, the cobalt atom lies in the least squares plane through the four corrin nitrogen atoms (max. deviation 0.01 Å in **HisCbl**). The fold angles of the corrin rings

are very similar in the two structures and were measured as 11.8(3)° and 12.0(3)° for **ImCbl** and **HisCbl**, respectively.

**Table 2.5. Crystallographic data for ImCbl and HisCbl (Hannibal, Bunge et al. 2007).**

	<b>ImCbl</b>	<b>HisCbl</b>
Empirical formula	C <sub>65</sub> H <sub>91</sub> N <sub>15</sub> O <sub>14</sub> PCo•22 H <sub>2</sub> O	C <sub>68</sub> H <sub>96</sub> N <sub>16</sub> O <sub>16</sub> PCo•20 H <sub>2</sub> O•0.5 HCl
H <sub>2</sub> O sites	22	27
Formula weight	1792.8	1862.1
Crystal system	orthorhombic	orthorhombic
space group	P2 <sub>1</sub> 2 <sub>1</sub> 2 <sub>1</sub>	P2 <sub>1</sub> 2 <sub>1</sub> 2 <sub>1</sub>
Unit cell dimensions:		
a [Å]	15.834(10)	15.697(1)
b [Å]	22.469(10)	22.422(1)
c [Å]	25.766(10)	25.417(1)
V [Å <sup>3</sup> ]	9167(8)	8946(1)
Z	4	4
D <sub>calc</sub> [g cm <sup>-3</sup> ]	1.299	1.383
μ [mm <sup>-1</sup> ]	0.293	0.318
F(000)	3840	3980
Crystal size [mm]	0.3 x 0.1 x 0.1	0.35 x 0.20 x 0.15
θ-range for data collection [°]	2.83-22.51	1.21-18.80
Temperature [K]	298	103
Wavelength [Å]	0.71073	0.71073
# of unique reflections	5976	6966
# of reflections with I>2σ <sub>I</sub>	3952	6050
R(int)	0.089	0.079
Data/restraints/ parameters	5976/1787/1076	6966/2611/1249
Final R indices:		
R1 (I>2σ <sub>I</sub> , all data)	0.0811 (0.1420)	0.0734 (0.0869)
wR2 (I>2σ <sub>I</sub> , all data)	0.1862 (0.2424)	0.1885 (0.2023)
Largest diff. peak/hole (e Å <sup>-3</sup> )	0.61/-0.48	0.56/-0.45

The fold angles are smaller than those typically observed for cobalamin structures with relatively short Co-N(DMB) bond distances (Gruber et al. 1998). The imidazole rings of **ImCbl** and **HisCbl** are oriented along the line connecting atoms C5 and C15 of the corrin ring, bisecting the angles between N21 and N22 as well as between N23 and N24. Both imidazole rings in each cobalamin structure are aligned with the lower  $\alpha$ -5,6-dimethylbenzimidazole ligand.

In principle, the  $\beta$ -ligand in **ImCbl** can either be a neutral imidazole or an anionic imidazolate. The compound itself was crystallized at neutral pH. Since the  $pK_a$  of cobalamin bound imidazole is  $\sim 10$  (Eilbeck and West 1976; Hamza and Pratt 1994; Hanania and Irvine 1964; Marques et al. 1990), only a very minor fraction is present as imidazolate in solution under these conditions. The current version of the Cambridge Structural Database (v5.27, November 2005) holds 46 entries with the term 'cobalamin' in the compound name. In most of these entries, the cobalamin complexes are overall neutral in charge. There are only five examples of non-neutral cobalamins in the database: ammonium sulfitocobalamin (refcodes: DEMSIX and NOJKIG) (Randaccio et al. 1999; Randaccio et al. 2002), sodium thiosulfatocobalamin (EJADIC), (Perry et al. 2003) thioureacobalamin chloride (DEMTUK) (Randaccio et al. 1999; Randaccio et al. 2002), thioureacobalamin hexafluorophosphate (NOJNOP) (Randaccio et al. 1999; Randaccio et al. 2002), and aquocobalamin perchlorate (SUNYEF) (Kratky et al. 1995). In the present crystal structure of **ImCbl**, there is no indication of a counter anion, which would be expected to be  $Cl^-$  or  $ClO_4^-$  (see method of synthesis). Of course, the occurrence of hydroxide at one of the modeled water sites cannot

be ruled out, but it is also conceivable that the minor fraction of imidazolotocobalamin present in solution preferentially crystallized.

In **HisCbl** the histidine ligand is clearly disordered over two approximately equally occupied (0.54 vs. 0.46) alternate conformations related by a 180° rotation around the Co-N bond. With respect to the protonation state of the  $\beta$ -ligand, it is assumed that the amino group is protonated and the carboxyl group is deprotonated. Difference electron density close to the carboxylate of one of the alternate histidine conformers was modeled as a chloride ion with ~50% occupancy indicating the presence of a mixture of histidine ligands with neutral and anionic imidazole moieties.

For **ImCbl** the Co-bound imidazole does not form any direct interactions with symmetry equivalent Cbl molecules. Two weak hydrogen bonds exist between N3 (of the major component) and two water molecules with heavy atom distances of 3.3 Å and 3.5 Å. In **HisCbl**, most of the interactions of the  $\beta$ -ligand are formed with water molecules. Only one hydrogen bond exists between one of the carboxylate oxygen atoms and the amide nitrogen of side chain d of a symmetry equivalent B<sub>12</sub> molecule.

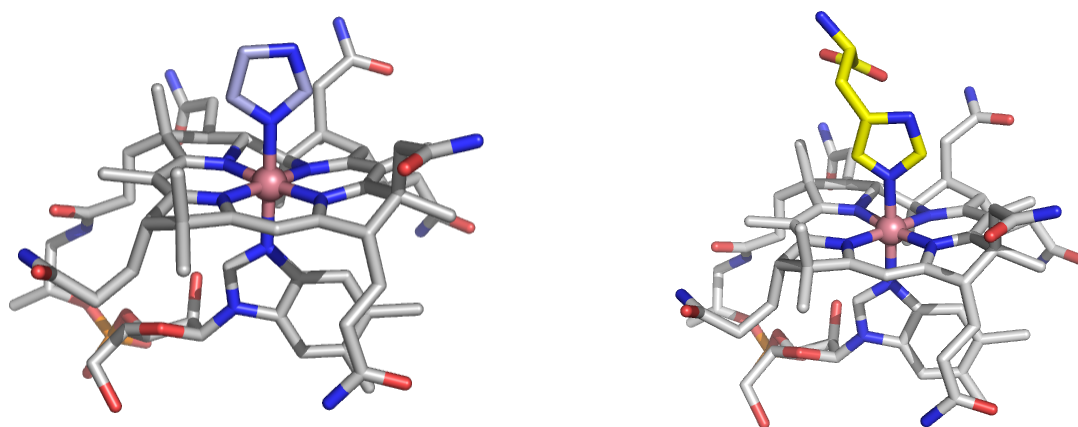


**Figure 2.17. A.** Molecular structure of **ImCbl** and **HisCbl** in a sticks-representation. The central cobalt atom is depicted as a pink sphere. N-, O- and P-atoms are drawn in blue, red and orange respectively. C-atoms are drawn in grey in the Cbl-trunk and in light blue in the  $\beta$ -ligand. **B.** Molecular structure of **HisCbl**. The central cobalt atom is depicted as a pink sphere. N-, O- and P-atoms are drawn in blue, red and orange respectively. C-atoms are drawn in grey in the  $B_{12}$ -trunk and in yellow or orange in the  $\beta$ -ligand. H-atoms have been omitted for clarity. The figure was prepared using the program PyMol (<http://www.pymol.org/>) (Hannibal, Bunge et al. 2007).

**Figure 2.18** shows the superposition of our HisCbl and its TC-bound counterpart obtained from the protein database (PDB-entry: 2BB6). Substantial differences were observed in the bond distances of the upper and lower axial ligands. Both bonds appeared to be longer in the TC-bound form compared to the free HisCbl complex. This could be explained by: a) limitations associated to restraints applied to the Cbl structure during data refinement of the protein bound Cbl, or b) as an actual structural change induced by the protein upon binding to Cbl.

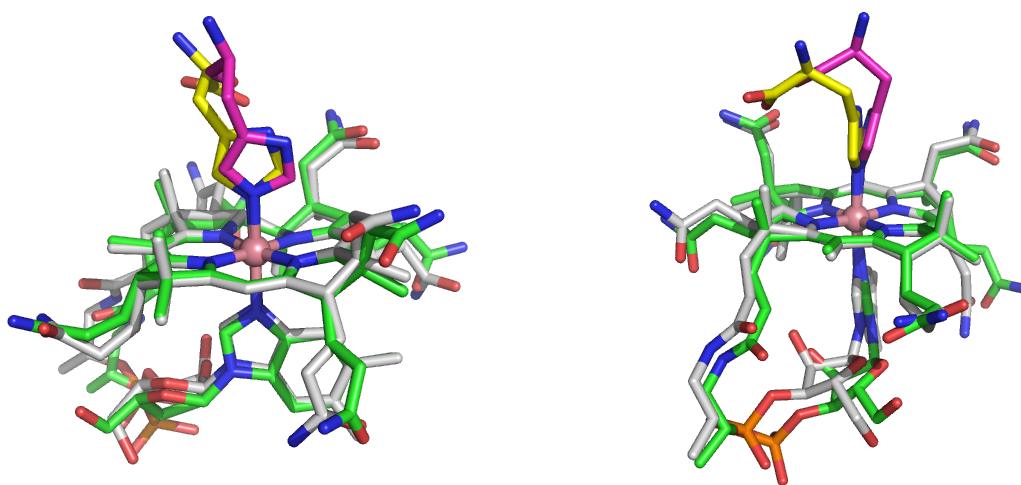


**Figure 2.18.** Two approximately perpendicular views of the superposition of one conformer of HisCbl with one of the Cbl-moieties present in the monoclinic structure of bovine transcobalamin (PDB-entry: 2BB6). The Cbl-trunks are shown in white (HisCbl) and green (TC) respectively. The histidine residues are shown in yellow and magenta (His-175 in TC) (Hannibal, Bunge et al. 2007).

## SUMMARY

The crystal structures and syntheses of imidazolylcobalamin and histidinylcobalamin are presented. The axial Co-N bond distances of HisCbl are significantly shorter than the restrained values reported for the crystal structures of bovine recombinant HisCbl-bound TC,

and the corrin fold angle is slightly smaller (by  $2^\circ$ ) in TC-bound HisCbl compared with the free cofactor.

## MATERIALS AND METHODS

**General procedures and chemicals.** Hydroxycobalamin hydrochloride (HOCbl•HCl; stated purity by manufacturer is  $\geq 96\%$ ; aromatic region of the  $^1\text{H}$  NMR shows it contains at least  $\sim 6\%$  impurities (Brasch and Finke 1999)) was purchased from Fluka BioChemica. Imidazole (99%) and L-histidine (98%) were purchased from ACROS Organics. All chemicals were used without further purification. Water was purified using a Barnstead Nanopure Diamond water purification system and/or HPLC grade water was used.

UV-visible spectra were recorded on a Cary 5000 spectrophotometer equipped with a thermostatted cell holder, operating with WinUV Bio software (version 3.00).  $^1\text{H}$  NMR spectra were recorded on a Varian Inova 500 MHz spectrometer equipped with a 5 mm thermostatted ( $22.0 \pm 0.5$  °C) probe. Solutions were prepared in  $\text{D}_2\text{O}$  and TSP (3-(trimethylsilyl)propionic-2,2,3,3- $\text{d}_4$  acid,  $\text{Na}^+$  salt) used as an internal reference.

pH measurements were made at room temperature with a Corning Model 445 pH meter equipped with a Mettler-Toledo Inlab 423 electrode. The electrode was filled with 3 M KCl/saturated AgCl solution, pH 7.0, and standardized with standard BDH buffer solutions at pH 4.00 and 7.00.

**Synthesis of imidazolylcobalamin (ImCbl).** Imidazole (5.7 mg, 1.2 equiv.) was added to HOCbl•HCl (100 mg) dissolved in TES buffer (1.0 mL, 0.10 M, pH 7.4) and the

mixture reacted for 2 h at room temperature. The product was precipitated by addition of cold (-20 °C) acetone, vacuum filtered and dried overnight under vacuum at 60 °C. <sup>1</sup>H NMR (D<sub>2</sub>O, δ, ppm): 5.95, 6.20, 6.35, 6.80, 6.72, 6.93, 7.08 and 7.27; ~96% purity. (Brasch and Finke 1999) The percentage of non-cobalamin impurities determined by converting the products to dicyanocobalamin, (CN)<sub>2</sub>Cbl<sup>-</sup> (0.10 M KCN, pH 10.0, ε<sub>368</sub> = 3.04 × 10<sup>4</sup> M<sup>-1</sup>cm<sup>-1</sup>), (Barker et al. 1960) was 5 ± 1 %. ES/MS, m/z: 1396.1 (calcd [ImCbl]<sup>+</sup>, C<sub>65</sub>H<sub>92</sub>N<sub>15</sub>O<sub>14</sub>PCo = 1396.6); 698.6 (calcd [ImCbl + H]<sup>2+</sup>, C<sub>65</sub>H<sub>93</sub>N<sub>15</sub>O<sub>14</sub>PCo = 698.3).

**Synthesis of histidinylcobalamin (HisCbl).** The procedure was identical to that for imidazolylcobalamin, except that 1.5 equiv. L-His was used. <sup>1</sup>H NMR (D<sub>2</sub>O, δ, ppm): 5.67, 6.19, 6.32 (d), 6.69, 6.70, 7.06 and 7.25; ~95% purity. The percentage of non-cobalamin impurities determined by converting the products to (CN)<sub>2</sub>Cbl<sup>-</sup> was 4 ± 2. ES/MS, m/z: 1484.3 (calcd [HisCbl]<sup>+</sup>, C<sub>68</sub>H<sub>96</sub>N<sub>16</sub>O<sub>16</sub>PCo = 1484.6); 1482.5 (calcd [HisCbl - 2H]<sup>-</sup>, C<sub>68</sub>H<sub>94</sub>N<sub>16</sub>O<sub>16</sub>PCo = 1482.6); 742.3 (calcd [HisCbl + H]<sup>2+</sup>, C<sub>68</sub>H<sub>97</sub>N<sub>15</sub>O<sub>14</sub>PCo = 742.3).

**X-Ray diffraction studies.** Crystals of **ImCbl** were grown from water. Briefly, HOcbl•HCl (8.85 mg) and imidazole (4.00 mg) were dissolved in water (0.50 mL), NaClO<sub>4</sub> (1.50 mg) added and the pH adjusted to ~7.5 using concentrated HClO<sub>4</sub>. The sample was kept at room temperature and crystals appeared after 24 h. A crystal specimen was mounted in a glass capillary and diffraction data were collected at room temperature on a modified Stoe 4-circle diffractometer using Mo-Kα radiation (λ = 0.71073 Å). Note: the crystallization of ImCbl was carried out by Dr. Nicola E. Brasch a few years ago, in the laboratory of Prof. Dr. Rudi van Eldik, and the corresponding X-ray analysis was incorporated into a single manuscript together with the structural analysis of HisCbl.

Crystals of **HisCbl** were grown by adding a solution of histidine (~100 mg/ml, pH=7.5) to an aqueous solution of HOCbl•HCl (100 mg/ml). Crystals appeared after about 32 h. X-ray diffraction data for **HisCbl** were measured at 100 K (Oxford 700 Series Cryostream) on a Bruker AXS platform single crystal X-ray diffractometer upgraded with an APEX II CCD detector. Graphite monochromatized Mo K $\alpha$  radiation was used. Crystals were mounted on a thin glass fiber from a pool of Fluorolube™ and placed under a stream of nitrogen.

Both structures were solved by direct methods to yield the Co-atoms plus most remaining atoms of the structure. Missing atoms (mostly in the solvent region) were located in subsequent electron-density maps. Full-matrix least-squares refinement on  $F^2$  was performed with the program SHELXL-97.(Sheldrick and Schneider 1997) No absorption correction was applied to the data. Scattering factors including real and imaginary dispersion corrections were taken from the ‘International Tables of Crystallography’. H-atom positions were calculated and refined as ‘riding’ on their respective non-H-atom. The isotropic adp for each H-atom was set to 1.5 times the equiv. isotropic adp of the adjacent non-H-atom. Crystallographic residuals at the close of the refinement are also given in **Table 2.5**.

In **ImCbl**, the B<sub>12</sub> complex was very well defined except for the hydroxymethyl group of the ribose in the nucleotide loop, which was found to be disordered over two alternate conformations. The solvent electron density was modeled with 22 fully occupied and anisotropically refined H<sub>2</sub>O molecules.

In **HisCbl**, the Co-bound histidine is disordered over two alternate conformations. Discrete disorder was also observed for the amide side chains A and E, as well as for the

ribose hydroxymethyl group. The solvent comprises 20 (partially occupied) water molecules distributed over 27 sites, and a half occupied chloride ion.

### **2.3 Project 3: Synthesis and characterization of the MeCbl analogues ethyl-, propyl-, butyl-, pentyl-, and hexyl-cobalamin.**

#### **INTRODUCTION**

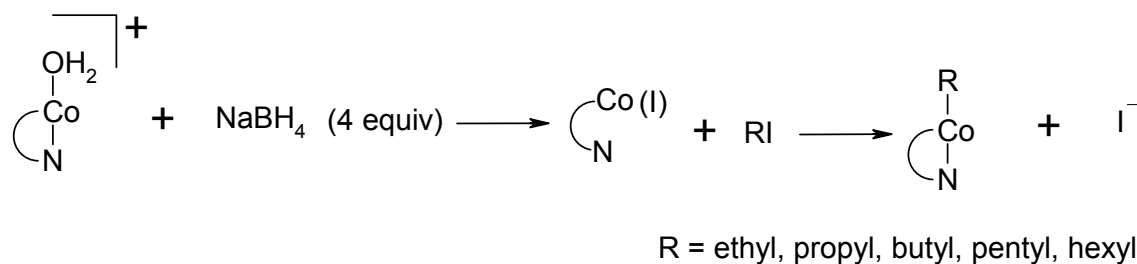
The ability of cells to convert CNCbl into MeCbl and AdoCbl depends on the MMACHC gene product. Recently, Kim et al. discovered that the *MMACHC* gene product catalyzes the reductive decyanation of CNCbl (Kim, Gherasim, and Banerjee 2008). Because the natural alkylcobalamins MeCbl and AdoCbl are the major cobalamin forms found in mammalian tissues, plasma and milk (Gimsing, Nexo, and Hippe 1983; Gimsing and Nexo 1983; Raaberg et al. 1989), we hypothesized that the MMACHC gene product would also catalyze the dealkylation of newly internalized (dietary) alkylcobalamins (see Chapter 3). *Project 3* describes the synthesis and characterization of a series of MeCbl analogs with increasing  $\beta$ -axial alkyl chain length, that will serve as substrates for dealkylation studies in cultured cells. The characterization of these MeCbl analogs includes: UV-vis and  $^1\text{H}$  NMR spectroscopies, ES/MS, HPLC, and X-ray crystallography. Part of this work has been published (Hannibal et al. 2009).

## RESULTS AND DISCUSSION

### A. Synthesis and characterization of alkylcobalamins

All alkylcobalamins were synthesized from the reaction of cob(I)alamin with the corresponding alkyl halide under anaerobic conditions and protected from exposure to light. A general scheme of the reaction (aliphatic nucleophilic substitution) is given in **Scheme 2.6**.

The reactions proceeded to completion rapidly (less than 5 min) in the presence of a 5 molar excess of the alkyl ligand. All alkylcobalamins were obtained in high purity (> 97%) as judged by  $^1\text{H}$  NMR spectroscopy analysis (Brasch and Finke 1999). Attempts to synthesize and isolate *iso*-propylcobalamin were unsuccessful. The instability of this derivative has been reported in the literature (Pratt 1972). Precipitation of the alkylcobalamins from acetone facilitated the removal of excess alkyl halide by dissolution and as a result, the percentage of non-cobalamin impurities in the dried cobalamin material was less than 3 % as determined by the dicyanocobalamin test (Barker et al. 1960). UV-visible and  $^1\text{H}$  NMR characterization data is presented in **Table 2.6**. A significant blue-shift in the UV-visible spectrum was observed for all alkylcobalamins compared to MeCbl. Similarly,  $^1\text{H}$  NMR chemical shifts in the aromatic region of the spectrum were also very similar amongst all alkylcobalamins, and differed from that of MeCbl. The chemical shift of the C10 hydrogen showed the greatest shift compared to MeCbl, probably as a result of the stronger electron donation provided by the longer alkyl ligands.



**Scheme 2.6.** Reaction of Cbl(I) with alkyl halides to form alkylcobalamins. The reactions were carried out under strictly anaerobic conditions (to prevent oxidation of Cbl(I)), in the dark (to prevent decomposition of the products).

The products were also characterized by mass spectrometry and X-ray synchrotron diffraction (the later for EtCbl and BuCbl only). The partial characterization of alkylcobalamins other than MeCbl has been previously reported by other laboratories and our UV-visible and  $^1\text{H}$  NMR spectroscopic data for EtCbl and BuCbl (**Table 2.6**) were in excellent agreement with the literature (Cole et al. 2002; Taylor et al. 1973; Pratt 1972; Smith et al. 1964). UV-vis and  $^1\text{H}$  NMR spectra were almost identical for the MeCbl analogs and differed significantly from that of MeCbl (**Table 2.6**). The  $\gamma$ -band of the UV-visible spectrum of corrinoids, which is the most intense band in the near ultraviolet region, reflects the amount of negative charge donated by the upper axial ligand to the cobalt via the  $\sigma$ -bond (Pratt 1972). This was observed for EtCbl and BuCbl when compared to MeCbl (**Table 2.6**). On the other hand, the  $^1\text{H}$  NMR resonance of the C10 hydrogen for EtCbl and BuCbl are considerably downfield compared with MeCbl (6.06 and 6.08 ppm respectively, versus 5.91 ppm for MeCbl). The effect of the upper axial ligands of the Cbl on the hydrogen atom on C10, the bridge carbon between rings B and C (**Figure 1.1**) has been previously studied (Pratt 1972).

**Table 2.6. UV visible and <sup>1</sup>H NMR spectroscopy data for alkylcobalamins (Hannibal et al. 2009).**

Cobalamin	UV-visible wavelength maxima (nm)	Chemical shifts (ppm)				
MeCbl	340, 377, 528 <sup>a</sup>	7.20	6.98	6.29	6.28	5.91
EtCbl	319, 349, 513	7.18	7.00	6.27	6.26	6.06
PrCbl	319, 349, 514	7.18	7.02	6.29	6.26	6.08
BuCbl	319, 349, 515	7.18	7.01	6.29	6.26	6.08
PeCbl	318, 346, 512	7.18	7.00	6.29	6.26	6.08
HxCbl	320, 346, 512	7.18	7.00	6.29	6.27	6.08

<sup>a</sup> Comprehensive B<sub>12</sub>. Z. Schneider; A. Stroinski, Walter de Gruyter, Berlin, New York, 1987. UV-visible measurements were performed in water, pH 6.80, at 25°C. <sup>1</sup>H NMR measurements were carried out in D<sub>2</sub>O, pD 7.5, at 25°C.

Examination of MeCbl, EtCbl, PrCbl and BuCbl showed that strong electron donating ligands in the β-axial position of hexacoordinated corrinoids induced a downfield shift in the magnetic resonance of the C10 hydrogen (Pratt 1972). Our results follow the same pattern (**Table 2.6**). Also, replacement of the C10 hydrogen by another substituent affects the electronic structure of the corrin macrocycle and influences the binding properties of the cobalt center (Brown et al. 1997; Knapton and Marques 2005; Marques et al. 2002). These findings indicate that the hydrogen atom in C10 is extremely sensitive to its electronic environment and *vice versa*. Thus, the chemical shifts of the hydrogen in C10 for EtCbl and BuCbl display the correlation expected for the stronger electron donating ability of the respective alkyl ligands compared to that of the methyl group in MeCbl (**Table 2.6**).

## B. X-RAY ANALYSIS OF EtCbl AND BuCbl.

Suitable crystals for X-ray analysis were obtained for EtCbl and BuCbl. The synthesis of propylcobalamin (PrCbl), pentylcobalamin (PnCbl) and hexylcobalamin (HxCbl) was also carried out, but attempts to obtain crystals of these derivatives were unsuccessful. Both EtCbl and BuCbl crystallized in the orthorhombic space group  $P2_12_12_1$  with cell parameters 16.00 Å x 21.02 Å x 24.54 Å, and 16.03 Å x 20.73 Å x 24.62 Å, respectively. A summary of the crystallographic data and refinement parameters is presented in **Table 2.7**. The crystal structure and the crystal packing of the cobalamin molecule in this space group has been described exhaustively in the literature and the current structures do not deviate markedly from the cobalamin structures known to date. The final crystallographic residuals of 0.0462 and 0.0492 for the two structures are amongst the lowest ever achieved for cobalamin structures, and this can be directly correlated with the quality of the diffraction data. The merging R-factors for the synchrotron data were extremely good (0.0281 and 0.0262 for the symmetry-related reflections) and the average signal to noise values ( $I/\sigma$ ) were 57.2 and 31.4 for EtCbl and BuCbl, respectively. Comparison of the two data sets indicates that although they both extend to approximately the same resolution (around 0.71 Å), the EtCbl data is almost twice as strong as the BuCbl data (as judged by the  $I/\sigma$  values quoted above). Despite the fact that the data resulted from two data sets merged together, the better signal to noise ratio clearly results in a more accurately-determined crystal structure.

The crystal packing of the cobalamin molecule in the  $P2_12_12_1$  space group is generally analyzed by comparison of the ratios of the  $c/a$  and  $b/a$  unit cell dimensions (Garau et al. 2003). The EtCbl ratios of  $c/a = 1.534$  and  $b/a = 1.314$ , and the BuCbl ratios of  $c/a =$

1.536 and  $b/a = 1.293$  indicate that these crystals are typical of cluster I packing (Garau et al. 2003).

**Table 2.7. Refinement parameters for EtCbl and BuCbl (Hannibal et al. 2009).**

	EtCbl	BuCbl
Empirical formula	C <sub>64</sub> H <sub>91</sub> N <sub>13</sub> O <sub>31</sub> CoP	C <sub>66</sub> H <sub>93</sub> N <sub>13</sub> O <sub>29</sub> CoP
H <sub>2</sub> O sites	17	20
Formula weight	1628.40	1622.44
Crystal system	orthorhombic	orthorhombic
space group	P2 <sub>1</sub> 2 <sub>1</sub> 2 <sub>1</sub>	P2 <sub>1</sub> 2 <sub>1</sub> 2 <sub>1</sub>
Unit cell dimensions:		
<i>a</i> [Å]	16.00	16.03
<i>b</i> [Å]	21.02	20.73
<i>c</i> [Å]	24.54	24.62
<i>V</i> [Å <sup>3</sup> ]	8253.29	8181.27
<i>Z</i>	4	4
<i>D</i> <sub>calc</sub> [g cm <sup>-3</sup> ]	1.106	1.139
$\mu$ [mm <sup>-1</sup> ]	0.29	0.29
<i>F</i> (000)	2924	2988
Crystal size [mm]	0.6 x 0.1 x 0.1	0.7 x 0.1 x 0.1
$\theta$ -range for data collection [°]	67.1	67.0
Temperature [K]	100	100
Wavelength [Å]	0.78468	0.78468
# of unique reflections	18317	20451
# of reflections with $I > 4\sigma_I$	18291	20273
<i>R</i> (int)	0.0281	0.0262
Data/restraints/parameters	18317 / 0 / 1037	20451 / 0 / 1131
GOF on <i>F</i> <sup>2</sup>		
Final <i>R</i> indices:		
<i>R</i> <sub>1</sub> ( $I > 4\sigma_I$ / all data)	0.0462 / 0.0462	0.0489 / 0.0492
<i>wR</i> <sub>2</sub> (all data)	0.1324	0.1371
Largest diff. peak/hole [e/Å <sup>-3</sup> ]	0.92 / -0.74	0.81 / -0.65

Cobalamins that belong to the same crystal packing type display remarkably similar conformations of their side chains as well as a similar pattern of intra and intermolecular hydrogen bonding (Randaccio et al. 2000).

The cobalamin molecules are oriented in the crystal such that the plane of the corrin ring is almost parallel to the *ab* plane of the unit cell, tilted by approximately 5-10°, and when viewed down the *a*-axis, the molecules appear to adopt a slight zig-zag sheet-like pattern due to this tilt, running parallel to the *ab* plane. Layers of solvent molecules lie between the tilted cobalamin sheets, with the axial base and the upper axial ligand projecting into this layer. Long solvent channels are also evident when viewed down the *c* axis. In both cases the solvent was modeled very accurately, with 17 placed in EtCbl and 20 in BuCbl, with the residual peaks in the electron density less than 1 e/Å<sup>3</sup> in both structures. Thermal ellipsoids plots for EtCbl and BuCbl (drawn at 75% probability) are presented in **Figure 2.19**.

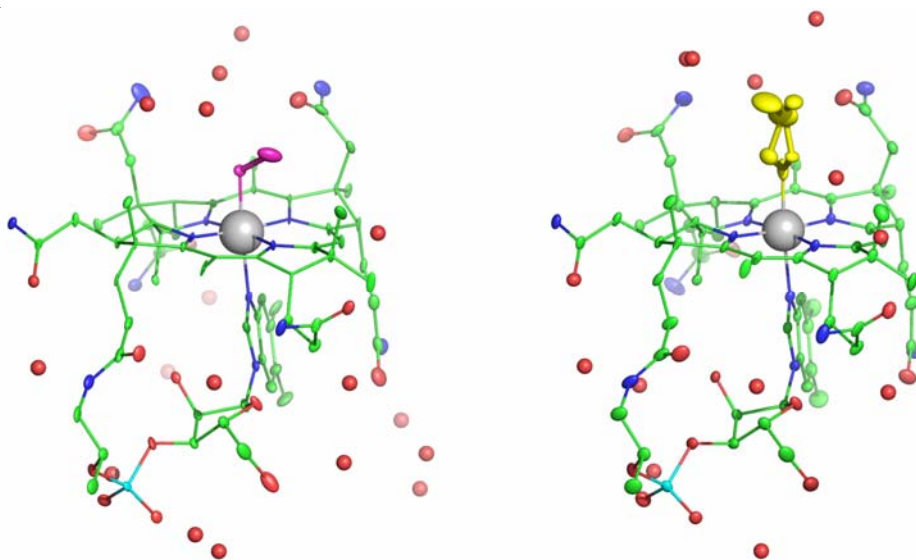


**Figure 2.19.** Thermal ellipsoid plots of EtCbl (left) and BuCbl (right). The ethyl  $\beta$ -axial ligand in EtCbl is shown in magenta and the butyl ligand (two conformations) in BuCbl is shown in yellow. The rest of the cobalamin complex is colored green (C), red (O), blue (N) and orange (P). The cobalt in each case is shown as a grey sphere. The thermal ellipsoids were drawn at 75% probability for all the atoms except for the cobalt and the water molecules (shown as red spheres) (Hannibal et

Of the 20 water molecules in the BuCbl structure, ten were in fully occupied positions and the rest were refined with partial occupancy, initially set at 0.5 based upon the observed increase in their anisotropic displacement parameters when refined with full occupancy. Conversely, all 17 water molecules in the EtCbl structure were at fully occupied positions. In the two structures, all the water molecules are in hydrogen bonding contact with either oxygen or nitrogen atoms on the cobalamin moiety, or with other water molecules.

The conformation of the corrin ring is generally quantified by the fold angle around the Co-C10 axis, between the planes of the conjugated ring systems (plane 1: N21, C4, C5, C6, N22, C9, C10) and plane 2: N24, C16, C15, C14, N23, C11, C10; see **Figure 1.1**). In EtCbl and BuCbl this corrin fold angle is 14.7° and 13.1° respectively, the direction of the fold being towards the  $\beta$  face of the corrin (away from the  $\alpha$ -5,6-dimethylbenzimidazole group). The corresponding values for a number of other alkylcobalamins are given in **Table 2.8**.

**Table 2.8.** Comparison of the Co coordination sphere in EtCbl, BuCbl and other alkylcobalamin complexes. Values are also given for CNCbl (Hannibal et al. 2009).

<b>Cobalamin</b>	<b>Co-X (Å)</b>	<b>Co-N3B (Å)</b>	<b>Fold angle (°)</b>	<b>Reference</b>
EtCbl	2.025(2)	2.232(2)	14.7	This work
BuCbl	2.018(9)	2.244(2)	13.1	This work
MeCbl	1.979(4)	2.162(4)	14.7	(Randaccio et al. 2000)
AdoCbl	2.033(4)	2.237(3)	15.9	(Ouyang et al. 2004)
AdoCbl (neutron)	2.023(10)	2.214(9)	13.3	(Lenhert and Hodgkin)
AdePrCbl	1.959(10)	2.212(8)	10.9	(Pagano et al. 1991)
CNCbl	1.885(4)	2.041(3)	18.7	(Randaccio et al. 2000)
CHF <sub>2</sub> Cbl	1.949(7)	2.187(7)	15.6	(Wagner et al. 1999)
CF <sub>3</sub> Cbl	1.878(12)	2.047(10)	15.6	(Zou and Brown 1998)
vinylCbl	1.911(7)	2.165(6)	12.5(2)	(McCauley et al. 2005)
<i>cis</i> -chlorovinylCbl	1.951(7)	2.144(5)	5.7 (9)	(McCauley et al. 2005)
isoamylCbl	2.044(3)	2.277(2)	10.6	(Perry, Fernandes, and Marques 2004)
<i>R</i> -2,3-dihydroxypropylCbl	2.002(23)	2.269	10.6	(Alcock, Dixon, and Golding 1985)
<i>S</i> -2,3-dihydroxypropylCbl	2.079(30)	2.367	13.0	(Alcock, Dixon, and Golding 1985)

Recently, van der Donk and coworkers reported the X-ray structure of *cis*-chlorovinylcobalamin and vinylcobalamin (McCauley et al. 2005). Interestingly, *cis*-chlorovinylcobalamin exhibited a fold angle of  $5.7 (9)^\circ$  which is the smallest reported value for cobalamins (others fall in the  $13.3^\circ$  (AdoCbl) to  $18.7^\circ$  ( $\text{H}_2\text{OCbl}^+$ ) range) (McCauley et al. 2005). The authors attributed this result to interactions between the chlorine and the corrin ring and its  $\beta$ -substituents on the tetrapyrrolic macrocycle (McCauley et al. 2005). It was originally proposed that the extent of folding of the corrin ring was inversely related to the steric bulk of the  $\beta$ -axial ligand but it is now generally believed that the *trans* influence of the ligand is the critical factor (Randaccio et al. 2000; Randaccio et al. 2006). There is a rough correlation between the corrin fold angle and the length of the Co-NB3 bond (Randaccio et al. 2006) (**Figure 2.20**). Although there is considerable scattering, the parameters obtained for EtCbl and BuCbl are similar to those reported for AdoCbl structures (**Figure 2.20**).

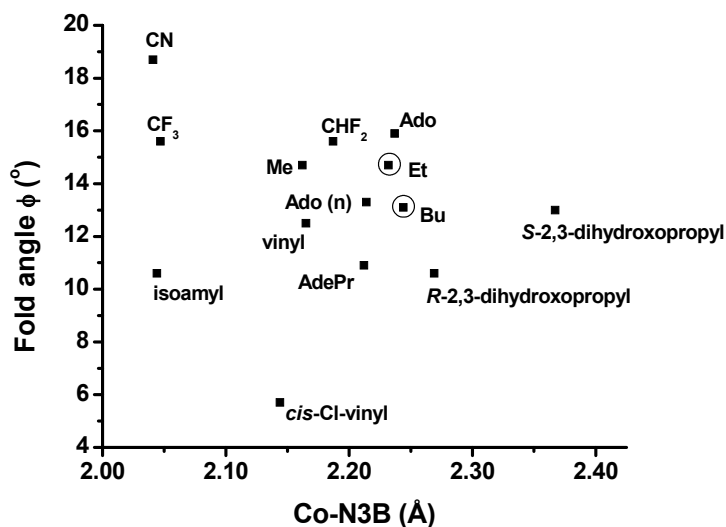


**Figure 2.20.** Scatter plot of the corrin fold angle ( $\phi$ ) versus the axial Co-N3B distance for Co-C bonded cobalamins. EtCbl and BuCbl are indicated with circled dots (Hannibal et al. 2009).

The Co-C bond distances in the two complexes are 2.025(2) Å and 2.018 Å for EtCbl and BuCbl, respectively. These distances are comparable to other Co-C bond lengths observed in cobalamin complexes (**Table 2.8**). In the EtCbl complex, the second carbon atom (C72) is directed away from the two amide groups which project up from the  $\beta$  face of the corrin at carbons C2 and C7, and points almost directly towards the C46 methyl group (attached to carbon C12 of the corrin, see **Figure 1.1**). This results in a Co-C71-C72 angle of 117.5°. By calculating a plane through the cobalt atom, C71 and C46, the degree of rotation of the C72 carbon out of this plane can be estimated at approximately 5°. In the BuCbl complex, two orientations of the butyl group were observed in the electron density, as presented in **Figure 2.21**.

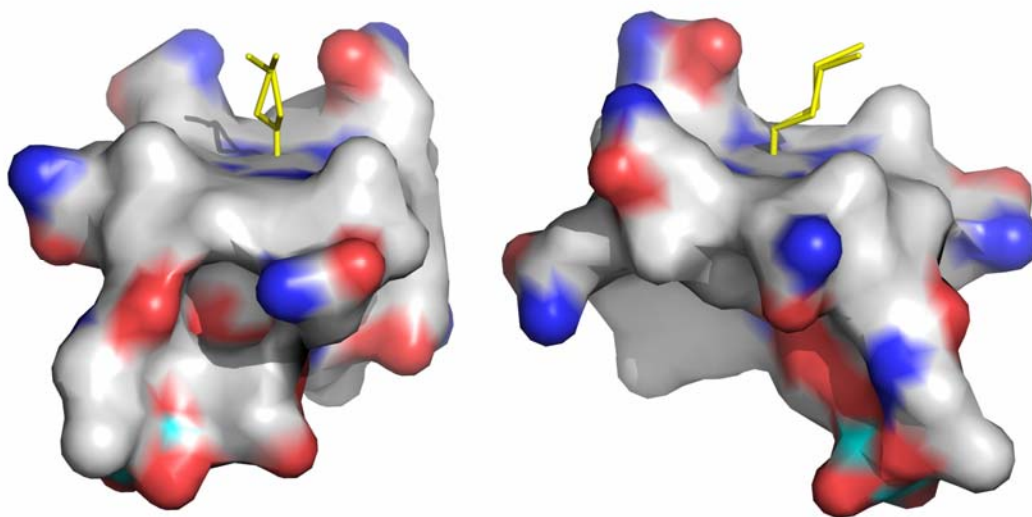


**Figure 2.21.** Surface maps of BuCbl in two different orientations. The butyl group is directed towards the hydrophobic side of the corrin ring, similar to the ethyl group in EtCbl (Hannibal et al. 2009).

The first and third carbon atoms of both conformations were in identical positions, with the second and fourth carbon atoms occupying two distinct positions. The net effect is a rotation of the butyl group about an axis running between the first and third carbon atoms. The butyl group in both orientations is in a typical elongated conformation, also directed towards the hydrophobic side of the corrin ring similar to the ethyl group (**Figure 2.21**). However, neither of the two conformations of the butyl group have the C72 carbon atom in the same position as in the ethyl group with the C72 atoms rotated by approximately 29° and 62°, respectively, from the Co-C71-C46 plane. The Co-C71-C72 angles in the two conformations are 119.0 and 119.6°.

Analysis of other cobalamin complexes containing a Co-C bond (AdoCbl, vinylCbl, chlorovinylCbl) shows a similar pattern with the upper axial ligand directed towards the hydrophobic side of the  $\beta$  face of the corrin ring, between the C46 methyl and the C54 methyl groups. In vinyl- and chlorovinylcobalamin, the former, possessing a similar steric bulk to that of EtCbl, the second carbon is rotated almost 49° towards the C54 methyl (McCauley et al. 2005). The four independent molecules in the asymmetric unit of the chlorovinylcobalamin complex show a range of values from 29° to 44° from the Co-C71-C46 plane. Adenosylcobalamin shows the largest rotation from this plane of almost 84°, which has the C atoms of the ribose moiety pointed almost directly at the C54 methyl group. Consequently, there appears to be no correlation between the size or the substituents on the second carbon atom and the direction in which the ligand points. Extending the analysis to other cobalamin complexes including those with Co-N, Co-O and Co-S bonds showed that in all cases the substituent is directed toward this side of the corrin ring with a mean rotation from the Co-C71-C46 plane of approximately 44°, which bisects almost exactly the angular

spread between the C46 and C54 methyl groups ( $87^\circ$ ). In fact, the  $15^\circ$  variation observed in the four chlorovinylcobalamin molecules (McCauley et al. 2005) would indicate a large energy minimum delineated by the C46 and C54 methyl groups and dominated primarily by the hydrophobicity of this side of the corrin ring and the lack of any ordered hydrogen-bonded water molecules. Importantly, it has been proposed that the methyl groups on C46 and C54, and the methylene groups in side chains *a* and *c* protect the reactive methyl or adenosyl groups in the coenzymes during catalytic turnover (Perry and Marques 2004) (see also references therein).

A superposition of the structure of EtCbl with that of the naturally occurring MeCbl is shown in **Figures 2.22**.

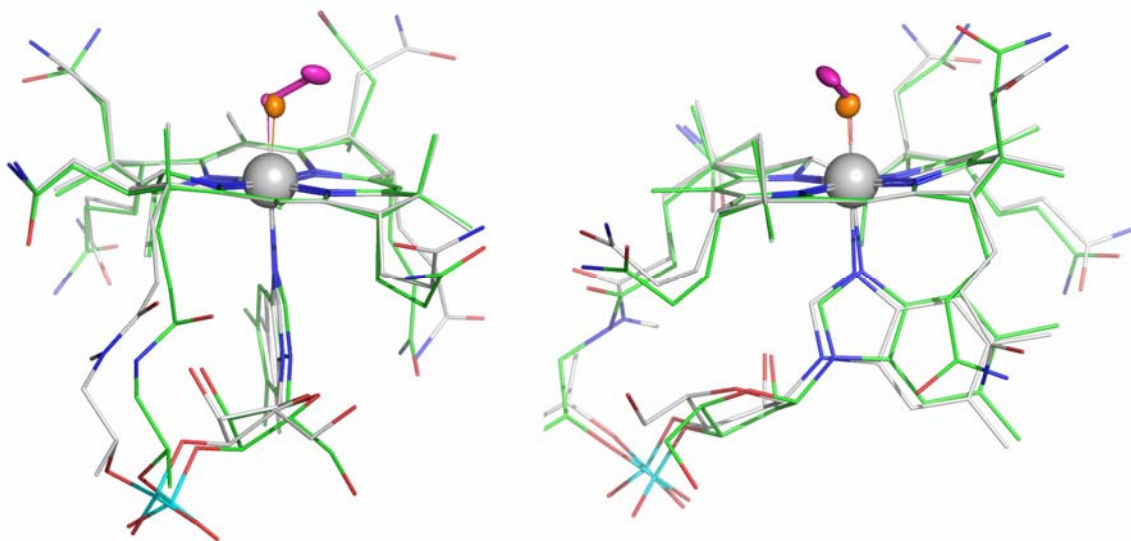


**Figure 2.22.** Superposition of the structures of MeCbl and EtCbl. Two approximately perpendicular views are shown (Hannibal et al. 2009).

There is high structural similarity amongst the structures as expected. The positions of the carbon atoms are visually similar in both complexes. However, a clear distinction of the two alkylcobalamins was possible by direct superposition of the two structures. Although the Co-N3B bond is significantly longer in EtCbl (2.232(2) Å) compared to MeCbl (2.162(4) Å), the orientation of the  $\alpha$ -5,6-dimethylbenzimidazole moiety with respect to the corrin ring is the same in both complexes.

There are seven amide side chains incorporated in the corrin ring. Three short acetamide side chains (*a*, *c*, and *g*), which project above the plane of the corrin and four propionamide (*b*, *d*, *e* and *f*) side chains which extend below the plane of the corrin ring. There is remarkably consistency in the conformation of the side chains amongst cobalamin structures, although side chains *c*, *d*, and *e* display greater flexibility with respect to *a*, *b*, *g* and *f* side chains (Perry and Marques 2004). The overall conformation of the side chains in EtCbl and BuCbl does not differ from that observed in other cobalamins. However, the superposition of the structures of MeCbl and EtCbl showed that there is considerable variation in the general orientation of their respective side chains. This could be explained by the presence of van der Waals forces between the longer alkyl  $\beta$ -axial ligands (such as ethyl and butyl groups in EtCbl and BuCbl) with the side chains in the corrin ring, compared to the inability of the methyl group in MeCbl to establish interactions with rather distant side chains projecting above and below the plane of the corrin ring.

It has been established that all alkylcobalamins display the so called “inverse” *trans* influence (Randaccio et al. 2006), where the distances of both axial ligands lengthen or shorten when the electron donating ability of the upper axial ligand (R) increases or decreases, respectively. EtCbl and BuCbl are no exception, as evidenced by comparison with

other available structures (**Table 2.8**). A linear correlation ( $r^2 = 0.919$ ) was obtained by plotting Co-C *versus* Co-N3B bond distances for a number of alkylcobalamins, as shown in **Figure 2.23**.

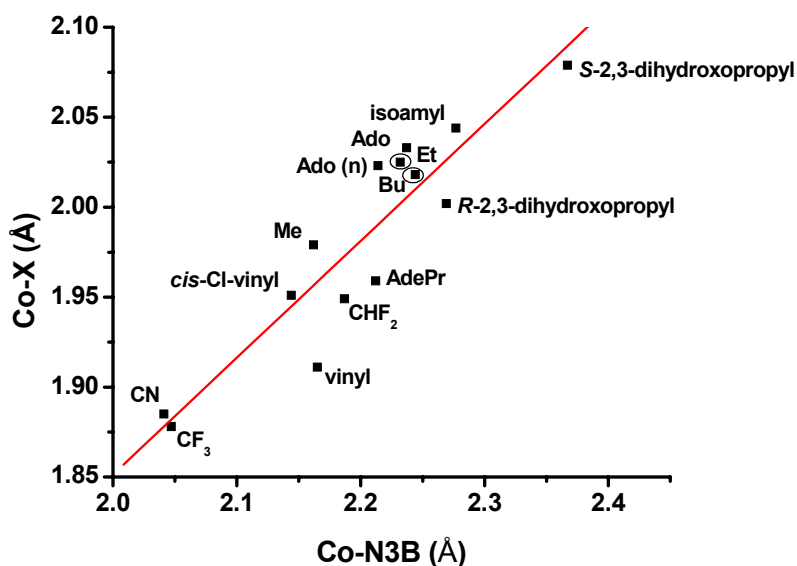


**Figure 2.23.** Plot of the axial Co-C against Co-N3B for Co-C bonded cobalamins. EtCbl and BuCbl are indicated with circled dots. The equation of linear regression is:  $0.552 + 0.649X$ ,  $r^2 = 0.919$ , (N= 14) (Hannibal et al. 2009).

Lengthening of the Co-C bond in alkylcobalamins is thought to be a consequence of the steric repulsion caused by bulky  $\beta$ -axial ligands (such as ethyl and butyl groups), whereas lengthening of the Co-N3B bond appears to be electronic in nature, as a consequence of the strong  $\sigma$ -donation from the alkyl ligands (Randaccio et al. 2006).

### C. SEPARATION OF ALKYLCOBALAMINS BY HPLC.

A simple reverse-phase HPLC procedure was developed for the separation of all alkylcobalamins. A representative chromatogram is presented in **Figure 2.24**. Retention times were consistent with the increasing hydrophobicity of the different alkylcobalamins ( $C_1 \rightarrow C_6$ ), as follows: MeCbl: 8.2 min; EtCbl: 9.1 min; PrCbl: 9.5 min; BuCbl: 9.9 min; PnCbl: 10.3 min and HxCbl: 10.8 min. The structure of these cobalamin derivatives was further confirmed by ES/MS, as described in Materials and Methods.

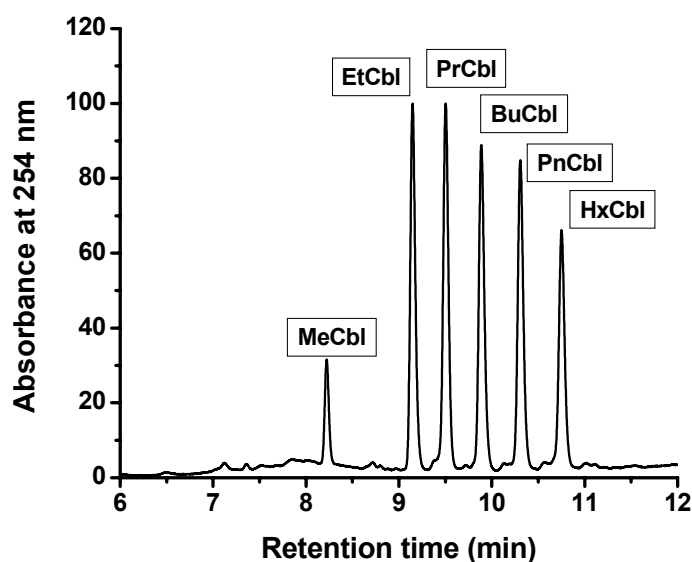


**Figure 2.24.** HPLC chromatogram of a mixture of alkylcobalamins separated on a Zorbax SB C-18 column (4.6 x 250 mm, 5  $\mu$ m particle size, Agilent). Solvent A contains 0.1% acetic acid/acetate buffer titrated to pH 3.5 with  $NH_4OH$  and Solvent B is acetonitrile containing 0.1% acetic acid. Gradient conditions were as follows: 0-2 min, 10% B; 2-14 min, 70% B; 14-15 min, 70% B; 15-16 min, 10% B; 16-17 min, 10% B, at a flow rate of 1 ml/min. Retention times were: MeCbl: 8.2 min; EtCbl: 9.1 min; PrCbl: 9.5 min; BuCbl: 9.9 min; PnCbl: 10.3 min and HxCbl: 10.8 min (Hannibal et al. 2009).

## SUMMARY

The X-ray crystal structures of EtCbl and BuCbl were obtained at high resolution ( $R = 0.0462$  and  $0.0492$ , respectively). Both EtCbl and BuCbl exhibited an “inverse” *trans* influence, as depicted by the lengthening of their Co-C and Co-N3B bonds. Analysis of the surface maps showed that both alkyl ligands in EtCbl and BuCbl project towards the hydrophobic side of the corrin ring. Comparison with other cobalamins showed that in general the  $\beta$ -axial substituent is directed towards the hydrophobic side of the  $\beta$  face of the corrin somewhere between the C46 methyl and the C54 methyl groups. To that end, it has been proposed that the hydrophobic axial groups (methyl groups on C46 and C54 and the methylene groups of the *a* and *c* side chains) protect the reactive methyl or adenosyl groups in the coenzymes during catalytic turnover (Perry and Marques 2004). These findings together with the results presented herein strengthen the notion that very fine structural and conformational relationships must be involved in the biological roles of Nature’s most beautiful cofactor (Stubbe 1994).

## MATERIALS AND METHODS

### General procedures and chemicals

Hydroxycobalamin hydrochloride (HOCbl•HCl) was purchased from Fluka. Stated purity by manufacturer is  $\geq 96\%$ . However, the aromatic region of the  $^1\text{H}$  NMR spectrum shows it contains at least  $\sim 6\%$  impurities (Brasch and Finke 1999). Alkyl halides (bromoethane, 99%, FW 108.97, d 1.46 g/mL, and 1-bromobutane, 99%, FW 137.02, d 1.276

g/mL) were purchased from Sigma. All chemicals were used without further purification. Water was purified using a Barnstead Nanopure Diamond water purification system and/or HPLC grade water was used. All solutions used for the synthesis of the alkylcobalamins were degassed by at least three freeze-pump-thaw cycles under argon using standard Schlenk techniques. Syntheses were carried out in an MBraun Labmaster 130(1250/78) glove box operating under argon atmosphere, or in an anaerobic cuvette with continuous argon bubbling. Both synthesis and handling of the alkylcobalamins were performed in the darkness under red-dim light illumination.

UV-visible spectra were recorded on a Cary 5000 spectrophotometer equipped with a thermostatted cell holder, operating with WinUV Bio software (version 3.00).  $^1\text{H}$  NMR spectra were recorded on a Varian Inova 500 MHz spectrometer equipped with a 5 mm thermostatted ( $22.0 \pm 0.5$  °C) probe. Solutions were prepared in  $\text{D}_2\text{O}$  and TSP (3-(trimethylsilyl)propionic-2,2,3,3- $\text{d}_4$  acid,  $\text{Na}^+$  salt) used as an internal reference. pH measurements were made at room temperature with a Corning Model 445 pH meter equipped with a Mettler-Toledo Inlab 423 electrode.

Liquid chromatography electrospray ionization mass spectrometry (LC-ESI-MS) was carried out using a Thermo Finnigan Triple Stage Quadrupole (TSQ) Quantum Ultra mass spectrometer (Thermo Electron Corporation, Waltham, MA, USA). Each alkylcobalamin was dissolved in 95%MeOH/5%H<sub>2</sub>O at a concentration of 10 mg/L and infused at a rate of 10  $\mu\text{L}/\text{min}$ .

### Synthesis of alkylcobalamins

All alkylcobalamins were synthesized by reacting cob(I)alamin with the corresponding alkyl halide for ~10 min in the absence of light under anaerobic conditions according to literature methods (Kim et al. 1988; Pratt 1972). In all cases, cob(I)alamin was generated by reduction of aquacobalamin with 10 equivalents of sodium borohydride ( $\text{NaBH}_4$ ). Prior to adding the alkyl halide, excess  $\text{NaBH}_4$  was decomposed by the addition of a small excess of anaerobic acetone. The product precipitated upon drop-wise addition into cold acetone ( $4^\circ\text{C}$ , 20 mL) and was filtered and dried overnight under vacuum at  $60^\circ\text{C}$ . Alkyl halides are soluble in acetone; hence it is unlikely that unreacted alkyl halide co-precipitates with the product. The percentage of non-cobalamin impurities was determined by converting the products to dicyanocobalamin,  $(\text{CN})_2\text{Cbl}^-$  (0.10 M KCN, pH 10.0,  $\epsilon_{368} = 3.04 \times 10^4 \text{ M}^{-1} \text{cm}^{-1}$ ) (Barker et al. 1960).

**EtCbl.** Bromoethane (5 equiv.,  $1.27 \times 10^{-4}$  moles, 9.5  $\mu\text{L}$ ) was added to  $\text{HOCbl}\cdot\text{HCl}$  (35 mg,  $2.53 \times 10^{-5}$  moles) dissolved in  $\text{H}_2\text{O}$  (1.0 mL). Yield:  $\geq 90\%$ .  $^1\text{H}$  NMR ( $\text{D}_2\text{O}$ ,  $\delta$ , ppm): 6.06, 6.26, 6.27, 7.00 and 7.18, ;  $\sim 98\%$  purity (Brasch and Finke 1999). ES/MS (+ve), m/z: 1358.8 (calcd for  $[\text{EtCbl} + \text{H}]^+$ ,  $\text{C}_{64}\text{H}_{94}\text{N}_{13}\text{O}_{14}\text{PCo} = 1358.6$ ); 1380.7 (calcd for  $[\text{EtCbl} + \text{Na}]^+$ ,  $\text{C}_{64}\text{H}_{93}\text{N}_{13}\text{O}_{14}\text{PCoNa} = 1380.6$ ); 1381.6 (calcd for  $[\text{EtCbl} + \text{H} + \text{Na}]^{2+}$ ,  $\text{C}_{64}\text{H}_{94}\text{N}_{13}\text{O}_{14}\text{PCoNa} = 1381.6$ ); 680.0 (calcd for  $[\text{EtCbl} + 2\text{H}]^{2+}$ ,  $\text{C}_{64}\text{H}_{95}\text{N}_{13}\text{O}_{14}\text{PCo} = 679.8$ ).

**PrCbl.** 1-Bromopropane (5 equiv.,  $1.27 \times 10^{-4}$  moles, 11.5  $\mu\text{L}$ ) was added to  $\text{HOCbl}\cdot\text{HCl}$  (35 mg,  $2.53 \times 10^{-5}$  moles) dissolved in  $\text{H}_2\text{O}$  (1.0 mL). Yield:  $\geq 84\%$ .  $^1\text{H}$  NMR ( $\text{D}_2\text{O}$ ,  $\delta$ , ppm): 6.08, 6.26, 6.29, 7.02 and 7.18;  $\sim 98\%$  purity (Brasch and Finke 1999). ES/MS (+ve), m/z: 1372.9 (calcd for  $[\text{PrCbl} + \text{H}]^+$ ,  $\text{C}_{65}\text{H}_{96}\text{N}_{13}\text{O}_{14}\text{PCo} = 1372.6$ ); 1394.2

(calcd for  $[\text{PrCbl} + \text{Na}]^+$ ,  $\text{C}_{65}\text{H}_{95}\text{N}_{13}\text{O}_{14}\text{PCoNa} = 1394.6$ ); 1395.9 (calcd for  $[\text{PrCbl} + \text{H} + \text{Na}]^{2+}$ ,  $\text{C}_{65}\text{H}_{96}\text{N}_{13}\text{O}_{14}\text{PCoNa} = 1395.6$ ).

**BuCbl.** 1-Bromobutane (5 equiv.,  $1.27 \times 10^{-4}$  moles, 13.6  $\mu\text{L}$ ) was added to  $\text{HOcbl}\cdot\text{HCl}$  (35 mg,  $2.53 \times 10^{-5}$  moles) dissolved in  $\text{H}_2\text{O}$  (1.0 mL). Yield:  $\geq 90\%$ .  $^1\text{H}$  NMR ( $\text{D}_2\text{O}$ ,  $\delta$ , ppm): 6.08, 6.26, 6.29, 7.01 and 7.18;  $\sim 98\%$  purity (Brasch and Finke 1999). ES/MS (+ve), m/z: 1386.7 (calcd for  $[\text{BuCbl} + \text{H}]^+$ ,  $\text{C}_{66}\text{H}_{98}\text{N}_{13}\text{O}_{14}\text{PCo} = 1386.6$ ); 1408.7 (calcd for  $[\text{BuCbl} + \text{Na}]^+$ ,  $\text{C}_{66}\text{H}_{97}\text{N}_{13}\text{O}_{14}\text{PCoNa} = 1408.6$ ); 1409.8 (calcd for  $[\text{BuCbl} + \text{H} + \text{Na}]^{2+}$ ,  $\text{C}_{66}\text{H}_{98}\text{N}_{13}\text{O}_{14}\text{PCoNa} = 1409.6$ ); 693.9 (calcd for  $[\text{BuCbl} + 2\text{H}]^{2+}$ ,  $\text{C}_{66}\text{H}_{99}\text{N}_{13}\text{O}_{14}\text{PCo} = 693.8$ ).

**PnCbl.** 1-Bromopentane (5 equiv.,  $1.27 \times 10^{-4}$  moles, 15.7  $\mu\text{L}$ ) was added to  $\text{HOcbl}\cdot\text{HCl}$  (35 mg,  $2.53 \times 10^{-5}$  moles) dissolved in  $\text{H}_2\text{O}$  (1.0 mL). Yield:  $\geq 90\%$ .  $^1\text{H}$  NMR ( $\text{D}_2\text{O}$ ,  $\delta$ , ppm): 6.08, 6.26, 6.29, 7.01 and 7.18;  $\sim 98\%$  purity (Brasch and Finke 1999). ES/MS (+ve), m/z: 1400.9 (calcd for  $[\text{PeCbl} + \text{H}]^+$ ,  $\text{C}_{67}\text{H}_{100}\text{N}_{13}\text{O}_{14}\text{PCo} = 1400.6$ ); 1422.6 (calcd for  $[\text{PeCbl} + \text{Na}]^+$ ,  $\text{C}_{67}\text{H}_{99}\text{N}_{13}\text{O}_{14}\text{PCoNa} = 1422.6$ ); 701.0 (calcd for  $[\text{PeCbl} + 2\text{H}]^{2+}$ ,  $\text{C}_{67}\text{H}_{101}\text{N}_{13}\text{O}_{14}\text{PCo} = 700.8$ ); 1329.4 (calcd for  $[\text{Cbl} + \text{H}]^+$ ,  $\text{C}_{62}\text{H}_{89}\text{N}_{13}\text{O}_{14}\text{PCo} = 1329.6$ ).

**HxCbl.** 1-Iodohexane (5 equiv.,  $1.27 \times 10^{-4}$  moles, 18.7  $\mu\text{L}$ ) was added to  $\text{HOcbl}\cdot\text{HCl}$  (35 mg,  $2.53 \times 10^{-5}$  moles) dissolved in  $\text{H}_2\text{O}$  (1.0 mL). Yield:  $\geq 90\%$ .  $^1\text{H}$  NMR ( $\text{D}_2\text{O}$ ,  $\delta$ , ppm): 6.08, 6.27, 6.29, 7.01 and 7.18;  $\sim 98\%$  purity (Brasch and Finke 1999). ES/MS (+ve), m/z: 1417.1 (calcd for  $[\text{HxCbl} + \text{H}]^+$ ,  $\text{C}_{68}\text{H}_{102}\text{N}_{13}\text{O}_{14}\text{PCo} = 1417.6$ ); 1439.6 (calcd for  $[\text{HxCbl} + \text{Na}]^+$ ,  $\text{C}_{68}\text{H}_{101}\text{N}_{13}\text{O}_{14}\text{PCoNa} = 1439.6$ ); 709.2 (calcd for  $[\text{HxCbl} + 2\text{H}]^{2+}$ ,  $\text{C}_{68}\text{H}_{103}\text{N}_{13}\text{O}_{14}\text{PCo} = 709.3$ ); 1329.4 (calcd for  $[\text{Cbl} + \text{H}]^+$ ,  $\text{C}_{62}\text{H}_{89}\text{N}_{13}\text{O}_{14}\text{PCo} = 1329.6$ ).

### **X-ray diffraction studies**

Crystals of EtCbl and BuCbl were grown from their corresponding synthesis mixtures, at room temperature, under anaerobic conditions. Crystals suitable for X-ray analysis appeared after 1 week. The EtCbl and BuCbl crystals were transferred into paratone oil and any residual synthesis mixture was carefully removed by dragging the crystals through the oil. The crystals were then mounted in thin nylon loops on copper magnetic pins (Hampton Research) and flash-cooled in liquid nitrogen. X-ray diffraction experiments were carried out at beamline BL9-2 at the Stanford Synchrotron Radiation Laboratory (SSRL). Data from both complexes were collected on a MarMosaic 325 CCD detector using X-rays produced by a 16-pole wiggler insertion device through a flat Rh-coated collimating mirror, a liquid nitrogen-cooled double Si(111) crystal monochromator and a toroidal focusing mirror. The X-ray wavelength used for both crystals was 0.78468 Å (15800 eV). For EtCbl, two data sets were collected, both consisting of 360 0.5° images covering the same 180° angular range and with a crystal to detector distance of 95.0 mm. The first data set was recorded with an exposure time of 5 s and no beam attenuation, and the second data set had the same exposure time but the beam was attenuated by 75%. The two data sets were processed with the program XDS and scaled together with the program XSCALE (Kabsch 1993). Symmetry-equivalent and Bijvoet pairs were not merged and no absorption correction was applied. A total of 132135 reflections were measured, resulting in 18317 unique reflections to a nominal resolution of 0.71 Å, with a merging R-factor of 0.028 for common reflections on all images. For BuCbl only one data set was recorded comprising 360 0.5 images with an exposure time of 15 s and a crystal to detector distance of 95.0 mm. The data were processed and scaled with XDS and XSCALE (Kabsch 1993), with the symmetry-equivalent and

Bijvoet pairs unmerged. A total of 66437 reflections were measured, giving a final unique data set of 20451 reflections to a resolution of 0.71 Å with a merging R-factor of 0.026.

Both structures were solved by Patterson methods as implemented in the program SHELXS (Sheldrick and Schneider 1997). The cobalt, phosphorus and some of the nitrogen atoms were readily located, the remainder of the lighter atoms later identified by difference Fourier synthesis. The structures were refined by full-matrix least-squares methods using SHELXL (Sheldrick and Schneider 1997). A correction for the anomalous scattering from cobalt at 15800 eV was applied during refinement. All non-hydrogen atoms were refined with anisotropic thermal parameters and hydrogen atoms were added in idealized positions and refined in riding positions at the very end of the refinement. Additional difference electron density peaks were modeled as water molecules. Seventeen water molecules were added to the EtCbl structure and refined with full occupancy. Twenty water molecules were added to BuCbl, ten with fractional occupancies. The final crystallographic R factor (R1) for EtCbl was 0.0462 for 18291 reflections with  $F_o > 4\sigma_F$ , and for BuCbl R1 was 0.0492 for 20273 reflections with  $F_o > 4\sigma_F$ .

## CHAPTER 3

### MECHANISMS OF COBALAMIN PROCESSING IN CELLS

#### 3.1 Project 1: Development of a method for the accurate assessment of intracellular cobalamins.

#### INTRODUCTION

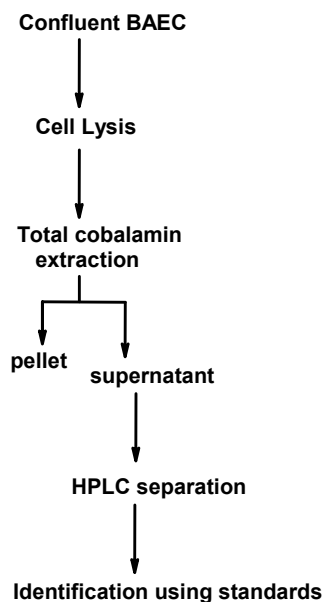
The identification of new Cbl derivatives in cells has been a matter of active research in the vitamin B<sub>12</sub> field. The major cellular Cbl forms are AdoCbl, MeCbl, as well as Cbl(II) generated during enzymatic turnover. Cbl(II) is recovered as H<sub>2</sub>OCbl<sup>+</sup> upon cell lysis due to oxidation by O<sub>2</sub>. Our laboratory has a long standing interest on the isolation and identification of: 1) GSCbl, which has been proposed to be a key intermediate in the biosynthesis of MeCbl and AdoCbl (Pezacka, Green, and Jacobsen 1990), and 2) NO<sub>2</sub>Cbl, which has been reported as a naturally occurring derivative by others (Anes et al. 1994; Begley and Hall 1979; Begley and Hall 1979). NO<sub>2</sub>Cbl could also represent the only isolatable fingerprint for the existence of the air-sensitive NOCbl. However, it is important to note that NO<sub>2</sub>Cbl can also be formed from the reaction of H<sub>2</sub>OCbl<sup>+</sup> and NO<sub>2</sub><sup>-</sup>. Model chemistry studies have shown that the reaction of H<sub>2</sub>OCbl<sup>+</sup> with ligands that are present in the intracellular milieu such as GSH and NO<sub>2</sub><sup>-</sup> is fast (seconds) (Knapton and Marques 2005; Marques 1991; Xia et al. 2004), suggesting that formation of GSCbl and NO<sub>2</sub>Cbl is feasible under physiological conditions. Cell lysis is accompanied by the release of intracellular GSH and NO<sub>2</sub><sup>-</sup>, and therefore β-axial ligand exchange of these ligands with H<sub>2</sub>OCbl<sup>+</sup> to form GSCbl and NO<sub>2</sub>Cbl, respectively, is likely to occur and represents an artifact caused by the

Cbl extraction procedure. *Project 1* describes a new procedure to prevent the formation of artifacts, which is based on the use of non-radioactive  $\text{H}_2\text{OCbl}^+$  as a ligand trap to scavenge intracellular anions that are released upon cell lysis, thus preventing their reaction with newly formed  $\text{H}_2\text{OCbl}^+$  (Hannibal et al. 2008). This permitted the identification of Cbl forms that were synthesized prior to cell lysis, i.e., the Cbl forms that occur naturally. The strategy is herein designated as “cold-trapping”. Part of this work has been published (Hannibal et al. 2008).

## RESULTS AND DISCUSSION

### A. Extraction of cobalamins from cultured cells

The identification and quantitation of cobalamins from biological materials relies on the extraction procedure that is utilized. We adjusted the extraction conditions to maximize the overall recovery and to minimize decomposition of potentially labile cobalamin derivatives. A flow-diagram of the extraction procedure is presented in **Scheme 3.1**. The overall recovery of cobalamins was ~75-85%. Approximately 15-25% remained bound to protein. The reproducibility of the extraction was: a) intra-assay: 12% variation and b) inter-assay: 18% variation.



**Scheme 3.1.** Flow-diagram of the method utilized for the extraction of cobalamins from cultured cells.

### **B. Development of a reproducible HPLC method for the separation of Cbls**

A reproducible HPLC method was developed for the efficient separation of seven Cbl forms as shown in **Figure 3.1**. In addition, simple procedures for the synthesis of Cbl standards that are not available commercially, such as GSCbl, NO<sub>2</sub>Cbl and SO<sub>3</sub>Cbl have been developed (Suarez-Moreira et al. 2006). Intracellular Cbls were extracted with 80% EtOH, separated by HPLC, fractions were collected, and the radioactivity present in each fraction was counted in a  $\gamma$ -counter. The radioactive profile of intracellular Cbl was then overlapped with the chromatogram of pure Cbl standards. **Figure 3.2** shows a typical chromatogram of the intracellular Cbl profile in BAEC. AdoCbl, MeCbl and H<sub>2</sub>OCbl<sup>+</sup> appear to be the major intracellular forms, in agreement with the literature available for other cell

types (Gimsing and Nexø 1983). As predicted,  $\beta$ -axial ligand exchange does occur for the non-alkylCbIs during cell lysis (**Figure 3.3**) (Hannibal et al. 2008). In addition,  $\text{SO}_3\text{Cbl}$ ,  $\text{NO}_2\text{Cbl}$  and  $\text{GSCbl}$  underwent substantial decomposition during the extraction procedure; 30, 35 and 65%, respectively.  $\text{AdoCbl}$ ,  $\text{MeCbl}$  and  $\text{CNCbl}$  do not exchange with other ligands and proved to be very stable during the extraction procedure (decomposition was lower than 0.25%).

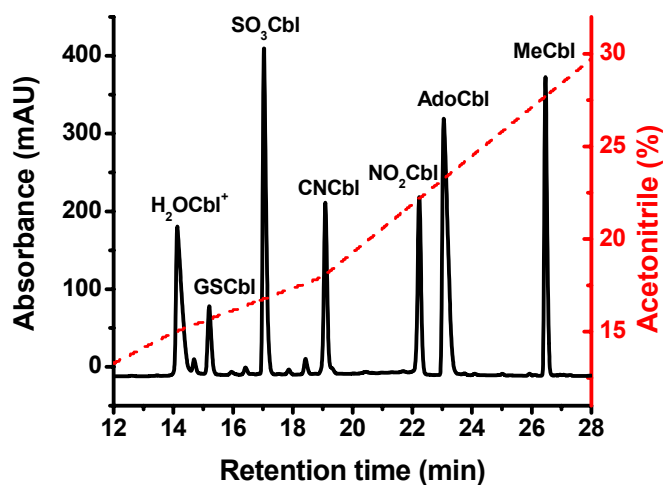


**Figure 3.1.** Reverse-phase HPLC of a mixture of seven cobalamin standards. Gradient conditions: (A) 0.1 % acetic acid, pH 3.5; (B) acetonitrile containing 0.1% acetic acid. (dashed line, % change in B) (Hannibal et al. 2008).

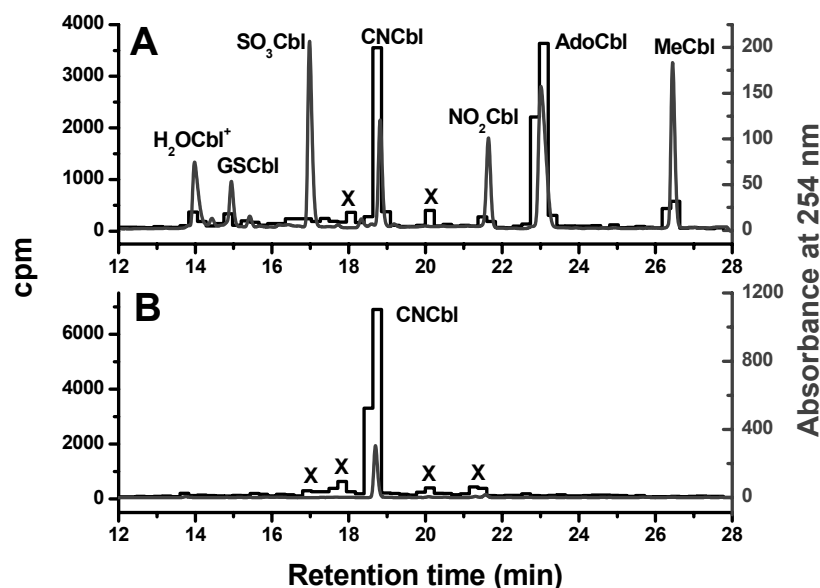


**Figure 3.2.** Profile of [ $^{57}\text{Co}$ ]-cobalamins in cultured BAEC extracted in the absence of excess  $\text{H}_2\text{OCbl}^+$ . **A.** [ $^{57}\text{Co}$ ]-AdoCbl, [ $^{57}\text{Co}$ ]-MeCbl and [ $^{57}\text{Co}$ ]-CNCbl (the source of  $\text{B}_{12}$  given to the cells) were the most abundant forms present in BAEC. However, smaller amounts of [ $^{57}\text{Co}$ ]- $\text{H}_2\text{OCbl}^+$ , [ $^{57}\text{Co}$ ]-GSCbl, [ $^{57}\text{Co}$ ]- $\text{SO}_3\text{Cbl}$  and [ $^{57}\text{Co}$ ]- $\text{NO}_2\text{Cbl}$  were also observed. X denotes as yet unidentified corrinoids. **B.** Conversion of intracellular [ $^{57}\text{Co}$ ]-Cbls to [ $^{57}\text{Co}$ ]-CNCbl. X denotes unknown corrinoids that were not able to convert to [ $^{57}\text{Co}$ ]-CNCbl (Hannibal et al. 2008).

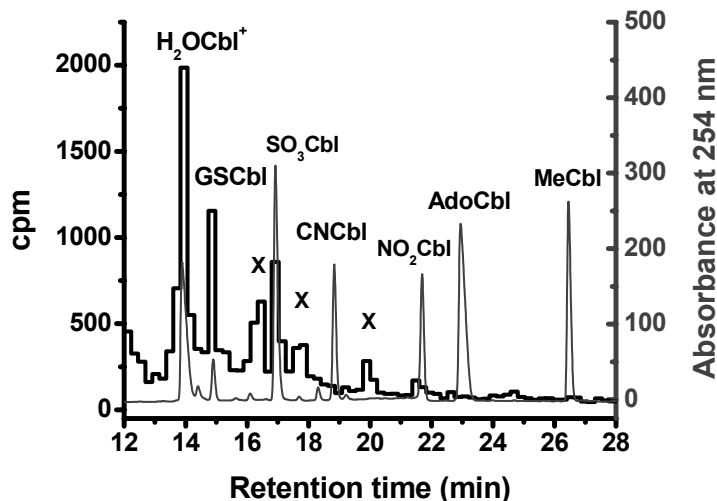


**Figure 3.3.** Formation of [ $^{57}\text{Co}$ ]-cobalamins as a result of  $\beta$ -axial ligand exchange. BAEC grown in the presence of non-radioactive CNCbl were harvested and pelleted. Immediately before lysis, the pellet was spiked with [ $^{57}\text{Co}$ ]- $\text{H}_2\text{OCbl}^+$ , lysed and extracted in the absence of excess  $\text{H}_2\text{OCbl}^+$ . This figure shows that substantial amounts of [ $^{57}\text{Co}$ ]-GSCbl, [ $^{57}\text{Co}$ ]- $\text{SO}_3\text{Cbl}$  and [ $^{57}\text{Co}$ ]- $\text{NO}_2\text{Cbl}$  were formed during the extraction in contrast to the lack of formation of [ $^{57}\text{Co}$ ]-AdoCbl and [ $^{57}\text{Co}$ ]-MeCbl. Unknown corrinoids (X) are also observed (Hannibal et al. 2008).

### C. Accurate assessment of intracellular Cbls: cold-trapping

Cobalamins were extracted from BAEC pellets in the presence of 7.5 mM  $\text{H}_2\text{OCbl}^+$ , which was added to the cells just before lysis and extraction. We reasoned that excess  $\text{H}_2\text{OCbl}^+$  would serve as a scavenger for intracellular ligands that might exchange with  $[\text{}^{57}\text{Co}]\text{-H}_2\text{OCbl}^+$  and other labile  $[\text{}^{57}\text{Co}]\text{-Cbls}$ . The HPLC Cbl profile is shown in **Figure 3.4**, panel A. As expected a broad region of UV absorbance at 254 nm corresponding to excess

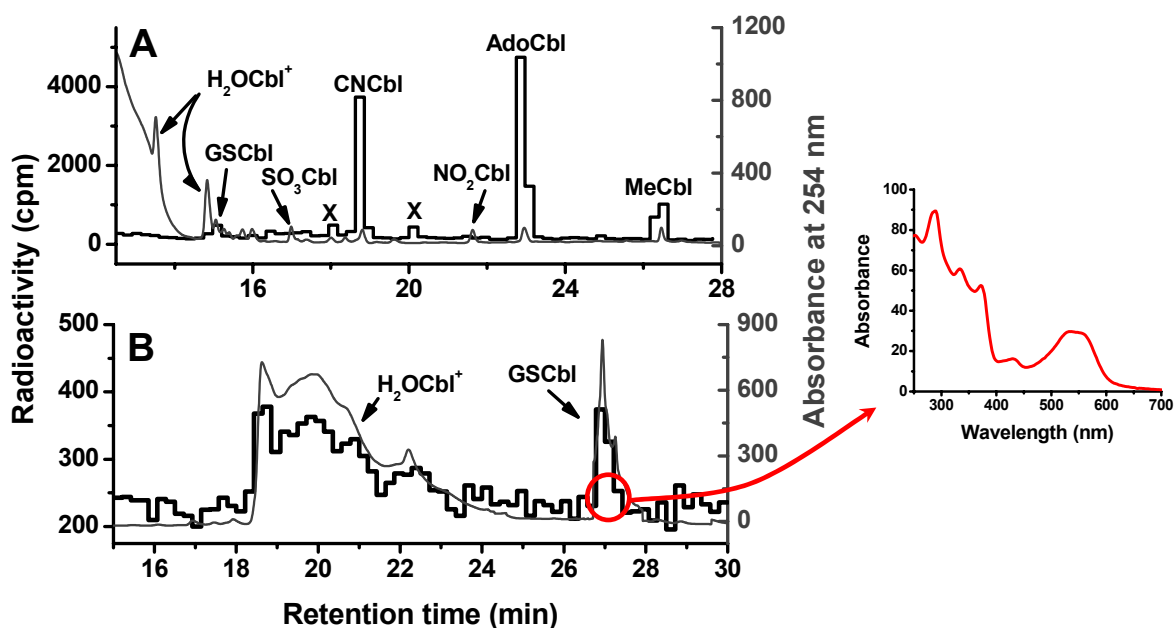


**Figure 3.4. Profile of  $[\text{}^{57}\text{Co}]\text{-cobalamins}$  in cultured BAEC extracted in the presence of excess  $\text{H}_2\text{OCbl}^+$  (“cold trapping”).** A.  $[\text{}^{57}\text{Co}]\text{-AdoCbl}$ ,  $[\text{}^{57}\text{Co}]\text{-MeCbl}$  and  $[\text{}^{57}\text{Co}]\text{-CNCbl}$  (the source of  $\text{B}_{12}$  given to the cells) were the most abundant forms present in BAEC and were similar to the levels shown in **Figure 3.2** panel A. However, the level of the non-alkylcobalamins  $[\text{}^{57}\text{Co}]\text{-GSCbl}$  and  $[\text{}^{57}\text{Co}]\text{-SO}_3\text{Cbl}$  decreased significantly, and  $[\text{}^{57}\text{Co}]\text{-NO}_2\text{Cbl}$  was undetectable when the extraction was carried out in the presence of excess  $\text{H}_2\text{OCbl}^+$ . Unknown corrinoids (X) were also observed. B. Improved separation of  $[\text{}^{57}\text{Co}]\text{-H}_2\text{OCbl}^+$  and  $[\text{}^{57}\text{Co}]\text{-GSCbl}$  using the “shallow” HPLC method. The red arrow points to the UV-visible spectrum of a GSCbl standard whose retention time matched that of the radioactive peak obtained after cold trapping of excess GSH (Hannibal et al. 2008).

$\text{H}_2\text{OCbl}^+$  in the extraction buffer was observed. The recovery of [ $^{57}\text{Co}$ ]-AdoCbl, [ $^{57}\text{Co}$ ]-MeCbl and [ $^{57}\text{Co}$ ]-CNCbl remained unchanged and comparable to the analyses shown in Fig. 2A. However, the amount of the non-alkylcobalamins [ $^{57}\text{Co}$ ]-GSCbl and [ $^{57}\text{Co}$ ]- $\text{SO}_3\text{Cbl}$  decreased substantially. [ $^{57}\text{Co}$ ]- $\text{NO}_2\text{Cbl}$  was undetectable under these conditions. A chromatogram of [ $^{57}\text{Co}$ ]-CbIs separated using the slow-gradient HPLC method (see Methods section) is shown in **Figure 3.4**, panel **B**.

The distribution of [ $^{57}\text{Co}$ ]-CbIs and unknown corrinoids in cultured BAEC and human cell lines is summarized in **Table 3.1**. Values were taken from the cold-trapping experiments, which reflect relative amounts of naturally-occurring cobalamins only. The high amount of CNCbl present does not reflect natural intracellular levels, since it was the source with which cells were fed for the experiments. Cbl-like analogues (“unknowns” in **Table 3.1**) made up the second largest fraction in endothelial cells ( $20.8 \pm 4.4\%$ ). Smaller amounts of  $\text{SO}_3\text{Cbl}$  ( $2.8 \pm 1.0\%$ ) and GSCbl ( $4.5 \pm 0.9\%$ ) were found in cultured BAEC. Also shown in the table is the total uptake of [ $^{57}\text{Co}$ ]-CNCbl and the intracellular concentration of total GSH at the time of cell harvest (48h).

**Table 3.1.** Total Cbl uptake, intracellular distribution of [<sup>57</sup>Co]-Cobalamins and Total GSH in BAEC, HFF and HepG2 (Hannibal et al. 2008).

	Total [ <sup>57</sup> Co]-CNCbl uptake (pmol/mg protein) <sup>1</sup>	[ <sup>57</sup> Co]-Cobalamin (%) <sup>2</sup>							Intracellular GSH (mM) <sup>3</sup>	
		HOCbl	GSCbl	SO <sub>3</sub> Cbl	CNCbl	NO <sub>2</sub> Cbl	AdoCbl	MeCbl		Unknowns
BAEC	0.54	7.8 ± 2.3 <sup>4</sup>	4.5 ± 0.9	2.8 ± 1.0	15.5 ± 2.5	ND	37.6 ± 2.9	10.2 ± 3.5	20.8 ± 4.4	2.39 ± 0.48
HFF	0.36	7.2 ± 0.6	ND <sup>5</sup>	ND	29.4 ± 8.1	ND	11.5 ± 1.9	51.8 ± 7.1	5.1 ± 2.2	6.39 ± 0.27
HepG2	5.1	11.9 ± 1.7	5.1 ± 0.8	ND	10.7 ± 0.5	ND	42.5 ± 0.4	26.7 ± 4.8	ND	0.30 ± 0.04

<sup>(1)</sup> Total [<sup>57</sup>Co]-CNCbl uptake was determined by measuring the amount of radioactivity in the washed cell pellets divided by total mg of protein. <sup>(2)</sup> [<sup>57</sup>Co]-Cobalamin (%) values were expressed as mean ± standard deviation (n = 3-6). <sup>(3)</sup> Intracellular GSH was determined by the HPLC method of Jacobsen et al. (Jacobsen et al. 1994) GSH concentrations are expressed as mean ± standard deviation (n = 3). <sup>(4)</sup> All values are statistically significant at a 99% confidence level as assessed by student t-test. <sup>(5)</sup> ND, not detected.

## SUMMARY

The objective of this study was to determine the extent of  $\beta$ -axial ligand exchange that occurs during the extraction of Cbls from mammalian cells. We hypothesized that non-covalent  $\beta$ -axial ligands would undergo exchange during the extraction procedure. We further hypothesized that non-covalent  $\beta$ -axial ligand exchange could be minimized by performing the extraction in the presence of a large excess of a ligand scavenger, in this case non-radioactive  $\text{H}_2\text{OCbl}^+$ , which serves as a “cold trapping” agent.

Accurate identification and quantification of Cbls in biological samples requires that the extraction procedure: a) efficiently releases Cbl from proteins (little or no Cbl exists in its free form in mammalian cells (Schneider et al. 1976)); b) maintains the chemical structures of the different cellular Cbl derivatives throughout the extraction procedure; and, c) results in a near quantitative recovery of total cellular Cbl. Therefore, the recovery and stability of all the Cbls expected to be present in the cell lines studied was assessed and taken into consideration when interpreting the results. The proportion of each Cbl derivative recovered after successive extractions steps remained basically unchanged, suggesting that the observed relative amounts of AdoCbl and MeCbl indeed represent the natural abundance of each derivative in cultured cells.

Analysis of individual recoveries showed that the  $[^{57}\text{Co}]$ -non-alkylcobalamins underwent different degrees of decomposition during the extraction procedure, which leads to an underestimation of their actual biological abundance.  $[^{57}\text{Co}]$ - $\text{H}_2\text{OCbl}^+$ , the product of decomposition, is in turn concomitantly overestimated.  $[^{57}\text{Co}]$ -AdoCbl and  $[^{57}\text{Co}]$ -MeCbl remained essentially unchanged under our experimental conditions, supporting the notion

that the alkylcobalamins can be considered as reliable indicators of Cbl metabolic activity in the cells.

The coenzymes AdoCbl and MeCbl were the major Cbl forms present in BAEC, HFF and HepG2 cells (Table 1). Non-metabolized [ $^{57}\text{Co}$ ]-CNCbl, the substrate used in these studies, was also present in substantial amounts (10.7% for HepG2 to 29.4% for HFF). Based on model studies (Xia et al. 2004; Marques 1991; Knapton and Marques 2005), we hypothesized that upon cell lysis [ $^{57}\text{Co}$ ]- $\text{H}_2\text{OCbl}^+$  would react with intracellular anions such as nitrite ( $\text{NO}_2^-$ ), sulfite ( $\text{SO}_3^{2-}$ ) and glutathione thiolate anion ( $\text{GS}^-$ ) to form the corresponding Cbl derivatives [ $^{57}\text{Co}$ ]- $\text{NO}_2\text{Cbl}$ , [ $^{57}\text{Co}$ ]- $\text{SO}_3\text{Cbl}$  and [ $^{57}\text{Co}$ ]- $\text{GSCbl}$ , respectively (**Figure 3.5**). These derivatives are readily formed upon cell lysis. A strategy was implemented to distinguish natural *versus* artifactual Cbls based on the use of an efficient anion trap (non-radioactive  $\text{H}_2\text{OCbl}^+$ ) to scavenge intracellular anions during the lysis and extraction procedure. To our knowledge, this is the first time that “cold trapping” of exchangeable anions has been utilized in the extraction of cellular Cbls.

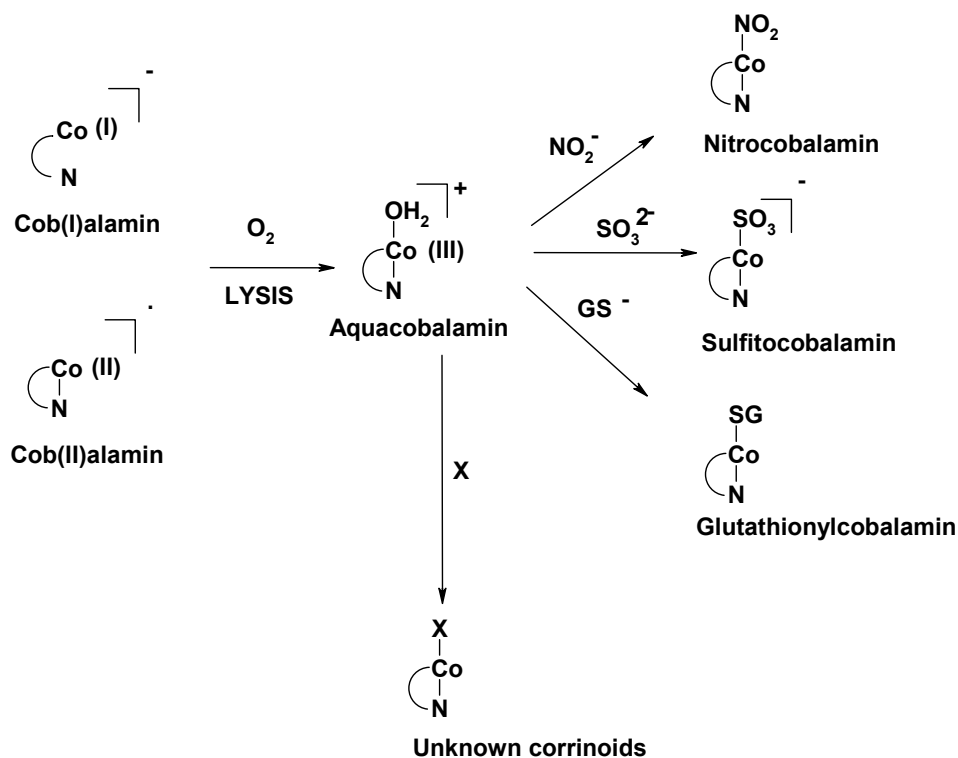


**Figure 3.5. Reactions of aquacobalamin (H<sub>2</sub>OCo<sup>+</sup>) with relevant biological ligands leading to the formation of artifactual derivatives during the cell lysis and cobalamin extraction procedures.** In the presence of oxygen, intracellular cob(I)alamin and cob(II)alamin are converted to H<sub>2</sub>OCo<sup>+</sup> (cob(III)alamin). H<sub>2</sub>OCo<sup>+</sup> reacts with free nitrite (NO<sub>2</sub><sup>-</sup>), sulfite (SO<sub>3</sub><sup>2-</sup>) and glutathione thiolate anion (GS<sup>-</sup>) and other currently unidentified ligands (X) to produce the corresponding derivatives NO<sub>2</sub>Cbl, SO<sub>3</sub>Cbl, GSCbl and XCbl, respectively (Hannibal et al. 2008).

Previous studies carried out in our laboratories suggested that GSCbl was an intermediate in the biosynthesis of AdoCbl and MeCbl (Pezacka, Green, and Jacobsen 1990; Pezacka 1993; Pezacka, Green, and Jacobsen 1990). The Cbl profile of cells grown in the presence of [<sup>57</sup>Co]-CNCbl as a source of vitamin B<sub>12</sub> showed that the following derivatives are formed: [<sup>57</sup>Co]-H<sub>2</sub>OCo<sup>+</sup>, [<sup>57</sup>Co]-GSCbl, [<sup>57</sup>Co]-SO<sub>3</sub>Cbl, [<sup>57</sup>Co]-CNCbl, [<sup>57</sup>Co]-AdoCbl, [<sup>57</sup>Co]-MeCbl as well as other yet unidentified corrinoids. When the extraction was performed in the presence of excess cold H<sub>2</sub>OCo<sup>+</sup>, the recovery of both [<sup>57</sup>Co]-GSCbl and

[<sup>57</sup>Co]-SO<sub>3</sub>Cbl decreased significantly. Moreover, preparation of cell lysates in the presence of freshly added [<sup>57</sup>Co]-H<sub>2</sub>OCbl<sup>+</sup> resulted in the formation of [<sup>57</sup>Co]-GSCbl and [<sup>57</sup>Co]-SO<sub>3</sub>Cbl but not [<sup>57</sup>Co]-AdoCbl or [<sup>57</sup>Co]-MeCbl, suggesting that β-ligand exchange occurs but only with non-covalently bound β-ligands. [<sup>57</sup>Co]-GSCbl was present in BAEC and HepG2, but not in HFF. The strikingly high level of [<sup>57</sup>Co]-MeCbl (52%) seen in HFF may suggest that GSCbl is being rapidly consumed as the proximal precursor in MeCbl coenzyme biosynthesis. Little or no [<sup>57</sup>Co]-SO<sub>3</sub>Cbl and [<sup>57</sup>Co]-NO<sub>2</sub>Cbl were present in any of the human cell lines, suggesting that previous findings by other investigators on the isolation of SO<sub>3</sub>Cbl and NO<sub>2</sub>Cbl may have been misleading due to the artifactual formation of these derivatives during the extraction procedures. NOCbl, which immediately decomposes to NO<sub>2</sub>Cbl in the presence of O<sub>2</sub> (Hannibal, Smith et al. 2007), is unlikely to be an isolatable naturally occurring Cbl.

According to the literature, most tissues contain higher levels of AdoCbl than MeCbl (Gimsing and Nexø 1983), and this was the case for BAEC and HepG2 cells. In contrast, it has been reported that human fibroblasts show higher amounts of MeCbl than AdoCbl (Suormala et al. 2004). In agreement, this study showed that HFF contained 52% MeCbl and 12% AdoCbl (**Table 3.1**). Whether these results represent actual physiological patterns or are just a result of cell culture conditions adjusted by manufacturers for optimal cell growth remains to be investigated. It is important to note that the ratio AdoCbl/MeCbl could be affected by cell culture conditions such as folate source, supplementation with different forms of Cbl, cell passage and time of incubation. Indeed, previous studies published by Quadros and coworkers have shown that AdoCbl and MeCbl are synthesized at different rates in leukemia cells, and as a result the corresponding yields of each cofactor vary over

time (Quadros et al. 1976). Moreover the metabolic need for AdoCbl and MeCbl may be cell specific, as both the literature (**Table 3.2** and references therein) and these results suggest. The total specific activities reported for methylmalonyl-CoA mutase are higher than those reported for methionine synthase (**Table 3.2**). Higher mutase activity could be responsible for and therefore correlate with a higher requirement of the corresponding cofactor, AdoCbl, as it was observed in BAEC and HepG2. However, this possibility does not hold true for the case of human fibroblasts, in which higher levels of MeCbl were observed.

**Table 3.2. Activity of the Cbl-dependent enzymes in different cell types. Values represent total enzyme activity.**

Source	Tissue/ Cell	Methionine synthase	Methylmalonyl -CoA mutase	Reference
Human ( $\text{pmol}\cdot\text{min}^{-1}\cdot\text{mg}^{-1}$ )	Fibroblasts	110-119	898-2483	(Mellman, Willard, and Rosenberg 1978)
Human ( $\text{pmol}\cdot\text{min}^{-1}\cdot\text{mg}^{-1}$ )	Fibroblasts	139-625	585-2570	(Suormala et al. 2004)
Human ( $\text{nmol}\cdot\text{h}^{-1}\cdot\text{mg}^{-1}$ )	Glioma cells	$19.7 \pm 0.55$	$105.6 \pm 2.8$	(Riedel et al. 1999)
Rat ( $\text{nmol}\cdot\text{min}^{-1}\cdot\text{mg}^{-1}$ )	Liver	$0.28 \pm 0.08$	$8.2 \pm 0.16$	(Riedel, Ueland, and Svardal 1995; Yamada et al. 2000)
	Liver	$4.5 \pm 0.18$	$430 \pm 80$	(Kennedy et al. 1990)
	Kidney	$2.8 \pm 0.27$	$56 \pm 6.7$	(Kennedy et al. 1990)
Sheep ( $\mu\text{mol}\cdot\text{min}^{-1}\cdot\text{mg}^{-1}$ )	Brain	$4.7 \pm 0.18$	$47 \pm 10$	(Kennedy et al. 1990)
	Spinal cord	$2.8 \pm 0.54$	$28 \pm 3.3$	(Kennedy et al. 1990)
	Liver	2.4	124	(Kennedy et al. 1995)
Cattle ( $\mu\text{mol}\cdot\text{min}^{-1}\cdot\text{g}^{-1}$ )	Heart	0.55	45	(Kennedy et al. 1995)
	Brain	0.35	3.2	(Kennedy et al. 1995)

The total cobalamin uptake was similar for BAEC and HFF, although considerably higher in the case of HepG2 (**Table 3.1**). This result was not surprising, since it is well established that tumor cells take up and accumulate higher amounts of Cbl than normal cells in order to sustain high rates of cell division (Flodh and Ullberg 1968).

In summary, I have designed a simple procedure for the characterization of naturally- occurring Cbls in cultured cells. The distinction between natural versus artifactual formation of non-alkylcobalamins was made possible by means of *cold-trapping* of exchangeable anions with excess non-radioactive  $\text{H}_2\text{OCbl}^+$ .  $\beta$ -axial ligand exchange does occur during the extraction procedure, causing an increase in the relative recovery of the radiolabeled non-alkylcobalamins. Scavenging of  $\text{GS}^-$  and  $\text{SO}_3^{2-}$  did not result in the total loss of  $[\text{}^{57}\text{Co}]\text{-GSCbl}$  and  $[\text{}^{57}\text{Co}]\text{-SO}_3\text{Cbl}$  in BAEC, suggesting that these derivatives do occur naturally in endothelial cells. However, their abundance is probably underestimated given the instability of these compounds, especially of GSCbl, during the extraction procedure. The isolation and identification of  $[\text{}^{57}\text{Co}]\text{-GSCbl}$  as a naturally-occurring Cbl in both BAEC and HepG2 strengthens the notion of its role as a key intermediate in the biosynthesis of AdoCbl and MeCbl (Pezacka, Green, and Jacobsen 1990). Although proposed by others as naturally-occurring,  $[\text{}^{57}\text{Co}]\text{-NO}_2\text{Cbl}$  was not present in detectable amounts in any of the cell types investigated herein. Significant levels of the analogues have been previously observed in biological samples (Kondo, Kolhouse, and Allen 1980; Gimsing 1995), and their structure and function are still a matter of debate. Further research toward the isolation and identification of the Cbl analogues in cultured BAEC is currently in progress. It is recommended that metabolic labeling studies on cultured cells and tissues and perfused

organs use the cold-trapping approach to provide more reliable estimates of Cbls in these systems.

## MATERIALS AND METHODS

**Materials.** Dulbecco's phosphate buffered saline (DPBS), AdoCbl, MeCbl, HOCbl, cyanocobalamin (CNCbl), glutathione (GSH), sodium sulfite and sodium nitrite were purchased from SIGMA. [ $^{57}\text{Co}$ ]-CNCbl (specific activity 379  $\mu\text{Ci}/\mu\text{g}$  CNCbl) was purchased from MP Biomedical. Glacial acetic acid, acetonitrile (both HPLC grade) and ethanol were purchased from Fisher Scientific. Bovine aortic endothelial cells (BAEC) and fetal bovine serum (FBS) were purchased from CAMBREX.  $\text{SO}_3\text{Cbl}$ ,  $\text{GSCbl}$  and  $\text{NO}_2\text{Cbl}$  were synthesized by reacting  $\text{H}_2\text{OCbl}^+$  with sodium sulfite, GSH and sodium nitrite, respectively, according to our recently published procedure (Suarez-Moreira et al. 2006). Synthesis of [ $^{57}\text{Co}$ ]- $\text{H}_2\text{OCbl}^+$  was performed according to published procedures (Mahoney and Rosenberg 1971), using [ $^{57}\text{Co}$ ]-CNCbl as the starting material.

**Cell culture and [ $^{57}\text{Co}$ ]-cobalamin metabolic labeling.** The following cultured cells were used in this study: 1) BAEC were cultured in 162  $\text{cm}^3$  flasks (Corning) and grown in vitamin  $\text{B}_{12}$ -free, folic acid-free Ham's F12/DME (1:1) medium supplemented with 5% FBS ( $\sim 33$  pM Cbl), 2.0 mM L-glutamine, penicillin (100 units/mL), streptomycin (0.1 mg/mL) and 50 nM (6S)- $N^5$ -methyltetrahydrofolic acid (Eprova AG); 2) Human foreskin fibroblasts (HFF) were obtained from the Lerner Research Institute tissue culture core. HFF were grown in Advanced Dulbecco's Modified Eagle Medium (Invitrogen) supplemented with 10% FBS ( $\sim 67$  pM Cbl), 2 mM L-glutamine, penicillin (100 units/mL), and streptomycin (0.1 mg/mL).

Note: commercially available advanced DMEM contains 9.07 $\mu$ M folic acid. 3) Human hepatoma cells (HepG2) were obtained from ATCC (HB-8065<sup>TM</sup>). HepG2 were grown in ATCC complete growth medium (#30-2003) supplemented with 10% FBS (~67 pM Cbl), penicillin (100 units/mL) and streptomycin (0.1 mg/mL). Note: ATCC (HB-8065<sup>TM</sup>) complete medium contains 2.27  $\mu$ M of folic acid as the source of folate. Total Cbl concentration in commercial FBS was determined using a commercial assay (MP Biomedicals). The amount of Cbl present in the culture medium via supplementation with FBS was shown to be sufficient to support normal growth in all three cell types. For [<sup>57</sup>Co] metabolic-labeling experiments, cells were passaged at a ratio of 1:2. [<sup>57</sup>Co]-CNCbl was added to achieve a final concentration of 0.2 nM (0.1  $\mu$ Ci per mL of culture medium), and cells were grown to 100% confluency (~48 h).

**Extraction of cellular cobalamins.** Confluent cells were harvested by trypsinization and washed three times with DPBS. Cell lysis was performed by treatment with 0.5 mL 50 mM Tris, pH 7.4 containing 0.15 M NaCl and 1% Triton X-100 for 20 min at room temperature. (Note: extraction and handling of the samples were performed under dim-red light to prevent decomposition of the photosensitive Cbls). An aliquot of the cell lysate was taken for protein and total GSH determinations. Extractions were performed by addition of 0.75 mL of absolute ethanol to the cell lysate and incubated for 20 min at room temperature. Protein precipitates were removed by centrifugation at 9,302 x g for 3 min at room temperature. The resulting supernatant was taken to dryness in a Speed Vac at 45°C. The Cbl-enriched residue was washed three times with acetone, re-suspended with 0.3 mL DPBS and passed through an Amicon microfuge filter (0.22  $\mu$ m). Cbl extracts were stable for at least 2 months at -20°C.

**Identification of intracellular cobalamins by HPLC.** Extracted Cbls were separated by gradient reverse-phase HPLC using an Agilent 1100 System equipped with a Zorbax SB C-18 column (4.6 x 250 mm, 5  $\mu$ m particle size, Agilent). Solvent A contained 0.1% acetic acid/acetate buffer titrated to pH 3.50 with  $\text{NH}_4\text{OH}$  and Solvent B was acetonitrile containing 0.1% acetic acid. Prior to injection, Cbl extracts were spiked with a mixture of pure non-radioactive Cbl standards to assist in the identification of the intracellular Cbls. Gradient conditions were as follows: 0-2 min, 5% B; 2-14 min, 15% B; 14-19 min, 18% B; 19-32 min, 35% B; 32-33 min, 60% B; 33-35 min, 5% B at a flow rate of 1 mL/min. Elution was monitored with UV detection at 254 nm. Peak areas were obtained using HP Chemstation LC 3D software provided with the instrument. In typical runs, 70 fractions (~0.23 mL) were collected between 12 and 28 min. When required, a HPLC method consisting of a shallow linear gradient was used to improve separation of  $\text{H}_2\text{OCbl}^+$  from GSCbl (see “cold-trapping” experiments below). Gradient conditions for such runs were as follows: 0-2 min, 5% B; 2-14 min, 15% B; 14-39 min, 18% B; 39-42 min, 35% B; 42-43 min, 60% B; 43-45 min, 5% B and 70 fractions (~0.23 mL) were collected between 15 and 30 min. The radioactivity associated with each fraction was counted using a gamma-counter (Gamma 4000, BECKMAN-Coulter).

**Recovery of total and individual cobalamins.** Total recovery of Cbl was calculated as the radioactivity present in the final Cbl extract divided by the radioactivity present in the washed cell pellets. The individual recovery of the different Cbl derivatives during the extraction procedure was also assessed. Briefly, unlabeled cell pellets were spiked with a known amount of the [ $^{57}\text{Co}$ ]-Cbl derivative to be tested immediately before cell lysis. The cells were then lysed, extracted and the HPLC/radioactive assay performed as described

before. Recovery of the individual cobalamin derivatives was calculated as the ratio of the corresponding [ $^{57}\text{Co}$ ]-Cbl radioactive peak present in the final Cbl extract versus the radioactivity initially added to the cell pellets.

**Assessment of  $\beta$ -axial ligand exchange during cobalamin extraction.** GSH is the primary soluble thiol in cells (Meister 1995). Because GSH readily reacts with  $\text{H}_2\text{OCbl}^+$  (Xia et al. 2004), formation of GSCbl is likely to be a product of  $\beta$ -axial ligand exchange during extraction. To test this hypothesis, cells were grown in the presence of non-radioactive CNCbl, harvested, and lysed in the presence of [ $^{57}\text{Co}$ ]- $\text{H}_2\text{OCbl}^+$  (0.33  $\mu\text{Ci}$ , specific activity = 305  $\mu\text{Ci}/\mu\text{g}$ ; chemical level comparable to the amount of [ $^{57}\text{Co}$ ]-CNCbl that is imported by cells in culture investigated herein). Intracellular GSH was determined by the method of Jacobsen et al. (Jacobsen et al. 1994).

**“Cold trapping” of exchangeable ligands with excess aquacobalamin.** Cells were grown in the presence of [ $^{57}\text{Co}$ ]-CNCbl, harvested and lysed with buffer containing 7.5 mM  $\text{H}_2\text{OCbl}^+$ . We hypothesized that a high excess concentration of non-radioactive  $\text{H}_2\text{OCbl}^+$  would trap ligands that might undergo  $\beta$ -axial ligand exchange reactions with non-alkylcobalamins during lysis and extraction (designated “cold trapping”). The ratio of excess  $\text{H}_2\text{OCbl}^+$  to total intracellular GSH in these studies ranged from 150 to 2,500 depending on cell type. Accurate identification and quantification of the radioactivity associated with GSCbl was conducted for Cbl profiles analyzed by the slow-gradient HPLC method as described herein. It should be noted that  $\beta$ -axial ligand exchange between endogenously formed [ $^{57}\text{Co}$ ]-Cbls and cold excess  $\text{H}_2\text{OCbl}^+$  was <2% (see supplemental data). Finally, to further examine the nature of the radioactive Cbls extracted from cultured cells, an aliquot of

the Cbl extract was treated with excess KCN under alkaline conditions followed by exposure to light in the presence of acetic acid. This procedure converts true Cbl to CNCbl (Weissbach et al. 1960). The samples were then separated by HPLC and the resulting radioactive signal/s assigned according to pure Cbl standards as described.

**Statistical analysis.** Statistical analysis was performed using Microcal Origin<sup>®</sup> v7.0 (OriginLab Corporation). Unless otherwise indicated, all values are expressed as mean  $\pm$  standard deviation, with  $n \geq 3$ . The statistical significance for establishing presence and amount of each Cbl derivative was determined by a directional (one-tailed) student t-test at 99% confidence level. Briefly, an experimental HPLC baseline was obtained by injecting DPBS into the HPLC, collecting fractions and counting them in the gamma counter as described for the routine sample analysis. The limit of detection for a [<sup>57</sup>Co] signal to be considered different from the instrumental noise was set as the lowest positive value that differs from the mean of the baseline values at a 99% confidence level.

### 3.2 ***Project 2***: Processing of alkylcobalamins in mammalian cells: a role for the *MMACHC* (*cbIC*) gene product.

#### INTRODUCTION

The *MMACHC* gene product of the *cbIC* complementation group, referred to as the *cbIC* protein, catalyzes the *in vitro* and *in vivo* decyanation of cyanocobalamin (vitamin B<sub>12</sub>). We hypothesized that the *cbIC* protein would also catalyze the *dealkylation* of newly internalized methylcobalamin (MeCbl) and 5'-deoxyadenosylcobalamin (AdoCbl), the naturally occurring *alkylcobalamins* that are present in the diet. The hypothesis was tested in cultured endothelial cells using [<sup>57</sup>Co]-AdoCbl and MeCbl analogs consisting of [<sup>57</sup>Co]-labeled straight-chain alkylcobalamins ranging from C2 (ethylcobalamin) to C6 (hexylcobalamin). [<sup>57</sup>Co]-AdoCbl was converted to [<sup>57</sup>Co]-MeCbl by cultured bovine aortic endothelial cells, suggesting that a dealkylation process likely involving the *cbIC* protein removed the 5'-deoxyadenosyl alkyl group. Surprisingly, all of the straight-chain alkylcobalamins served as substrates for the biosynthesis of both AdoCbl and MeCbl. Dealkylation was then assessed in normal skin fibroblasts and fibroblasts derived from 3 patients with mutations in the *MMACHC* gene. While normal skin fibroblasts readily converted [<sup>57</sup>Co]-propylcobalamin to [<sup>57</sup>Co]-AdoCbl and [<sup>57</sup>Co]-MeCbl, there was little or no conversion in *cbIC* mutant fibroblasts. ***Project 2*** presents strong evidence that the *cbIC* protein is responsible for early processing of both CNCbl (decyanation) and alkylcobalamins (dealkylation) in mammalian cells. Part of this work has been published (Hannibal et al. 2009 ).

## RESULTS AND DISCUSSION

### A. Cobalamin uptake and cofactor biosynthesis by BAEC.

The ability of BAEC to internalize [ $^{57}\text{Co}$ ]-CNCbl and synthesize [ $^{57}\text{Co}$ ]-AdoCbl and [ $^{57}\text{Co}$ ]-MeCbl was first determined, because little is known about B<sub>12</sub> metabolism in cardiovascular cells and tissues. [ $^{57}\text{Co}$ ]-CNCbl was added to pre-confluent cells in culture and total cobalamin uptake was measured at 6, 12, 24, 48 and 72 h in washed cell pellets. Data for uptake of [ $^{57}\text{Co}$ ]-CNCbl by BAEC are shown in **Table 3.3**. Maximum uptake occurs at ~48 h of growth under the culture conditions described above. For each time point, the intracellular cobalamin profile was also examined and the results for cofactor biosynthesis are summarized in **Table 3.3**.

**Table 3.3. Uptake and processing of [ $^{57}\text{Co}$ ]-CNCbl by BAEC (Hannibal et al. 2009).**

Time (h)	[ $^{57}\text{Co}$ ]-Cbl uptake <sup>1</sup> (fmol/mg protein)		[ $^{57}\text{Co}$ ]-Cofactor biosynthesis <sup>2</sup> (fmol/mg protein)	
	Conditioned medium	Intracellular	AdoCbl	MeCbl
6	10.5	0.36	0.006 ± 0.002	0.003 ± 0.001
12	8.8	0.44	0.035 ± 0.005	0.007 ± 0.002
24	8.4	0.54	0.044 ± 0.014	0.008 ± 0.001
48	8.3	0.59	0.090 ± 0.021	0.012 ± 0.003
72	8.5	0.60	0.113 ± 0.016	0.008 ± 0.002

<sup>1</sup>Uptake results represent three pooled samples per time point.

<sup>2</sup>Cofactor biosynthesis is expressed as mean ± standard deviation (n=3)

The kinetics of biosynthesis of the active cofactors, AdoCbl and MeCbl is shown in **Figure 3.6**. Although AdoCbl appeared to be the most abundant cobalamin form at all times,

the ratio AdoCbl/MeCbl varied over time. BAEC also utilized [ $^{57}\text{Co}$ ]-hydroxocobalamin ([ $^{57}\text{Co}$ ]-HOCbl) and [ $^{57}\text{Co}$ ]-AdoCbl as substrates for cofactor biosynthesis (**Figure 3.7**).

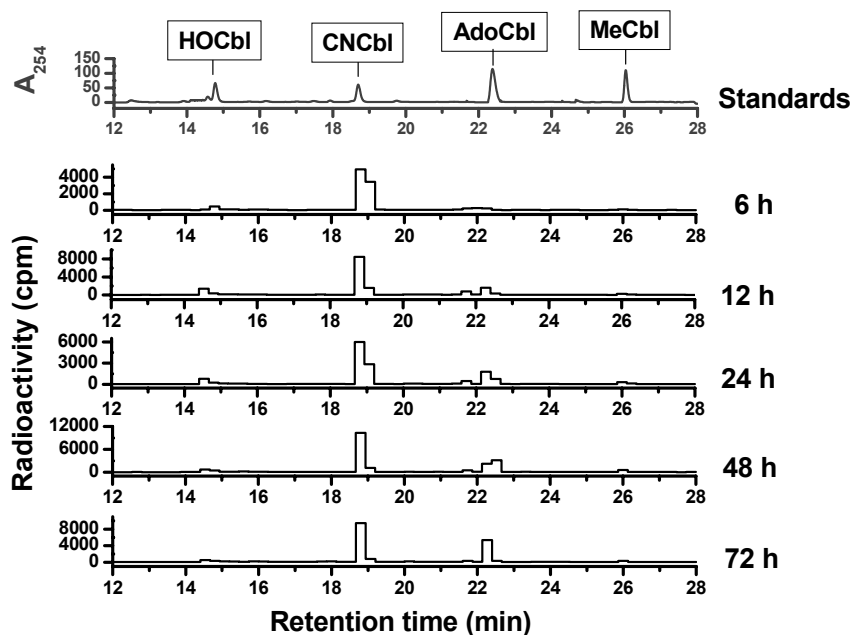


**Figure 3.6. Processing [ $^{57}\text{Co}$ ]-CNCbl in BAEC.** Kinetics of cobalamin biosynthesis in BAEC for 6, 12, 24, 48 and 72 h. BAEC were grown in the presence of [ $^{57}\text{Co}$ ]-CNCbl (0.2 nM final concentration; 0.1  $\mu\text{Ci}/\text{mL}$  culture medium) as the cobalamin source. Absorbance at 254 nm for cobalamin standards is shown in the upper chromatogram. Radioactivity for [ $^{57}\text{Co}$ ]-cobalamins at 6, 12, 24, 48 and 72 h is shown in the bottom chromatograms (Hannibal et al. 2009).

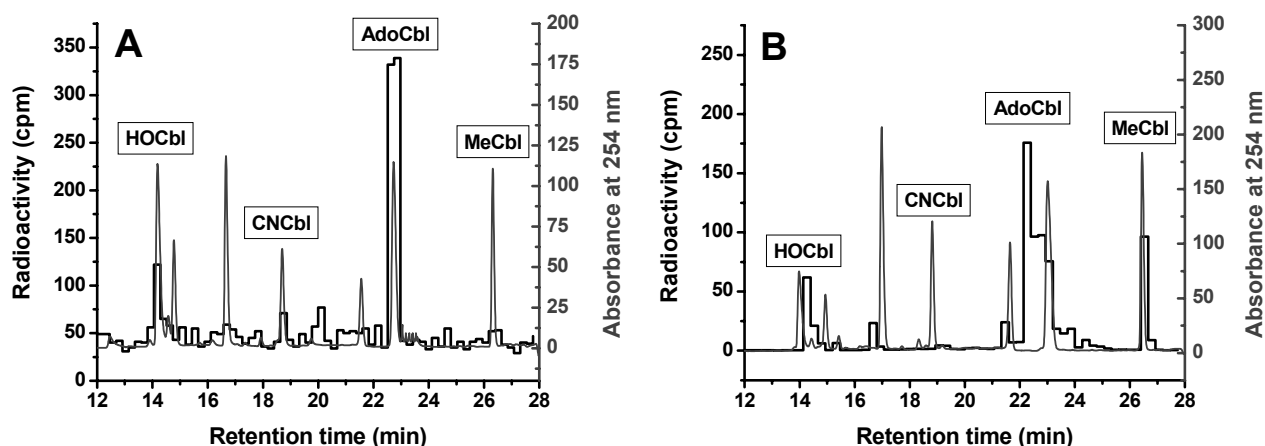


**Figure 3.7. Processing of [ $^{57}\text{Co}$ ]-HOCbl and [ $^{57}\text{Co}$ ]-AdoCbl by BAEC. A.** Representative profile of intracellular cobalamins in BAEC grown in the presence of [ $^{57}\text{Co}$ ]-HOCbl as the source of cobalamin. **B.** Representative profile of cells grown in the presence of [ $^{57}\text{Co}$ ]-AdoCbl as the source of cobalamin for 48 h (Hannibal et al. 2009 ).

Thus, endothelial cells possess the machinery for the efficient conversion of the natural cofactor AdoCbl into MeCbl as well as for utilizing HOCbl (**Figure 3.7**) and CNCbl as substrates for cofactor biosynthesis (see **Table 3.3**).

### B. Cytotoxicity of xenobiotic alkylcobalamins.

It has been reported that EtCbl and PrCbl form inactive complexes with apomethionine synthase *in vitro* (Yamada et al. 1999). Therefore, the effects of high concentrations of each of the non-radioactive xenobiotic alkylcobalamins on cultured BAEC were examined. None of the xenobiotic alkylcobalamins appeared to be cytotoxic (**Figure 3.8**).

In addition, cell viability (MTT assay), senescence ( $\beta$ -galactosidase activity), and export of homocysteine and methylmalonic acid into the culture medium were also

examined. None of these markers were altered in the presence of xenobiotic cobalamins compared to cells supplemented with CNCbl, AdoCbl or no cobalamin at all (data not shown). The lack of cytotoxicity of EtCbl, PrCbl and the longer-chained alkylcobalamins suggests that they are converted to non-toxic cobalamins, which serve as substrates for the biosynthesis of MeCbl and AdoCbl.

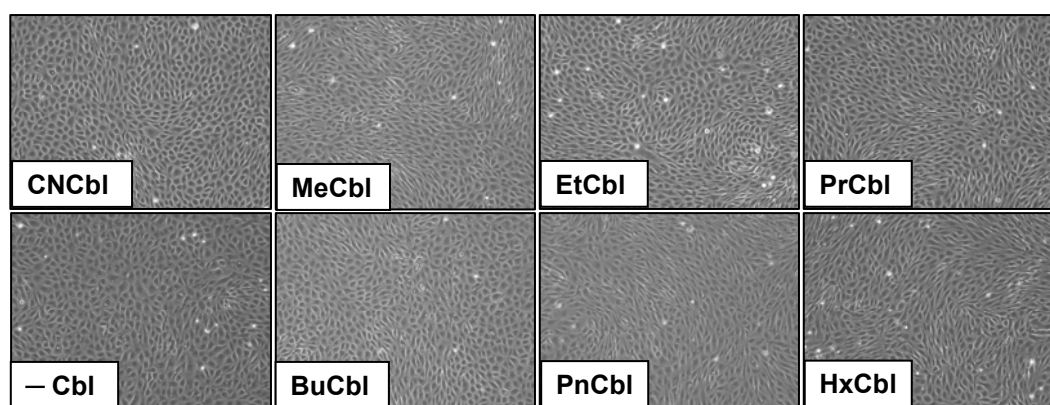


**Figure 3.8.** Growth of BAEC on CNCbl, MeCbl and xenobiotic alkylcobalamins. BAEC were grown for 2 weeks with 1  $\mu$ M Cbls. Culture medium was replaced every three days. After 2 weeks of growth, total homocysteine and methylmalonic acid levels in spent media were identical (data not shown) suggesting that all xenobiotic alkylcobalamins served as substrates for coenzyme biosynthesis and were not cytotoxic to cell growth. Cell cultures were protected from light exposure at all times (Hannibal et al. 2009).

### C. Dealkylation of xenobiotic alkylcobalamins by BAEC.

The ability of BAEC to convert a series of [ $^{57}\text{Co}$ ]-labeled xenobiotic alkylcobalamins with increasing  $\beta$ -axial alkyl ligand chain length into the active coenzyme forms was determined. Cells were grown for 48 h in the presence of 125 pM [ $^{57}\text{Co}$ ]-alkylcobalamin. Cobalamins present in cells and in the conditioned culture medium were extracted and analyzed as described under Materials and Methods. The intracellular cobalamin profile of

cells grown in the presence of [ $^{57}\text{Co}$ ]-PrCbl is shown in **Figure 3.9**, panel **A**. Cells were able to dealkylate [ $^{57}\text{Co}$ ]-PrCbl and efficiently convert it to the two natural cofactors AdoCbl and MeCbl. Little [ $^{57}\text{Co}$ ]-PrCbl was recovered from the cell extracts (**Figure 3.9**, panel **A**).

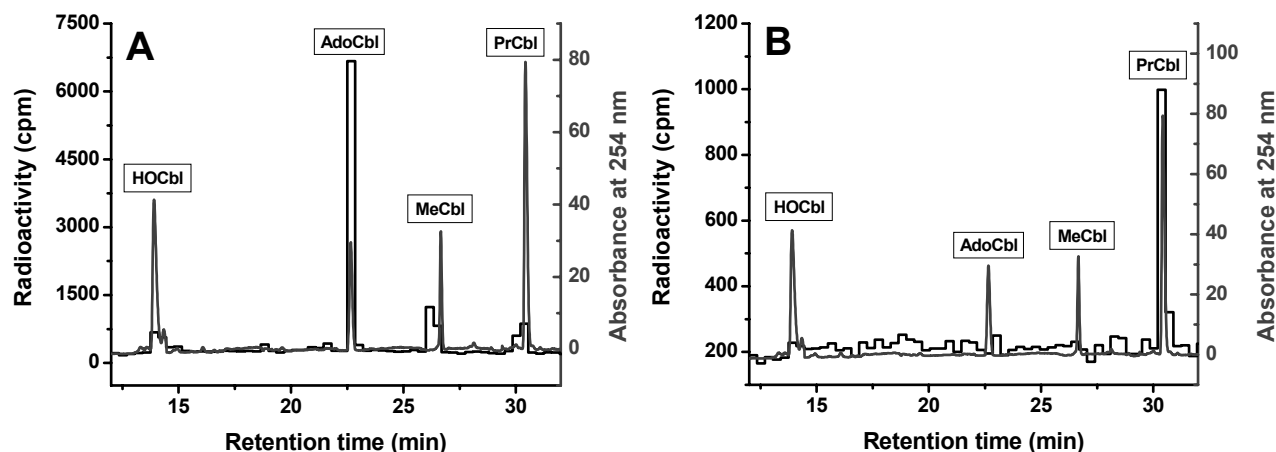


**Figure 3.9. Processing [ $^{57}\text{Co}$ ]-PrCbl in BAEC.** **A.** Typical cobalamin profile from BAEC grown in the presence of [ $^{57}\text{Co}$ ]-PrCbl (0.125 nM final concentration; 0.06  $\mu\text{Ci/ml}$  culture medium) as the cobalamin source for 48 h. Absorbance at 254 nm for cobalamin standards is shown in the lighter tracing; radioactivity for [ $^{57}\text{Co}$ ]-cobalamins is shown in the darker tracing. **B.** Cobalamins extracted from conditioned medium after 48 h. The darker tracing shows that [ $^{57}\text{Co}$ ]-PrCbl is largely intact after 48 h in the culture medium (Hannibal et al. 2009).

Examination of the 48-h conditioned culture medium (**Figure 3.9**, panel **B**) revealed a prominent [ $^{57}\text{Co}$ ]-PrCbl peak but little or no other [ $^{57}\text{Co}$ ]-labeled cobalamins suggesting that the [ $^{57}\text{Co}$ ]-PrCbl substrate was stable and that there was negligible export of cellular cobalamins from BAEC into the conditioned medium. Similarly, all of the other [ $^{57}\text{Co}$ ]-labeled alkylcobalamins used in this study were stable and did not degrade in the culture medium. [ $^{57}\text{Co}$ ]-AdoCbl was the major form of cobalamin found in BAEC after feeding with [ $^{57}\text{Co}$ ]-labeled alkylcobalamins. **Table 3.4** summarizes the results obtained for the xenobiotic alkylcobalamin series (EtCbl, PrCbl, BuCbl, PnCbl, HxCbl), as well as results from the naturally occurring cobalamin forms (AdoCbl, CNCbl and HOCbl).

**Table 3.4. Processing of natural and xenobiotic cobalamins by BAEC (Hannibal et al. 2009 ).<sup>1</sup>**

Source	Intracellular cobalamin (%)					Ratio AdoCbl/MeCbl
	AdoCbl	MeCbl	HOcbl	CNCbl	Others <sup>2</sup>	
	58.1	4.5	20.4	<1	17.0	12.9
	33.6	7.5	3.7	47.1	8.1	4.5
	57.1	8.6	10.2	<1	23.1	6.6
	59.1	5.5	15.4	<1	20.0	10.7
	32.7	8.1	7.7	<1	51.5	4.0
	28.8	4.0	12.4	<1	54.8	7.2
	43.2	7.4	15.1	<1	34.3	5.8
	48.5	8.7	16.2	<1	26.6	5.6

<sup>1</sup> BAEC were cultured in the presence of [<sup>57</sup>Co]-cobalamins for 48 h. Intracellular [<sup>57</sup>Co]-cobalamins were extracted from washed cells and separated by HPLC as described in Experimental Procedures.

<sup>2</sup> “Others” includes unprocessed Cbl source and unidentified corrinoids.

**D. Genetic background, biochemical characterization and ability of the *cbIC* cell lines to perform decyanation of [<sup>57</sup>Co]-CNCbl.**

A summary of the mutations present in the *cbIC* cell lines used in this study and the age of onset of the disease are presented in **Table 3.5**. The three patient *cbIC* cell lines present distinct mutations in the *MMACHC* gene, which led in all cases to a severe impairment of cobalamin metabolism. Total levels of homocysteine and methylmalonic acid were assessed in the conditioned culture medium of normal and *cbIC* mutant fibroblasts grown for 7 days, and are shown in **Table 3.5**. All *cbIC* cell lines excreted increased levels of both Hcy and MMA compared to normal fibroblasts. In addition, all *cbIC* cell lines were unable to decyanate [<sup>57</sup>Co]-CNCbl and synthesize [<sup>57</sup>Co]-MeCbl and [<sup>57</sup>Co]-AdoCbl (**Table 3.5**). In contrast normal fibroblasts performed decyanation and subsequent cofactor biosynthesis efficiently. Patient cell line WG3354 performed decyanation to form HOCbl, however, there was no detectable AdoCbl and MeCbl biosynthesis (**Table 3.5**). Overall, this is the biochemical phenotype expected for combined methylmalonic aciduria and homocystinuria, hence, the *cbIC* patient cell lines selected herein represent a suitable model to investigate the role of the *cbIC* protein in the dealkylation process.

**Table 3.5. Genetic and biochemical background of the *cbfC* patient cell lines used in this study (Hannibal et al. 2009 ).**

Cell line	Mutation 1	Mutation 2	Age of Onset	Metabolites in conditioned culture medium <sup>a</sup>		Decyanation of [ <sup>57</sup> Co]-CNCbl and cofactor biosynthesis (%) <sup>b</sup>			
				Hcy (nmol/mg protein)	MMA (nmol/mg protein)	HOCbl	CNCbl	AdoCbl	MeCbl
Normal	-	-	-	11.2 ± 11.8	0.76 ± 0.07	19.5 ± 3.7	28.9 ± 2.6	25.3 ± 4.8	26.4 ± 1.1
WG1801	c.217C>T	c.217C>T	<2 months	52.8 ± 25.5	6.67 ± 0.09	ND <sup>c</sup>	100	ND	ND
WG2176	c.1-234A>G	c.609G>A	Birth	92.3 ± 23.2	3.57 ± 0.03	ND	100	ND	ND
WG3354	c.435_436delAT	c.435_436delAT	<2 months	48.1 ± 8.1	2.46 ± 0.27	27.9 ± 5.9	72 ± 5.9	ND	ND

<sup>a</sup> Values represent mean ± standard deviation (n=3). Total Hcy and MMA were determined in the conditioned culture medium of cells grown for 7 days. Differences in Hcy and MMA levels between the normal and the *cbfC* mutant cell lines were statistically significant, as determined by Student's t-test at the 95% level of confidence (p<0.05).

<sup>b</sup> Values represent mean ± standard deviation (n=3). Cells were grown in the presence of [<sup>57</sup>Co]-CNCbl for 48 h.

<sup>c</sup>ND: not detectable.

**E. Dealkylation of xenobiotic alkylcobalamins by normal and *cbIC* mutant fibroblasts.**

Because patients with a defective *MMACHC* gene are unable to utilize CNCbl as a substrate for cofactor biosynthesis (Rosenberg, Patel, and Lilljeqvist 1975; Rosenblatt and Fenton 2001; Suormala et al. 2004) (**Table 3.5**), we hypothesized that *cbIC*-derived skin fibroblasts would be incapable of dealkylating newly internalized alkylcobalamins. To test this hypothesis, normal and *cbIC* mutant cell lines were incubated with [<sup>57</sup>Co]-MeCbl (natural Cbl) or with [<sup>57</sup>Co]-PrCbl (xenobiotic Cbl) as described, and after 48 h, the intracellular cobalamin profiles were examined. **Figure 3.10** shows the results obtained from normal and *cbIC* mutant cells grown in the presence of [<sup>57</sup>Co]-MeCbl as the sole Cbl source. While normal fibroblasts utilized [<sup>57</sup>Co]-MeCbl for [<sup>57</sup>Co]-AdoCbl synthesis efficiently, the *cbIC* mutant cell lines performed very little synthesis of [<sup>57</sup>Co]-AdoCbl (**Table 3.6** and **Figure 3.10**).

**Table 3.6. Processing of [<sup>57</sup>Co]-MeCbl by human normal and *cbIC* mutant fibroblasts (Hannibal et al. 2009).**

	% intracellular Cbl <sup>a</sup>			
	HFF	WG1801	WG2176	WG3354
<b>HOcbl</b>	11.3 ± 0.7	7.3 ± 3.2	4.8 ± 0.1	4.9 ± 0.1
<b>Others<sup>b</sup></b>	23.8 ± 4.1	5.6 ± 3.1	3.9 ± 1.6	0.6 ± 0.8
<b>AdoCbl</b>	27.1 ± 2.3	6.9 ± 2.2	7.0 ± 4.2	4.4 ± 1.9
<b>MeCbl</b>	37.8 ± 2.5	80.3 ± 4.3	84.2 ± 5.7	90.2 ± 2.1

<sup>a</sup> Results are expressed as mean ± standard deviation (n = 3).

<sup>b</sup> Cobalamins not quantitatively determined in the present study include glutathionylcobalamin, sulphitocobalamin and nitrocobalamin. See ref (Hannibal et al. 2008).

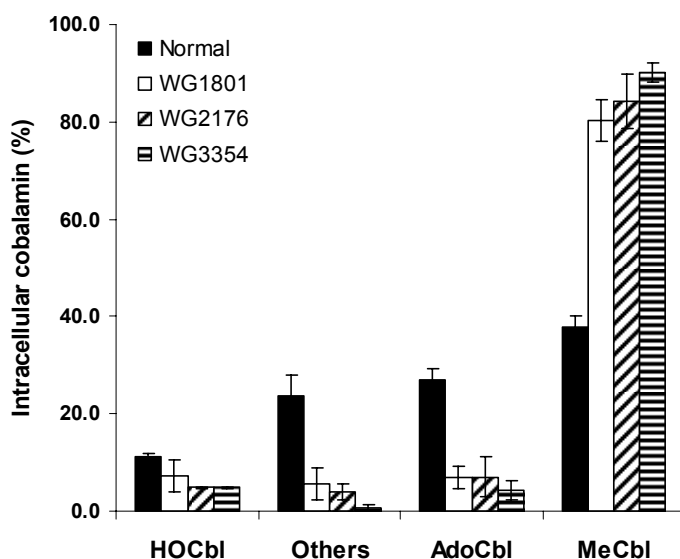


**Figure 3.10. Processing of [ $^{57}\text{Co}$ ]-MeCbl by human normal and *cbIC* mutant fibroblasts (WG1801, WG2176 and WG3354) (Hannibal et al. 2009 ).** Cells were cultured in the presence of 0.125 nM [ $^{57}\text{Co}$ ]-MeCbl (0.06  $\mu\text{Ci/ml}$  culture medium) for 48 h. [ $^{57}\text{Co}$ ]-labeled cobalamins were then extracted and analyzed by HPLC as described (Hannibal et al. 2008).

The ability of normal and *cbIC* fibroblasts to process [ $^{57}\text{Co}$ ]-PrCbl was also investigated. As shown in **Figure 3.11**, there was a much reduced capacity for the *cbIC* mutant lines to convert [ $^{57}\text{Co}$ ]-PrCbl to [ $^{57}\text{Co}$ ]-AdoCbl and [ $^{57}\text{Co}$ ]-MeCbl, and most of the cobalamin in the mutant cells was unprocessed [ $^{57}\text{Co}$ ]-PrCbl. However, normal fibroblasts were efficient at converting [ $^{57}\text{Co}$ ]-PrCbl into [ $^{57}\text{Co}$ ]-MeCbl, the predominate form, and, to a lesser extent, [ $^{57}\text{Co}$ ]-AdoCbl (**Figure 3.11**). These results are consistent with a role for the *cbIC* protein in removing alkyl groups from the  $\beta$ -axial ligand position of alkylcobalamins.

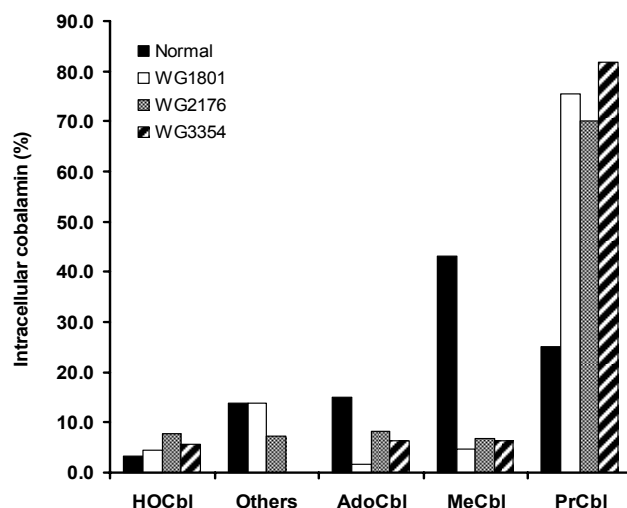


**Figure 3.11. Processing of [ $^{57}\text{Co}$ ]-PrCbl by human normal and *cbIC* mutant fibroblasts (WG1801, WG2176 and WG3354) (Hannibal et al. 2009 ).** Cells were cultured in the presence of 0.125 nM [ $^{57}\text{Co}$ ]-PrCbl (0.06  $\mu\text{Ci/ml}$  culture medium) for 48 h. [ $^{57}\text{Co}$ ]-labeled cobalamins were then extracted and analyzed by HPLC as described (Hannibal et al. 2008). Results represent two pooled samples per cell line. “Others” refers to cobalamins not quantitatively determined in the present study, which include glutathionylcobalamin, sulphitocobalamin and nitrocobalamin (See ref (Hannibal et al. 2008)).

## SUMMARY

The primary objective of the current work was to demonstrate that mammalian cells are capable of processing alkylcobalamins and to provide evidence that the processing is mediated by the *cbIC* protein. BAEC were used for assessing dealkylation processing and conversion to AdoCbl and MeCbl. The vascular endothelium appears to play important roles in cobalamin homeostasis. For example, endothelial cells synthesize and secrete considerable amounts of TC, the serum B<sub>12</sub>-binding protein that delivers the vitamin to cells throughout the body (Quadros, Rothenberg, and Jaffe 1989). However, there is little information on

cobalamin processing and coenzyme biosynthesis by vascular endothelial cells. We hypothesized that the vascular endothelium is able to utilize CNCbl and alkylcobalamins as substrates for the synthesis of AdoCbl and MeCbl and that the *cbfC* protein recently shown to catalyze the *in vitro* decyanation of CNCbl (Kim, Gherasim, and Banerjee 2008), also catalyzes the dealkylation of alkylcobalamins in BAEC.

Our results demonstrate that cultured BAEC convert CNCbl to both AdoCbl and MeCbl. The amount of AdoCbl synthesized is always greater than the amount of MeCbl synthesized (**Table 3.3**). However, there was considerable variation in the AdoCbl/MeCbl product ratio depending on the substrate. When HOCbl and CNCbl were used as substrates, the AdoCbl/MeCbl product ratio was 12.9 and 4.5, respectively. Next, we assessed the ability of BAEC to utilize AdoCbl as a substrate for the biosynthesis of MeCbl as reported for cultured human lymphocytes several years ago (Quadros et al. 1979). Since AdoCbl and MeCbl are naturally occurring alkylcobalamins in circulation (Gimsing 1983; Gimsing, Nexø, and Hippe 1983), BAEC must have a system for dealkylating these endogenous alkylcobalamins that are delivered to the cell. We find that BAEC are indeed capable of converting AdoCbl to MeCbl.

We then determined whether the putative “dealkylase” activity would remove other alkyl groups from the  $\beta$ -axial position of cobalamins. Xenobiotic straight-chain alkylcobalamins were synthesized and purified, ranging from  $\text{CH}_3\text{CH}_2$ - (ethylcobalamin) to  $\text{CH}_3(\text{CH}_2)_5$ - (hexylcobalamin). None of the alkylcobalamins appeared to be cytotoxic to cultured BAEC. Surprisingly, all of the xenobiotic alkylcobalamins served as substrates for the synthesis of AdoCbl and MeCbl with AdoCbl/MeCbl product ratios ranging from 4.0 to 10.7 (**Table 3.4**). While our study demonstrates that the dealkylase system has broad

substrate specificity for the ligand coordinating at the  $\beta$ -axial position of the cobalamin molecule, it does not address whether this activity is associated with one or more proteins.

The mystery of how decyanation of CNCbl occurs was recently solved by the *in vitro* studies of Kim et al. (Kim, Gherasim, and Banerjee 2008). Decyanation is a process that is dependent on the activity of the *cbIC* protein. The protein is a monomer of ~29 kDa, which catalyzes the reductive decyanation of CNCbl using a flavoprotein oxidoreductase for transferring reducing equivalents from NADPH (Kim, Gherasim, and Banerjee 2008). Human fibroblasts that carry mutations in the *MMACHC* gene exhibit impaired cobalamin processing of CNCbl and little or no AdoCbl and MeCbl biosynthesis (Rosenblatt et al. 1997; Suormala et al. 2004). Three *cbIC* mutant fibroblasts isolated from severely ill and genetically unrelated patients were used in the present study to assess dealkylation *in vivo*. The biochemical profile of the *cbIC* mutant cell lines WG1801, WG2176 and WG3354 resembled that reported for other *cbIC* cell lines, i.e., substantial export of Hcy and MMA into culture medium (indicative of functional cobalamin deficiency) and poor or negligible utilization of CNCbl as a substrate for cofactor biosynthesis. The inability of the *cbIC* mutant fibroblasts to utilize [ $^{57}\text{Co}$ ]-PrCbl as a substrate for AdoCbl and MeCbl biosynthesis is consistent with the hypothesis that the *cbIC* protein catalyzes the dealkylation. In contrast, normal fibroblasts were able to use PrCbl efficiently to generate both AdoCbl and MeCbl. Based on the observations that 1) human recombinant *MMACHC* catalyzes decyanation of CNCbl (Kim, Gherasim, and Banerjee 2008); 2) *cbIC* mutant fibroblasts are unable to utilize CNCbl as a substrate for coenzyme biosynthesis (Rosenblatt 2001; Suormala et al. 2004); and, 3) *cbIC* mutant fibroblasts are unable to perform dealkylation of [ $^{57}\text{Co}$ ]-PrCbl (this

study), we propose that the *cbIC* protein is responsible for catalyzing the removal of alkyl groups from the  $\beta$ -ligand position of alkylcobalamins.

The phenotypic expression of combined hyperhomocysteinemia and methylmalonicacidemia is associated with patients from the *cbIF*, *cbIC* and *cbID* complementation groups. Of these, *cbIF* is unlikely to be a dealkylase since its impairment leads to accumulation of newly internalized B<sub>12</sub> in lysosomes (Rosenblatt et al. 1985; Watkins and Rosenblatt 1986; Shih et al. 1989). Recent work now shows that the *cbIF* gene product is a B<sub>12</sub> lysosomal membrane transporter (Rutsch et al. 2009). The *cbID* locus is complex since it can lead to either isolated or combined defects in methionine synthase and methylmalonyl-CoA mutase (Suormala et al. 2004; Coelho et al. 2008) and, for this reason, is also unlikely to encode a dealkylase that is shared by both AdoCbl and MeCbl synthesis pathways. Hence, the *cbIC* locus appears to be the most likely candidate for encoding an alkylcobalamin dealkylase function.

The current work shows that newly internalized alkylcobalamins undergo dealkylation processing, a likely prerequisite for generating the biologically active cobalamin forms AdoCbl and MeCbl, and that the *dealkylase* activity requires the *cbIC* protein. In light of our results and previous findings, alternative mechanisms for cobalamin processing *in vivo* should be considered. Our current thoughts on the possible mechanisms by which the *cbIC* protein could process newly internalized natural and xenobiotic alkylcobalamins are summarized in **Figure 3.12**. Binding of the natural alkylcobalamins MeCbl and AdoCbl to the *MMACHC* chaperone has been shown to induce the “base-off” conformation in which the  $\alpha$ -axial dimethylbenzimidazole ligand is not coordinated to the cobalt. This could be important in enhancing the reactivity of the  $\beta$ -axial ligand [6]. A variety of mechanistic

alternatives can be considered for the removal of an alkyl group from the  $\beta$ -axial position of cobalamins (**Figure 3.12**). First, homolysis of the cobalt-carbon bond would generate cob(II)alamin and an alkyl radical (*Reaction 1*, **Fig. 3.12**). Second, nucleophilic displacement of the alkyl group would result in the formation of cob(I)alamin and the transfer of the alkyl carbocation to the acceptor (*Reaction 2*, **Fig. 3.12**) (Hogenkamp, Bratt, and Sun 1985; Hogenkamp, Bratt, and Kotchevar 1987). Third, reductive dealkylation could occur resulting in the formation of either cob(II)alamin or cob(I)alamin and the departure of the alkyl group as a carbanion or a radical, respectively (*Reactions 3 and 4*, **Fig. 3.12**). A number of *in vitro* studies with human recombinant *cbIC* protein are currently underway in our laboratories to elucidate the mechanism of dealkylation catalyzed by the surprisingly versatile *cbIC* protein.

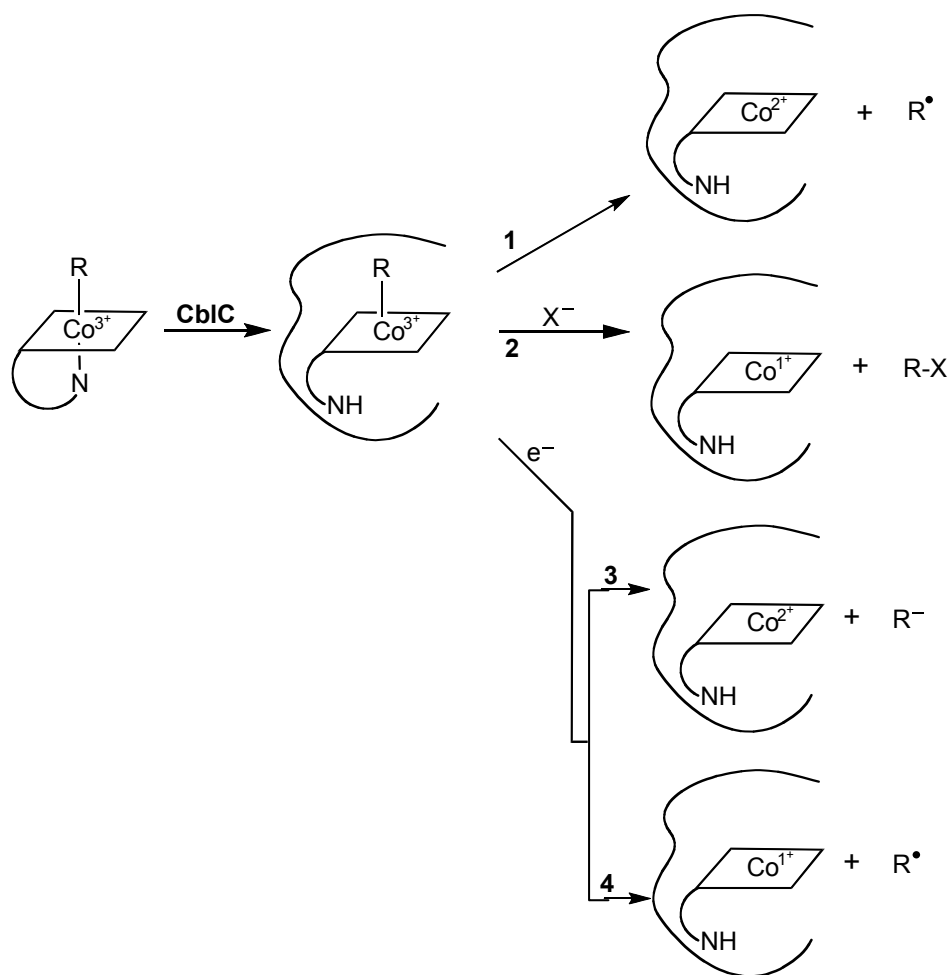


**Figure 3.12. Possible mechanisms for the dealkylation of alkylcobalamins mediated by the *cblC* protein.** Formation of the base-off conformation of the cobalamin leads to an enhanced reactivity of the upper axial ligand. *Reaction 1*: homolysis of the cobalt-carbon bond would generate cob(II)alamin and an alkyl radical. *Reaction 2*: nucleophilic displacement of the alkyl group would result in the formation of cob(I)alamin and the transfer of the alkyl carbocation to the acceptor as described by model studies (Hogenkamp, Bratt, and Sun 1985; Hogenkamp, Bratt, and Kotchevar 1987). *Reactions 3 and 4*: reductive dealkylation could occur resulting in the formation of either cob(II)alamin or cob(I)alamin and the departure of the alkyl group as a carbanion or a radical, respectively (Hannibal et al. 2009).

## MATERIALS AND METHODS

**Synthesis and purification of ethylcobalamin (EtCbl), propylcobalamin (PrCbl), butylcobalamin (BuCbl), pentylcobalamin (PnCbl) and hexylcobalamin (HxCbl).** Xenobiotic alkylcobalamins were synthesized by the reaction of cob(I)alamin with the corresponding alkylhalide (Kim et al. 1988; Pratt 1972). Cob(I)alamin was generated by reduction of CNCbl (Sigma) with 10 equivalents of sodium borohydride (NaBH<sub>4</sub>, Sigma). Before addition of the alkylhalide, excess NaBH<sub>4</sub> was eliminated by reaction with excess anaerobic acetone. The syntheses were carried out by a bolus addition of the alkylhalide [ethylbromide for EtCbl, propylbromide for PrCbl, butyliodide for BuCbl, pentylbromide for PnCbl and hexyliodide for HxCbl (all from Sigma-Aldrich)] to the cob(I)alamin solution, followed by rapid mixing of the reactants for 10 min at room temperature using dim-red light under anaerobic conditions. Alkylcobalamins were then purified by gradient reverse-phase HPLC using an Agilent 1100 System equipped with a Zorbax SB C-18 column (4.6 x 250 mm, 5 µm particle size, Agilent). Solvent A contained 0.1% acetic acid/acetate buffer titrated to pH 3.50 with NH<sub>4</sub>OH and Solvent B was acetonitrile (100%) containing 0.1% acetic acid. Gradient conditions were as follows: 0-2 min, 10% B; 2-14 min, 70 % B; 14-15 min, 70% B; 15-16 min, 10% B; 16-17 min, 10% B, at a flow rate of 1 mL/min. Retention times were: MeCbl, 8.2 min; EtCbl, 9.1 min; PrCbl, 9.5 min; BuCbl, 9.9 min; PnCbl, 10.3 min and HxCbl, 10.8 min (**Chapter 2, Figure 2.27**). Products collected after HPLC separation were dried using a Speedvac, resuspended in PBS and sterilized by filtration (Millipore 0.22 µm) before addition to the cell cultures. [<sup>57</sup>Co]-Alkylcobalamins were synthesized as described above using [<sup>57</sup>Co]-CNCbl (MP Biomedicals, Solon, OH) as the starting material (specific

activity: 379  $\mu\text{Ci}/\mu\text{g}$ ). 5'-Chloro-5'-deoxyadenosine, synthesized as described by Jacobsen et al. [12], was used to synthesize [ $^{57}\text{Co}$ ]-AdoCbl.

**Cell culture lines and [ $^{57}\text{Co}$ ]-cobalamin metabolic labeling.** Bovine aortic endothelial cells (BAEC) were cultured in 162  $\text{cm}^3$  flasks (Corning) and grown in vitamin B<sub>12</sub>-free, folic acid-free Ham's F12/DME (1:1) medium supplemented with 5% FBS, 2.0 mM L-glutamine, penicillin (100 units/mL), streptomycin (0.1 mg/ml) and 50 nM (6S)-N<sup>5</sup>-methyltetrahydrofolic acid (Eprova AG). The amount of cobalamin present in the 5% FBS-supplemented culture medium (33 pM) was shown to be sufficient to support normal growth of BAEC. Normal and *cbIC* mutant fibroblasts were grown in Advanced DMEM (Gibco) culture medium supplemented with 10% FBS (final cobalamin concentration, 66 pM). Note: the concentration of folic acid in the culture medium is 9.07  $\mu\text{M}$ . For [ $^{57}\text{Co}$ ]-Cbl metabolic labeling experiments, cells were passaged at a ratio of 1:2. [ $^{57}\text{Co}$ ]-CNCbl was added to achieve a final concentration of 0.2 nM, and cells were grown to 100% confluency (~48 h).

***cbIC* patient cell lines.** Dr. David Watkins, McGill University, kindly provided human *cbIC* mutant skin fibroblasts from patients with severe disease (WG1801, WG2176 and WG3354). The Repository for Mutant Human Cell Strains, Montreal Children's Hospital, Montreal, Canada (<http://www.cellbank.mcgill.ca/>) provided patient information on the *cbIC* lines. Patient WG1801 was a 2 month-old male of Turkish ethnicity, son of first cousins, with two brothers who were possible carriers of the inborn error. Patient WG2176 was a 7-month old male of Hong Kong Chinese ethnicity with a healthy older sister and an affected fetal brother who was aborted. Patient WG3354 was a female of Pakistani ethnicity with both parents and younger siblings heterozygous for the *cbIC* mutation.

**Assessment of dealkylation in BAEC and human fibroblasts.** Cells were passaged at a ratio of 1:2 in medium containing 0.125 nM (specific activity: 379 mCi/mg) of the desired [<sup>57</sup>Co]-cobalamin. After 48 h, cells were harvested, total cobalamins extracted with 80% aqueous ethanol and the intracellular cobalamin profile determined as recently described by Hannibal et al. (Hannibal et al. 2008). The cell cultures were protected from light at all times to prevent photolysis of the alkylcobalamins.

**Stability of [<sup>57</sup>Co]-alkylcobalamins in the culture medium.** Conditioned medium (1 ml) from 48-h old cultures was extracted with a 1:1 mixture of phenol/chloroform, taken to dryness in a Speedvac, reconstituted with 0.4 ml of phosphate-buffered saline (PBS). Cobalamin standards were added to the sample, the mixture was filtered (0.22 µm filter) and analyzed by HPLC as previously described (Hannibal et al. 2008). Workup of the conditioned culture medium was conducted under dim-red light.

**Extraction and analysis of intracellular cobalamins.** Confluent cells were harvested by trypsinization and washed three times with Dulbecco's PBS. Extraction of cobalamins from cell pellets was performed as previously described (Hannibal et al. 2008). Extracted [<sup>57</sup>Co]-cobalamins were mixed with unlabeled cobalamin standards and separated by gradient reverse-phase HPLC using an Agilent 1100 System equipped with a Zorbax SB C-18 column (4.6 x 250 mm, 5 µm particle size, Agilent) as previously described (Hannibal et al. 2008). Elution was monitored with UV detection at 254 nm. In typical runs, 60 fractions were collected. The radioactivity associated with each fraction was counted using a gamma-counter (Gamma 4000 Beckman-Coulter).

**Cobalamin uptake studies.** Cells were seeded at an initial density of ~50% and allowed to grow for 24 h. After 24 h, half of the conditioned culture medium was replaced

with fresh medium and [ $^{57}\text{Co}$ ]-CNCbl added to a final concentration of 0.2 nM (specific activity: 379  $\mu\text{Ci}/\text{mg}$ ). Uptake was followed by counting the radioactivity in a  $\gamma$ -counter at 6, 12, 24, 48 and 72 h, both in spent medium and in washed cell pellets. Total cobalamin values were normalized to cellular protein concentration.

**Cytotoxicity.** To rule out cytotoxic effects of the xenobiotic alkylcobalamins under our culture conditions, BAEC were grown in the presence of 1  $\mu\text{M}$  of each of the xenobiotic alkylcobalamins (supraphysiological concentration) as the major source of cobalamin for two weeks, with medium plus fresh alkylcobalamin changes every three days. Morphological changes were monitored by phase-contrast microscopy. To assess for cobalamin deficiency, total homocysteine and methylmalonic acid concentrations were determined in the conditioned culture medium. Cell number and cell viability were determined by hemocytometry and the 3-(4,5-dimethylthiazol-2-yl)-2,5-diphenyltetrazolium bromide (MTT) assay (Mosmann 1983), respectively. Cellular senescence was assessed by determining  $\beta$ -galactosidase activity using a commercial kit (Sigma).

**Biochemical analyses.** Total homocysteine in conditioned culture medium was determined by the method of Jacobsen et al. using monobromobimane and HPLC with fluorescence detection (Jacobsen et al. 1994). Values were normalized to cellular protein concentration. The concentration of methylmalonic acid in conditioned culture medium was determined by gas chromatography and mass spectrometry (GC/MS) in the Department of Clinical Pathology, Cleveland Clinic by a method modified from Hoffmann et al (Hoffmann et al. 1989). Total protein concentration was determined by the bicinchoninic acid assay (Thermo Scientific) using bovine serum albumin as a standard.

### 3.3 **Project 3: Dealkylation of alkylcobalamins by the *MMACHC* (*cbIC*) gene product: *in vitro* studies.**

#### INTRODUCTION

The *MMACHC* gene product of the *cbIC* complementation group, referred to as the *cbIC* protein, catalyzes the *in vitro* and *in vivo* decyanation of cyanocobalamin (vitamin B<sub>12</sub>). We hypothesized that the *cbIC* protein would also catalyze the *dealkylation* of newly internalized methylcobalamin (MeCbl) and 5'-deoxyadenosylcobalamin (AdoCbl), the naturally occurring *alkylcobalamins* that are present in the diet. In **Project 2** we described, for the first time, that the *cbIC* protein is required for the processing of upper axial ligands that are bound to the Co center through a Co-C bond (alkylcobalamins). A recent study by Kim and Banerjee showed that the *CbIC* protein binds both MeCbl and AdoCbl and induces the base-off conformation of both natural alkylcobalamins. However, no dealkylation was observed under the conditions required for the decyanation of CNCbl. This suggested that: a) the *cbIC* protein was not responsible for dealkylating the natural cofactors, or b) the *cbIC* protein is responsible for the dealkylation of alkylcobalamins, however, the chemistry of these reactions differs substantially from what has been described for the decyanation of CNCbl.

In order to decipher this new mystery, we embarked in a series of *in vitro* experiments in collaboration with the laboratory of Dr. Ruma Banerjee, at Ann Arbor, University of Michigan. **Project 3** describes a series of *in vitro* experiments done with human recombinant *cbIC* protein and a series of alkylcobalamins (MeCbl, AdoCbl and the MeCbl analogs that

were investigated in *Project 2*) as substrates for dealkylation. Part of this work is in preparation for publication (Kim et al. 2009).

## RESULTS AND DISCUSSION

### A. Dealkylation of MeCbl and AdoCbl *in vitro*.

The reaction of MeCbl and AdoCbl with the *cbiC* protein has been reexamined. The results obtained in *Project 2* on the processing of alkylcobalamins by cultured normal and *cbiC* fibroblasts in addition to the observation that *in vitro*, the *cbiC* protein induces the base-off conformation of MeCbl and AdoCbl suggests that *cbiC* could be involved in the dealkylation of dietary cobalamins *in vivo*. Studies carried out by the laboratory of Dr. Banerjee at Ann Arbor, University of Michigan showed that the *cbiC* protein binds

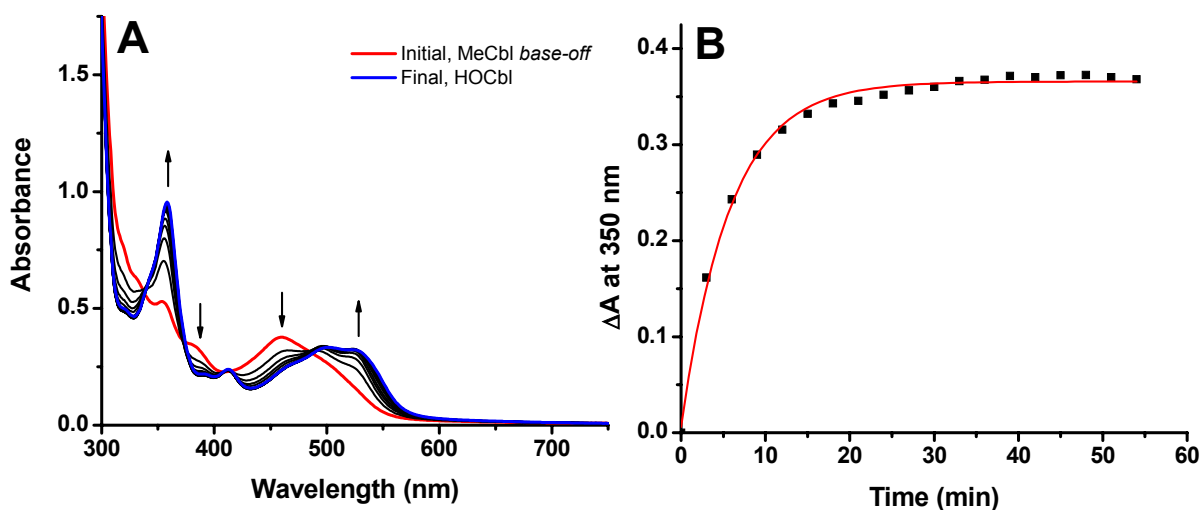


**Figure 3.13. Dealkylation of MeCbl by *CbiC* in the presence of GSH.** **A.** Kinetics of conversion of MeCbl into HOCbl (in the presence of air). **B.** Time course for the formation of HOCbl at 350 nm. Conditions: [*cbiC* protein] = 100  $\mu$ M, [Cbl] = 30  $\mu$ M, [GSH] = 1.0 mM, 100 mM HEPES, pH 8.0, 150 mM KCl, 10% glycerol, T = 20  $^{\circ}$ C (Kim et al. 2009).

glutathione tightly, although it was not required for the decyanation of CNCbl. It was then discovered that GSH is required for the removal of alkyl groups from the cofactors MeCbl and AdoCbl. In the presence of excess GSH MeCbl bound to *cbIC* undergo dealkylation to form HOCbl (**Figure 3.13**, panel **A**). A time course for the reaction is given in **Figure 3.13**, panel **B**.

In the absence of oxygen, the reaction products are cob(I)alamin and S-methylglutathione. In the presence of oxygen cob(I)alamin is oxidized to HOCbl/H<sub>2</sub>O Cbl<sup>+</sup>. The rate of the reaction (determined in the presence of air) was 0.1956 min<sup>-1</sup>.

The reaction with AdoCbl as a substrate was studied under the same conditions. The kinetics and time course plots are given in **Figure 3.14**, panels **A** and **B** respectively. Interestingly, AdoCbl bound to *cbIC* displays a substantially slower reaction than that observed for MeCbl. The rate constant was calculated to be 0.00129 min<sup>-1</sup>.

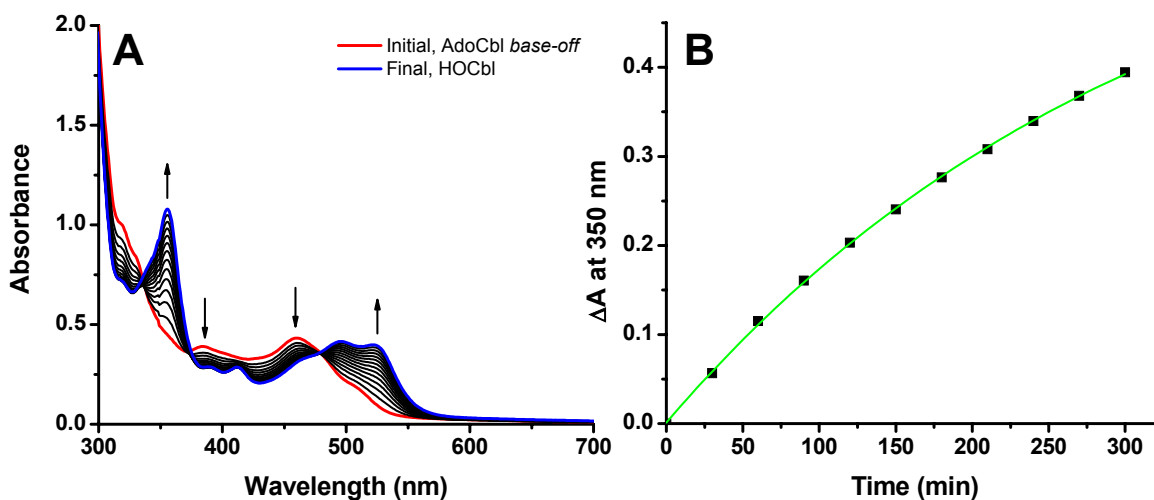


**Figure 3.14. Dealkylation of AdoCbl by *cbIC* in the presence of GSH.** **A.** Kinetics of conversion of AdoCbl into HOCbl (in the presence of air). **B.** Time course for the formation of HOCbl at 350 nm. Conditions: [*cbIC* protein] = 100 μM, [Cbl] = 30 μM, [GSH] = 1.0 mM, 100 mM HEPES, pH 8.0, 150 mM KCl, 10% glycerol, T = 20 °C (Kim et al. 2009).

Our results confirm that, in addition to decyanation of CNCbl, the *cbiC* protein is also capable of performing dealkylation of the natural cofactors MeCbl and AdoCbl. This finding strengthens the biological relevance of these reactions as the two cofactors represent the most abundant Cbl forms present in the human diet (unprocessed foods such as meat, eggs, milk, etc), therefore, the most likely candidate substrates for dealkylation *in vivo*.

Because our cell culture studies suggested that the intracellular machinery responsible for dealkylation of cobalamins displayed broad specificity for its substrates, I decided to investigate: **a)** the ability of the *cbiC* protein to bind the MeCbl analogs EtCbl, PrCbl, BuCbl, PnCbl and HxCbl as it is observed for the natural cofactors, and **b)** the ability of the *CbiC*/GSH system to catalyze the removal of the upper axial ligand.

### **B. Binding of the *cbiC* protein to analogs of MeCbl.**

We found that incubation of the *cbiC* protein with the MeCbl analogs EtCbl, PrCbl, BuCbl, PnCbl and BuCbl generates the base-off conformation of the cobalamin molecule rapidly (less than 30 seconds). **Figure 3.15** shows the spectra of EtCbl in its free form in solution (free) and upon addition of *cbiC* (*+cbiC*). The inset shows the UV-visible spectrum of authentic base-off EtCbl, at pH 1.5.

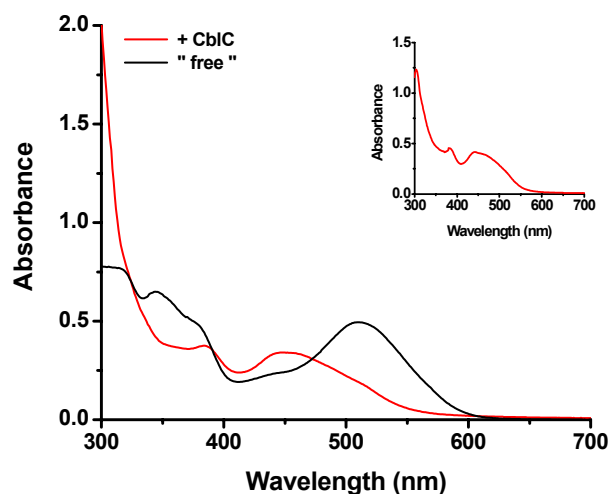


**Figure 3.15. Binding of *cbIC* to EtCbl and induction of the base-off conformation.** Addition of *cbIC* to a solution of EtCbl rapidly converts the Cbl to its base-off conformation. Conditions: [*cbIC* protein] = 50  $\mu$ M, [Cbl] = 30  $\mu$ M, 100 mM HEPES, pH 8.0, 150 mM KCl, 10% glycerol, T = 20  $^{\circ}$ C. Inset: UV-visible spectrum of authentic base-off EtCbl at pH 1.50 (Kim et al. 2009).

The *cbIC* protein appeared to bind all the MeCbl analogs tested herein indistinctively, suggesting that an increase in the size of the upper axial ligand does not affect the ability of the protein to bind Cbl and induce its base-off conformation.

### C. Dealkylation of MeCbl analogs by *cbIC* and GSH.

The fact that *cbIC* binds a series of MeCbl analogs regardless of the identity of the upper axial ligand made it of interest to investigate whether the enzyme would be capable of dealkylating foreign cobalamins. The reaction of *cbIC*-RCbl with GSH was carried out under the same conditions tested for the dealkylation of the natural cofactors.

**Figure 3.16, panel A** shows a representative reaction for the dealkylation of EtCbl. **Figure 3.16, panel B** shows a time course for the reaction. *cbIC* catalyzes the dealkylation of

EtCbl to form HOCbl. The reaction was an order of magnitude slower than the removal of the methyl group from MeCbl.

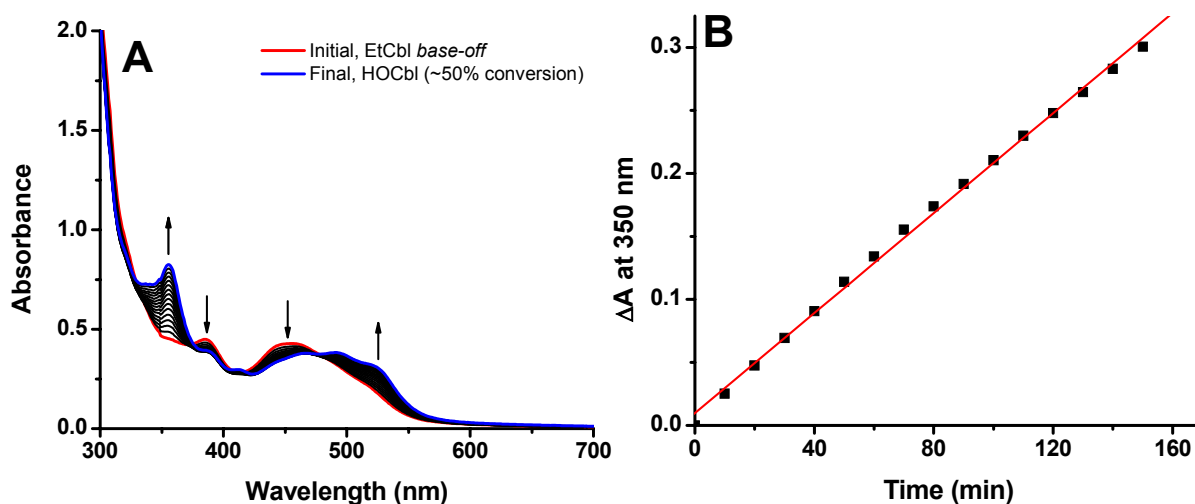


**Figure 3.16. Dealkylation of EtCbl by the *CblC*/GSH system.** Base-off EtCbl reacts with GSH to form HOCbl. Conditions: [*cblC* protein] = 50  $\mu$ M, [Cbl] = 30  $\mu$ M, [GSH] = 1.0 mM, 100 mM HEPES, pH 8.0, 150 mM KCl, 10% glycerol, T = 20  $^{\circ}$ C (Kim et al. 2009).

Interestingly, the rate of dealkylation decreased with increasing size of the upper axial ligand in the Cbl molecule. **Figure 3.17**, panels **A** and **B** presents the kinetic plot and time course, respectively, for the dealkylation of *cblC*-HxCbl with GSH. The spectral changes were rather modest, and at long incubation times, the *cblC* protein precipitated making the study of the slower reactions very difficult. The product of the reaction is presumably HOCbl, although this could not be assessed accurately since the reaction did not progress to an extent such that the Cbl product could be unequivocally identified.

Another feature of the reaction of the higher alkylcobalamins with the *cblC*/GSH system was the presence of a lag phase during the first 30 minutes of the reaction after

addition of GSH (see **Figure 3.17**, panel **B**). At present, we do not have a clear explanation for this observation. Our current thoughts on this will be discussed in the next section.

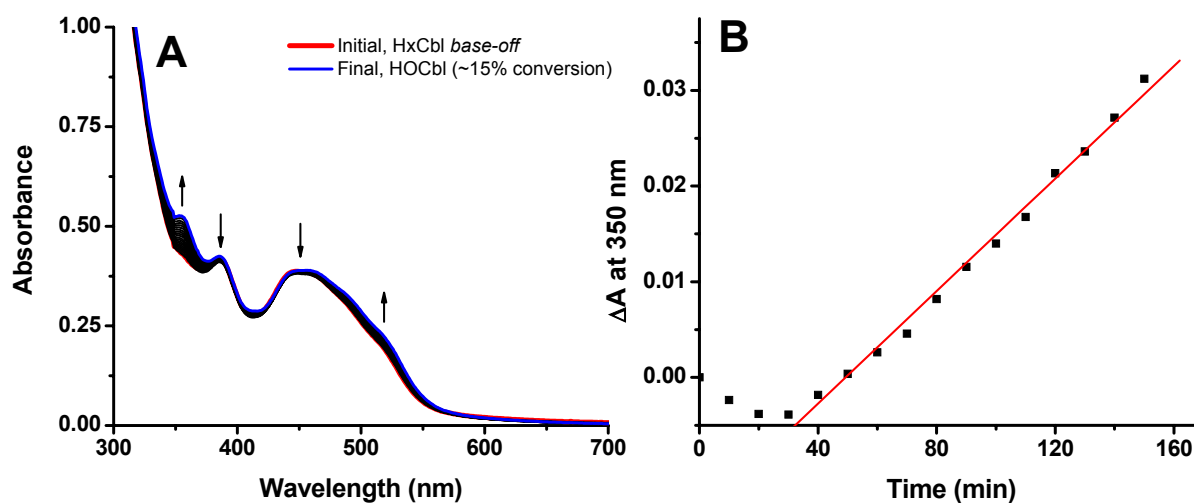


**Figure 3.17. Dealkylation of HxCbl by the *cbIC*/GSH system.** Base-off HxCbl reacts with GSH to form presumably HOCbl. Conditions:  $[CbIC] = 50 \mu\text{M}$ ,  $[Cbl] = 30 \mu\text{M}$ ,  $[GSH] = 1.0 \text{ mM}$ , 100 mM HEPES, pH 8.0, 150 mM KCl, 10% glycerol,  $T = 20 \text{ }^\circ\text{C}$  (Kim et al. 2009).

**Table 3.7** and **Figure 3.18** summarize the reaction rates obtained for the entire series of MeCbl analogs.

**Table 3.7. Dealkylation rates for the natural cofactors and a series of MeCbl analogs.**

Cbl	Rate ( $\text{min}^{-1}$ )
MeCbl	0.2065
EtCbl	0.0290
PrCbl	0.0023
BuCbl	0.0007
PnCbl	0.0004
HxCbl	0.0004
AdoCbl	0.0025

Conditions: [*cbiC* protein] = 50  $\mu\text{M}$ , [Cbl] = 30  $\mu\text{M}$ , [GSH] = 1.0 mM, 100 mM HEPES, pH 8.0, 150 mM KCl, 10% glycerol, T = 20  $^{\circ}\text{C}$  (Kim et al. 2009).

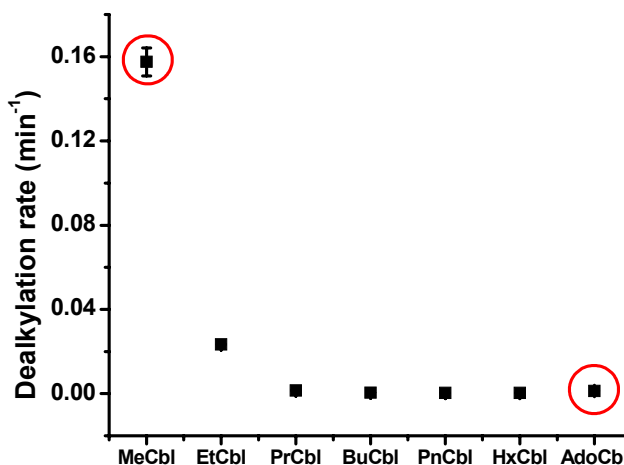


**Figure 3.18. Dealkylation rates of natural and foreign alkylcobalamins by the *CbiC*/GSH system.** Conditions: [*cbiC* protein] = 50  $\mu\text{M}$ , [Cbl] = 30  $\mu\text{M}$ , [GSH] = 1.0 mM, 100 mM HEPES, pH 8.0, 150 mM KCl, 10% glycerol, T = 20  $^{\circ}\text{C}$  (Kim et al. 2009).

Our results indicate that MeCbl is the preferred substrate for the *cbiC*/GSH system and that an increase in the length of the alkyl chain of upper axial ligand in Cbls leads to a reduced efficiency of the *cbiC*/GSH system to perform dealkylation. One factor contributing to the observed trends in the dealkylation rates could be that the transfer of higher alkyl groups to GSH is more difficult than it is for a methyl moiety. This probably holds true for bulky groups like 5'-deoxyadenosine in AdoCbl. In addition, we can speculate on the role of at least two important conformational features that could be restricted to the size of the upper axial ligand. For example, the steric hindrance provoked by bulky ligands (compared to MeCbl) may alter the conformation required for catalysis without altering the ability of *cbiC*

to bind Cbl and induce the base-off conformation. On the other hand, positioning of the higher alkylcobalamins could limit the access of GSH to its binding site, thus impeding the nucleophilic attack of the Co-C bond.

#### **D. Identification of the reaction products by mass spectrometry.**

The Cbl products of the dealkylation reaction are cob(I)alamin and HOCbl under anaerobic and aerobic conditions, respectively. This could be followed by UV-visible spectrophotometry. We hypothesized that the alkyl upper ligand is transferred to glutathione, to produce the corresponding thioether. To determine the identity of the reaction products, dealkylation reaction mixtures were subjected to a partial clean-up HPLC procedure (to eliminate HEPES buffer, KCl and glycerol) and analyzed by mass spectrometry. **Figure 3.19 panels A and B** shows the spectra of the products found in a reaction mixture for the dealkylation of MeCbl. GSH (exact mass 307.08) and Me-SG were identified (mass 321.10).

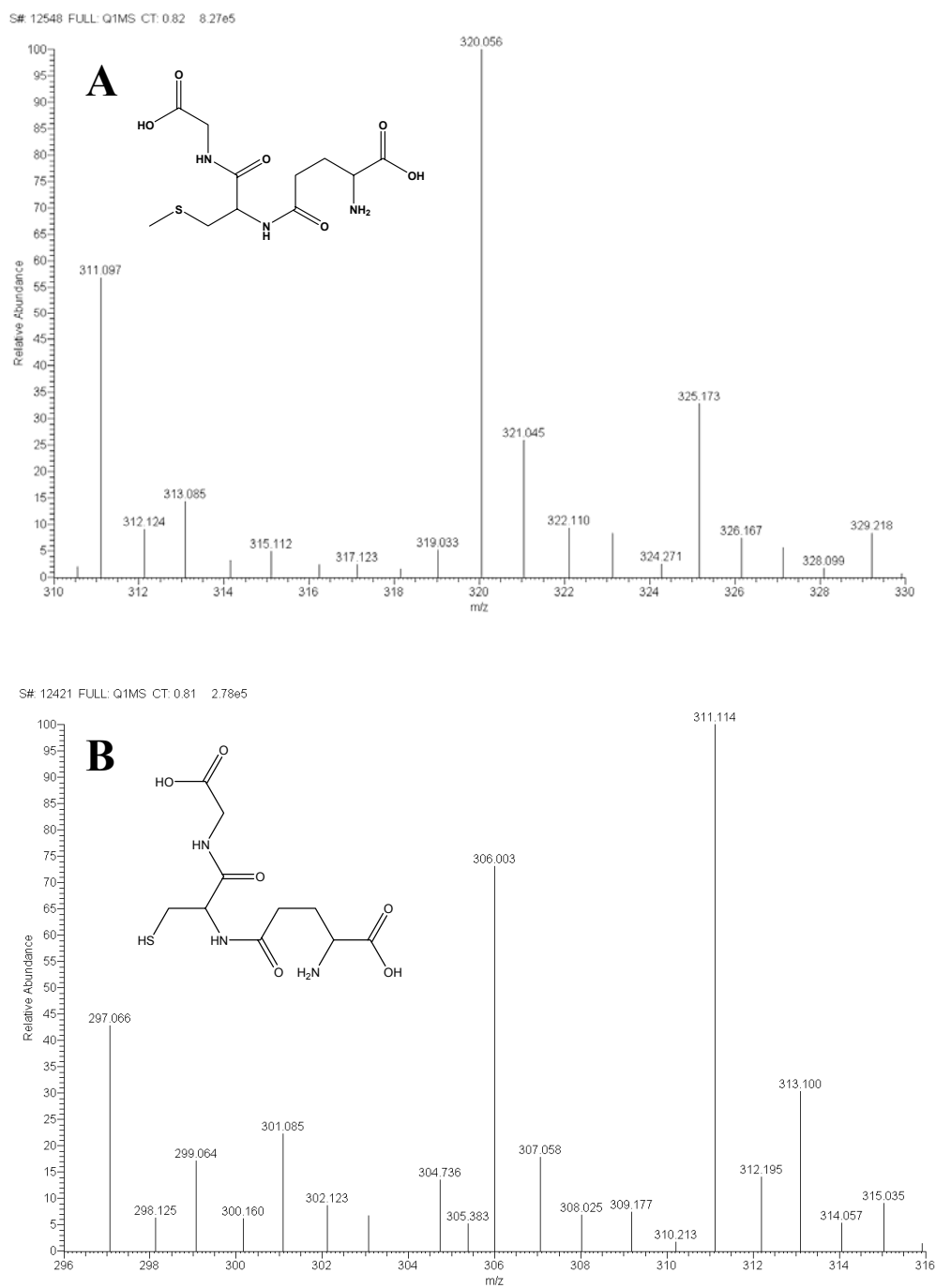


**Figure 3.19.** Identification of Me-SG as a product of the dealkylation of MeCbl catalyzed by *cbiC* protein. **A.** Spectrum (negative mode) showing the mass expected for Me-SG. **B.** Spectrum (negative mode) showing the mass expected for GSH (Kim et al. 2009).

Similarly, dealkylation of AdoCbl resulted in the transfer of the 5'-deoxyadenosyl group to glutathione, to generate Ado-SG (exact mass 556.17).

Based on these results, we propose that dealkylation of alkylcobalamins occurs through nucleophilic attack of the thiolate on the alkyl group to generate cob(I)alamin and the corresponding thioether, as originally proposed in **Figure 3.12**, *Reaction 2* of this chapter. We found that the thiolate form of glutathione operates as the nucleophile, hence the following reaction is proposed (**Figure 3.20**):

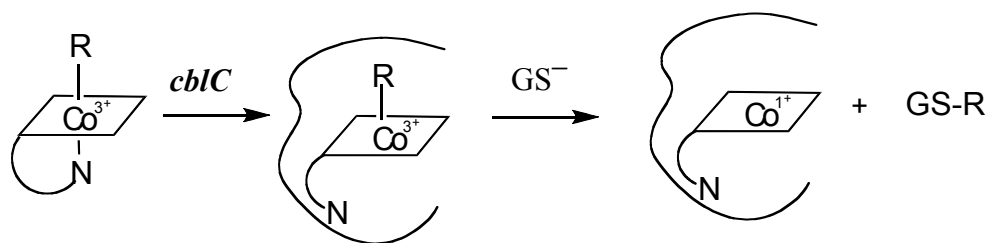


**Figure 3.20. A mechanism for the biological dealkylation of alkylcobalamins.** Nucleophilic displacement of the alkyl group results in the formation of cob(I)alamin and the transfer of the alkyl carbocation to the acceptor as described by model studies (Hogenkamp, Bratt, and Sun 1985; Hogenkamp, Bratt, and Kotchevar 1987).

## SUMMARY

A new function has been uncovered for the *MMACHC* gene product or *cbIC*: dealkylation of MeCbl and AdoCbl catalyzed by GSH. We observed that normal cells in culture could interconvert AdoCbl and MeCbl, demonstrating that mammalian cells possess the machinery for the processing of Co-C bonds in alkylcobalamins and carrying out the biosynthesis of the cofactors. The intracellular component/s involved in the dealkylation displayed broad specificity for the cobalamin substrate provided to the cell culture as the sole

source of Cbl. BAEC were able to utilize EtCbl, PrCbl, BuCbl, PnCbl and HxCbl as substrates for both MeCbl and AdoCbl biosynthesis.

The dealkylation was then examined *in vivo* in normal human and *cbIC* mutant fibroblasts, to assess whether the *cbIC* protein was required for the dealkylation of alkylcobalamins such as it is required for the decyanation of CNCbl. While normal human fibroblasts performed dealkylation of both [<sup>57</sup>Co]-MeCbl (natural) and [<sup>57</sup>Co]-PrCbl (foreign), all of the *cbIC* mutant cell lines displayed impaired or negligible dealkylation and cofactor biosynthesis. This was the first piece of evidence suggesting that the *MMACHC* gene product is required for dealkylation of dietary cobalamins.

A series of *in vitro* experiments utilizing human recombinant *MMACHC* followed, in collaboration with the laboratory of Dr. Ruma Banerjee. We found that the *cbIC* protein catalyzed the dealkylation of MeCbl and AdoCbl in the presence of excess reduced glutathione. Demethylation of MeCbl was much faster than the removal of the 5'-adenosyl group from AdoCbl. In addition, we examined the ability of *cbIC* to dealkylate the series of MeCbl analogues previously described in **Project 2**. *cbIC* catalyzed the removal of the alkyl group at the upper axial position of the MeCbl analogs, in essentially all the derivatives examined herein. However, the rate of dealkylation decreased with increasing alkyl chain length. Whether the later is a result of conformational alterations in the *cbIC* protein induced by the more bulky alkyl moieties or due to an unfavorable incorporation of the longer alkyl carbocations into glutathione remains to be elucidated.

## MATERIALS AND METHODS

**Synthesis and purification of ethylcobalamin (EtCbl), propylcobalamin (PrCbl), butylcobalamin (BuCbl), pentylcobalamin (PnCbl) and hexylcobalamin (HxCbl).** Xenobiotic alkylcobalamins were synthesized by the reaction of cob(I)alamin with the corresponding alkylhalide (Kim et al. 1988; Pratt 1972) and purified by HPLC as described in **Chapter 2, Figure 2.27** (Hannibal et al. 2009). [ $^{57}\text{Co}$ ]-Alkylcobalamins were synthesized as described above using [ $^{57}\text{Co}$ ]-CNCbl (MP Biomedicals, Solon, OH) as the starting material (specific activity: 379  $\mu\text{Ci}/\mu\text{g}$ ). 5'-Chloro-5'-deoxyadenosine, synthesized as described by Jacobsen et al., (Jacobsen, DiGirolamo, and Huennekens 1975) was used to synthesize [ $^{57}\text{Co}$ ]-AdoCbl.

**Cell culture lines and [ $^{57}\text{Co}$ ]-cobalamin metabolic labeling.** Bovine aortic endothelial cells (BAEC) were cultured in 162  $\text{cm}^3$  flasks (Corning) and grown in vitamin B<sub>12</sub>-free, folic acid-free Ham's F12/DME (1:1) medium supplemented with 5% FBS, 2.0 mM L-glutamine, penicillin (100 units/mL), streptomycin (0.1 mg/ml) and 50 nM (6S)-N<sup>5</sup>-methyltetrahydrofolic acid (Eprova AG). The amount of cobalamin present in the 5% FBS-supplemented culture medium (33 pM) was shown to be sufficient to support normal growth of BAEC. Normal and *cbiC* mutant fibroblasts were grown in Advanced DMEM (Gibco) culture medium supplemented with 10% FBS (final cobalamin concentration, 66 pM). Note: the concentration of folic acid in the culture medium is 9.07  $\mu\text{M}$ . For [ $^{57}\text{Co}$ ]-Cbl metabolic labeling experiments, cells were passaged at a ratio of 1:2. [ $^{57}\text{Co}$ ]-CNCbl was added to achieve a final concentration of 0.2 nM, and cells were grown to 100% confluency (~48 h).

***cb1C* patient cell lines.** Dr. David Watkins, McGill University, kindly provided human *cb1C* mutant skin fibroblasts from patients with severe disease (WG1801, WG2176 and WG3354). The Repository for Mutant Human Cell Strains, Montreal Children's Hospital, Montreal, Canada (<http://www.cellbank.mcgill.ca/>) provided patient information on the *cb1C* lines. Patient WG1801 was a 2 month-old male of Turkish ethnicity, son of first cousins, with two brothers who were possible carriers of the inborn error. Patient WG2176 was a 7-month old male of Hong Kong Chinese ethnicity with a healthy older sister and an affected fetal brother who was aborted. Patient WG3354 was a female of Pakistani ethnicity with both parents and younger siblings heterozygous for the *cb1C* mutation.

**Assessment of dealkylation in BAEC and human fibroblasts.** Cells were passaged at a ratio of 1:2 in medium containing 0.125 nM (specific activity: 379 mCi/mg) of the desired [<sup>57</sup>Co]-cobalamin. After 48 h, cells were harvested, total cobalamins extracted with 80% aqueous ethanol and the intracellular cobalamin profile determined as recently described by Hannibal et al. (Hannibal et al. 2008). The cell cultures were protected from light at all times to prevent photolysis of the alkylcobalamins.

**Stability of [<sup>57</sup>Co]-alkylcobalamins in the culture medium.** Conditioned medium (1 ml) from 48-h old cultures was extracted with a 1:1 mixture of phenol/chloroform, taken to dryness in a Speedvac, reconstituted with 0.4 ml of phosphate-buffered saline (PBS). Cobalamin standards were added to the sample, the mixture was filtered (0.22 μ filter) and analyzed by HPLC as previously described (Hannibal et al. 2008). Workup of the conditioned culture medium was conducted under dim-red light.

**Extraction and analysis of intracellular Cbls.** Confluent cells were harvested by trypsinization and washed three times with Dulbecco's PBS. Extraction of cobalamins from

cell pellets was performed as previously described (Hannibal et al. 2008). Extracted [ $^{57}\text{Co}$ ]-cobalamins were mixed with unlabeled cobalamin standards and separated by gradient reverse-phase HPLC using an Agilent 1100 System equipped with a Zorbax SB C-18 column (4.6 x 250 mm, 5  $\mu\text{m}$  particle size, Agilent) as previously described (Hannibal et al. 2008). Elution was monitored with UV detection at 254 nm. In typical runs, 60 fractions were collected. The radioactivity associated with each fraction was counted using a gamma-counter (Gamma 4000 Beckman-Coulter).

**Cobalamin uptake studies.** Cells were seeded at an initial density of  $\sim 50\%$  and allowed to grow for 24 h. After 24 h, half of the conditioned culture medium was replaced with fresh medium and [ $^{57}\text{Co}$ ]-CNCbl added to a final concentration of 0.2 nM (specific activity: 379  $\mu\text{Ci}/\text{mg}$ ). Uptake was followed by counting the radioactivity in a  $\gamma$ -counter at 6, 12, 24, 48 and 72 h, both in spent medium and in washed cell pellets. Total cobalamin values were normalized to cellular protein concentration.

**Cytotoxicity.** To rule out cytotoxic effects of the xenobiotic alkylcobalamins under our culture conditions, BAEC were grown in the presence of 1  $\mu\text{M}$  of each of the xenobiotic alkylcobalamins (supraphysiological concentration) as the major source of cobalamin for two weeks, with medium plus fresh alkylcobalamin changes every three days. Morphological changes were monitored by phase-contrast microscopy. To assess for cobalamin deficiency, total homocysteine and methylmalonic acid concentrations were determined in the conditioned culture medium. Cell number and cell viability were determined by hemocytometry and the 3-(4,5-dimethylthiazol-2-yl)-2,5-diphenyltetrazolium bromide (MTT) assay (Mosmann 1983), respectively. Cellular senescence was assessed by determining  $\beta$ -galactosidase activity using a commercial kit (Sigma).

**Biochemical analyses.** Total homocysteine in conditioned culture medium was determined by the method of Jacobsen et al. using monobromobimane and HPLC with fluorescence detection (Jacobsen et al. 1994). Values were normalized to cellular protein concentration. The concentration of methylmalonic acid in conditioned culture medium was determined by gas chromatography and mass spectrometry (GC/MS) in the Department of Clinical Pathology, Cleveland Clinic by a method modified from Hoffmann et al (Hoffmann et al. 1989). Total protein concentration was determined by the bicinchoninic acid assay (Thermo Scientific) using bovine serum albumin as a standard.

**Expression and purification of *cbIC*.** The recombinant protein utilized in our studies was expressed and purified according to the recent report of Kim et al. (Kim, Gherasim, and Banerjee 2008). All the workup procedure was carried out by Dr. Carmen Gherasim in the laboratory of Dr. Ruma Banerjee, Ann Arbor, Michigan.

**Dealkylation of alkylcobalamins *in vitro*.** The reactions were carried out in 100 mM HEPES, pH 8.0, 150 mM KCl and 10% glycerol. The reaction was initiated by addition of 1.0 mM GSH to premixed *cbIC*-Cbl (1.7/1 molar ratio). Spectra were recorded at 20 °C on a Cary100 spectrophotometer. The dealkylation rate was monitored at 350 nm.

**Identification of reaction products by HPLC and mass spectrometry.** Reaction mixtures were subjected to an HPLC “clean-up” procedure since the presence of HEPES buffer, KCl and glycerol diffculted the analysis of the products by mass spectrometry. Reaction mixtures were first lyophilized, resuspended in a final volume of 120  $\mu$ L (of which ~ 50  $\mu$ L was glycerol) and run onto a Synergi Hydro-RP C18 (4  $\mu$ m) with polar endcapping HPLC column (Phenomenex) under an isocratic gradient of 0.1% formic acid /acetonitrile in a 99:1 ratio, for 30 min. Identification of GSH, GSSG, and Me-SG was done using

commercially available standards (Sigma, St Louis, MO, USA). Ado-SG eluted in between GSH and GSSG. The void volume for this column is 1.79 min. HEPES, KCl and glycerol eluted in the void volume. The retention times for the commercial standards were: GSH: 4.14 min, Me-SG: 7.07 min and GSSG 10.3 min. Fractions were collected between 3 and 15 minutes, lyophilized or evaporated using a Speedvac, and reconstituted with 90%MeOH/10%H<sub>2</sub>O for mass spectrometry analysis. Liquid chromatography electrospray ionization mass spectrometry was carried out using a Thermo Finnigan Triple Stage Quadrupole (TSQ) Quantum Ultra mass spectrometer (Thermo Electron Corporation, Waltham, MA, USA). Each sample was dissolved in 90%MeOH/10%H<sub>2</sub>O and infused at a rate of 0.3  $\mu$ L/min. Identification of the products was carried out by comparison with commercial standards.

**CHAPTER 4**  
**BIOCHEMISTRY OF THE *cbIC* DISORDER AND COBALAMIN**  
**DEFICIENCY IN HUMANS**

**4.1 Project 1. Metabolic profile of human fibroblasts carrying the *cbIC* mutation**

**INTRODUCTION**

Synthesis of AdoCbl and MeCbl from other Cbl derivatives is dependent on the *MMACHC* gene product, which defines the *cbIC* complementation group (Lerner-Ellis et al. 2006). The absence of MeCbl results in increased concentrations of Hcy in blood, as well as decreased blood levels of methionine. On the other side, without AdoCbl, MM is unable to convert methylmalonyl-CoA into succinyl-CoA, resulting in increased levels of methylmalonic acid in blood and urine. Three *cbIC* fibroblast cell lines were provided by Drs. Watkins and Rosenblatt, McGill University, Montreal, Canada. These cell lines were isolated from three genetically unrelated patients diagnosed with severe *cbIC* disorder (patient information, genetic background and other relevant information was provided in **Chapter 3, Project 2, Table 3.5**).

## RESULTS AND DISCUSSION

### A. Production of Hcy and MMA.

According to the expected failure to synthesize both AdoCbl and MeCbl by these patient fibroblasts, we hypothesized that *cb1C* cells in culture will produce and export higher levels of both Hcy and MMA into the culture medium compared to normal cells, as a result of functional Cbl deficiency. **Figure 4.1** shows the levels of Hcy and MMA measured in the conditioned culture medium after 7 days. All *cb1C* cell lines produced significantly higher levels of both Hcy and MMA compared to the control cell line. Importantly, it was observed that MMA levels were maintained close to normal values in *cb1C* mutants supplemented with HOcbl, whereas a similar response was not observed for Hcy production. These results suggest that the *cb1C* fibroblast cell lines undergo functional Cbl deficiency.

### B. Cobalamin uptake and cofactor biosynthesis.

Cobalamin uptake and the ability of the *cb1C* cell lines to synthesize AdoCbl and MeCbl were also examined. All *cb1C* cell lines displayed decreased [ $^{57}\text{Co}$ ]-HOcbl uptake and failure to retain intracellular Cbls beyond 48 h in culture, as depicted in **Figure 4.2**. The ability of *cb1C* cell lines to synthesize AdoCbl and MeCbl was evaluated after 48 h of incubation with the [ $^{57}\text{Co}$ ]-Cbl source.

Fowler et al. have recently reported the inability of *cb1C* to synthesize AdoCbl and MeCbl from [ $^{57}\text{Co}$ ]-CNCbl (Suormala et al. 2004). On the other hand, Rosenberg et al.

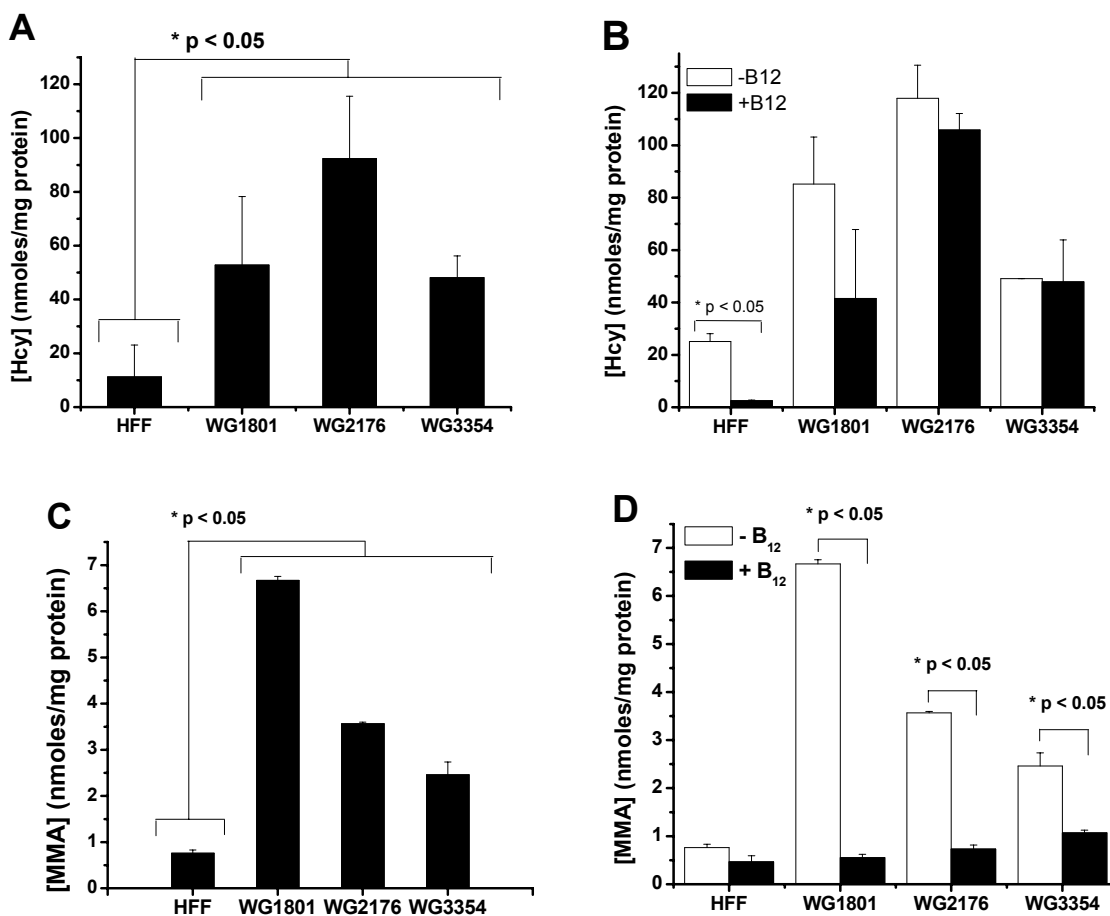


**Figure 4.1.** Determination of Hcy and MMA in conditioned culture media of normal and *cb1C* fibroblast cell lines, after 7 days. All three *cb1C* patients produced significantly higher amounts of Hcy and MMA compared to normal cells (panels A and C). Supplementation of the culture medium with 723 nM HOCbl did not cause a significant decrease in the levels of Hcy observed in the culture medium, but proved to be very efficient at maintaining MMA levels close to normal values in all patients (panels B and D, respectively). Statistically significant differences were established by independent Student's t-test, at  $\alpha=0.05$ . N=3, two independent experiments.

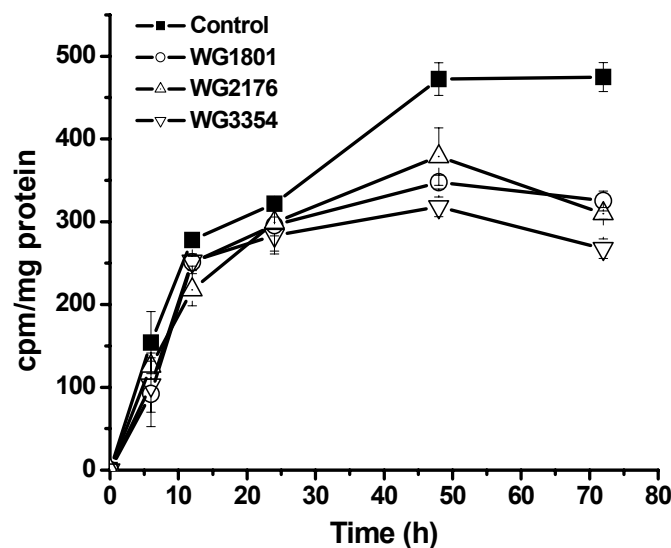


**Figure 4.2.** [ $^{57}\text{Co}$ ]-HOCbl uptake by control and *cbIC* fibroblasts. Cells were washed twice with PBS, lysed and the radioactivity counted on a  $\gamma$ -counter. Values (mean  $\pm$  standard deviation, n=3) were normalized by mg protein.

reported that mitochondria have the necessary machinery to synthesize AdoCbl from HOCbl (Fenton, Ambani, and Rosenberg 1976; Fenton and Rosenberg 1978); i.e. independently of the *cbIC* gene product. Could this be responsible for the effect of HOCbl supplementation in maintaining the levels of MMA close to that of control cells (**Figure 4.1, panel D**)? We believed that this could be the case. The extent of cofactor biosynthesis by cells grown in the presence of [ $^{57}\text{Co}$ ]-CNCbl was evaluated in **Chapter 3, Project 2**. Little decyanation and cofactor biosynthesis was observed for all three *cbIC* mutant cell lines, whereas normal fibroblasts were able to utilize CNCbl as a substrate for cofactor biosynthesis efficiently. The ability of *cbIC* cell lines to utilize [ $^{57}\text{Co}$ ]-HOCbl as a substrate for cofactor biosynthesis was

investigated (**Table 4.1**). While the normal cell line utilized HOCbl as substrate for MeCbl and AdoCbl biosynthesis, none of the *cbIC* fibroblasts were able to synthesize either AdoCbl or MeCbl, except for patient WG1801 (21.7% AdoCbl, no MeCbl). Unprocessed HOCbl was the principal intracellular form isolated from the *cbIC* mutant cell lines. These data also suggests that, with the exception of patient cell line WG1801, the *cbIC* mutants cannot utilize HOCbl as a substrate for the biosynthesis of AdoCbl through the putative mitochondrial machinery originally suggested in the literature (Fenton, Ambani, and Rosenberg 1976; Fenton and Rosenberg 1978).

**Table 4.1. Processing of [<sup>57</sup>Co]-HOCbl by human normal and *cbIC* mutant fibroblasts.**

	% intracellular Cbl <sup>a</sup>			
	HFF	WG1801	WG2176	WG3354
<b>HOCbl</b>	25.9 ± 5.3	78.3 ± 18.4	100	100
<b>Others<sup>b</sup></b>	ND	ND	ND	ND
<b>AdoCbl</b>	13.4 ± 6.8	21.7 ± 1.7	ND	ND
<b>MeCbl</b>	60.7 ± 3.0	ND	ND	ND

<sup>a</sup> Results are expressed as mean ± standard deviation (n = 3).  
<sup>b</sup> Cobalamins not quantitatively determined in the present study include glutathionylcobalamin, sulphitocobalamin and nitrocobalamin. See ref (Hannibal et al. 2008).

### C. Cell morphology.

Mutant fibroblasts from the *cbIC* complementation group, especially WG2176 and WG3354, display an altered cell morphology compared to control cell lines (**Figure 4.3**). However, all cell lines appeared to divide normally and no signs of necrosis were observed. Apoptosis and senescence were also examined by DNA laddering (**Figure 4.4**) and measurement of β-galactosidase activity respectively *in situ* (**Figure 4.5**), and no significant

differences were found between normal and *cb1C* fibroblasts (not shown). Supplementation with HOCbl did not affect the cell's morphology. Therefore, the causes underlying the altered cell morphology remain to be elucidated. Mutants WG2176 and WG3354 showed enlarged cell body (megaloblastosis) and disruption of the characteristic fibroblast growth pattern in culture. Megaloblastosis is one of the major features of Cbl deficiency and is utilized as a tool for clinical diagnostics (mcv: mean red cell volume).

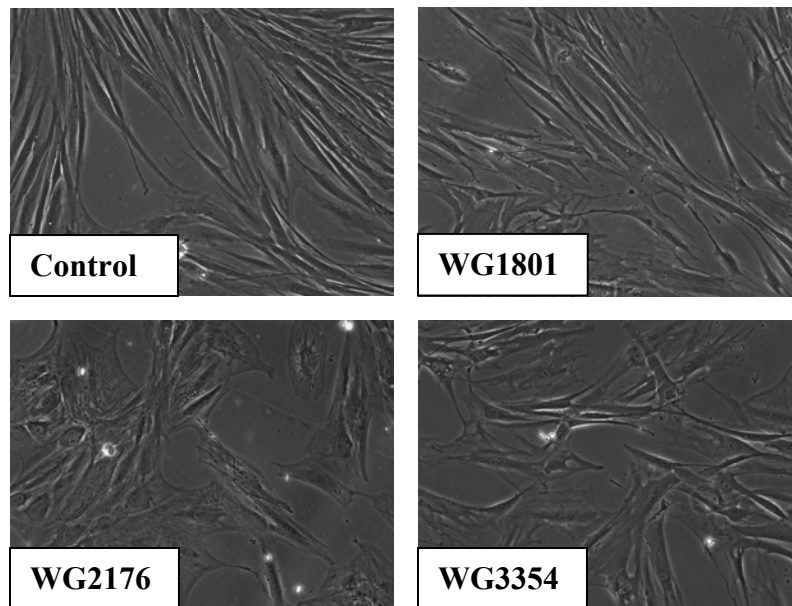


**Figure 4.3.** Morphology of control (normal fibroblasts) and *cblC* mutants by inverted phase contrast microscopy. Magnification: 100X.

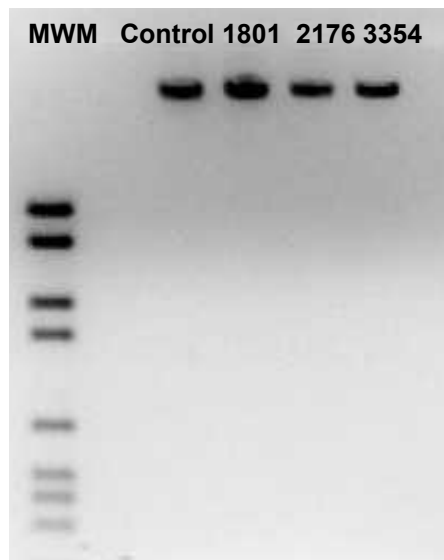


**Figure 4.4.** DNA laddering assay. MWM: molecular weight marker (1-10 Kb). ~1  $\mu$ g of total DNA per lane.

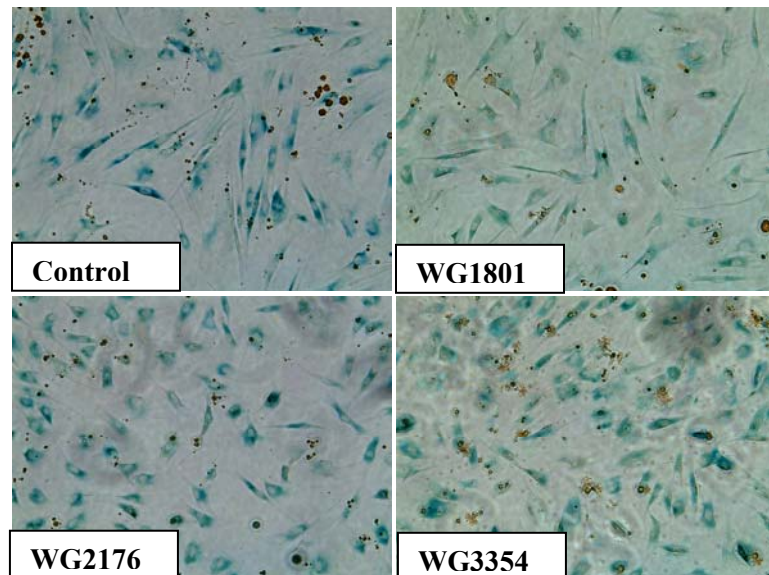


**Figure 4.5.**  $\beta$ -galactosidase staining of normal and *cblC* cells in culture. Brown granules are precipitates of the dye used in the assay. Senescent (viable but with an arrested cell cycle) cells express higher levels of  $\beta$ -galactosidase than normally dividing cells. No differences were observed between normal and *cblC* mutant cells.

#### D. Intracellular levels of cobalamin and folic acid.

We observed that the *cbiC* mutant cell lines failed to retain intracellular cobalamin at incubation times longer than 48 h, and moreover, an efflux of cellular cobalamins appeared to occur at  $t \sim 72$  h. This was not observed in the normal cell line. It was of interest to determine the total levels of intracellular cobalamin in normal versus *cbiC* mutant cell lines that were grown with and without supplementation with HOCbl. Surprisingly, the *cbiC* cell lines displayed slightly higher levels of total intracellular cobalamin compared to normal fibroblasts when grown in the absence of exogenous HOCbl (**Table 4.2**). Supplementation of the cell cultures with 723 nM HOCbl (supraphysiological concentration) increased the levels of intracellular cobalamin in all four cell lines, normal and *cbiC* mutants, however the *cbiC* cell lines did not achieve the levels observed in the normal cell line. One simple explanation for this result is that *cbiC* cell lines do not retain cobalamin because they are unable to utilize it.

**Table 4.2. Intracellular levels of cobalamin and folic acid in normal and *cbiC* mutant fibroblasts.<sup>1</sup>**

Cell line	Total intracellular Cbl		Total intracellular folates	
	(pg/mg protein)		(ng/mg protein)	
	- OHCbl	+ HOCbl	-HOCbl	+HOCbl
<b>Normal</b>	930.73	9894.98	18.42	68.52
<b>WG1801</b>	1286.66	6803.40	17.15	35.98
<b>WG2176</b>	1250.99	4663.16	10.85	22.08
<b>WG3354</b>	1366.97	4822.22	11.99	25.01

<sup>1</sup> Total intracellular Cbl and folates were determined on lysates from cells grown in the presence or in the absence of exogenous HOCbl (723 nM), for 7 days.

We examined the total levels of intracellular folate in normal and mutant *cbIC* cell lines, since folate biosynthesis depends on the activity of methionine synthase. With the exception of patient cell line WG1801, the *cbIC* cell lines displayed lower levels of intracellular folate compared to normal cells, in the absence of exogenous HOCbl. Supplementation of the cell cultures with HOCbl resulted in increased levels of total folates in all the cell lines. However, none of the *cbIC* mutant fibroblasts reached the intracellular levels of Cbl or folate observed in the normal cell line. This suggests that a functional *cbIC* protein is required not only for the decyanation and dealkylation of cobalamins, but also to maintain the homeostasis of related metabolites. Tetrahydrofolate (THF), the biologically active form required for DNA biosynthesis, is regenerated by the enzyme methionine synthase. Presumably, the inability of the *cbIC* cell lines to utilize HOCbl as a substrate for the biosynthesis of MeCbl leads to a partial blockage in the biosynthesis of THF by methionine synthase. This could explain the observation that *cbIC* mutant cell lines displayed lower levels of folate compared to the normal cell lines under conditions of cobalamin sufficiency.

## **SUMMARY**

A general assessment of the metabolic and morphological features of the *cbIC* cell lines was carried out and compared to that of normal human fibroblasts. All *cbIC* cell lines exported increased levels of Hcy and MMA compared to the normal cell line. Supplementation with HOCbl reduced the levels of MMA exported by the *cbIC* cell lines, however, this was not effective in substantially reducing the levels of Hcy. In addition, the

*cb1C* cell lines displayed reduced uptake and impaired processing of HOCbl compared to the normal cell line. Only one of the three *cb1C* cell lines was able to utilize HOCbl as substrate for AdoCbl biosynthesis. This was in line with the finding that all *cb1C* mutant cell lines take up or retain less amount of cobalamin compared to the normal fibroblasts, and this is also mirrored in the total levels of intracellular folates. Therefore, it appears that the positive response of the *cb1C* cell lines to HOCbl supplementation (lowering of MMA) may not be directly associated with the activity of mitochondrial methylmalonyl-CoA mutase, as we hypothesized based on previous reports.

The altered morphology observed in the *cb1C* cell lines could be due to: a) toxicity mediated by Hcy and MMA and/or b) functional deficiency of cobalamin, as a result of a defective *MMACHC* gene. No signs of necrosis, late-stage apoptosis or senescence were observed, therefore, the abnormal morphology could be related to alterations in cytoskeletal proteins and/or other major structural components of the cells.

## MATERIALS AND METHODS

**Human fibroblasts cell lines.** Normal and *cb1C* mutant fibroblasts were grown in Advanced DMEM (Gibco) culture medium supplemented with 10% FBS (final cobalamin concentration, 66 pM). Note: this culture medium contains 9.07  $\mu$ M folic acid as the source of folate. When indicated, cells were supplemented with 723 nM of filter-sterilized HOCbl dissolved in PBS. Additional information about the *cb1C* cell lines used in this study was given in **Chapter 3, Project 2, Table 3.5** and in the Materials and Methods section.

**Determination of Hcy and MMA in conditioned culture medium.** Cells were cultured as described and at the end point of the experiment the conditioned culture medium was collected, centrifuged at 1000 rpm for 10 min (to remove dead cells), filtered with a 0.22  $\mu\text{m}$  filter (Millipore) and stored at 4 °C until further use. Assays for Hcy and MMA quantification were carried out as described in **Chapter 3, Project 2**, in the Materials and Methods section. Total Hcy and MMA values were normalized to cellular protein concentration.

**Determination of total intracellular cobalamin and folates.** Total intracellular cobalamin and folates were determined using the SimulTRAC-SNB Radioassay kit vitamin B<sub>12</sub>[<sup>57</sup>Co]/Folate [<sup>125</sup>I], MP Biomedicals (Orangeburg, NY, USA). Cbl and folate values were normalized to cellular protein concentration.

**Assessment of cellular apoptosis (DNA laddering) and senescence ( $\beta$ -galactosidase activity).** Cellular apoptosis (late stage) was assessed by determining the degree of genomic DNA fragmentation. Total genomic DNA was extracted (Wizard Genomic DNA purification kit, Promega, Madison, WI, USA) from cells grown in the absence of exogenous Cbl and run on a 1% agarose gel. The gel was stained with ethidium bromide and photographed under UV light. Senescence was assessed *in situ* using a commercially available kit (Senescence Cells Histochemical Staining Kit, Sigma, St Louis, MO, USA). Cells were seeded at a ~ 30% density and grown in regular cultured medium for 24 hours. The conditioned cultured medium was removed and cells were washed three times with 1X PBS. The assay was conducted according to the manufacturer's instructions.

**Cobalamin uptake studies.** Cells were seeded at an initial density of ~25-30% and allowed to grow for 24 h. After 24 h, half of the conditioned culture medium was replaced

with fresh medium and [ $^{57}\text{Co}$ ]-HOCbl added to a final concentration of 0.2 nM (specific activity: 379  $\mu\text{Ci}/\text{mg}$ ). Uptake was followed by counting the radioactivity in a  $\gamma$ -counter at 6, 12, 24, 48 and 72 h, both in spent medium and in washed cell pellets. Total cobalamin values were normalized to cellular protein concentration.

**Processing of [ $^{57}\text{Co}$ ]-HOCbl by normal and *cb1C* fibroblasts.** Briefly, processing experiments were done as described in previous sections, utilizing [ $^{57}\text{Co}$ ]-HOCbl (final concentration in the culture medium  $\sim 0.125$  nM) as the sole source of Cbl. Cells were grown for 48 h, harvested and the intracellular Cbl profile examined as described previously (Hannibal et al. 2008).

**4.2. Project 2: Assessment of the human proteome of patients with a defective *MMACHC* gene (*cb1C*) by 2D-DIGE.**

**INTRODUCTION**

*cb1C* was initially thought to be a disease of infancy, which presents with failure to thrive, acute neurological deterioration, mental retardation, muscular hypotonia, ligament laxity, retinopathy, multisystem organ dysfunction, and haematological abnormalities including megaloblastic anemia (Andersson, Marble, and Shapira 1999; Rosenblatt and Fenton 2001). The late-onset form of the *cb1C* disease was established in 1984 (Shinnar and Singer 1984). A previously asymptomatic 14-year old girl presented with an acute onset of neurological symptoms including dementia, myelopathy, and motor-neuron disease (Shinnar and Singer 1984). The patient was diagnosed to belong to the *cb1C* complementation group, thus establishing the heterogeneity of this condition. In 1997, Rosenblatt et al., reviewed 50 *cb1C* patients, of whom six patients had late-onset (Rosenblatt et al. 1997). The authors noted that late-onset patients had better survival and response to treatment, and less neurological sequelae compared to early-onset patients (Rosenblatt et al. 1997).

Herein, we investigate the proteome of *cb1C* fibroblasts isolated from genetically unrelated and severely ill patients with early-onset of the disease. The primary molecular and morphological characterizations of the *cb1C* mutant cell lines was presented in **Chapter 3** and **section 4.1** of this chapter, and suggested that functional Cbl deficiency must be at least partially responsible for the observed phenotype. We observed that the *cb1C* cell lines

produced increased levels of both Hcy and MMA compared to the normal cell line, and that supplementation of the cell cultures with HOCbl did not reduce the export of Hcy or MMA in *cbIC* cell lines to the levels observed in normal fibroblasts. Moreover, supplementation of the *cbIC* cell lines with a supraphysiological dose of HOCbl (723 nM) did not restore the levels of intracellular folates to those found in the normal cell line. Therefore, alterations in folate homeostasis should be taken into account for understanding the *cbIC* phenotype.

An assessment of the *cbIC* proteome and its comparison with that of normal fibroblasts was conducted using two-dimensional differential gel electrophoresis (2D-DIGE). The identification of changes at the protein level will bridge the gap existing between the role/s of the *MMACHC* gene product *in vivo* and the clinical information retrieved from patients belonging to the *cbIC* complementation group.

## RESULTS AND DISCUSSION

A recent study reported by Wu et al. provided a head-to-head comparison of the three most popular techniques in proteomics: 2D-DIGE, cICAT (cleavable isotope-coded affinity tags) and iTRAQ (isobaric tags for relative and absolute quantification (Wu et al. 2006). The authors concluded that in the 2D-DIGE approach, comigration and partial comigration of proteins could compromise the accuracy of the quantification, especially for nonabundant proteins in complex samples (Wu et al. 2006). The cICAT procedure was shown to be as sensitive as the 2D DIGE (limit of detection ~ 1 ng), but is cysteine-content biased (proteins without Cys or with naturally low abundance of Cys are not detected). The iTRAQ method is the most sensitive, but the labeling step needs to be handled separately for each sample,

which could introduce potential sources of errors such as sample handling or variable degrees of tryptic digestion between two samples (Wu et al. 2006). The 2D-DIGE technology is readily available in our laboratory and offers the advantage of multiplex analysis of samples. In addition, the results presented in this dissertation will be validated by other conventional techniques (western blot, enzyme activity, etc) whenever possible, and will be complemented with a bioinformatics analysis. *In silico* analysis of the differentially expressed proteins could reveal relationships with low expression proteins or enzymes that are not detectable by 2D-DIGE.

#### **A. Cy-dye labeling of the normal and *cb1C* proteomes.**

To detect and identify differentially expressed proteins between normal and *cb1C* mutant fibroblasts, we used the novel fluorescence technique 2D-DIGE, in which differences in protein expression can be detected and identified with an increased confidence in comparison with the traditional two dimensional electrophoresis technique (Marouga, David, and Hawkins 2005). In addition, we investigated the effect of HOCbl on the proteome of normal and *cb1C* fibroblasts. In order to minimize variations associated to growth conditions, cell extracts for 2D-DIGE analysis were prepared from a single batch of normal and *cb1C* fibroblasts (i.e, same passage number), which were split and grown simultaneously for 7 days, either in the presence or in the absence of 723 nM HOCbl supplied in the culture medium.

Cells were then harvested by trypsinization, washed 3 times with PBS and the resulting cell pellets were treated as described in Materials and Methods. Proteins from

normal and *cbiC* cell lines were individually labeled with the fluorescent dyes Cy2, Cy3, and Cy5 as recommended by the manufacturer (see Materials and Methods), mixed, and co-resolved on three different analytical gels (total protein ~150  $\mu$ g). A preparative gel containing ~600  $\mu$ g of total unlabelled protein (pooled normal and *cbiC* samples) was run simultaneously. **Table 4.3** summarizes our experimental set up.

<b>Table 4.3. Gel set up for 2D-DIGE experiments and fluorophore labeling scheme.</b>				
		<b>Cy2</b>	<b>Cy5</b>	<b>Cy3</b>
<b>-HOCbl</b>	Gel 1 <sup>a</sup>	Pooled, normal + WG1801	Normal	WG1801
	Gel 2	Pooled, normal + WG2176	Normal	WG2176
	Gel 3	Pooled, normal + WG3354	Normal	WG3354
	Gel P1	Pooled: normal + WG1801 + WG2176 + WG3354		
<b>+HOCbl</b>	Gel 4	Pooled, normal + WG1801	Normal	WG1801
	Gel 5	Pooled, normal + WG2176	Normal	WG2176
	Gel 6	Pooled, normal + WG3354	Normal	WG3354
	Gel P2	Pooled: normal + WG1801 + WG2176 + WG3354		

<sup>a</sup>Gels 1-6: analytical gels; <sup>b</sup>Gels P1 and P2: preparative gels.

### **B. Decyder® image analysis of differentially expressed proteins.**

**Figures 4.6** and **4.7** show the images obtained from fluorescence detection of the normal and *cbiC* Cy-labeled proteins for patient fibroblasts WG1801, without and with HOCbl supplementation, respectively. The data obtained from the fluorescence scan was analyzed using the Decyder® software. **Figure 4.8** shows a summary of the steps that were followed to select candidate spots. Only the spots containing differentially expressed proteins with a normal/*cbiC* ratio  $\geq 2.0$  and with a t-test with  $p < 0.05$  were selected, and then matched

to the same spots in the corresponding preparative gel (stained with Coomassie Blue). Candidate spots were cut manually, trypsinized and analyzed by ESI/MS.

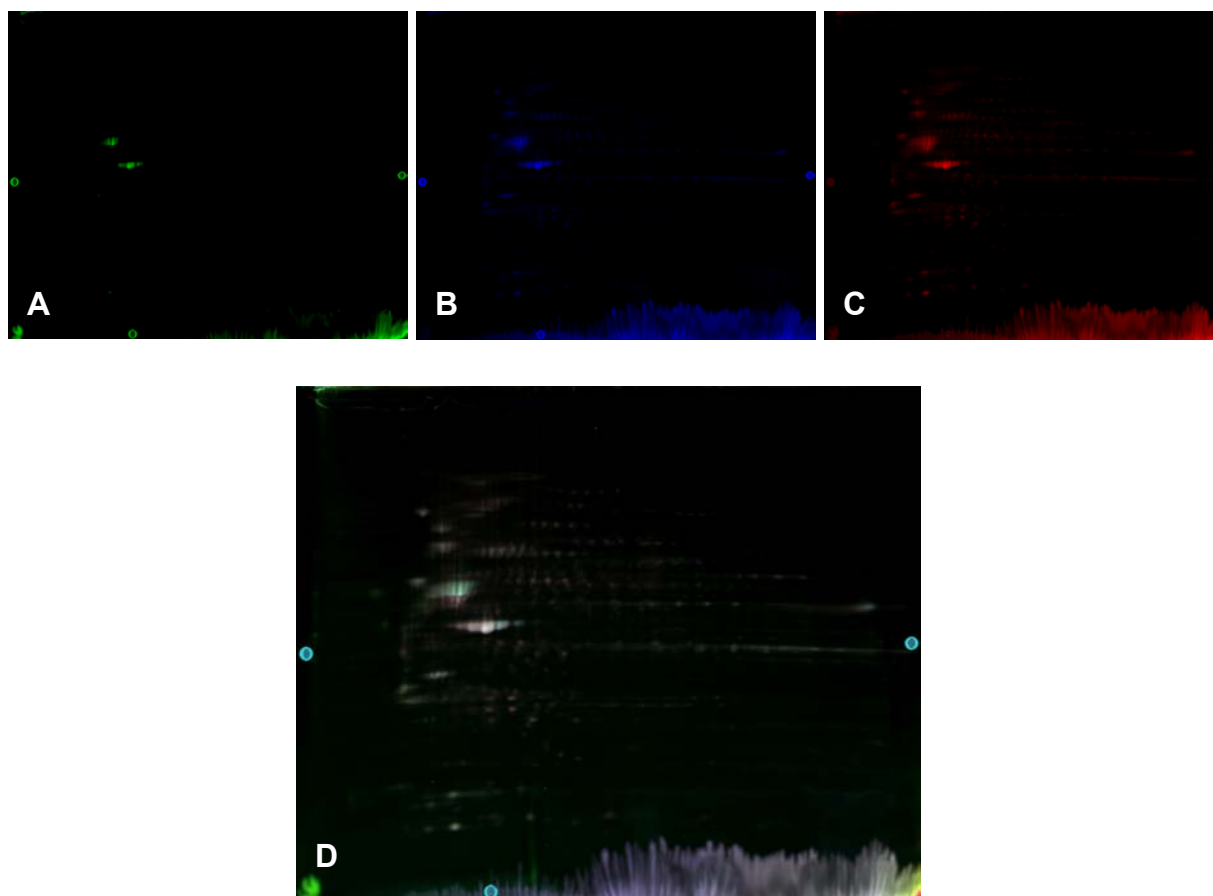


**Figure 4.6.** Fluorescence scans for normal and *cblC* (patient WG1801) proteins from cells grown without exogenous HOCl. **A.** Cy2, internal standard; **B.** Cy5, proteins from normal cell line; **C.** Cy3, proteins from *cblC* patient WG1801; **D.** Merge of the three images.

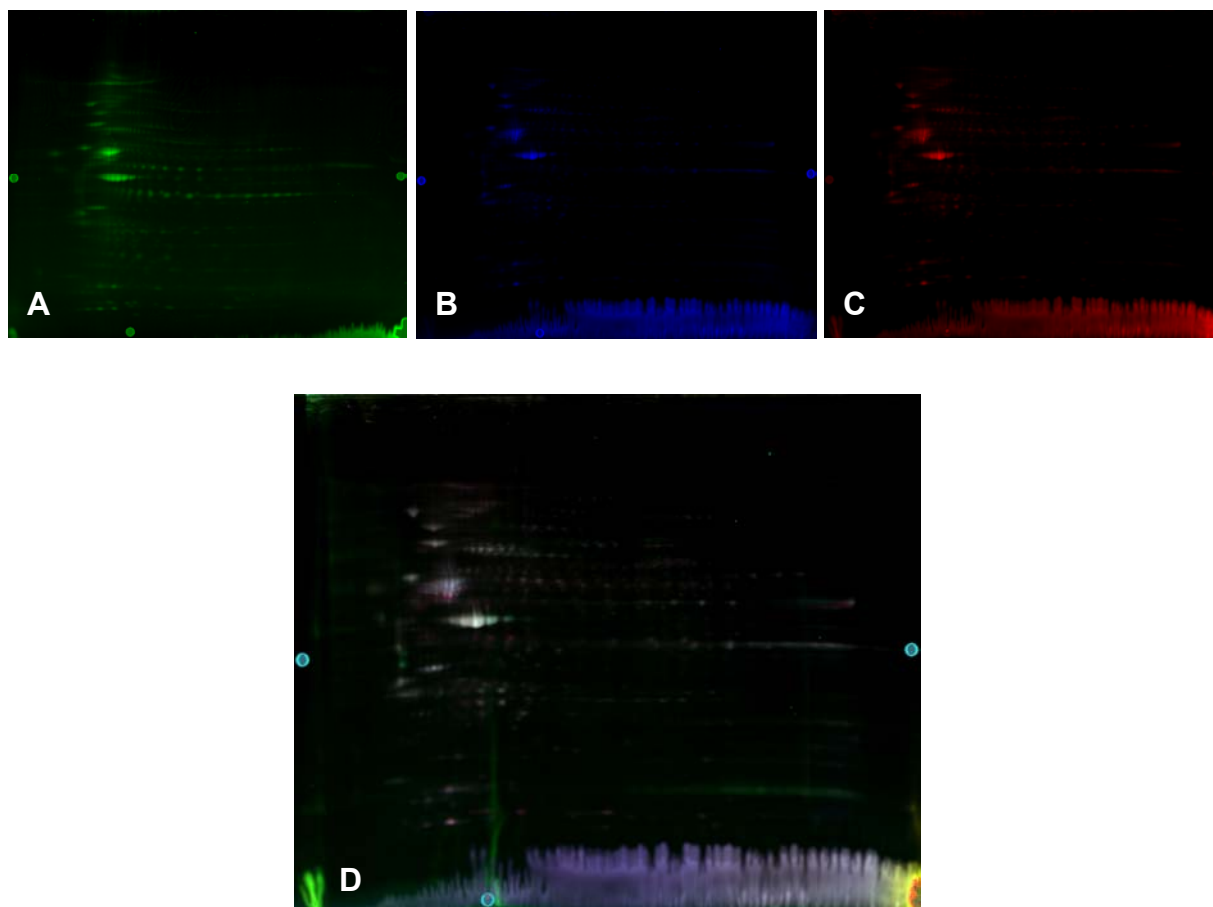


**Figure 4.7.** Fluorescence scans for normal and *cbIC* (patient WG1801) proteins from cells grown with HOCbl supplementation. **A.** Cy2, internal standard; **B.** Cy5, proteins from normal cell line; **C.** Cy3, proteins from *cbIC* patient WG1801; **D.** Merge of the three images.

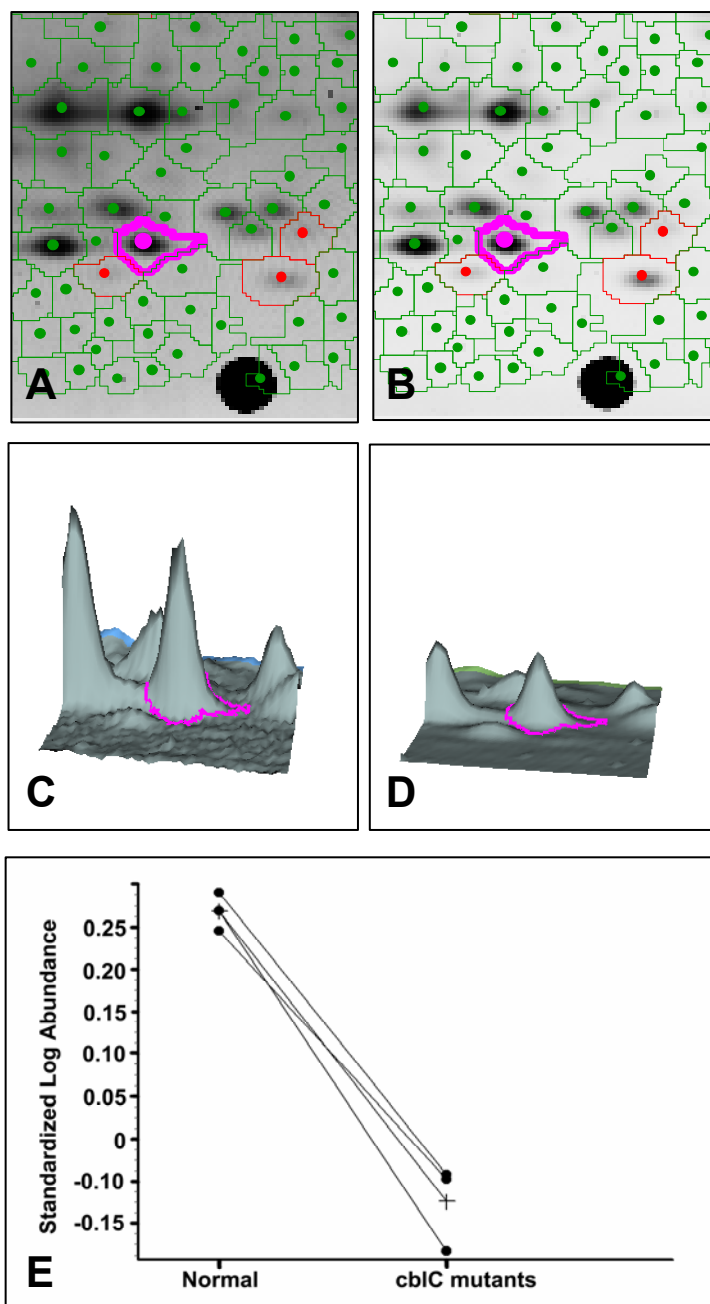


**Figure 4.8.** A representative scheme for 2D-DIGE image analysis. As an example, Spot 39 from gel P2 (panels **A** and **B**, Cy5 and Cy3 for normal and patient WG1801 cell lines, respectively) displayed a fold change of -2.19 according to 3D Decyder® analysis of the spot volumes (panels **C** and **D**, Cy5 and Cy3, respectively). A plot of Log of the standardized abundance for normal and *cb1C* fibroblasts is shown in panel **E** (n=3). Mass spectrometry analysis revealed that the expression change exemplified herein corresponded to protein S100A6. Fold change cut-off:  $\pm 2.0$ . Statistical significance:  $p < 0.05$ , n=3.

The study was designed to identify statistically significant changes in the protein levels of normal versus the *cb1C* proteome, rather than looking into changes in individual patients. Therefore, the comparative analysis was carried out by contrasting three runs for the normal proteome (Cy5 scans from gels 1, 2 and 3) *versus* three runs for the *cb1C* proteome (one per patient; Cy3 scans gels 1, 2 and 3 corresponding to patients WG1801, WG2176 and WG3354 respectively).

We first analyzed the proteome of normal and *cb1C* fibroblasts grown in the absence of exogenous HOCbl. Comparison of normal/*cb1C* fibroblasts relative amounts of 3516 detected spots allowed us to select 15 spots with significant variation (**Figure 4.9**). These protein spots exhibited differences in standardized average spot volume ratios  $\geq 2.0$  and a t-test with  $p < 0.05$  ( $n=3$ ).

Among 15 spots, 5 were more abundantly expressed in the *cb1C* mutants, whereas 10 were expressed at lower levels in the *cb1C* fibroblasts. These differentially expressed proteins spots were picked manually and analyzed by LC/MS as described. All of the spots were positively identified, with some of them having multiple protein components.

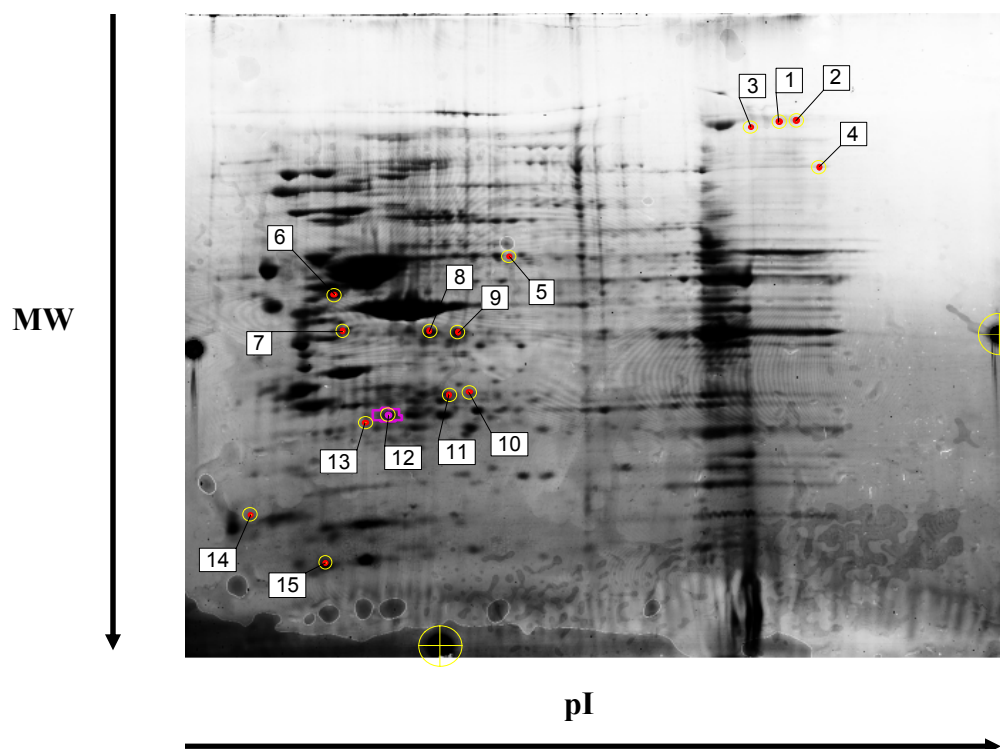


**Figure 4.9.** Differential expression of proteins in three *cb1C* mutants compared to normal fibroblasts (Gel P1). Labels 1-15 indicate the spots selected for identification by mass spectrometry. A statistical significance of 95% confidence was set and a stringency of 2-fold +/- in the expression ratio of control versus *cb1C* mutants. The preparative gel shown in the picture was loaded with 600  $\mu$ g of total protein and stained with Coomassie blue overnight.

### C. Identification of proteins by LC/MS and validation assays.

**Table 4.4** shows a summary of the proteins that were differentially expressed in normal *versus cb1C* fibroblasts. Major changes were observed in proteins related to cytoskeleton, nervous system, signaling and cellular detoxification. Further validation of the results using alternative techniques was also conducted, especially in cases where one spot contained more than one protein. **Figure 4.10** shows western blots for protein disulfide isomerase (PDI, **panel A**), chloride intracellular channel 4 (CLIC4, **panel B**) and ubiquitin C-terminal esterase L1 (UCHL1, **panel C**).

**Table 4.4.** Differentially expressed proteins in *cb1C* mutants compared to normal fibroblasts (N=3,  $\alpha=0.05$ ) grown in the absence of exogenous HOCbl. Proteins that were more abundantly expressed in the *cb1C* fibroblasts are listed in bold.

Spot	Protein	Gene ID	Fold Change	Mascot score	t-test (p value)
1	<b>HDL binding protein</b>	<b>42716280</b>	<b>2.87</b>	<b>807</b>	<b>0.029</b>
4	<b>Eukaryotic translation elongation factor 2</b>	<b>4503483</b>	<b>2.5</b>	<b>1234</b>	<b>0.042</b>
7	Serine (or Cys) proteinase inhibitor (protease inhibitor 6, PI-6, or serpin B6)	41152086	-2.09	2322	0.032
7	Caldesmon-1, isoform 2, Ct truncated	4826657	-2.09	956	0.032
8	$\beta$ -actin	4501885	-2.11	1116	0.024
9	Tubulin alpha, ubiquitous	57013276	-2.17	907	0.028
11	Chloride intracellular channel 4 (CLIC4)	7330335	-2.04	1507	0.018
3	<b>Collagen type VI, alpha 2, isoform 2C2</b>	<b>115527062</b>	<b>2.1</b>	<b>295</b>	<b>0.028</b>
3	<b>Collagen type VI, alpha 1 precursor</b>	<b>87196339</b>	<b>2.1</b>	<b>662</b>	<b>0.028</b>
12	Ubiquitin carboxyl esterase L1	21361091	-2.19	1261	0.021
5	Plastin 3	7549809	-2.9	1471	0.023
6	Vimentin	62414289	-2.44	3652	0.032
10	Glutathione transferase omega 1	4758484	-2.1	172	0.0096
13	Glutathione transferase	4504183	-2.84	821	0.016
12	Glutathione transferase M3	2306552	-2.19	281	0.021
5	PDI associated 3 precursor	21361657	-2.9	529	0.023
15	SH3 domain binding Glu-rich protein like 3	13775198	-2.23	312	0.042
15	S100 Ca-binding protein A6	7657532	-2.23	121	0.042
14	<b>ribosomal protein S14</b>	<b>5032051</b>	<b>2.45</b>	<b>260</b>	<b>0.033</b>
14	<b>H2B histone family member A</b>	<b>4504257</b>	<b>2.45</b>	<b>90</b>	<b>0.033</b>
8	GAPDH	7669492	-2.11	761	0.024

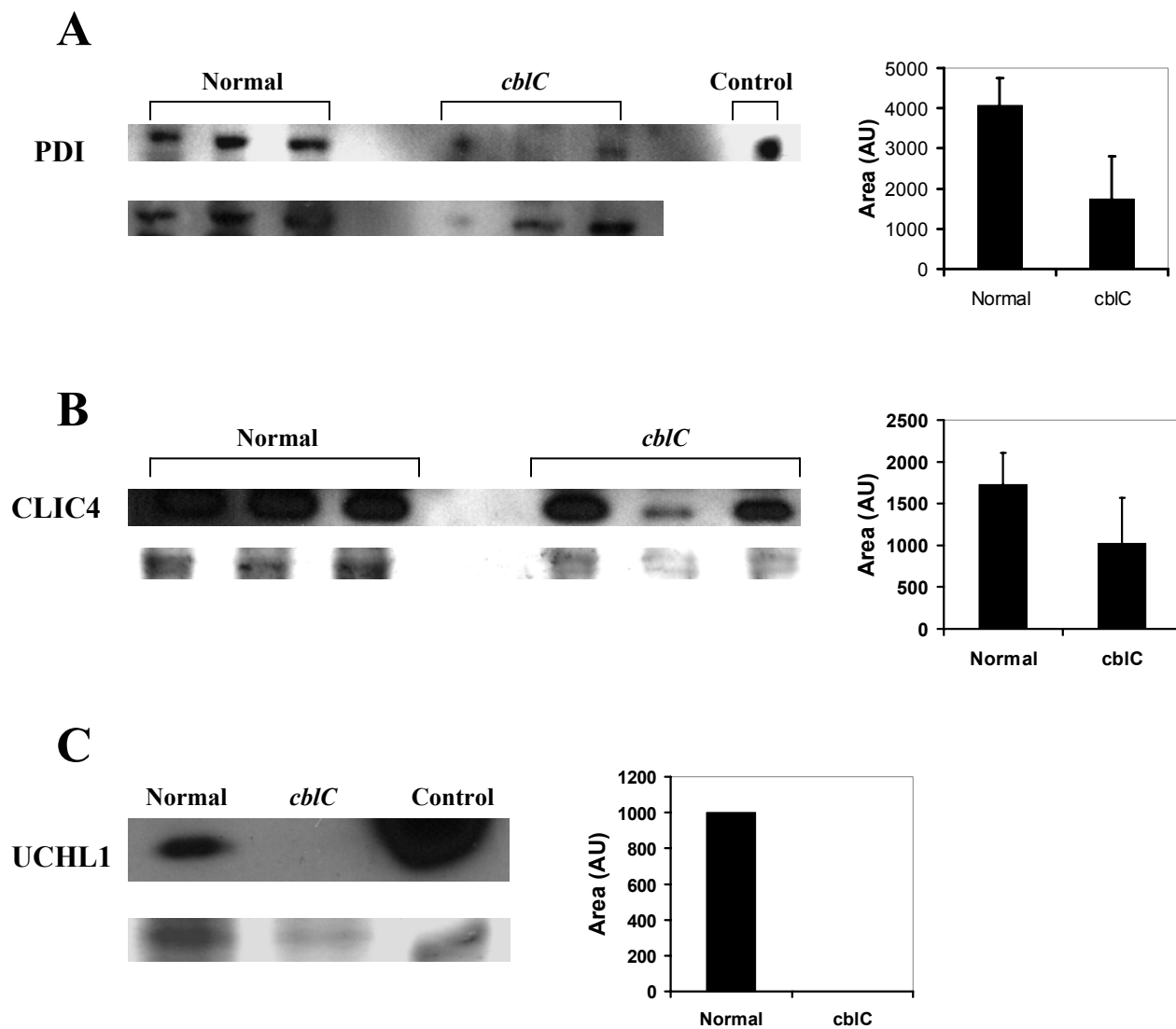


**Figure 4.10.** Western blots of PDI (**panel A**), CLIC4 (**panel B**) and UCHL1 (**panel C**). Cell lysates were obtained from cells grown without HOCbl supplementation. Protein load was normalized by western blotting of GRP 94, a protein whose expression was not altered in normal versus *cbIC* fibroblasts (bottom gels in each panel). Pooled samples were run for UCHL1 (n=3). Band density was determined using ImageJ software.

The effect of HOCbl supplementation on the proteome of *cb1C* fibroblasts was then examined. Of the 3500 protein spots detected, 41 spots displayed significant changes (ratio normal/*cb1C*  $\geq 2.0$ ,  $p < 0.05$ ,  $n=3$ ) (**Figure 4.11**). These 41 candidate spots were analyzed by LC/MS.

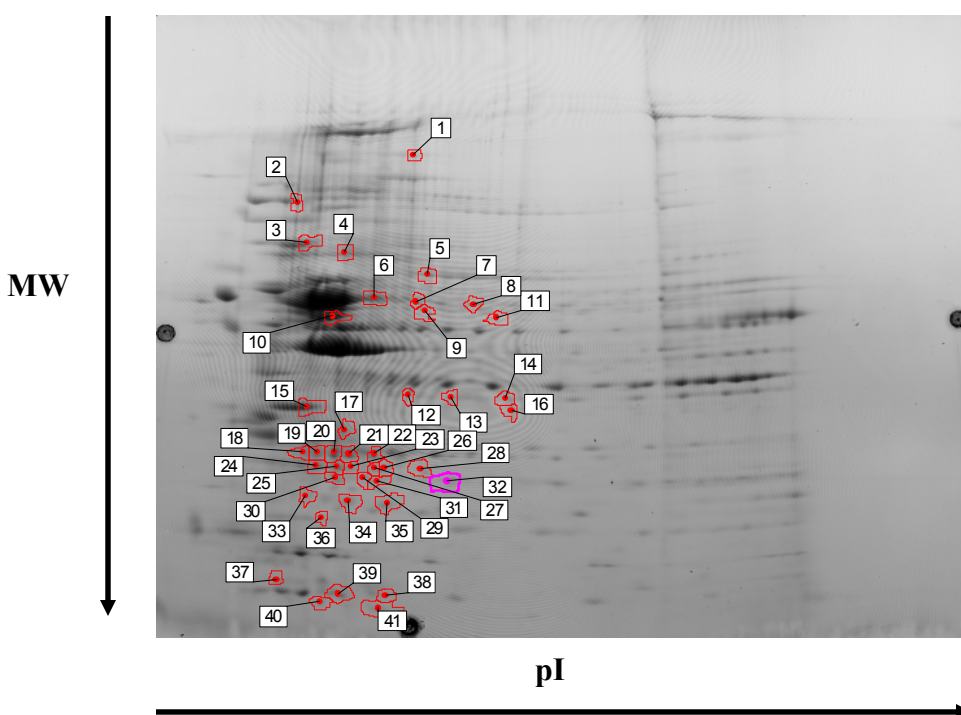


**Figure 4.11.** Differential expression of proteins in three *cb1C* mutants compared to normal fibroblasts grown in the presence of 723 nM HOCbl. Labels 1-41 indicate the spots selected for identification by mass spectrometry. A statistical significance of 95% confidence was set and a stringency of 2-fold +/- in the expression ratio of control versus *cb1C* mutants. The preparative gel shown in the picture was loaded with 600  $\mu\text{g}$  of total protein and stained with Coomassie blue overnight.

All of the spots were positively identified as some of them had multiple proteins.

**Table 4.5** presents a list of the differentially expressed proteins found under conditions of HOCbl supplementation. Among the 41 spots analyzed, 37 proteins were identified as differentially expressed.

**Table 4.5.** Differentially expressed proteins in *cb1C* mutants compared to normal fibroblasts (N=3,  $\alpha=0.05$ ) grown in the presence of 723 nM HOCbl.

Spot	Protein	Gene ID	Fold Change	Mascot score	t-test (p value)
1	Collagen type VI, isoform 2C2	17402875	-2.72	953	0.039
1	Vinculin isoform VCL	4507877	-2.72	660	0.039
2	Hsp 90 protein 1, beta	20149594	-2.03	1758	0.042
2	Hsp 90 alpha (cytosolic), class A, member 1, isoform 2	40254816	-2.03	1393	0.042
3	Hsp 70, protein 5,	16507237	-2.28	3310	0.031
3	PDI associated 4	4758304	-2.28	435	0.031
4	Hsp70 protein 8, isoform 1	5729877	-2.15	2218	0.042
4	Annexin VI isoform 1	71773329	-2.15	1678	0.042
4	ATPase, H <sup>+</sup> transporting, lysosomal	19913424	-2.15	701	0.042
5	Lamin A/C, isoform 2	5031875	-2.3	2672	0.049
5	Dihydropyrimidase -like 2	4503377	-2.3	1622	0.049
5	chaperonine containing TCP1, sub3	63162572	-2.3	829	0.049
15	Annexin 5	4502107	-2.08	1285	0.031
6	Vimentin	62414289	-5.03	3908	0.031
10	PDI associated 3 precursor	21361657	-2.38	1140	0.042
6	Tubulin alpha 6	14389309	-2.38	1014	0.042
8	Phosphoglycerate dehydrogenase	23308577	-2.13	2316	0.033
7	tryptophanyl-tRNA synthetase isoform a	47419914	-2.63	2129	0.033
8	inosine monophosphate dehydrogenase 2	66933016	-2.13	778	0.042
11	Septin 11	8922712	-2.25	1237	0.031
13	Annexin 5, A2, isoform I	50845388	-2.90	355	0.039

(Continued on next page)

**Table 4.5 (continued)**

Spot	Protein	Gene ID	Fold Change	Mascot score	t-test (p value)
16	Voltage dependent anion channel 1	4507879	-2.17	657	0.034
16	Voltage dependent anion channel 2	42476281	-2.17	405	0.034
17	Chloride intracellular Channel 4	7330335	-2.38	621	0.034
18	Ubiquitin carboxyl esterase L1	21361091	-3.16	949	0.037
18	Triosephosphate isomerase 1	4507645	-2.93	954	0.039
22	Peroxiredoxin 6	4758638	-2.34	600	0.042
26	DJ-1	31543380	-2.52	152	0.031
24	Glutathione transferase	4504183	-2.54	926	0.031
29	Peroxiredoxin 2, isoform a	32189392	-2.23	899	0.031
31	Transgelin 2	4507357	-2.03	1364	0.04
33	Cofilin 1	5031635	-2.26	473	0.031
37	SH3 domain binding Glu-rich protein like 3	13775198	-3.1	565	0.032
39	S100 Ca-binding protein A6	7657532	-2.19	141	0.031
40	Ubiquitin and ribosomal protein S27a precursor	4506713	-2.79	382	0.031
32	Peroxiredoxin 1	4505591	-2.29	269	0.031

Remarkably, all 37 proteins identified as differentially expressed were downregulated in the *cb1C* fibroblasts. This indicates that supplementation of the cell cultures with a supraphysiological dose of HOCbl induced a global downregulation of the *cb1C* proteome with respect to the normal cell lines. Of interest, no differences in the expression of HDL binding protein, col VI alpha 1 precursor, eEF2, GST omega 1, GST M3 and GAPDH were observed between normal and *cb1C* fibroblasts upon supplementation with HOCbl. This suggests that supplementation with HOCbl corrected for the alterations caused by its deficiency or insufficiency.

In the absence of exogenous HOCbl col VI isoform 2C2 was upregulated in the *cb1C* fibroblasts (normal/*cb1C* ratio + 2.1), whereas the opposite result was obtained for cells

grown in the presence of HOCbl (normal/*cb1C* ratio – 2.72). This indicates a profound effect of HOCbl supplementation on the expression levels of this important structural protein.

A remarkable result was observed in the expression levels of vimentin. Supplementation of the cell cultures with HOCbl exacerbated the differences between normal and *cb1C* fibroblasts further. In the absence of HOCbl, normal/*cb1C* vimentin was -2.44, whereas in the presence of exogenous HOCbl this ratio decreased to -5.03. This remarkable finding was validated further by immunocytochemistry and western blot experiments. **Figure 4.12** shows the results for immunocytochemistry for human vimentin from cells cultures grown in the absence of exogenous HOCbl. *cb1C* cell lines presented decreased staining compared to the normal cell line. Patient fibroblasts WG3354 appeared to present an almost normal vimentin phenotype according to the image. Western blot were performed for vimentin expression in cells grown with HOCbl supplementation (**Figure 4.13**). The expression pattern resembled that observed in 2D-DIGE experiments, i.e., significantly decreased levels of vimentin were observed in the *cb1C* cell lines compared to normal fibroblasts.

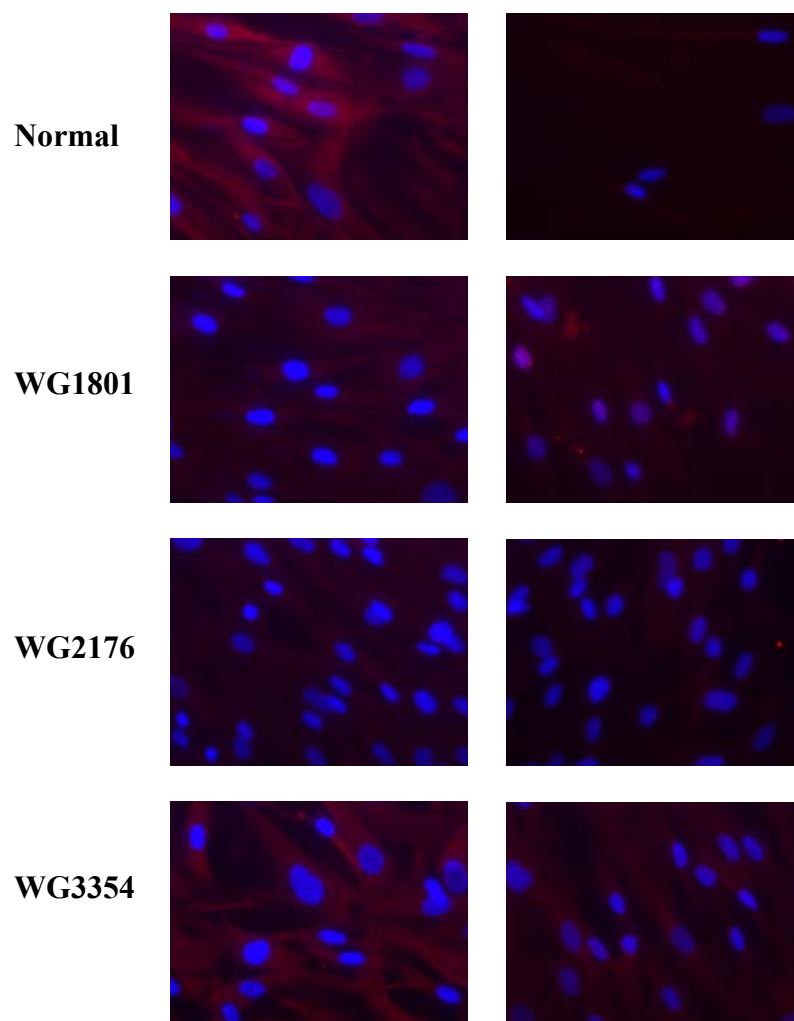


**Figure 4.12.** Immunocytochemistry of human normal and *cbIC* fibroblasts with anti-hrVimentin. Cells were grown without HOCbl supplementation. Left column: detection; right column: negative controls (no primary antibody added). Vimentin was stained with Texas Red whereas nuclei were stained with DAPI.

On the other hand, a number of proteins in the *cbIC* proteome remained as downregulated regardless of supplementation with HOCbl. This includes PDI associated precursor 3, CLIC4, UCHL1, GST, SH3DBGRP and S100A6. It is important to consider

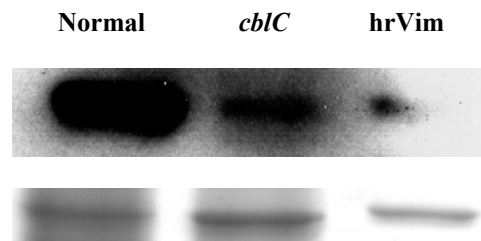


**Figure 4.13.** Western blots for vimentin. Human normal and *cbIC* fibroblasts grown in the presence of 723 nM HOCbl were stained with anti-hrVimentin. Upper row: detection; Bottom row: coomassie staining of the SDS-PAGE. Vimentin was stained with Texas Red whereas nuclei were stained with DAPI. Each lane represents pooled normal and *cbIC* patient samples (n=3). hrVim: human recombinant vimentin.

that the global downregulation can be due to a partial or total inability of the *cbIC* cell lines to respond and adapt to the changes induced by supplementation with HOCbl, which were fully functional in the normal cell line, rather than a direct effect of HOCbl on the *cbIC* proteome. Supplementation with HOCbl caused the differential expression of a number of proteins that were not identified or differentially expressed in cells that were grown without exogenous HOCbl. These included: vinculin VCL, Hsp90, Hsp70, annexins VI and V, septin 11, peroxiredoxins 1 and 6, cofilin 1, DJ-1, transgelin 1 and others (see **Table 4.5**). When possible, additional validation assays were conducted. As an example, **Figure 4.14**, panels **A** and **B** show activity assays for GST and Annexin V. Lower GST activity was determined in *cbIC* fibroblasts compared to the normal cell line, which correlates with the lower levels of expression observed in the 2D-DIGE experiments. Lower concentrations of annexin V (determined using an ELISA assay kit) were found in *cbIC* fibroblasts compared to normal cells, which again confirms our 2D-DIGE results.

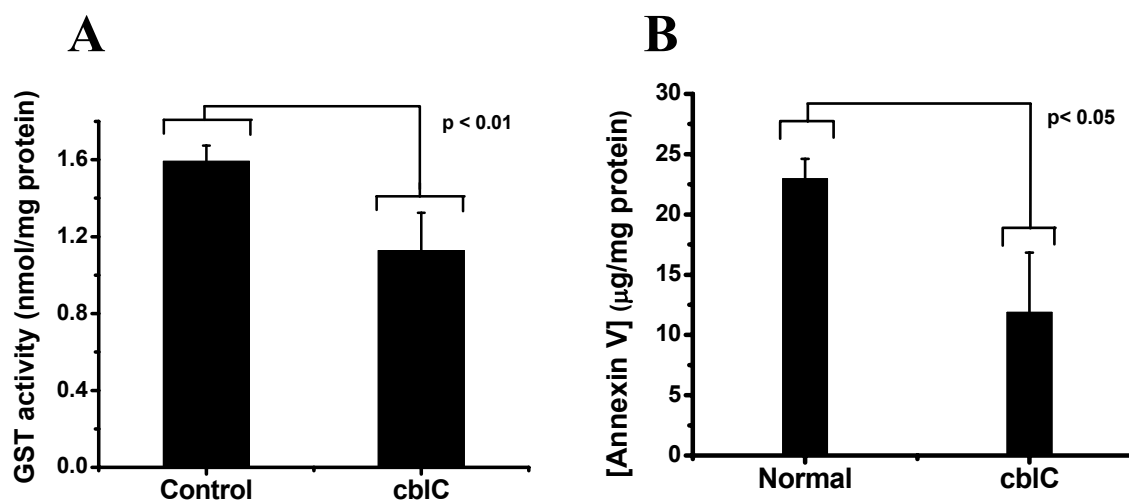


**Figure 4.14.** Glutathione transferase activity (**panel A**) and concentration of annexin V (**panel B**) in normal and *cbIC* fibroblasts grown in the presence of 723 nM HOCbl. Fresh cell lysates were prepared and the assays conducted according to the manufacturer's directions (see Materials and Methods).

Overall, these results indicate that: 1) the *cbIC* proteome differs substantially from that of normal cells, and 2) supplementation with HOCbl does not completely restore the *cbIC* proteome to that observed in normal fibroblasts.

### **Cytoskeleton: assembly and remodeling.**

Substantial changes in protein expression levels between normal and *cbIC* fibroblasts were found for cytoskeletal proteins with structural and regulatory roles. These included collagen VI, alpha 1 and 2C2 isoforms, vimentin, tubulin alpha,  $\beta$ -actin, vinculin VCL, plastin 3, lamin A/C isoform 2, chaperonin TCP1, caldesmon 1, cofilin, 1 and transgelin 2.

Interestingly, changes in cytoskeletal proteins have been reported for a patient cell line belonging to the complementation group D (*cbID*) (Richard et al. 2006) and also, for

human fibroblasts grown under conditions of folate deficiency (Katula, Heinloth, and Paules 2007).

Our results showed that the production of collagen VI, 2C2, was upregulated in *cb1C* fibroblasts grown without HOCbl supplementation, and downregulated in *cb1C* cells grown in the presence of 723 nM HOCbl. In the absence of HOCbl supplementation, *cb1C* fibroblasts exported increased levels of both Hcy and MMA. Supplementation of the cell cultures with 723 nM HOCbl corrected the levels of MMA to some extent, but very mild correction was observed in the levels of Hcy. These findings suggest that increased levels of Hcy may be responsible for the upregulation of collagen VI, 2C2, in *cb1C* fibroblasts and that even a modest decrease in the levels of Hcy could have a substantial impact in the expression pattern of this protein.

Collagen VI is a major structural component of microfibrils. Mutations in the genes that code for collagen VI subunits result in Ullrich syndrome (Jimenez-Mallebrera et al. 2006) and Bethlem myopathy (Kanagawa and Toda 2006), an autosomal dominant disorder. In a 2D-DIGE proteomic study performed with normal and patient fibroblasts belonging to the *cb1D* complementation group, an upregulation of collagen VI  $\alpha 2$  was also noted (Richard et al. 2006). The patient described in the study presented with isolated methylmalonic aciduria.

In addition, a study performed in human smooth muscle cells demonstrated that high levels of Hcy cause an upregulation in the production of collagen, which could be related to the pathogenesis of homocystinuria (Majors et al. 2002). In support of this proposal, patients

with untreated homocystinuria have widespread premature atherosclerosis with intimal thickening and collagen-rich fibrous plaques (Majors, Ehrhart, and Pezacka 1997).

Based on these findings, it is reasonable to hypothesize that muscular dystrophias and cardiomyopathies, two common presentations of the *cb1C* disorder, are caused by an excessive production of collagens as a result of increased levels of Hcy. This is further supported by the observation that *cb1C* patients show some improvement of their motor functions after prolonged therapy with HOCbl (Andersson, Marble, and Shapira 1999; Andersson and Shapira 1998).

Human vimentin was also downregulated in *cb1C* fibroblasts. Vimentin is a cytoskeletal protein whose major role was initially thought to be stabilizing the architecture of the cytoplasm. An *in vitro* study conducted by Mor-Vaknin et al. showed that monocyte-derived macrophages secrete vimentin into the extracellular space (Mor-Vaknin et al. 2003). Secretion of vimentin was stimulated by TNF- $\alpha$  and inhibited by IL10, suggesting that the protein is also involved in immune response (Mor-Vaknin et al. 2003).

We found that *cb1C* fibroblasts expressed lower levels of vimentin compared to normal cells, and that the difference was further exacerbated by supplementation with HOCbl. It is important to mention that the expression pattern of vimentin is highly tissue-specific (Perreau et al. 1988); therefore, correlations between the expression levels of this protein in fibroblasts with the clinical manifestation of the *cb1C* disorder are difficult. However, low levels of vimentin could be at least partially responsible for the altered morphology of the *cb1C* fibroblasts in culture. To that end, low levels of some major cytoskeleton structural proteins, namely  $\beta$ -actin and tubulin alpha, were also found in *cb1C*

fibroblasts compared to normal cells grown without HOCbl. Supplementation of the cell cultures with HOCbl corrected for the observed downregulation of  $\beta$ -actin, but was without effect on the levels of tubulin alpha. To our knowledge, there is only one report linking cobalamin administration with the expression of actin (the alpha-smooth muscle actin isoform) (Isoda et al. 2008). Isoda et al. reported that the overexpression of actin in liver (a marker of fibrosis) induced by the carcinogenic agent dimethylnitrosamine can be suppressed by administration of CNCbl (Isoda et al. 2008).

Two proteins related to the actin-cytoskeleton, namely caldesmon 1 and plastin 3, were differentially expressed in normal *versus cb1C* fibroblasts. Caldesmon 1 isoform 2 was downregulated in *cb1C* fibroblasts grown in the absence of exogenous HOCbl. Caldesmon 1 is a calmodulin and actin-binding protein that plays an essential role in the regulation of smooth muscle and nonmuscle contraction (Yoshio et al. 2007). Of interest, caldesmon has been proposed to suppress cancer cell invasion by regulating podosome/invadopodium formation (Yoshio et al. 2007). The podosome and invadopodium are cell-adhesion structures that degrade the extracellular matrix thus promoting cell invasion (Yoshio et al. 2007). Supplementation of the cell cultures with HOCbl corrected for the low levels of caldesmon in *cb1C* fibroblasts. Therefore, HOCbl therapy in patients with the *cb1C* disorder could have protective effects against cancer cell invasion by preventing downregulation of caldesmon.

Plastins are a family of actin-binding proteins, which are expressed in most tissues and appear to be differentially expressed in normal and malignant cells (Lin et al. 1993). A recent study demonstrated that plastin 3 is important for axonogenesis through increasing the F-actin level (Oprea et al. 2008). The authors proposed that defects in axonogenesis are the

major cause of spinal muscular atrophy, a neuromuscular disease (Oprea et al. 2008). Of interest, *cb1C* fibroblasts present with neurological and muscular disorders, which are usually alleviated by administration of HOCbl. Our 2D-DIGE study showed that plastin 3 levels in normal and *cb1C* fibroblasts are comparable in cells grown with exogenous HOCbl. This suggests that the physiological role of plastin 3 and its responsiveness to HOCbl could account for some of the symptoms and its alleviation in *cb1C* patients.

Finally, the expression of vinculin VCL, lamin A/C, chaperonin containing TCP1, cofilin 1 and transgelin 2 was downregulated in *cb1C* fibroblasts grown in the presence of exogenous HOCbl but not in cells grown without HOCbl. The interpretation of these results is complex, as none of these proteins were differentially expressed in cells grown without HOCbl supplementation. In principle, we could speculate that supraphysiological levels of HOCbl (723 nM) induce an overexpression of these proteins in the normal cell line that could not be achieved in *cb1C* fibroblasts. Thus, a comparison of the normal and the *cb1C* proteome results translated into downregulation of these proteins in *cb1C* fibroblasts.

Vinculin VCL is a cytoskeletal protein with a role in cell-cell and cell-matrix junctions, and it is thought to be one of the interacting proteins responsible for the anchoring of F-actin to the membrane (Hu et al. 2007). Defects in vinculin VCL are the cause of cardiomyopathy dilated type 1W, which ultimately leads to congestive heart failure and arrhythmia (Olson et al. 2002).

Cofilin 1 is a widespread intracellular actin-binding protein that binds and depolymerizes filamentous F-actin and inhibits polymerization of monomeric G-actin in a

pH dependent manner (Ghosh et al. 2004). Cofilin 1 is involved in the translocation of the actin-cofilin complex from the cytoplasm to the nucleus (Ghosh et al. 2004).

Transgelin 2 is one of the earliest markers of differentiated smooth muscle. The function of this protein has not yet been determined (Nagase et al. 1995; Stanier et al. 1998). The sequence indicates a calponin homology domain which is also found in cytoskeletal and signal transduction proteins, including actin-binding proteins like spectrin, alpha-actinin, dystrophin and proteins essential for the regulation of cell shape such as cortexillins.

Lamin A/C is a family of proteins that make up the extracellular matrix. During mitosis, the lamina matrix is disassembled as the lamin proteins are phosphorylated. It is thought that lamins are involved in nuclear stability, chromatin structure and gene expression. Mutations in this gene lead to several diseases, such as Emery-Dreifuss and limb girdle muscular dystrophies, lipodystrophy and cardiomyopathy (Genschel and Schmidt 2000).

Chaperonine containing TCP1 is a molecular chaperone also known as the TCP1 ring complex. Unfolded peptides enter the ring cavity of the complex and are folded in an ATP-dependent manner (Frydman et al. 1992). The complex folds several proteins including actin and tubulin (Frydman et al. 1992). The fact that lower levels of this protein were observed in *cb1C* fibroblasts could account for the low levels of tubulin that were also found in *cb1C* cells.

### **Nervous system and signaling.**

One of the most remarkable findings of our proteomic assessment was the identification of ubiquitin carboxy-terminal hydrolase L1 (UCHL1) as one of the proteins

that is downregulated in *cb1C* fibroblasts. UCHL1, also known as PGP9.5, is a major component of the ubiquitin-proteasome system (UPS), a major pathway for protein degradation (Gong and Leznik 2007). UCHL1 is one of the most abundant proteins in the brain (1-2% of the total soluble protein) and was reported to be exclusively localized in neurons (Wilson et al. 1988) and in cells of the diffuse neuroendocrine system and their tumors (Doran et al. 1983). Downregulation and extensive oxidative modification of UCHL1 have been observed in brain tissue of patients with Alzheimer's, as well as Parkinson's diseases (Castegna et al. 2002; Choi et al. 2004; Butterfield et al. 2006). Downregulation of UCHL1 in *cb1C* fibroblasts was not restored to normal levels upon supplementation with HOCbl. Therefore, downregulation of UCHL1 could be partially responsible for the documented inability of *cb1C* patients to achieve normal cognitive performance after prolonged treatment with HOCbl (Andersson, Marble, and Shapira 1999).

Another protein that was downregulated in *cb1C* fibroblasts and whose levels of expression were not altered by supplementation with HOCbl was SH3 domain binding Glu-rich protein like 3 (SH3BGRP3). SH3BGRP3 is a highly conserved protein that presents significant similarity to glutaredoxin 1 of *E. coli* (Mazzocco et al. 2001). Little is known about the function of this protein in humans; however, its structure suggests that it could function as an endogenous modulator of glutaredoxin biological activity (Mazzocco et al. 2001). A recent report suggests that SH3BGRP3 may also play a role in the all-trans retinoic acid –induced signaling pathway (Xu et al. 2005).

On the other hand, serpinB6, a member of the intracellular serine protease inhibitors was downregulated in *cb1C* fibroblasts grown without exogenous HOCbl, however its expression level compared to that of normal fibroblasts when the cell cultures were

supplemented with HOCbl. SerpinB6 is thought to prevent cellular damage by scavenging leaking lysosomal proteases. A recent report showed that serpinB6 localized mainly in the cytoplasm of endothelial and epithelial cells, monocytes and neutrophils (Strik et al. 2004).

Importantly, there were three proteins that appeared to be downregulated in *cb1C* fibroblasts grown in the presence of exogenous HOCbl: DJ-1 (Parkinson disease protein 7), dihydropyrimidase-like2, and annexin V A2 isoform I.

DJ-1 belongs to a family of peptidases that acts as a positive regulator of androgen receptor-dependent transcription. DJ-1 may also function as a redox-sensitive chaperone, as a sensor for oxidative stress, and it is thought to protect neurons from oxidative damage (Abou-Sleiman et al. 2003). Defects in this gene are the cause of early-onset Parkinson disease 7 (Abou-Sleiman et al. 2003; Annesi et al. 2005).

Dihydropyrimidase-like2 is a protein that presents homology to dihydropyrimidase and is expressed mainly in the fetal and neonatal brains of mammals and chickens. Little is known about this family of proteins, however, they are thought to be intracellular transducers in the development of the nervous system (Kitamura et al. 1999).

### **Gene regulation and protein synthesis.**

*cb1C* fibroblasts grown in the absence of exogenous HOCbl displayed an upregulation in the expression levels of eukaryotic elongation factor 2 (eEF2), ribosomal protein S14 (RPS14) and H2B member A, and a downregulation in the levels of the calcium binding protein S100A6. Supplementation with HOCbl restored the expression of eEF2, RPS14 and H2B to normal levels in *cb1C* fibroblasts, however, the expression pattern of

S100A6 was unaffected. eEF2 is a GTP-binding translation elongation factor which is essential for protein synthesis (Kaneda et al. 1984). eEF2 promotes the GTP-dependent translocation of the nascent protein chain from the A-site to the P-site of the ribosome (Kaneda et al. 1984). RPS14 is a component of the 40s ribosomal subunit, thus playing an essential role in catalyzing protein synthesis (Rhoads, Dixit, and Roufa 1986). H2B member A is the most abundant member of the H2B histone family, which are responsible for nucleosome structure of the chromosomal fiber (Bonenfant et al. 2006). S100A6 is a calcium binding protein. Proteins belonging to the S100 family localize in the cytoplasm and/or nucleus of a wide range of cells and are thought to be involved in a number of cellular processes such as cell cycle progression and differentiation (Tsoporis, Izhar, and Parker 2008). A recent report showed that in cardiac myocytes, S100A6 is induced by TNF- $\alpha$  via a NF- $\kappa$ B-dependent mechanism, serving a role in homeostasis to limit TNF- $\alpha$  -induced apoptosis by regulating p53 phosphorylation (Tsoporis, Izhar, and Parker 2008). We found that *cb1C* fibroblasts displayed lower levels of S100A6 compared to the normal cell lines, and this was not affected by the presence or absence of exogenous HOCbl.

Two proteins, septin 11 and ubiquitin and ribosomal protein S27a precursor (URPS27a) were downregulated in *cb1C* fibroblast grown in the presence of HOCbl. Septins are a novel family of GTP-binding proteins that appear to play an important role in cytokinesis, membrane dynamics, vesicle trafficking, apoptosis, and cell polarity (Ito et al. 2005). In addition, a recent report suggests a role in the development of proliferative retinal membranes (Xin et al. 2007). Septin 11 was also shown to be downregulated in fibroblasts from patients with the *cb1D* disorder (Richard et al. 2006). URPS27a is a component of the 40s subunit of the ribosome (Redman and Rechsteiner 1989). URPS27a is a cytoplasmic

protein that contains C4-type zinc finger domains. URPS27a is a fusion precursor protein consisting of ubiquitin at the N-terminus and ribosomal protein S27a at the C-terminus (Redman and Rechsteiner 1989). This protein is a precursor of ubiquitin, which is responsible for targeting proteins for degradation by the 26S proteasome (Redman and Rechsteiner 1989). The downregulation observed for URPS27a in *cb1C* fibroblasts suggests that protein turnover may be compromised in patients with the *cb1C* disorder.

### **Intracellular trafficking and protein folding.**

A number of proteins involved in protein folding and intracellular trafficking were downregulated in *cb1C* fibroblasts compared to the normal cell line, which was not reversed by exogenously added HOCbl to the cell cultures. These include: PDI precursor 3 and PDI associated 4, Hsp90 1 and Hsp90 alpha class A member 1 isoform 2, Hsp70 proteins 5 and 8, annexin VI isoform 1, annexin 5, annexin V A2, a lysosomal  $-H^+$  transporting ATPase, and voltage dependent anion channels 1 and 2. Importantly, PDI, Hsp70 and Hsp90 play important roles in folding of newly synthesized proteins or stabilizing and refolding of denatured proteins after stress (Appenzeller-Herzog and Ellgaard 2008; Gregersen 2006). Annexins are a family of Ca-dependent and membrane-binding proteins, which are involved in membrane trafficking and various other processes including signaling, proliferation, differentiation, and inflammation (Raynal and Pollard 1994; Gerke, Creutz, and Moss 2005; Grewal and Enrich 2006). Lysosomal  $H^+$ -transporting ATPase is a vacuolar multisubunit enzyme that mediates acidification of eukaryotic intracellular organelles, a critical step for processes such as protein sorting, zymogen activation, receptor-mediated endocytosis and synaptic vesicle proton gradient generation (Stevens and Forgac 1997). The voltage dependent anion channels (VDACs) are the major channels by which small hydrophilic

molecules can pass through the mitochondrial outer membrane. There is increasing evidence that VDAC isoforms in mammals may act in the cross-talk between mitochondria and the cytoplasm by direct interaction with enzymes involved in energy metabolism and proteins involved in mitochondrial-induced apoptosis (Meins, Vorrhein, and Zeth 2008). VDACS also interact with anti-apoptotic proteins from the Bcl-2 family, and this interaction inhibits the release of apoptogenic proteins from the mitochondria (Hiller et al. 2008). The expression of both VDAC1 and VDAC2 was lower in *cb1C* fibroblasts than in normal cells, a pattern that did not vary when cells were grown in the presence of HOCbl.

#### **General metabolism and cellular detoxification.**

A number of proteins involved in general metabolism and cellular detoxification were identified as downregulated in the *cb1C* proteome. These include: high density lipoprotein binding protein (HDLBP), glycerol phosphate-3-dehydrogenase (GAPDH), glutathione-S-transferase (GST) (various isoforms), chloride intracellular channel 4 (CLIC4), phosphoglycerate dehydrogenase, tryptophanyl-tRNA synthetase isoform a, inosine monophosphate dehydrogenase 2, triosephosphate isomerase 1, and peroxiredoxins 1, 2 and 6. HDLBP was upregulated in *cb1C* fibroblasts grown without exogenous HOCbl; however no differences in the expression levels of this protein were found for cells grown with HOCbl supplementation. HDLBP, also known as vigilin, specifically binds to HDL and may function in the removal of excess cellular cholesterol (Plenz et al. 1994).

There were two proteins whose expression patterns were unaffected by the presence of added HOCbl: CLIC4 and GST. CLIC4 encompasses a group of proteins that regulate fundamental cellular processes such as stabilization of cell membrane potential,

transepithelial transport, maintenance of intracellular pH and regulation of cell volume. CLIC4 is a cytoplasmic and mitochondrial protein that is regulated by p53 and TNF-alpha (Fernandez-Salas et al. 1999; Fernandez-Salas et al. 2002). The observed downregulation of CLIC4 could therefore be partially responsible for the altered cellular morphology that was described in previous sections.

GAPDH levels were lower in *cb1C* fibroblasts grown without HOCbl compared to that of normal cells, but no differences were detected in fibroblasts supplemented with HOCbl. Two other enzymes involved in glycolysis were also downregulated in *cb1C* fibroblasts grown in the presence of exogenous HOCbl: phosphoglycerate dehydrogenase and triose phosphate isomerase.

*cb1C* fibroblasts supplemented with HOCbl also showed decreased expression of tryptophanyl-tRNA synthetase isoform a and inosine monophosphate dehydrogenase 2, compared to the normal cell line. The former enzyme catalyzes the aminoacylation of tRNA by their cognate amino acid, trp (Shen et al. 2008). Inosine monophosphate dehydrogenase 2 is the rate-limiting enzyme responsible for the *de novo* biosynthesis of guanine nucleotide (Zimmermann, Spychala, and Mitchell 1995). Its function is to maintain adequate pools of deoxy-guanine and ribonucleotides for DNA and RNA synthesis, respectively (Zimmermann, Spychala, and Mitchell 1995).

Importantly, three isoforms of GST were downregulated in *cb1C* fibroblasts grown without HOCbl supplementation: GST omega 1, GST, and GST M3. Of these, only GST remained downregulated under conditions of HOCbl supplementation, whereas the expression levels GST omega 1 and GST M3 did not differ significantly from that of normal

cell lines. The GST family of proteins uses glutathione in the process of biotransformation of drugs, xenobiotics and oxidative stress. A recent report showed significant associations between the age of onset of Alzheimer's and Parkinson's diseases and polymorphisms of GST omega 1 and 2 (Takeshita et al. 2009). The mu (M) class of GST functions in the detoxification of electrophilic compounds, including carcinogens, therapeutic drugs, environmental toxins and products of oxidative stress by conjugation with GST (Inskip et al. 1995). Immunoblotting analysis revealed that GST M3 is the predominant isoform found in brain (Campbell et al. 1990). Our activity assays confirmed that *cb1C* fibroblasts have reduced total GST activity. This may compromise the detoxification of metabolites that could potentially aggravate the manifestation of the *cb1C* disease.

Three members of the peroxiredoxin family were downregulated in *cb1C* fibroblasts grown with HOCbl supplementation: peroxiredoxins 1, 2 and 6. Peroxiredoxins are responsible for the detoxification of hydrogen peroxide as well as of organic peroxides, thus exerting a protective role against oxidative damage (Knoops, Loumaye, and Van Der Eecken 2007). Peroxiredoxins have been also implicated in the regulation of phospholipid turnover and may contribute to the antiviral activity of CD8(+) T-cells (Knoops, Loumaye, and Van Der Eecken 2007).

## **SUMMARY**

Examination of the *cb1C* proteome indicated that protein expression patterns are significantly different in the biochemical background of a defective *MMACHC* gene. We observed that major changes affect various aspects of cellular metabolism and regulation,

including cytoskeleton assembly and reorganization, nervous system proteins, signaling and cellular detoxification. Some of the proteins identified by this study have been strongly associated with skeletal and muscular diseases as well as neurological diseases. This is consistent with the clinical manifestations of the *cb1C* disorder. We anticipate that the identification of some proteins whose expression was strongly affected by the *cb1C* mutation, could be useful for designing alternative therapies to alleviate the symptoms of the *cb1C* disease that do not respond sufficiently to the current approaches (HOCbl supplementation alone or in combination with other drugs). For instance, administration of UCHL1 (a protein that is mutated or downregulated in patients with Alzheimer's and Parkinson's disease, and also downregulated in *cb1C* fibroblasts from three patients) was shown to alleviate the  $\beta$ -amyloid-induced synaptic dysfunction and memory loss associated with a mouse model of Alzheimer's disease (Gong et al. 2006).

By the same reasoning, it could be interesting to test whether some of the therapies utilized to treat patients with skeletal and muscular diseases would be also effective for alleviating related symptoms in patients with mutations in the *cb1C* gene; we now know that at least some of the proteins involved in the progression of these diseases appear to have a common functional relationship (collagen VI, vimentin, actin cytoskeleton). Although these notions remain speculative until further research is conducted, our results open new avenues for the investigation of the most common inborn error in human cobalamin metabolism.

## MATERIALS AND METHODS

**Human fibroblasts cell lines.** Normal and *cb1C* fibroblasts were grown in Advanced DMEM supplemented with 10% FBS (final total Cbl concentration: 66 pM) as described in **Chapter 4, Project 1.**

**Preparation of cell lysates for activity assays.** Fresh cell lysates for activity assays and/or ELISA were prepared according to the manufacturer's directions.

**Preparation of cell lysates for 2D-DIGE experiments.** Fibroblast cell lines were cultured to confluency in T- 150 flasks (1 flask/cell line) for 7 days. Cells were then harvested by incubation with trypsin, the pellets were washed, resuspended in PBS and counted using an hemacytometer. The cells pellets were isolated by centrifugation and stored at -20°C until further use. The frozen pellets were freeze-thawed three times, and lysed with 0.2 mL of homogenization buffer (40 mM Tris, 7 M Urea, 2 M Thiourea, 4% CHAPS, pH 8.6 containing the complete mini protease inhibitor cocktail (Roche) per cell pellet. The concentration of protein was determined on a 5 µL aliquot using the 2-D Quant kit (Amersham). 500 µg of total protein per cell line were divided into two aliquots of 250 µg of protein and were subjected to a "clean-up" procedure using the 2-D Clean up kit (Amersham). The final pellet from each tube was resuspended with 50 µL/pellet of lysis/homogenization buffer and the 2 aliquots of each sample were pooled prior to protein determination (Final volume = 100 µL). The protein concentration was determined on a 5 µL aliquot using the 2-D Quant kit. The samples were stored at -20 °C until CyDye labeling.

**CyDye labeling procedure.** CyDye stock solutions were prepared according to the manufacturer's recommendations. Briefly, each CyDye was resuspended to a final concentration of 1 nmol/mL with DMF, mixed by vortexing for 30 s, and collected by

centrifugation at 12000 rpm for 30 s. Store -20 °C until further use. An internal standard (IS) was prepared as follows: pool 250 µg of each sample together (1mg total protein in 500 µL). Add 268.3 µL of lysis buffer to adjust the concentration of protein to 2 mg/mL. The IS pool is used for two purposes: 1) One aliquot (200 µg) is labeled with Cy2 to be used as the IS on each of the 4 analytical gel and 2) the remainder (800 µg) was used for the Prep Gel that will be Spot Picked for MS analysis. 0.20 mg of the IS were labeled with Cy2 by addition of 1600 pmol of Cy2. Mix 2.4 µL of DMF with 1.6 µL of Stock Cy2 Dye (1,000 pmol/mL) to yield a final concentrations of 400 pmol/ µL. 200 µg of IS (100 µL) were then added to the 4 µL Cy2 working solution (400 pmol dye/50 µg protein). 150 µg of the HFF sample was labeled with Cy5 and 50 µg of each *cb1C* mutant sample was labeled with Cy3 under the same conditions, i.e., 400 pmol dye/50 µg protein. The samples were mixed, spun down and allowed to react for 30 min in the dark, at 4°C (on ice). The labeling reaction was stopped by addition of 1 µL of 10 mM lysine. The mixture was vortexed, spun down and left on ice for 10 min in the dark. Labeled samples can be stored for up to 3 months at -70°C.

**Sample preparation for isoelectrofocusing (IEF), 1st dimension.** The CyDye labeled samples were thawed to room temperature. For the analytical gels, three tubes containing mixtures of 50 µg (25 µL) of one Cy3-labeled sample, 50 µg (25 µL) of one Cy5 labeled sample and 50 µg (25 µL) of the Cy2 labeled standard mix were prepared. Disulfide bonds were reduced by addition of 2% DTT to the pooled samples (final concentration of DTT = 0.2%). Samples were vortexed and 0.37 mL of DeStreak solution (Amersham) was added to each mixture. The resulting protein concentration is ~ 0.33mg/mL (150 µg/450 µL). For the preparative gels (P1 and P2), an aliquot of 0.60mg (in 0.3 mL) of total protein was

placed into a microfuge tube. 2% DTT was added to a final concentration of 0.2%. The samples were vortexed, and 100  $\mu$ L of DeStreak solution (+0.5% Ampholytes (Amersham)) was added. The final concentration of protein was  $\sim$ 1.33 mg/mL (0.60 mg/450  $\mu$ L). Samples were isoelectrofocussed using an Amersham IPGphor IEF system. 0.45 mL of the sample was placed in the strip holder and assembly of the system was done according to the instrument's instructions. The IEF strips were rehydrated for 11 h at 20  $^{\circ}$ C using 50  $\mu$ Amp/strip and 30V. Rehydration with IEF was done according to the following scheme:

Step	Type of Step	Voltage	$\mu$ A/strip	W	Time (h)
1	Gradient	250	.05	0.1	0:30
2	Gradient	250-6000	.05	0.1	0:30
3	Gradient	6000	.05	0.1	5:00
4	Gradient	6000	.05	0.1	9:30
END					
Total					15:50

Note: although the analytical and preparative cannot be subjected to isoelectrofocusing together (due to voltage conditions), they were run together in the second dimension, SDS-PAGE.

**2nd Dimension: SDS-PAGE (Ettan Dalt Twelve Electrophoresis system).** The IPG strip was placed face up into an equilibration tube and equilibrated in a 2-step procedure. The strip was first covered with 7 mL of SDS Equilibration Buffer #1 (reducing buffer: 6 M urea, 2% SDS, 30% glycerol, 1.6% DTT, 50 mM Tris and 0.002% BPB, pH 8.8) and incubated with gentle shaking for 15 min, at room temperature. The solution was carefully removed and 10 mL of SDS Equilibration Buffer #2 (alkylation buffer: 6 M urea, 2% SDS,

30% glycerol, 2% Iodoacetamide, 50 mM Tris and 0.002 % BPB, pH 8.8) were added. The strip was incubated with gentle shaking for 15 min at room temperature. Note: the incubation time appears to be critical for reproducibility. The gel was casted as directed by the manufacturer, covered with 1X running buffer (BioRad) and ran for 6-7 h at constant power according to the following program: Step 1: 1 h at 2.5watts/strip; Step 2: 7 h at 180 watts max; 17 watts/gel. After the run was complete, the gels were rinsed with H<sub>2</sub>O. The gels were wrapped in cellophane paper and stored at 4°C until imaged.

**Staining of the preparative gels.** The top cover was removed and the gel was rinsed briefly with H<sub>2</sub>O. The gel was then fixed in 10% ethanol/ 7.5% acetic acid for 30 min with gentle shaking, and stained overnight with Pierce GelCode Blue with gentle shaking at room temperature. The gel was destained with H<sub>2</sub>O.

**Imaging and data analysis.** Fluorescence images of the gels were acquired on a Typhoon 9400 scanner (GE Healthcare). Cy2, Cy3, and Cy5 images for each gel were scanned with a resolution of 200 pixels. The image files were then analyzed with DeCyder software using published (Marouga, David, and Hawkins 2005; Karp, Kreil, and Lilley 2004) and manufacturer's recommendations (GE Healthcare). Only proteins with a fold change equal or greater than  $\pm 2.0$  and a statistical significance of at least 95% ( $p \leq 0.05$ ) were selected for identification.

**Protein digestion, mass spectrometry and protein identification.** For the protein digestion, the bands were cut to minimize excess polyacrylamide, divided into a number of smaller pieces, washed and destained. The gel pieces were then washed with water and dehydrated in acetonitrile. The bands were alkylated with iodoacetamide prior to the in-gel digestion step. All the bands were digested in-gel by adding 5  $\mu$ L 20 ng/ $\mu$ L trypsin in 50

mM ammonium bicarbonate and incubating the samples overnight, at room temperature. The resulting peptides were extracted from the polyacrylamide gel in two aliquots of 30  $\mu$ L using 50% acetonitrile with 5% formic acid. These extracts were combined and evaporated to a final volume of less than 10  $\mu$ L in a Speedvac, and were then resuspended in 1% acetic acid to make up a final volume of  $\sim$ 30  $\mu$ L for LC-MS analysis. The LC-MS system was a Finnigan LTQ linear ion trap mass spectrometer system. The HPLC column was a self-packed 9 cm x 75  $\mu$ m id Phenomenex Jupiter C18 reversed-phase capillary chromatography column. Ten  $\mu$ L volumes of the extract were injected, and the peptides eluted from the column (acetonitrile/0.05 M acetic acid gradient, flow rate: 0.3  $\mu$ L/min) were introduced into the source of the mass spectrometer online. The microelectrospray ion source was operated at 2.5 kV. The tryptic digest was analyzed using the data dependent multitask capability of the instrument acquiring full scan mass spectra to determine peptide molecular weights and product ion spectra to determine amino acid sequence in successive instrument scans. This mode of analysis produces approximately 2,500 collisionally induced dissociation (CID) spectra of ions ranging in abundance over several orders of magnitude. Please note that not all CID spectra are derived from peptides. The data were analyzed by using all CID spectra collected in the experiment to search the NCBI non-redundant database with the search program Mascot using mammalian taxonomy filter. All matching spectra were verified by manual interpretation. The interpretation process was aided by additional searches using the programs Sequest and Blast as needed.

**Western blots.** Western blots for CLIC4, vimentin, PDI, GRP94, UCHL1 were done according to standard procedures. Total proteins (50  $\mu$ g per lane) were resolved on a 12.5% SDS-PAGE, transferred onto a PVDF immobilon membrane, and blotted with the desired

antibody. Antibodies for CLIC4 and UCHL1 were purchased from Abcam (Cambridge, MA, USA). Antibodies for PDI and GRP94 (anti-KDEL monoclonal antibody) were purchased from Stratagene (Ann Arbor, MI, USA). Antibody for vimentin and hrVimentin were purchased from R&D Systems (Minneapolis, MN, USA). Detection was done by chemoluminescence using a commercially available kit (ECL Western Lightning Chemiluminescent Kit, Perkin-Elmer NEL104, Waltham, MA, USA). Quantitation of Western blots was done using ImageJ software (<http://rsbweb.nih.gov/ij/>).

**Immunocytochemistry -Vimentin.** Immunostaining of human vimentin was performed according to a protocol provided by Abcam. Briefly, cells were grown on NUNC 8-well chamber slides (Fisher Scientific, Pittsburgh, PA, USA) to a final density of ~ 50%, the conditioned culture medium discarded and the cells were rinsed briefly in PBS. The samples were then fixed with ice-cold acetone for 4 min. The samples were then washed twice with PBS. Note: fixation with acetone also results in the partial destruction of the cell membrane, this permeabilization is not needed. Cells were incubated in a solution containing 1% BSA in PBST (PBS + 0.25% Triton X-100) for 30 min to block unspecific binding of the antibodies. Cells were then incubated in the diluted antibody in 1% BSA in PBST overnight at 4°C. Negative controls were incubated in the same solution without the primary antibody. The solution was then decanted and the cells were washed three times in PBS, 5 min each wash. The cells were then incubated with the secondary antibody in 1% BSA for 1 h at room temperature in the dark. The solution of secondary antibody was decanted and the cells were washed three times with PBS for 5 min each in the dark. Counter staining was done by addition of mounting medium containing Hoechst or DAPI (DNA stain) for 1 min. The

coverslips when then sealed with nail polish to prevent drying and movement under the microscope. Stained coverslips were stored in the dark at 4°C until microscopic visualization.

**Activity assays and ELISA.** GST activity was determined using a commercial kit (Cayman Chemical, Ann Arbor, MI, USA). Annexin V was determined using an ELISA kit (Immunoclone® Annexin V ELISA kit, American diagnostica Inc, Stanford, CT, USA).

### **4.3. Project 3: Bioinformatic analysis of the pathways perturbed in the *cb1C* disorder/cobalamin deficiency.**

#### **INTRODUCTION**

Proteins that were identified as differentially expressed in *cb1C* fibroblasts compared to normal cells (**Chapter 4, Project 2**) were submitted to the Ingenuity Pathway Analysis (IPA) server ([www.ingenuity.com](http://www.ingenuity.com)) to uncover and explore relevant biological networks.

IPA constructs hypothetical protein interaction clusters on the basis of a regularly updated "Ingenuity Pathways Knowledge Base". The Ingenuity Pathways Knowledge Base is a very large curated database that consists of millions of individual relationships between proteins, culled from the biological literature. These relationships involve direct protein interactions, including physical binding interactions, enzyme substrate relationships, and cis-trans relationships in transcriptional control. The networks are displayed graphically as nodes (individual proteins) and edges (the biological relationships between the nodes). In practice, a data set that contains the GenBank identifiers of differentially expressed proteins identified in the DIGE experiment is uploaded into IPA. IPA then builds hypothetical networks from these proteins, and other non-DIGE-identified proteins from the database that are needed fill out a protein cluster. Network generation is optimized for inclusion of as many proteins from the inputted expression profile as possible and aims for highly connected networks. IPA computes a score for each possible network according to the fit of that network to the inputted proteins. The score is calculated as the negative base-10 logarithm of the P value that indicates the likelihood of the inputted proteins in a given network being found together

as a result of random chance. Therefore, scores of 2 or higher have at least a 99% confidence of not being generated by random chance alone. IPA has been successfully applied in a number of studies (Raponi et al. 2004; Siripurapu et al. 2005; Hoorn, Hoffert, and Knepper 2005; Peddinti et al. 2008). An advantage of combining 2D-DIGE results with bioinformatics is that bioinformatics facilitates the prediction of low abundance regulatory proteins and transcription factors that could be involved in the process under investigation.

## RESULTS AND DISCUSSION

### A. Analysis of the normal and *cbIC* proteomes in the absence of exogenous HOCbl.

A comparative analysis of the normal and *cbIC* proteomes and relevant metabolites (Hcy, MMA, folate and vitamin B<sub>12</sub>) generated two statistically significant cellular networks:

a) Network 1 depicts associations with cell cycle, gene expression and drug metabolism, and b) Network 2 established associations with genetic disorders, skeletal and muscular disorders and lipid disorders (**Figures 4.15** and **4.16**, respectively). A list of the genes involved in these two networks is shown in **Table 4.6**.

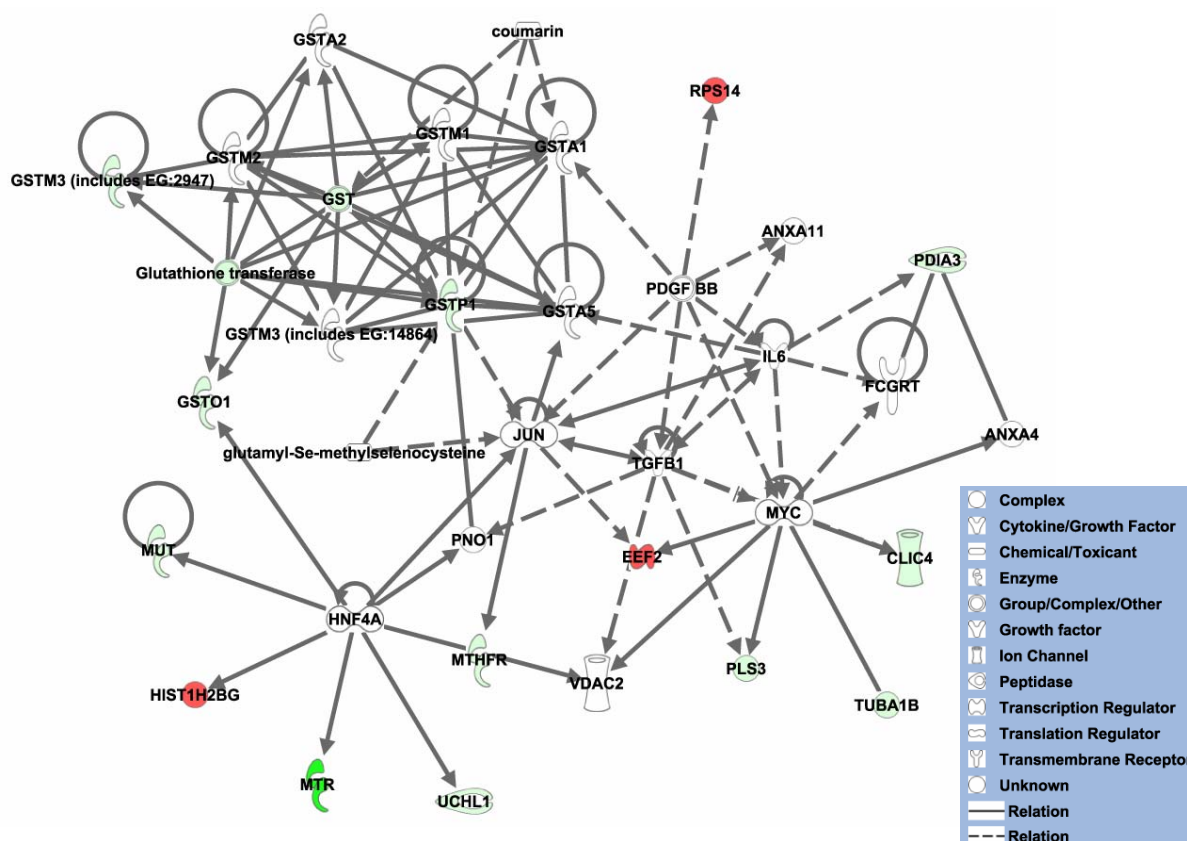


**Figure 4.15. Cell cycle, gene expression and drug metabolism network** generated from 2D-DIGE and metabolites data through comparative analysis of normal and *cb1c* fibroblasts grown without exogenous HOCbl. Solid lines represent direct interactions between molecules, whereas dashed lines represent indirect interactions between molecules. Color code: red: upregulated proteins or metabolites; green: downregulated proteins or metabolites. The intensity of green and red node colors indicates the degree of down or upregulation, respectively.

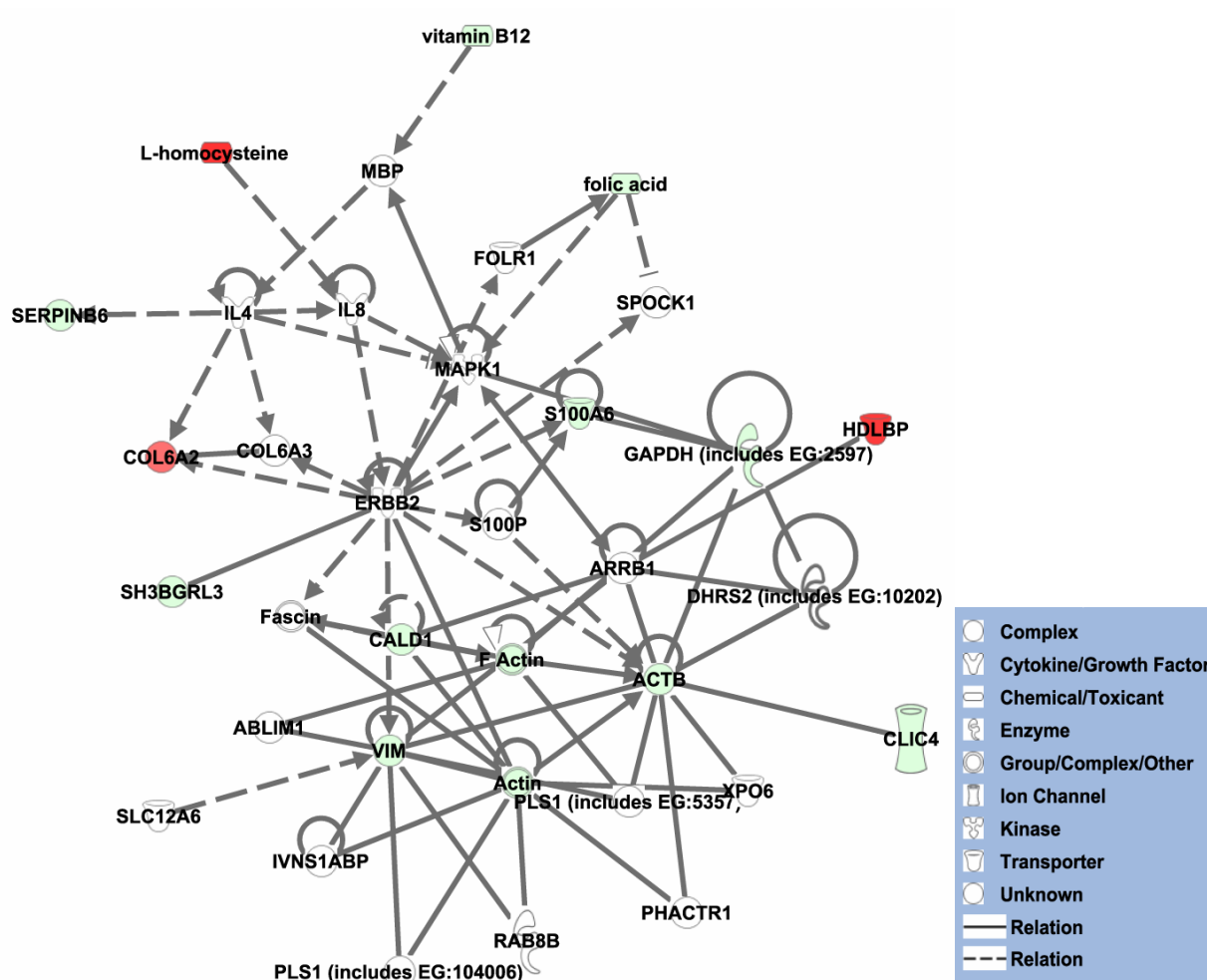


**Figure 4.16. Genetic disorders, skeletal and muscular disorders and lipid disorders network** generated from 2D-DIGE and metabolites data through comparative analysis of normal and *cb1c* fibroblasts grown without exogenous HOCbl. Solid lines represent direct interactions between molecules, whereas dashed lines represent indirect interactions between molecules. Color code: red: upregulated proteins or metabolites; green: downregulated proteins or metabolites. The intensity of green and red node colors indicates the degree of down or upregulation, respectively.

**Table 4.6. List of molecules displaying direct or indirect interactions with differentially expressed proteins determined by 2D-DIGE. Each set of molecules (IDs 1 and 2) was found to belong to a common functional network.**

<b>ID</b>	<b>Molecules in Network</b>	<b>Score</b>	<b>Focus Molecules</b>	<b>Top Functions</b>
1	ANXA4, ANXA11, CLIC4, coumarin, EEF2, FCGRT, glutamyl-Se-methylselenocysteine, Glutathione transferase, GST, GSTA1, GSTA2, GSTA5, GSTM1, GSTM2, GSTM3 (includes EG:14864), GSTM3 (includes EG:2947), GSTO1, GSTP1, HIST1H2BG, HNF4A, IL6, JUN, MTHFR, MTR, MUT, MYC, PDGF BB, PDIA3, PLS3, PNO1, RPS14, TGFB1, TUBA1B, UCHL1, VDACC2	34	14	Cell Cycle, Gene Expression, Drug Metabolism
2	ABLIM1, ACTB, Actin, ARRB1, CALD1, CLIC4, COL6A2, COL6A3, DHRS2 (includes EG:10202), ERBB2, F Actin, Fascin, folic acid, FOLR1, GAPDH (includes EG:2597), HDLBP, IL4, IL8, IVNS1ABP, L-homocysteine, MAPK1, MBP, PHACTR1, PLS1 (includes EG:104006), PLS1 (includes EG:5357), RAB8B, S100A6, S100P, SERPINB6, SH3BGRL3, SLC12A6, SPOCK1, VIM, vitamin B <sub>12</sub> , XPO6	31	13	Genetic Disorder, Skeletal and Muscular Disorders, Lipid Metabolism

The analysis of a total of 28 proteins and metabolites resulted in the detection of direct and indirect interactions with 55 new molecules, which are summarized in **Table 4.6**. IPA® analysis of these interactions established ranks for diseases and disorders derived from the proteome of patients with the *cb1C* disorder. A summary of the top ranked diseases and disorders derived from the analysis of normal *versus cb1C* fibroblasts grown in the absence of exogenous HOCbl is shown in **Figure 4.17**.

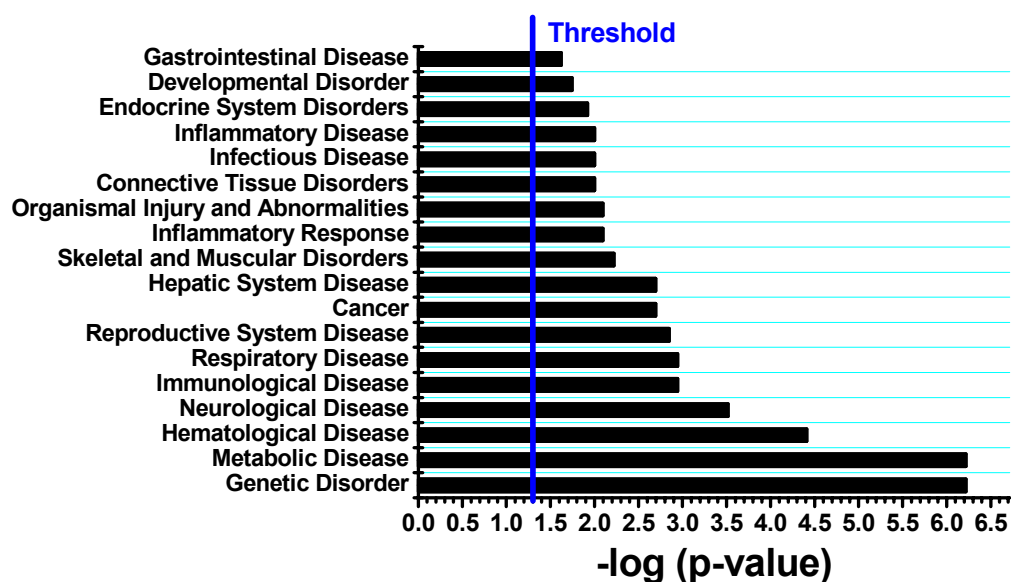


**Figure 4.17.** Top ranked associations for diseases and disorders predicted by IPA® based on 2D-DIGE and metabolite data for normal and *cb1C* fibroblasts grown without exogenous HOCbl. Threshold:  $-\log p$  value ( $p = 0.05$ ).

These associations confirm that the *cb1C* mutation leads to broad dysfunction of the metabolism, leading to manifestations that are typical of genetic and metabolic disorders, hematological and neurological disease, etc. (95% confidence level, threshold  $p = 0.05$ ).

This is consistent with the clinical manifestations of the *cb1C* disease. This supports the reliability of combining 2D-DIGE with bioinformatics for investigating the differential

expression of proteins and for determining direct and indirect associations with proteins that cannot be detected using standard experimental procedures. **Figure 4.18** shows a summary of the statistically significant associations with physiological systems development and functions found from the comparative analysis of normal and *cb1C* fibroblasts grown in the absence of exogenous HOCbl.

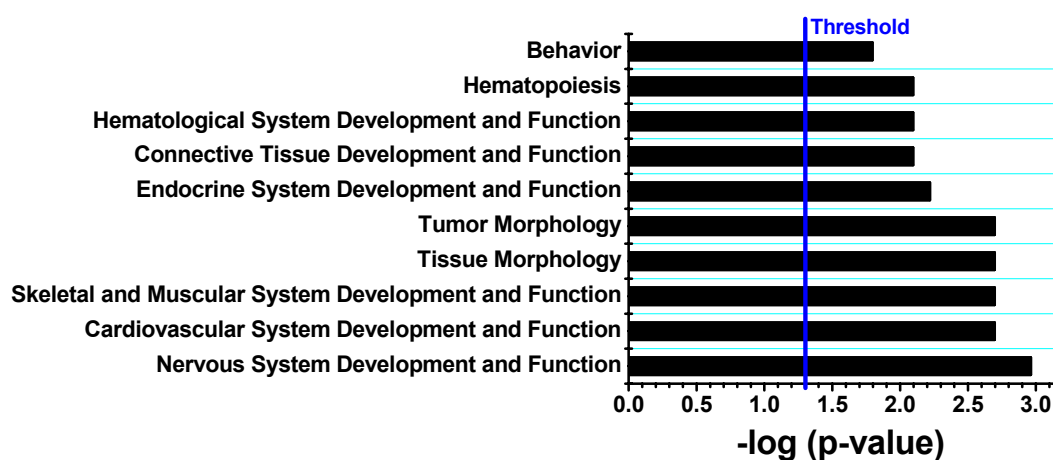


**Figure 4.18.** Top ranked associations for physiological systems development and functions predicted by IPA<sup>®</sup> based on 2D-DIGE and metabolite data for normal and *cb1C* fibroblasts grown without exogenous HOCbl. Threshold:  $-\log p$  value ( $p = 0.05$ ).

The analysis performed by IPA correlates with the clinical features of the *cb1C* disorder: *cb1C* is a genetic and metabolic disease, which presents with neurological, hematological, cardiovascular, skeletal and muscular abnormalities as the principal clinical manifestations. Statistically significant associations with other functions (hepatic system disease, behavioral problems) were also found, some of which have been described less commonly in patients with the *cb1C* disease. This confirms that the *cb1C* patient cell lines chosen in this study provided global insights into the general biochemical and functional hallmarks of the *cb1C* disease, rather than focusing in the case-specific metabolic changes.

## B. Analysis of the normal and *cb1C* proteomes supplemented with HOCbl.

The same analysis was conducted utilizing the 2D-DIGE and metabolite data gathered from normal and *cb1C* fibroblasts supplemented with HOCbl. **Figures 4.19, 4.20 and 4.21** show the top three networks found by IPA®.

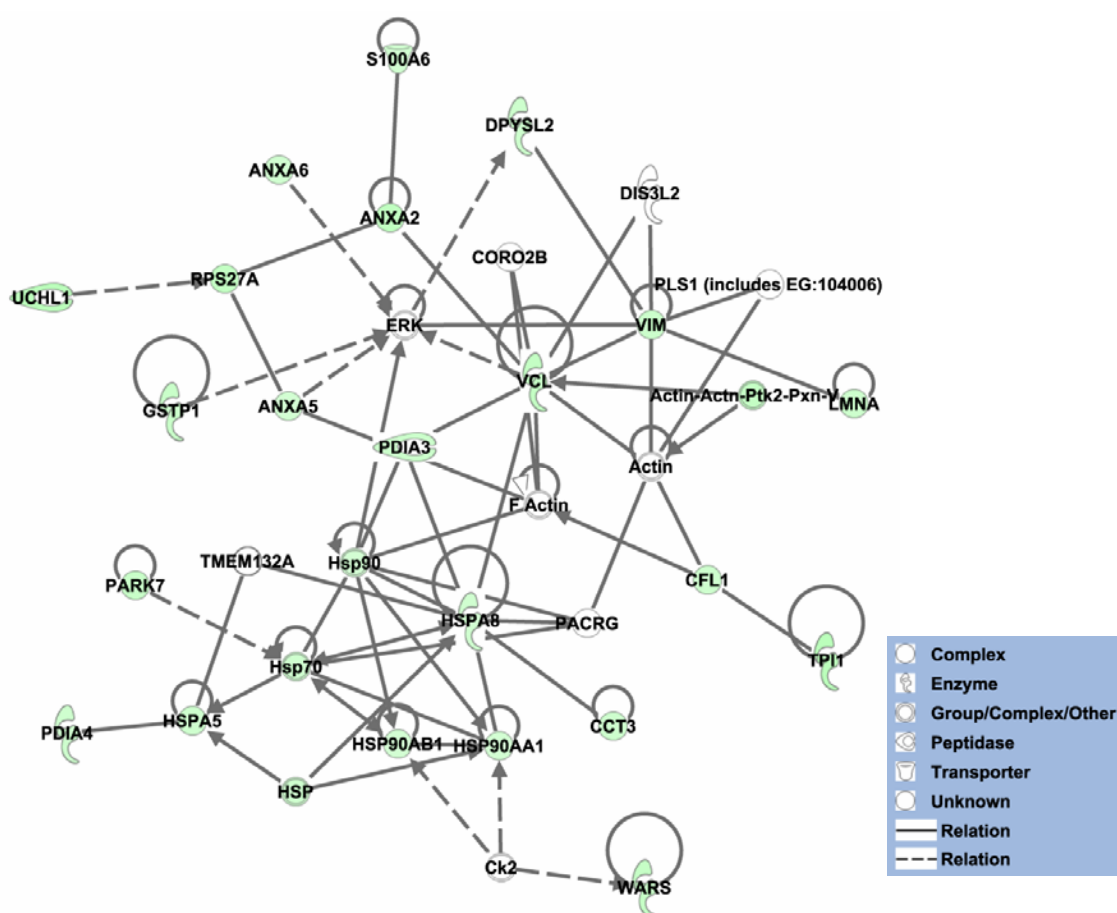


**Figure 4.19. Cancer, post-translational modification and protein folding network** generated from 2D-DIGE and metabolites data through comparative analysis of normal and *cb1C* fibroblasts supplemented with HOCbl. Solid lines represent direct interactions between molecules, whereas dashed lines represent indirect interactions between molecules. Color code: red: upregulated proteins or metabolites; green: downregulated proteins or metabolites. The intensity of green and red node colors indicates the degree of down or upregulation, respectively.

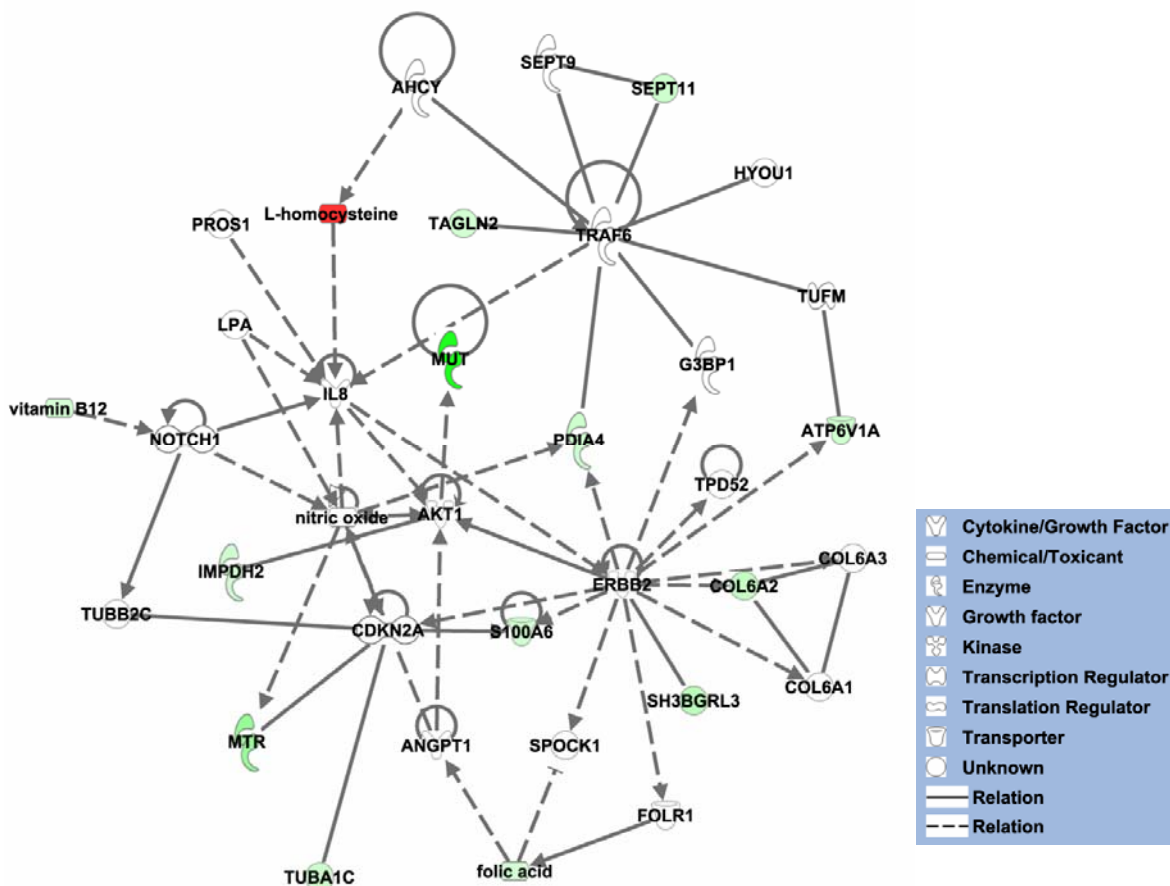


**Figure 4.20. Genetic disorders, skeletal and muscular disorders and cancer network** generated from 2D-DIGE and metabolites data through comparative analysis of normal and *cb1C* fibroblasts supplemented with HOCbl. Solid lines represent direct interactions between molecules, whereas dashed lines represent indirect interactions between molecules. Color code: red: upregulated proteins or metabolites; green: downregulated proteins or metabolites. The intensity of green and red node colors indicates the degree of down or upregulation, respectively.

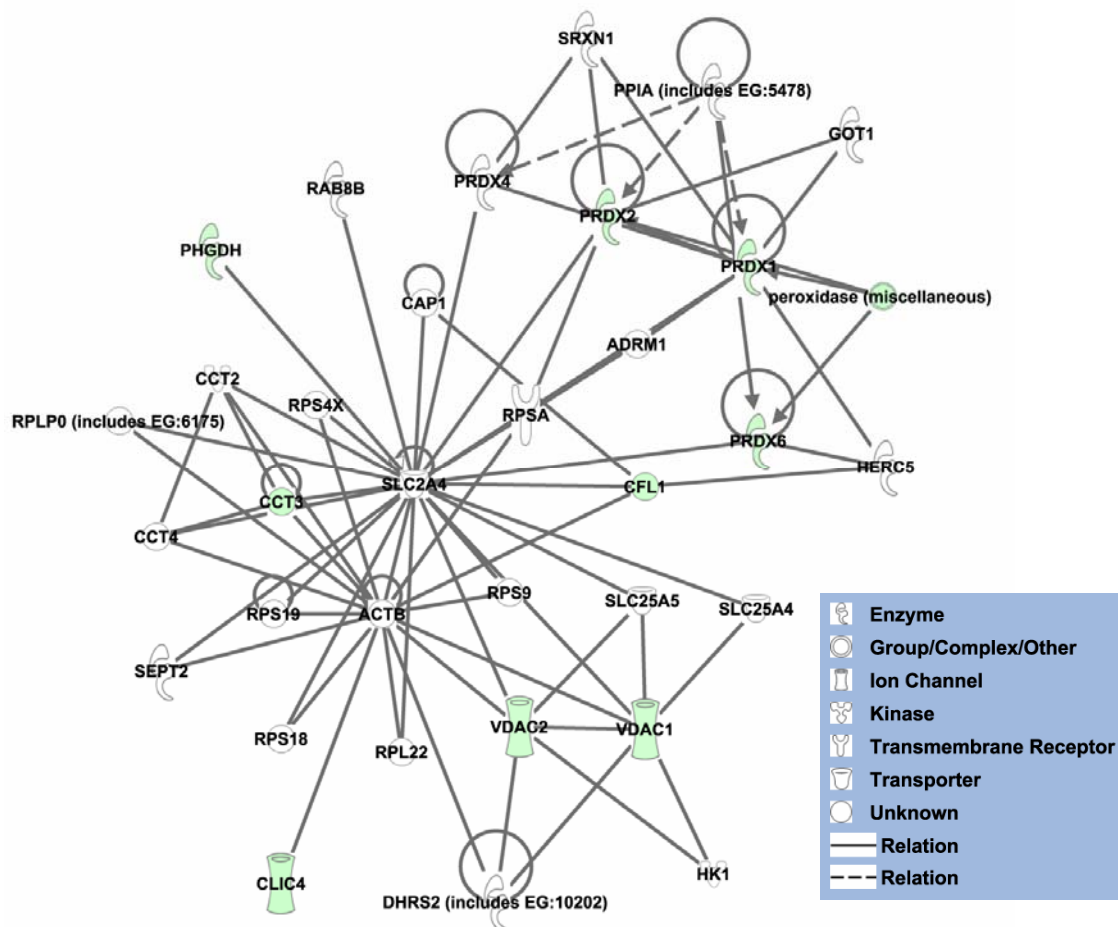


**Figure 4.21. Cellular assembly and organization, small molecule biochemistry and molecular transport network** generated from 2D-DIGE and metabolites data through comparative analysis of normal and *cb1C* fibroblasts supplemented with HOCl. Solid lines represent direct interactions between molecules, whereas dashed lines represent indirect interactions between molecules. Color code: red: upregulated proteins or metabolites; green: downregulated proteins or metabolites. The intensity of green and red node colors indicates the degree of down or upregulation, respectively.

A summary of the proteins involved in each network is given in **Table 4.7**.

**Table 4.7. Genes directly and indirectly associated with the *cb1C* phenotype supplemented with HOCbl, linked to functions by IPA®.**

ID	Molecules in Network	Score	Focus Molecules	Top Functions
1	Actin, Actin-Actn-Ptk2-Pxn-Vcl, ANXA2, ANXA5, ANXA6, CCT3, CFL1, Ck2, CORO2B, DIS3L2, DPYSL2, ERK, F Actin, GSTP1, HSP, Hsp70, Hsp90, HSP90AA1, HSP90AB1, HSPA5, HSPA8, LMNA, PACRG, PARK7, PDIA3, PDIA4, PLS1 (includes EG:104006), RPS27A, S100A6, TMEM132A, TP11, UCHL1, VCL, VIM, WARS	55	22	Cancer, Post-Translational Modification, Protein Folding
2	AHCY, AKT1, ANGPT1, ATP6V1A, CDKN2A, COL6A1, COL6A2, COL6A3, ERBB2, folic acid, FOLR1, G3BP1, HYOU1, IL8, IMPDH2, L-homocysteine, LPA, MTR, MUT, nitric oxide, NOTCH1, PDIA4, PROS1, S100A6, SEPT9, SEPT11, SH3BGRL3, SPOCK1, TAGLN2, TPD52, TRAF6, TUBA1C, TUBB2C, TUFM, vitamin B12	30	14	Genetic Disorder, Skeletal and Muscular Disorders, Cancer
3	ACTB, ADRM1, CAP1, CCT2, CCT3, CCT4, CFL1, CLIC4, DHRS2 (includes EG:10202), GOT1, HERC5, HK1, peroxidase (miscellaneous), PHGDH, PPIA (includes EG:5478), PRDX1, PRDX2, PRDX4, PRDX6, RAB8B, RPL22, RPLP0 (includes EG:6175), RPS9, RPS18, RPS19, RPS4X, RPSA, SEPT2, SLC25A4, SLC25A5, SLC2A4, SRXN1, VDAC1, VDAC2	18	9	Cellular Assembly and Organization, Small Molecule Biochemistry, Molecular Transport

The top ranked group of diseases and disorders, as well as the physiology systems development functions retrieved by IPA® for the normal versus *cb1C* proteome supplemented with HOCbl are shown in **Figures 4.22** and **4.23**.

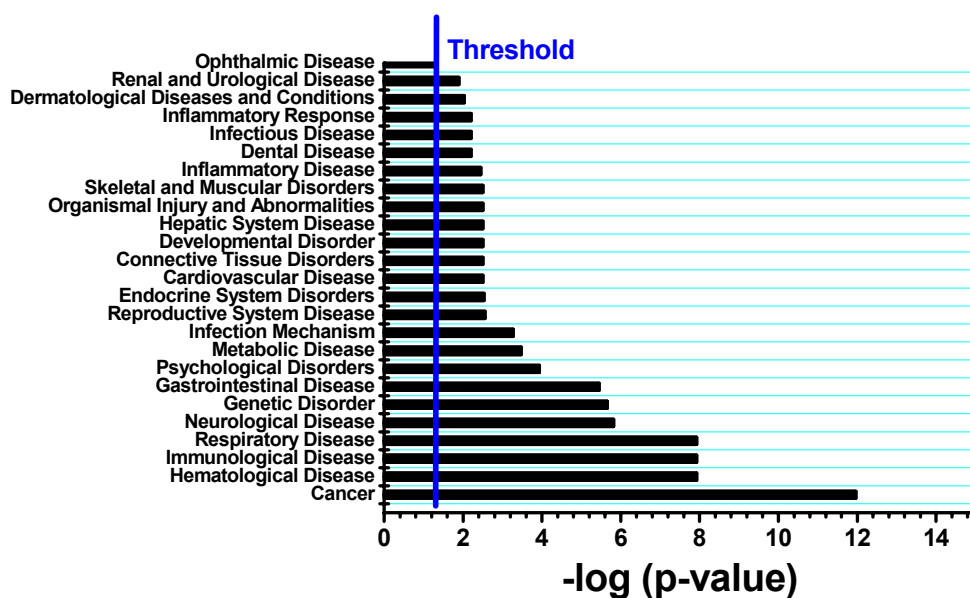


**Figure 4.22.** Top ranked associations for diseases and disorders predicted by IPA® based on 2D-DIGE and metabolite data for normal and *cb1C* fibroblasts supplemented with HOCbl.

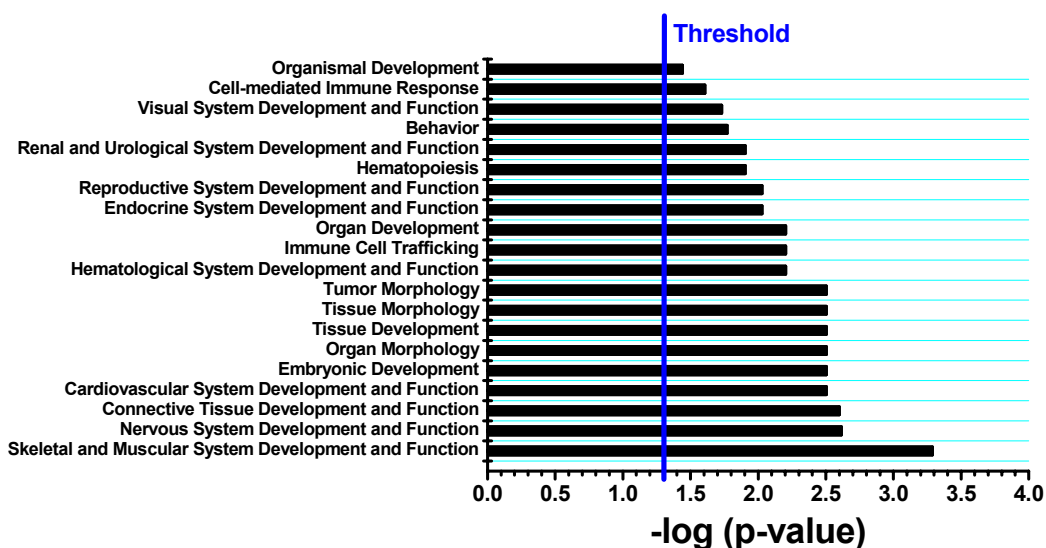


**Figure 4.23. Top ranked associations for physiological systems development and functions predicted by IPA<sup>®</sup> based on 2D-DIGE and metabolite data for normal and *cb1C* fibroblasts supplemented with HOCbl.**

Of interest, supplementation with HOCbl did not reverse the protein expression pattern of the *cb1C* cell lines to that observed in normal fibroblasts. The analysis performed by IPA<sup>®</sup> indicates strong associations with neurological, hematological and skeletal and muscular dysfunctions. This is consistent with the observation that patients with the *cb1C* inborn error are only partially responsive to therapy with HOCbl. Indeed, severely-ill patients do not show substantial improvement of their cognitive and motor functions upon long-term treatment with HOCbl (Rosenblatt et al. 1997).

## SUMMARY

The analysis of relevant pathways and networks revealed by IPA® based on 2D-DIGE results and measurement of relevant metabolites (Hcy, MMA, vitamin B<sub>12</sub> and folic acid) showed that the *cbIC* mutation strongly relates to dysfunctions involving the neurological, skeletal and muscular and hematological systems amongst others. This is in line with the commonly reported manifestations of the *cbIC*. This study provided new targets for the investigation of the biochemical hallmarks of the *cbIC* disease and suggests that alternative therapies usually utilized to treat neurological and skeletal and muscular related diseases could be effective to alleviate the symptoms observed in *cbIC* patients which were not completely eliminated by current therapies. This proposal is based on the finding that the proteins changes associated with these systems are also commonly altered in classical cases of neurological diseases (such as Alzheimer's and Parkinson's diseases) and muscular dystrophies (Bethlem, Ullrich dystrophies). The results obtained in **Projects 2** and **3** of this chapter open new avenues for the investigation of potential alternative treatments to alleviate the clinical manifestations of the *cbIC* disorder.

## MATERIALS AND METHODS

**Analysis of pathways and networks.** A bioinformatic analysis of the results was conducted using Ingenuity Pathway Analysis® software (IPA, [www.ingenuity.com](http://www.ingenuity.com)). Only proteins with a fold change of equal or greater than  $\pm 2.0$  ( $p < 0.05$ ) were included in the study. In addition, Hcy, MMA, folic acid and cobalamin were included, as these metabolites

were determined under the same conditions utilized for the 2D-DIGE experiments (7 days in culture, with and without HOCbl supplementation). The activities of the enzymes methionine synthase, methylmalonylCo-A mutase, cob(I)alamin adenosyltransferase and methyltetrahydrofolate reductase were included, as a comparison between normal and five other *cbIC* fibroblast cell lines was available from the literature and these activity of these enzymes appears to follow a highly reproducible pattern amongst patients (Suormala et al. 2004).

## CONCLUDING REMARKS

The synthesis and characterization of a number of cobalamin forms including NOCbl, HisCbl, EtCbl and BuCbl was carried out. Some of these cobalamin forms were utilized to assess the mechanisms of intracellular cobalamin processing in mammalian cells.

A method for the accurate assessment of intracellular cobalamins was developed. The procedure, which was tested in cultured cells, facilitated the identification and quantification of intracellular cobalamin forms that present exchangeable  $\beta$ -axial ligands.

A new role for the *MMACHC* gene product (*cbIC* protein) has been uncovered. Our *in vivo* studies suggested that the *cbIC* protein is responsible for early processing of both CNCbl (deacylation) and alkylcobalamins (dealkylation), the step preceding cofactor biosynthesis. Our *in vitro* studies confirmed that the *cbIC* protein catalyzes the dealkylation of Co-C bonded cobalamins by a reaction involving the nucleophilic attack of the Co-C bond by the thiolate anion of glutathione.

The proteome of normal and *cbIC* mutant fibroblasts was quantitatively examined by two-dimensional difference in-gel electrophoresis and mass spectrometry, in order to investigate the protein changes that accompany functional cobalamin deficiency in humans. Major changes were observed in the expression levels of proteins involved in cytoskeleton organization and assembly, the neurological system and cell signaling. *In silico* analysis of the differentially expressed proteins established strong associations with neurological disorders, muscular and skeletal disorders, and cardiovascular diseases. Supplementation of the cell cultures with HOCbl did not restore the *cbIC* proteome to the patterns of expression

observed in the normal cell line. Our findings concur with the clinical manifestations of the *cb1C* disorder, and the poor response of severely-ill patients to therapeutic doses of HOCbl.

**REFERENCES**

- Abou-Sleiman, P. M., D. G. Healy, N. Quinn, A. J. Lees, and N. W. Wood. 2003. The role of pathogenic DJ-1 mutations in Parkinson's disease. *Ann Neurol* 54 (3):283-6.
- Alcock, N.W., R.M. Dixon, and B.T. Golding. 1985. The crystal structures of (R)- and (S)-dihydroxypropylcobalamin; comparison with the structure of adenosylcobalamin. *J Chem Soc Chem Commun*:603-605. .
- Allen, R.H., S.P. Stabler, D.G. Savage, and J. Lindenbaum. 1990. Diagnosis of cobalamin deficiency I: Usefulness of serum methylmalonic acid and total homocysteine concentrations. *Am J Hematol* 34:90-98.
- Alpers, D.H., and G.L. Russell-Jones. 1999. Intrinsic factor, haptocorrin, and their receptors. In *Chemistry and Biochemistry of B12*, edited by R. Banerjee. New York: Wiley.
- Andersson, H. C., M. Marble, and E. Shapira. 1999. Long-term outcome in treated combined methylmalonic acidemia and homocystinemia. *Genet Med* 1 (4):146-50.
- Andersson, H.C., and E. Shapira. 1998. Biochemical and clinical response to hydroxocobalamin versus cyanocobalamin treatment in patients with methylmalonic acidemia and homocystinuria (cblC). *J Pediatr* 132:121-124.
- Anes, J. M., R. A. Beck, J. J. Brink, and R. J. Goldberg. 1994. Nitritocobalamin and nitrosocobalamin may be confused with sulfitecobalamin using cation-exchange chromatography. *J Chromatogr B Biomed Appl* 660 (1):180-5.
- Annesi, G., G. Savettieri, P. Pugliese, M. D'Amelio, P. Tarantino, P. Ragonese, V. La Bella, T. Piccoli, D. Civitelli, F. Annesi, B. Fierro, F. Piccoli, G. Arabia, M. Caracciolo, I.

- C. Ciro Candiano, and A. Quattrone. 2005. DJ-1 mutations and parkinsonism-dementia-amyotrophic lateral sclerosis complex. *Ann Neurol* 58 (5):803-7.
- Appenzeller-Herzog, C., and L. Ellgaard. 2008. The human PDI family: versatility packed into a single fold. *Biochim Biophys Acta* 1783 (4):535-48.
- Banerjee, R., Z.Q. Chen, and S. Gulati. 1997. Methionine synthase from pig liver. *Methods Enzymol* 281:189-196.
- Banerjee, R., and S. Chowdhury. 1999. Methylmalonyl-CoA mutase. In *Chemistry and Biochemistry of B<sub>12</sub>*, edited by R. Banerjee. New York: Wiley.
- Barker, H.A., R.D. Smyth, H. Weissbach, A. Munch-Petersen, J.I. Toohey, J.N. Ladd, B.E. Volcani, and R.M. Wilson. 1960. Assay, purification, and properties of the adenylobamide coenzyme. *J Biol Chem* 235:181-190.
- Beck, W.S. 1991. Diagnosis of megaloblastic anemia. *Annu Rev Med* 42:311-322.
- Begley, J. A., and C. A. Hall. 1979. Presence of sulfitocobalamin in cell extracts. Resolution and identification by SP-Sephadex C-25 cation exchange chromatography. In *Vitamin B<sub>12</sub>*, edited by B. Zagalak and W. Friedrich. Berlin: Walter de Gruyter.
- Begley, J.A., and C.A. Hall. 1979. Overestimation of cyanocobalamin due to coelution of sulfitocobalamin on SP-Sephadex C-25. *J Chromatogr.* 177:360-362.
- Bonenfant, D., M. Coulot, H. Towbin, P. Schindler, and J. van Oostrum. 2006. Characterization of histone H2A and H2B variants and their post-translational modifications by mass spectrometry. *Mol Cell Proteomics* 5 (3):541-52.
- Brasch, N.E., and R.G. Finke. 1999. A simple, convenient and direct method for assessing the purity of cobalamins. *J Inorg Biochem.* 73:215-219.

- Brattström, L., and A. Lindgren. 1992. Hyperhomocysteinemia as a risk factor for stroke. *Neurol Res* 14 (Suppl):81-84.
- Brink, C., D. C. Hodgkin, J. Lindsey, J. Pickworth, J. R. Robertson, and J. G. White. 1954. X-ray crystallographic evidence on the structure of vitamin B12. *Nature* 174 (4443):1169-71.
- Brouwer, M., W. Chamulitrat, G. Ferruzzi, D.L. Sauls, and J.B. Weinberg. 1996. Nitric oxide interactions with cobalamins: Biochemical and functional consequences. *Blood* 88:1857-1864.
- Brown, K. L. 2005. Chemistry and enzymology of vitamin B12. *Chem Rev* 105 (6):2075-149.
- Brown, K. L., S. Cheng, X. Zou, J. D. Zubkowski, E. J. Valente, L. Knapton, and H. M. Marques. 1997. Cis Effects in the Cobalt Corrins. 1. Crystal Structures of 10-Chloro-aquacobalamin Perchlorate, 10-Chlorocyanocobalamin, and 10-Chloromethylcobalamin. *Inorg Chem* 36 (17):3666-3675.
- Bultitude, J. , L.F. Larkworthy, J. Mason, D.C. Povey, and B. Sandell. 1984. Nitrogen-15 and cobalt-59 NMR study of the bent nitrosyl ligand in cobalt complexes. *Inorg Chem* 84 (22):3629 - 3633.
- Butterfield, D. A., A. Gnjec, H. F. Poon, A. Castegna, W. M. Pierce, J. B. Klein, and R. N. Martins. 2006. Redox proteomics identification of oxidatively modified brain proteins in inherited Alzheimer's disease: an initial assessment. *J Alzheimers Dis* 10 (4):391-7.
- Campbell, E., Y. Takahashi, M. Abramovitz, M. Peretz, and I. Listowsky. 1990. A distinct human testis and brain mu-class glutathione S-transferase. Molecular cloning and

- characterization of a form present even in individuals lacking hepatic type mu isoenzymes. *J Biol Chem* 265 (16):9188-93.
- Carmel, R. 2001. Cobalamin deficiency. In *Homocysteine in Health and Disease*, edited by R. Carmel and D. W. Jacobsen. Cambridge, UK: Cambridge University Press.
- Castegna, A., M. Aksenov, V. Thongboonkerd, J. B. Klein, W. M. Pierce, R. Booze, W. R. Markesbery, and D. A. Butterfield. 2002. Proteomic identification of oxidatively modified proteins in Alzheimer's disease brain. Part II: dihydropyrimidinase-related protein 2, alpha-enolase and heat shock cognate 71. *J Neurochem* 82 (6):1524-32.
- Champloy, F., K. Gruber, G. Jogl, and C. Kratky. 2000. XAS spectroscopy reveals X-ray-induced photoreduction of free and protein-bound B12 cofactors. *J Synchrotron Radiat* 7 (Pt 4):267-73.
- Chanarin, I. 1979. *The megaloblastic anemias*. 2 ed: Oxford, Blackwell.
- Chance, M. R. 1999. *Chemistry and Biochemistry of B12*:4371.
- Choi, J., A. I. Levey, S. T. Weintraub, H. D. Rees, M. Gearing, L. S. Chin, and L. Li. 2004. Oxidative modifications and down-regulation of ubiquitin carboxyl-terminal hydrolase L1 associated with idiopathic Parkinson's and Alzheimer's diseases. *J Biol Chem* 279 (13):13256-64.
- Coelho, D., T. Suormala, M. Stucki, J. P. Lerner-Ellis, D. S. Rosenblatt, R. F. Newbold, M. R. Baumgartner, and B. Fowler. 2008. Gene identification for the cblD defect of vitamin B12 metabolism. *N Engl J Med* 358 (14):1454-64.
- Cole, A. G., L. M. Yoder, J. J. Shiang, N. A. Anderson, L. A. Walker, 2nd, M. M. Banaszak Holl, and R. J. Sension. 2002. Time-resolved spectroscopic studies of B(12)

- coenzymes: a comparison of the primary photolysis mechanism in methyl-, ethyl-, n-propyl-, and 5'-deoxyadenosylcobalamin. *J Am Chem Soc* 124 (3):434-41.
- Cooper, B.A., and D.S. Rosenblatt. 1987. Inherited defects of vitamin B<sub>12</sub> metabolism. *Annu Rev Nutr* 7:291-320.
- Cregan, A. G., N. E. Brasch, and R. van Eldik. 2001. Thermodynamic and kinetic studies on the reaction between the vitamin B12 derivative beta-(N-methylimidazolyl)cobalamin and N-methylimidazole: ligand displacement at the alpha axial site of cobalamins. *Inorg Chem* 40 (7):1430-8.
- Diaz-Arrastia, R. 1998. Hyperhomocysteinemia - A new risk factor for Alzheimer disease? *Arch Neurol* 55:1407-1408.
- Doran, J. F., P. Jackson, P. A. Kynoch, and R. J. Thompson. 1983. Isolation of PGP 9.5, a new human neurone-specific protein detected by high-resolution two-dimensional electrophoresis. *J Neurochem* 40 (6):1542-7.
- Eilbeck, W. J., and M. S. West. 1976. Thermochemical studies of vitamin B<sub>12</sub>. Part II. Thermodynamic data for the interaction of imidazole and methylimidazoles with aquocobalamin (Vitamin B<sub>12a</sub>). *J Chem Soc Dalton Trans*:274-278.
- Ellison, M. K., and W. R. Scheidt. 1998. Tilt/Asymmetry in Nitrosyl Metalloporphyrin Complexes: The Cobalt Case. *Inorg Chem* 37 (3):382-383.
- Evans, G., and R.F. Pettifer. 2001. CHOOCH: a program for deriving anomalous-scattering factors from X-ray fluorescence spectra. *J Appl Cryst* 34:82-86.
- Fasching, M., W. Schmidt, B. Krautler, E. Stupperich, A. Schmidt, and C. Kratky. 2000. Co- $\alpha$ -(1H-Imidazolyl)-Co- $\beta$ -methylcob(III)amide: model for protein-bound corrinoid cofactors. *Helvet Chim Acta* 83 (9):2295-2316.

- Fenton, W.A., L.M. Ambani, and L.E. Rosenberg. 1976. Uptake of hydroxocobalamin by rat liver mitochondria. Binding to a mitochondrial protein. *J Biol Chem.* 251:6616-6623.
- Fenton, W.A., R.A. Gravel, and D.S. Rosenblatt. 2001. Disorders of propionate and methylmalonate metabolism. In *The Metabolic and Molecular Bases of Inherited Disease*, edited by C. R. Scriver, A. L. Beaudet, W. S. Sly, D. Valle, B. Childs, K. W. Kinzler and B. Vogelstein. New York: McGraw-Hill.
- Fenton, W.A., and L.E. Rosenberg. 1978. Mitochondrial metabolism of hydroxocobalamin: Synthesis of adenosylcobalamin by intact rat liver mitochondria. *Arch Biochem Biophys.* 189:441-447.
- Fernandez-Salas, E., M. Sagar, C. Cheng, S. H. Yuspa, and W. C. Weinberg. 1999. p53 and tumor necrosis factor alpha regulate the expression of a mitochondrial chloride channel protein. *J Biol Chem* 274 (51):36488-97.
- Fernandez-Salas, E., K. S. Suh, V. V. Speransky, W. L. Bowers, J. M. Levy, T. Adams, K. R. Pathak, L. E. Edwards, D. D. Hayes, C. Cheng, A. C. Steven, W. C. Weinberg, and S. H. Yuspa. 2002. mtCLIC/CLIC4, an organelular chloride channel protein, is increased by DNA damage and participates in the apoptotic response to p53. *Mol Cell Biol* 22 (11):3610-20.
- Finkelstein, J.D. 1990. Methionine metabolism in mammals. *J Nutr Biochem* 1:228-237.
- Firth, R.A, H.A.O. Hill, J.M. Pratt, R.G. Thorp, and R.J.P. Williams. 1969. The chemistry of vitamin B12. Part XI. Some further formation constants. *J Chem Soc (A).* 1:381-386.
- Flood, H., and S. Ullberg. 1968. Accumulation of labelled vitamin B12 in some transplanted tumours. *Int J Cancer* 3:694-699.

- Franz, K. J., L. H. Doerrer, B. Spingler, and S. J. Lippard. 2001. Pentacoordinate cobalt(III) thiolate and nitrosyl tropocoronand compounds. *Inorg Chem* 40 (15):3774-80.
- Frydman, J., E. Nimmesgern, H. Erdjument-Bromage, J. S. Wall, P. Tempst, and F. U. Hartl. 1992. Function in protein folding of TRiC, a cytosolic ring complex containing TCP-1 and structurally related subunits. *EMBO J* 11 (13):4767-78.
- Garau, G., S. Geremia, L. G. Marzilli, G. Nardin, L. Randaccio, and G. Tauzher. 2003. Crystal chemistry and binding of NO<sub>2</sub>, SCN and SeCN to Co in cobalamins. *Acta Crystallogr B* 59 (Pt 1):51-9.
- Genschel, J., and H. H. Schmidt. 2000. Mutations in the LMNA gene encoding lamin A/C. *Hum Mutat* 16 (6):451-9.
- Gerke, V., C. E. Creutz, and S. E. Moss. 2005. Annexins: linking Ca<sup>2+</sup> signalling to membrane dynamics. *Nat Rev Mol Cell Biol* 6 (6):449-61.
- Ghosh, M., X. Song, G. Mouneimne, M. Sidani, D. S. Lawrence, and J. S. Condeelis. 2004. Cofilin promotes actin polymerization and defines the direction of cell motility. *Science* 304 (5671):743-6.
- Gimsing, P. 1995. Cobalamin forms and analogues in plasma and myeloid cells during chronic myelogenous leukaemia related to clinical condition. *Br J Haematol* 89:812-819.
- Gimsing, P. 1983. Determination of cobalamins in biological materials. I. Improvement in the unequal recovery of cobalamins by preincubation with cadmium acetate. *Anal Biochem.* 129:288-295.
- Gimsing, P., and E. Nexø. 1983. The forms of cobalamin in biological materials. In *The Cobalamins Volume 10*, edited by C. A. Hall. New York: Churchill Livingstone.

- Gimsing, P., E. Nexø, and E. Hippe. 1983. Determination of cobalamins in biological material. II. The cobalamins in human plasma and erythrocytes after desalting on nonpolar adsorbent material, and separation by one-dimensional thin-layer chromatography. *Anal Biochem.* 129:296-304.
- Gong, B., Z. Cao, P. Zheng, O. V. Vitolo, S. Liu, A. Staniszewski, D. Moolman, H. Zhang, M. Shelanski, and O. Arancio. 2006. Ubiquitin hydrolase Uch-L1 rescues beta-amyloid-induced decreases in synaptic function and contextual memory. *Cell* 126 (4):775-88.
- Gong, B., and E. Leznik. 2007. The role of ubiquitin C-terminal hydrolase L1 in neurodegenerative disorders. *Drug News Perspect* 20 (6):365-70.
- Green, L. C., D. A. Wagner, J. Glogowski, P. L. Skipper, J. S. Wishnok, and S. R. Tannenbaum. 1982. Analysis of nitrate, nitrite, and [<sup>15</sup>N]nitrate in biological fluids. *Anal Biochem* 126 (1):131-8.
- Green, R., and D.W. Jacobsen. 1995. Clinical implications of hyperhomocysteinemia. In *Folate in Health and Disease*, edited by L. B. Bailey. New York: Marcell Dekker, Inc.
- Gregersen, N. 2006. Protein misfolding disorders: pathogenesis and intervention. *J Inherit Metab Dis* 29 (2-3):456-70.
- Grewal, T., and C. Enrich. 2006. Molecular mechanisms involved in Ras inactivation: the annexin A6-p120GAP complex. *Bioessays* 28 (12):1211-20.
- Griess, P. 1879. "Bemerkungen zu der abhandlung der H. H. Weselsky und Benedikt" "Über einige azorverbindungen". *Chem Ber* 12:426.

- Gruber, K., G. Jögl, G. Klintschar, and C. Kratky. 1998. Vitamin B<sub>12</sub> and B<sub>12</sub>-Proteins. Paper read at 4th European Symposium on Vitamin B<sub>12</sub> and B<sub>12</sub>-Proteins.
- Hamza, M. S. A., and J. M. Pratt. 1994. Hemes and hemoproteins. Part 10. Coordination of imidazole and other azoles by the iron(III) porphyrin microperoxidase-8. *J Chem Soc Dalton Trans*:1367-1371.
- Hanania, G. I. H., and D. H. Irvine. 1964. The effect of coordination on ionization. V. The imidazole complex of aquocobalamin. *J Chem Soc, Suppl.* 1:5694-5697.
- Hannibal, L., A. Axhemi, A. V. Glushchenko, E. S. Moreira, N. E. Brasch, and D. W. Jacobsen. 2008. Accurate assessment and identification of naturally occurring cellular cobalamins. *Clin Chem Lab Med* 46 (12):1739-46.
- Hannibal, L., S. D. Bunge, R. van Eldik, D. W. Jacobsen, C. Kratky, K. Gruber, and N. E. Brasch. 2007. X-ray structural characterization of imidazolylcobalamin and histidinylcobalamin: cobalamin models for aquacobalamin bound to the B12 transporter protein transcobalamin. *Inorg Chem* 46 (9):3613-8.
- Hannibal, L., J. Kim, N. E. Brasch, D. S. Rosenblatt, and D. W. Jacobsen. 2009. Processing of alkylcobalamins by mammalian cells: a role for the MMACHC (cblC) gene product. *Mol Genet Metabol.* In press.
- Hannibal, L., C. A. Smith, D. W. Jacobsen, and N. E. Brasch. 2007. Nitroxylcob(III)alamin: synthesis and X-ray structural characterization. *Angew Chem Int Ed Engl* 46 (27):5140-3.
- Hannibal, L., C. A. Smith, J. Smith, A. Axhemi, A. Miller, S. Wang, N. E. Brasch, and D. W. Jacobsen. 2009. High resolution crystal structure of the methylcobalamin analogs

- ethylcobalamin and butylcobalamin by X-ray synchrotron diffraction *Inorg Chem.* In press.
- Hassanin, H. A., L. Hannibal, D. W. Jacobsen, K. L. Brown, H. M. Marques, and N. E. Brasch. 2009. NMR spectroscopy and molecular modelling studies of nitrosylcobalamin: further evidence that the deprotonated, base-off form is important for nitrosylcobalamin in solution. *Dalton Trans* (3):424-33.
- Hassanin, H. A., L. Hannibal, D. W. Jacobsen, M.F. El-Shahat, M.S.A. Hamza, and N. E. Brasch. 2009. Mechanistic studies on the reaction between R<sub>2</sub>N-NONOates and aquacobalamin: evidence for direct transfer of a nitroxyl (NO<sup>-</sup>) group from R<sub>2</sub>N-NONOates to cobalt(III) centers. *Angew Chem Int Ed Engl.* Under revision.
- Healton, E.B., D.G. Savage, J.C.M. Brust, T.J. Garrett, and J. Lindenbaum. 1991. Neurological aspects of cobalamin deficiency. *Medicine* 70:229-245.
- Hiller, S., R. G. Garces, T. J. Malia, V. Y. Orekhov, M. Colombini, and G. Wagner. 2008. Solution structure of the integral human membrane protein VDAC-1 in detergent micelles. *Science* 321 (5893):1206-10.
- Hodgkin, D. C., J. Kamper, M. Mackay, J. Pickworth, K. N. Trueblood, and J. G. White. 1956. Structure of vitamin B<sub>12</sub>. *Nature* 178 (4524):64-6.
- Hoffmann, G., S. Aramaki, E. Blum-Hoffmann, W. L. Nyhan, and L. Sweetman. 1989. Quantitative analysis for organic acids in biological samples: batch isolation followed by gas chromatographic-mass spectrometric analysis. *Clin Chem* 35 (4):587-95.
- Hogenkamp, H.P.C., G.T. Bratt, and A.T. Kotchevar. 1987. Reaction of alkylcobalamins with thiols. *Biochemistry* 26:4723-4727.

- Hogenkamp, H.P.C., G.T. Bratt, and S.-Z. Sun. 1985. Methyl transfer from methylcobalamin to thiols. A reinvestigation. *Biochemistry* 24:6428-6432.
- Holleman-Wiberg. 2001. The compounds of transition metals: a comparative review. In *Inorganic Chemistry*, edited by N. Wiberg. Berlin. New York.: Academic Press, W DE G de Gruyter.
- Hoorn, E. J., J. D. Hoffert, and M. A. Knepper. 2005. Combined proteomics and pathways analysis of collecting duct reveals a protein regulatory network activated in vasopressin escape. *J Am Soc Nephrol* 16 (10):2852-63.
- Hu, K., L. Ji, K. T. Applegate, G. Danuser, and C. M. Waterman-Storer. 2007. Differential transmission of actin motion within focal adhesions. *Science* 315 (5808):111-5.
- Inskip, A., J. Elexperu-Camiruaga, N. Buxton, P. S. Dias, J. MacIntosh, D. Campbell, P. W. Jones, L. Yengi, J. A. Talbot, R. C. Strange, and et al. 1995. Identification of polymorphism at the glutathione S-transferase, GSTM3 locus: evidence for linkage with GSTM1\*A. *Biochem J* 312 (Pt 3):713-6.
- Isoda, K., N. Kagaya, S. Akamatsu, S. Hayashi, M. Tamesada, A. Watanabe, M. Kobayashi, Y. Tagawa, M. Kondoh, M. Kawase, and K. Yagi. 2008. Hepatoprotective effect of vitamin B12 on dimethylnitrosamine-induced liver injury. *Biol Pharm Bull* 31 (2):309-11.
- Ito, H., I. Iwamoto, R. Morishita, Y. Nozawa, S. Narumiya, T. Asano, and K. Nagata. 2005. Possible role of Rho/Rhotekin signaling in mammalian septin organization. *Oncogene* 24 (47):7064-72.

- Jacobsen, D.W., T. Amagasaki, and R. Green. 1990. Synthesis and recycling of the transcobalamin II receptor. In *Biomedicine and Physiology of Vitamin B12*, edited by J. Linnell and R. Bhatt. London: The Children's Medical Charity.
- Jacobsen, D.W., P.M. DiGirolamo, and F.M. Huennekens. 1975. Adenosylcobalamin analogues as inhibitors of ribonucleotide reductase and vitamin B12 transport. *Mol Pharmacol* 11:174-184.
- Jacobsen, D.W., V.J. Gatautis, R. Green, K. Robinson, S.R. Savon, M. Secic, J. Ji, J.M. Otto, and L.M. Taylor, Jr. 1994. Rapid HPLC determination of total homocysteine and other thiols in serum and plasma: sex differences and correlation with cobalamin and folate levels in normal subjects. *Clin Chem* 40:873-881.
- Jiang, F., C.G. Li, and M.J. Rand. 1997. Effect of hydroxocobalamin on vasodilatations to nitrenergic transmitter, nitric oxide and endothelium-derived relaxing factor in guinea-pig basilar artery. *Eur J Pharmacol* 340:181-186.
- Jimenez-Mallebrera, C., M. A. Maioli, J. Kim, S. C. Brown, L. Feng, A. K. Lampe, K. Bushby, D. Hicks, K. M. Flanigan, C. Bonnemann, C. A. Sewry, and F. Muntoni. 2006. A comparative analysis of collagen VI production in muscle, skin and fibroblasts from 14 Ullrich congenital muscular dystrophy patients with dominant and recessive COL6A mutations. *Neuromuscul Disord* 16 (9-10):571-82.
- Kabsch, W. 1993. Automatic processing of rotation diffraction data from crystals of initially unknown symmetry and cell constants. *J Appl Cryst* 2:795-800.
- Kambo, A., V. S. Sharma, D. E. Casteel, V. L. Woods, Jr., R. B. Pilz, and G. R. Boss. 2005. Nitric oxide inhibits mammalian methylmalonyl-CoA mutase. *J Biol Chem* 280 (11):10073-82.

- Kanagawa, M., and T. Toda. 2006. The genetic and molecular basis of muscular dystrophy: roles of cell-matrix linkage in the pathogenesis. *J Hum Genet* 51 (11):915-26.
- Kaneda, Y., M. C. Yoshida, K. Kohno, T. Uchida, and Y. Okada. 1984. Chromosomal assignment of the gene for human elongation factor 2. *Proc Natl Acad Sci U S A* 81 (10):3158-62.
- Karp, N. A., D. P. Kreil, and K. S. Lilley. 2004. Determining a significant change in protein expression with DeCyder during a pair-wise comparison using two-dimensional difference gel electrophoresis. *Proteomics* 4 (5):1421-32.
- Katula, K. S., A. N. Heinloth, and R. S. Paules. 2007. Folate deficiency in normal human fibroblasts leads to altered expression of genes primarily linked to cell signaling, the cytoskeleton and extracellular matrix. *J Nutr Biochem* 18 (8):541-52.
- Keefer, L. K., R. W. Nims, K. M. Davies, and D. A. Wink. 1996. "NONOates" (1-substituted diazen-1-ium-1,2-diolates) as nitric oxide donors: convenient nitric oxide dosage forms. *Methods Enzymol* 268:281-93.
- Kennedy, D. G., A. Cannavan, A. Molloy, F. O'Harte, S. M. Taylor, S. Kennedy, and W. J. Blanchflower. 1990. Methylmalonyl-CoA mutase (EC 5.4.99.2) and methionine synthetase (EC 2.1.1.13) in the tissues of cobalt-vitamin B12 deficient sheep. *Br J Nutr* 64 (3):721-32.
- Kennedy, D. G., P. B. Young, S. Kennedy, J. M. Scott, A. M. Molloy, D. G. Weir, and J. Price. 1995. Cobalt-vitamin B12 deficiency and the activity of methylmalonyl CoA mutase and methionine synthase in cattle. *Int J Vitam Nutr Res* 65 (4):241-7.
- Kim, J. , C. Gherasim, and R. Banerjee. 2008. Decyanation of vitamin B12 by a trafficking chaperone. *Proc Natl Acad Sci U S A* 105 (38):14551-4.

- Kim, J., L. Hannibal, C. Gherasim, D. W. Jacobsen, and R. Banerjee. 2009. The Glutathione S-transferase Activity of a Human B<sub>12</sub> Trafficking Protein for Processing Alkylcobalamins. Submitted.
- Kim, S.H., H.L. Chen, N. Feilchenfeld, and J. Halpern. 1988. Thermal decomposition and cobalt-carbon bond dissociation energies of organocobalamins: neopentyl-, (cyclopentylmethyl)-, (cyclohexylmethyl)-, (Tetrahydrofurfuryl)- and ((Tetrahydro-2H-pyryl)methyl)cobalamin. *J Am Chem Soc* 110:3120-3126.
- Kitamura, K., M. Takayama, N. Hamajima, M. Nakanishi, M. Sasaki, Y. Endo, T. Takemoto, H. Kimura, M. Iwaki, and M. Nonaka. 1999. Characterization of the human dihydropyrimidinase-related protein 2 (DRP-2) gene. *DNA Res* 6 (5):291-7.
- Knapton, L., and H. M. Marques. 2005. Probing the nature of the Co(III) ion in cobalamins: a comparison of the reaction of aquacobalamin (vitamin B<sub>12a</sub>) and aqua-10-chlorocobalamin with some anionic and N-donor ligands. *Dalton Trans* (5):889-95.
- Knoops, B., E. Loumaye, and V. Van Der Eecken. 2007. Evolution of the peroxiredoxins. *Subcell Biochem* 44:27-40.
- Kondo, H., J.F. Kolhouse, and R.H. Allen. 1980. Presence of cobalamin analogues in animal tissues. *Proc Natl Acad Sci U S A* 77:817-821.
- Kratky, C., G. Farber, K. Gruber, K. Wilson, Z. Dauter, H. F. Nolting, R. Konrat, and B. Krautler. 1995. Accurate structural data to demystify B<sub>12</sub>: High resolution solid-state structure of aquacobalamin perchlorate and structural analysis of the aquacobalamin ion in solution. *J Am Chem Soc* 117:4654-4670.
- Lenhart, P. G., and D. C. Hodgkin. 1961. Structure of the 5,6-dimethylbenzimidazolylcobamide coenzyme. *Nature* 192:937-8.

- Lenhert, P.G., and D.C. Hodgkin. 1961. Structure of the 5,6-dimethylbenzimidazolylcobamide coenzyme. *Nature* 192:937-938.
- Lerner-Ellis, J. P., J. C. Tirone, P. D. Pawelek, C. Dore, J. L. Atkinson, D. Watkins, C. F. Morel, T. M. Fujiwara, E. Moras, A. R. Hosack, G. V. Dunbar, H. Antonicka, V. Forgetta, C. M. Dobson, D. Leclerc, R. A. Gravel, E. A. Shoubbridge, J. W. Coulton, P. Lepage, J. M. Rommens, K. Morgan, and D. S. Rosenblatt. 2006. Identification of the gene responsible for methylmalonic aciduria and homocystinuria, cblC type. *Nat Genet* 38 (1):93-100.
- Lin, C. S., T. Park, Z. P. Chen, and J. Leavitt. 1993. Human plastin genes. Comparative gene structure, chromosome location, and differential expression in normal and neoplastic cells. *J Biol Chem* 268 (4):2781-92.
- Mahoney, M.J., and L.E. Rosenberg. 1971. Synthesis of cobalamin coenzymes by human cells in tissue culture. *J Lab Clin Med.* 78:302-308.
- Majors, A., L.A. Ehrhart, and E.H. Pezacka. 1997. Homocysteine as a risk factor for vascular disease - Enhanced collagen production and accumulation by smooth muscle cells. *Arteriosclerosis, Thrombosis, and Vascular Biology* 17:2074-2081.
- Majors, A.K., S. Sengupta, D.W. Jacobsen, and R.E. Pyeritz. 2002. Upregulation of smooth muscle cell collagen production by homocysteine-insight into the pathogenesis of homocystinuria. *Mol Genet Metabol* 76:92-99.
- Maragos, C. M., D. Morley, D. A. Wink, T. M. Dunams, J. E. Saavedra, A. Hoffman, A. A. Bove, L. Isaac, J. A. Hrabie, and L. K. Keefer. 1991. Complexes of .NO with nucleophiles as agents for the controlled biological release of nitric oxide. Vasorelaxant effects. *J Med Chem* 34 (11):3242-7.

- Marouga, R., S. David, and E. Hawkins. 2005. The development of the DIGE system: 2D fluorescence difference gel analysis technology. *Anal Bioanal Chem* 382 (3):669-78.
- Marques, H. M. . 1991. Activation parameters for the reaction of aquocobalamin (vitamin B12a) with small anionic and neutral ligands. *J Chem Soc Dalton Trans*:339-341.
- Marques, H. M., L. Knapton, X. Zou, and K. L. Brown. 2002. Probing the nature of the Co(III) ion in cobalamins: deactivation of the metal towards ligand substitution in 10-nitrosoaquacobalamin, and the kinetics of the ligand substitution reactions in iodocobalamin. *J Chem Soc Dalton Trans*:3195-3200.
- Marques, H. M., J. N. Marsh, J. R. Mellor, and O. Q. Munro. 1990. The coordination of imidazole and its derivatives by aquocobalamin. *Inorg Chim Acta* 170 (2):259-269.
- Mathews, F. S., M. M. Gordon, Z. Chen, K. R. Rajashankar, S. E. Ealick, D. H. Alpers, and N. Sukumar. 2007. Crystal structure of human intrinsic factor: Cobalamin complex at 2.6-Å resolution. *Proc Natl Acad Sci U S A* 104 (44):17311-6.
- Mazzocco, M., P. Arrigo, A. Egeo, M. Maffei, A. Vergano, R. Di Lisi, F. Ghiotto, E. Ciccone, R. Cinti, R. Ravazzolo, and P. Scartezzini. 2001. A novel human homologue of the SH3BGR gene encodes a small protein similar to Glutaredoxin 1 of *Escherichia coli*. *Biochem Biophys Res Commun* 285 (2):540-5.
- McCauley, K. M., D. A. Pratt, S. R. Wilson, J. Shey, T. J. Burkey, and W. A. van der Donk. 2005. Properties and reactivity of chlorovinylcobalamin and vinylcobalamin and their implications for vitamin B12-catalyzed reductive dechlorination of chlorinated alkenes. *J Am Chem Soc* 127 (4):1126-36.
- McCully, K.S. 1969. Vascular pathology of homocysteinemia: implications for the pathogenesis of arteriosclerosis. *Am J Pathol* 56:111-128.

- McCully, K.S., and B.D. Ragsdale. 1970. Production of arteriosclerosis by homocysteinemia. *Am J Pathol.* 61:1-8.
- Meins, T., C. Vornhein, and K. Zeth. 2008. Crystallization and preliminary X-ray crystallographic studies of human voltage-dependent anion channel isoform I (HVDAC1). *Acta Crystallogr Sect F Struct Biol Cryst Commun* 64 (Pt 7):651-5.
- Meister, A. 1995. Glutathione metabolism. *Methods Enzymol.* 251:3-7.
- Mellman, I., H.F. Willard, and L.E. Rosenberg. 1978. Cobalamin binding and cobalamin-dependent enzyme activity in normal and mutant fibroblasts. *J Clin Invest.* 62:952-960.
- Metz, J. 1993. Pathogenesis of cobalamin neuropathy: deficiency of nervous system S-adenosylmethionine? *Nutr Rev* 51:12-15.
- Mollin, D.L. 1960. The Megaloblastic Anemias. *Annu Rev Med* 11:333-352.
- Mor-Vaknin, N., A. Punturieri, K. Sitwala, and D. M. Markovitz. 2003. Vimentin is secreted by activated macrophages. *Nat Cell Biol* 5 (1):59-63.
- Morris, M. S. 2003. Homocysteine and Alzheimer's disease. *Lancet Neurol* 2 (7):425-8.
- Mosmann, T. 1983. Rapid colorimetric assay for cellular growth and survival: application to proliferation and cytotoxicity assays. *J Immunol Methods* 65 (1-2):55-63.
- Mudd, S.H., H.L. Levy, and R.H. Abeles. 1969. A derangement in B12 metabolism leading to homocystinemia, cystathioninemia and methylmalonic aciduria. *Biochem Biophys Res Commun* 35:121-126.
- Nagase, T., N. Miyajima, A. Tanaka, T. Sazuka, N. Seki, S. Sato, S. Tabata, K. Ishikawa, Y. Kawarabayasi, H. Kotani, and et al. 1995. Prediction of the coding sequences of unidentified human genes. III. The coding sequences of 40 new genes (KIAA0081-

- KIAA0120) deduced by analysis of cDNA clones from human cell line KG-1. *DNA Res* 2 (1):37-43.
- Nicolaou, A., S.H. Kenyon, J.M. Gibbons, T. Ast, and W.A. Gibbons. 1996. *In vitro* inactivation of mammalian methionine synthase by nitric oxide. *Eur J Clin Invest* 26:167-170.
- Olson, T. M., S. Illenberger, N. Y. Kishimoto, S. Huttelmaier, M. T. Keating, and B. M. Jockusch. 2002. Metavinculin mutations alter actin interaction in dilated cardiomyopathy. *Circulation* 105 (4):431-7.
- Olteanu, H., and R. Banerjee. 2001. Cobalamin-dependent remethylation. In *Homocysteine in Health and Disease*, edited by R. Carmel and D. W. Jacobsen. Cambridge, UK: Cambridge University Press.
- Oprea, G. E., S. Krober, M. L. McWhorter, W. Rossoll, S. Muller, M. Krawczak, G. J. Bassell, C. E. Beattie, and B. Wirth. 2008. Plastin 3 is a protective modifier of autosomal recessive spinal muscular atrophy. *Science* 320 (5875):524-7.
- Ouyang, L., P. Rulis, W. Y. Ching, G. Nardin, and L. Randaccio. 2004. Accurate redetermination of the X-ray structure and electronic bonding in adenosylcobalamin. *Inorg Chem* 43 (4):1235-41.
- Pagano, T. G. , L. G. Marzilli, M. M. Flocco, C. Tsai, H. L. Carrell, and J. P. Glusker. 1991. X-ray crystallographic and two-dimensional NMR investigations of a coenzyme B12 analogue with 5'-deoxyadenosine replaced by 9-(CH<sub>2</sub>)<sub>3</sub>-adenine. *J Am Chem Soc* 113:531-542.

- Peddinti, D., B. Nanduri, A. Kaya, J. M. Feugang, S. C. Burgess, and E. Memili. 2008. Comprehensive proteomic analysis of bovine spermatozoa of varying fertility rates and identification of biomarkers associated with fertility. *BMC Syst Biol* 2:19.
- Perreau, J., A. Lilienbaum, M. Vasseur, and D. Paulin. 1988. Nucleotide sequence of the human vimentin gene and regulation of its transcription in tissues and cultured cells. *Gene* 62 (1):7-16.
- Perry, B.P., M. A. Fernandes, K. L. Brown, X. Zou, E.J. Valente, and H.M. Marques. 2003. Probing the nature of the Co<sup>III</sup> ion in cobalamins -Spectroscopic and structural investigations of the reactions of aquacobalamin (Vitamin B<sub>12a</sub>) with ambident nucleophiles. *Eur J Inorg Biochem*:2095-2107.
- Perry, C. B. , and H. M. Marques. 2004. Fifty years of X-ray crystallography of vitamin B<sub>12</sub> and its derivatives. . *South Afr J Sci* 100:368-380.
- Perry, C. B., M. A. Fernandes, and H. M. Marques. 2004. Isoamylcobalamin-acetone-water (1/0.385/12.650). *Acta Crystallogr C* 60 (Pt 4):m165-7.
- Pezacka, E., R. Green, and D.W. Jacobsen. 1990. Glutathionylcobalamin as an intermediate in the formation of cobalamin coenzymes. *Biochem Biophys Res Commun* 169:443-450.
- Pezacka, E.H. 1993. Identification and characterization of two enzymes involved in the intracellular metabolism of cobalamin. Cyanocobalamin β-ligand transferase and microsomal cob(III)alamin reductase. *Biochim Biophys Acta* 1157:167-177.
- Pezacka, E.H., R. Green, and D.W. Jacobsen. 1990. Intracellular cobalamin metabolism: a thiol-cobalamin adduct as an intermediate in cobalamin coenzyme formation. *FASEB J* 4:A2126.

- Plenz, G., S. Kugler, S. Schnittger, H. Rieder, C. Fonatsch, and P. K. Muller. 1994. The human vigilin gene: identification, chromosomal localization and expression pattern. *Hum Genet* 93 (5):575-82.
- Pratt, JM. 1972. *Inorganic chemistry of vitamin B<sub>12</sub>*. United States, Academic Press Inc. ed. New York: Academic Press Inc (London) Ltd.
- Quadros, E. V., Y. Nakayama, and J. M. Sequeira. 2009. The protein and the gene encoding the receptor for the cellular uptake of transcobalamin bound cobalamin. *Blood*. 113 (1):186-92.
- Quadros, E.V., B. Jackson, A.V. Hoffbrand, and J.C. Linnell. 1979. Interconversion of cobalamins in human lymphocytes in vitro and the influence of nitrous oxide on synthesis of cobalamin coenzymes. In *Vitamin B<sub>12</sub>*, edited by B. Zagalak and W. Friedrich. Berlin: Walter de Gruyter.
- Quadros, E.V., D.M. Matthews, A.V. Hoffbrand, and J.C. Linnell. 1976. Synthesis of Cobalamin Coenzymes by Human Lymphocytes In Vitro and the Effect of Folates and Metabolic Inhibitors. *Blood* 48:609-619.
- Quadros, E.V., S.P. Rothenberg, and E.A. Jaffe. 1989. Endothelial cells from human umbilical vein secrete functional transcobalamin II. *Am J Physiol* 256:C296-C303.
- Raaberg, L., E. Nexø, S.S. Poulsen, and L. Tollund. 1989. Cobalamin and its binding protein in rat milk. *Scand J Clin Lab Invest* 49:529-535.
- Randaccio, L., M. Furlan, S. Geremia, M. Slouf, I. Srnova, and D. Toffoli. 2000. Similarities and differences between cobalamins and cobaloximes. Accurate structural determination of methylcobalamin and of LiCl- and KCl-containing cyanocobalamins by synchrotron radiation. *Inorg Chem* 39 (15):3403-13.

- Randaccio, L., S. Geremia, G. Nardin, M. S. Shlouf, and i. Srnova. 1999. Crystal chemistry of cobalamins. Structural characterization of the Co-S bond in cobalamins. *Inorg Chem* 38:4087-4092.
- Randaccio, L., S. Geremia, M. Stener, D. Toffoli, and E. Zangrando. 2002. Electronic properties of the axial Co-C and Co-S bonds in B<sub>12</sub> systems. A density functional study. *Eur J Inorg Chem*:93-103.
- Randaccio, Lucio, Silvano Geremia, Giorgio Nardin, and Jochen Wuerges. 2006. X-ray structural chemistry of cobalamins. *Coord Chem Rev* 250 (11+12):1332-1350.
- Raponi, M., R. T. Belly, J. E. Karp, J. E. Lancet, D. Atkins, and Y. Wang. 2004. Microarray analysis reveals genetic pathways modulated by tipifarnib in acute myeloid leukemia. *BMC Cancer* 4:56.
- Raynal, P., and H. B. Pollard. 1994. Annexins: the problem of assessing the biological role for a gene family of multifunctional calcium- and phospholipid-binding proteins. *Biochim Biophys Acta* 1197 (1):63-93.
- Redman, K. L., and M. Rechsteiner. 1989. Identification of the long ubiquitin extension as ribosomal protein S27a. *Nature* 338 (6214):438-40.
- Reenstra, W.W., and W.P. Jencks. 1979. Reactions of Cyanide with Cobalamins. *Journal of the American Chemical Society* 101:5780-5791.
- Regland, B., B.V. Johansson, B. Grenfeldt, L.-T. Hjelmgren, and M. Medhus. 1995. Homocysteinemia is a common feature of schizophrenia. *J Neur Transm* 100:165-169.
- Rhoads, D. D., A. Dixit, and D. J. Roufa. 1986. Primary structure of human ribosomal protein S14 and the gene that encodes it. *Mol Cell Biol* 6 (8):2774-83.

- Richard, E., L. Monteoliva, S. Juarez, B. Perez, L. R. Desviat, M. Ugarte, and J. P. Albar. 2006. Quantitative analysis of mitochondrial protein expression in methylmalonic acidemia by two-dimensional difference gel electrophoresis. *J Proteome Res* 5 (7):1602-10.
- Richter-Addo, G. B., S. J. Hodge, G. B. Yi, M. A. Khan, T. Ma, E. Van Caemelbecke, N. Guo, and K. M. Kadish. 1996. Synthesis, Characterization, and Spectroelectrochemistry of Cobalt Porphyrins Containing Axially Bound Nitric Oxide. *Inorg Chem* 35 (22):6530-6538.
- Rickes, E.L., N.G. Brink, F.R. Koniuszy, T.R. Wood, and K. Folkers. 1949. Crystalline vitamin B12. *Science* 107:396-397.
- Riedel, B., T. Fiskerstrand, H. Refsum, and P.M. Ueland. 1999. Co-ordinate variations in methylmalonyl-CoA mutase and methionine synthase, and the cobalamin cofactors in human glioma cells during nitrous oxide exposure and the subsequent recovery phase. *Biochem J.* 341:133-138.
- Riedel, B., P.M. Ueland, and A.M. Svardal. 1995. Fully automated assay for cobalamin-dependent methylmalonyl CoA mutase. *Clin Chem.* 41:1164-1170.
- Roncaroli, F., T. E. Shubina, T. Clark, and R. van Eldik. 2006. Nitrite Impurities Are Responsible for the Reaction Observed between Vitamin B(12) and Nitric Oxide in Acidic Aqueous Solution. *Inorg Chem* 45 (19):7869-7876.
- Rosenberg, L.E., L. Patel, and A.C. Lilljeqvist. 1975. Absence of an intracellular cobalamin-binding protein in cultured fibroblasts from patients with defective synthesis of 5'-deoxyadenosylcobalamin and methylcobalamin. *Proc Natl Acad Sci U S A* 72:4617-4621.

- Rosenblatt, D.S. 2001. Inborn errors of folate and cobalamin metabolism. In *Homocysteine in Health and Disease*, edited by R. Carmel and D. W. Jacobsen. Cambridge, UK: Cambridge University Press.
- Rosenblatt, D.S., A.L. Aspler, M.I. Shevell, B.A. Pletcher, W.A. Fenton, and M.R. Seashore. 1997. Clinical heterogeneity and prognosis in combined methylmalonic aciduria and homocystinuria (*cb1C*). *J Inherit Metab Dis.* 20:528-538.
- Rosenblatt, D.S., and W.A. Fenton. 2001. Inherited disorders of folate and cobalamin transport and metabolism. In *The Metabolic & Molecular Bases of Inherited Disease*, edited by C. R. Scriver, A. L. Beaudet, W. S. Sly, D. Valle, B. Childs, K. W. Kinzler and B. Vogelstein. New York: Mc-Graw Hill.
- Rosenblatt, D.S., A. Hosack, N.V. Matiaszuk, B.A. Cooper, and R. Laframboise. 1985. Defect in vitamin B12 release from lysosomes: Newly described inborn error of vitamin B12 metabolism. *Science* 228:1319-1321.
- Rosenblatt, D.S., and V.M. Whitehead. 1999. Cobalamin and folate deficiency: Acquired and hereditary disorders in children. *Semin.Hematol.* 36:19-34.
- Rossi, M., J.P. Glusker, L. Randaccio, M.F. Summers, P.J. Toscano, and L.G. Marzilli. 1985. The structure of a B<sub>12</sub> coenzyme: methylcobalamin studies by x-ray and NMR methods. *J Am Chem Soc* 107:1729-1738.
- Rutsch, F., S. Gailus, I. R. Miousse, T. Suormala, C. Sagne, M. R. Toliat, G. Nurnberg, T. Wittkamp, I. Buers, A. Sharifi, M. Stucki, C. Becker, M. Baumgartner, H. Robenek, T. Marquardt, W. Hohne, B. Gasnier, D. S. Rosenblatt, B. Fowler, and P. Nurnberg. 2009. Identification of a putative lysosomal cobalamin exporter altered in the *cb1F* defect of vitamin B12 metabolism. *Nat Genet* 41 (2):234-9.

- Scheidt, W. R., and J. L. Hoard. 1973. Stereochemistry of Low-spin cobalt porphyrins. I. Structure and Bonding in Nitrosylcobalt Porphyrin and Their Bearing on One Rational Model for the Oxygenated Protoheme. *J Am Chem Soc* 95 (25):8281-8288.
- Scheuring, E.M., I. Sagi, and M.R. Chance. 1994. Sulfur-containing cobalamins: X-ray absorption spectroscopic characterization. *Biochemistry* 33:6310-6315.
- Schneider, R.J., R.L. Burger, C.S. Mehlman, and R.H. Allen. 1976. The role and fate of rabbit and human transcobalamin II in the plasma transport of vitamin B12 in the rabbit. *J Clin Invest* 57:27-38.
- Schubert, R., U. Krien, I. Wulfsen, D. Schiemann, G. Lehmann, N. Ulfig, R. W. Veh, J. R. Schwarz, and H. Gago. 2004. Nitric oxide donor sodium nitroprusside dilates rat small arteries by activation of inward rectifier potassium channels. *Hypertension* 43 (4):891-6.
- Selcuki, C., R. Van Eldik, and T. Clark. 2004. NO Binding to Cobalamin: Influence of the Metal Oxidation State. *Inorg Chem* 43 (9):2828-33.
- Sheldrick, G.M., and T.R. Schneider. 1997. SHELXL: High Resolution Refinement. In *Methods Enzymol*, edited by R. M. Sweet and C. W. J. Carter: Academic Press; Orlando, Florida.
- Shen, N., M. Zhou, B. Yang, Y. Yu, X. Dong, and J. Ding. 2008. Catalytic mechanism of the tryptophan activation reaction revealed by crystal structures of human tryptophanyl-tRNA synthetase in different enzymatic states. *Nucleic Acids Res* 36 (4):1288-99.
- Shih, V.E., S.M. Axel, J.C. Tewksbury, D. Watkins, B.A. Cooper, and D.S. Rosenblatt. 1989. Defective lysosomal release of vitamin B12 (cblF): a hereditary cobalamin metabolic disorder associated with sudden death. *Am J Med Genet* 33:555-563.

- Shinawi, M. 2007. Hyperhomocysteinemia and cobalamin disorders. *Mol Genet Metab* 90 (2):113-21.
- Shinnar, S., and H.S. Singer. 1984. Cobalamin C Mutation (Methylmalonic Aciduria and Homocystinuria) in Adolescence A Treatable Cause of Dementia and Myelopathy. *N Engl J Med* 311 No.7:451-454.
- Shorb, M. S. . 1948. Activity of vitamin B12 for the growth of *Lactobacillus lactis*. *Science* 107:397-398.
- Siripurapu, V., J. Meth, N. Kobayashi, and M. Hamaguchi. 2005. DBC2 significantly influences cell-cycle, apoptosis, cytoskeleton and membrane-trafficking pathways. *J Mol Biol* 346 (1):83-9.
- Smith, E. L., L. Mervyn, P. W. Muggleton, A. W. Johnson, and N. Shaw. 1964. Chemical Routes to Coenzyme B12 and Analogues. *Ann N Y Acad Sci* 112:565-74.
- Stabler, S. P., and R. H. Allen. 2004. Vitamin B12 deficiency as a worldwide problem. *Annu Rev Nutr* 24:299-326.
- Stanier, P., S. Abu-Hayyeh, J. N. Murdoch, J. Eddleston, and A. J. Copp. 1998. Paralogous sm22alpha (Tagln) genes map to mouse chromosomes 1 and 9: further evidence for a paralogous relationship. *Genomics* 51 (1):144-7.
- Stevens, T. H., and M. Forgac. 1997. Structure, function and regulation of the vacuolar (H<sup>+</sup>)-ATPase. *Annu Rev Cell Dev Biol* 13:779-808.
- Strik, M. C., A. Wolbink, D. Wouters, B. A. Bladergroen, A. R. Verlaan, I. S. van Houdt, S. Hijlkema, C. E. Hack, and J. A. Kummer. 2004. Intracellular serpin SERPINB6 (PI6) is abundantly expressed by human mast cells and forms complexes with beta-tryptase monomers. *Blood* 103 (7):2710-7.

- Stubbe, J. 1994. Binding site revealed of nature's most beautiful cofactor. *Science* 266 (5191):1663-4.
- Suarez-Moreira, E., L. Hannibal, C. A. Smith, R. A. Chavez, D. W. Jacobsen, and N. E. Brasch. 2006. A simple, convenient method to synthesize cobalamins: synthesis of homocysteinylcobalamin, N-acetylcysteinylcobalamin, 2-N-acetylamino-2-carbomethoxyethanethiolatocobalamin, sulfitocobalamin and nitrocobalamin. *Dalton Trans* (44):5269-77.
- Suormala, T., M. R. Baumgartner, D. Coelho, P. Zavadakova, V. Kozich, H. G. Koch, M. Berghauer, J. E. Wraith, A. Burlina, A. Sewell, J. Herwig, and B. Fowler. 2004. The cblD defect causes either isolated or combined deficiency of methylcobalamin and adenosylcobalamin synthesis. *J Biol Chem* 279 (41):42742-9.
- Takeshita, H., J. Fujihara, H. Takastuka, T. Agusa, T. Yasuda, and T. Kunito. 2009. Diversity of glutathione s-transferase omega 1 (a140d) and 2 (n142d) gene polymorphisms in worldwide populations. *Clin Exp Pharmacol Physiol* 36 (3):283-6.
- Taylor, R.T., L. Smucker, M.L. Hanna, and J. Gill. 1973. Aerobic photolysis of alkylcobalamins: quantum yields and light-action spectra. *Arch Biochem Biophys* 156:521-533.
- Tsoporis, J. N., S. Izhar, and T. G. Parker. 2008. Expression of S100A6 in cardiac myocytes limits apoptosis induced by tumor necrosis factor-alpha. *J Biol Chem* 283 (44):30174-83.
- Wagner, T., C. E. Afshar, H. L. Carrell, J. P. Glusker, U. Englert, and H. P. Hogenkamp. 1999. Difluoromethylcobalamin: Structural Aspects of an Old Tree with a New Branch. *Inorg Chem* 38 (8):1785-1794.

- Watkins, D., and D.S. Rosenblatt. 1986. Failure of lysosomal release of vitamin B12: A new complementation group causing methylmalonic aciduria (cblF). *Am J Hum Genet.* 39:404-408.
- Weissbach, H., J.N. Ladd, B.E. Volcani, R.D. Smyth, and H.A. Barker. 1960. Structure of the adenylobamide coenzyme: degradation by cyanide, acid, and light. *J Biol Chem* 235:1462-1473.
- West, R. 1948. Activity of vitamin B12 in Addisonian pernicious anemia. *Science* 107:398.
- Wilson, P. O., P. C. Barber, Q. A. Hamid, B. F. Power, A. P. Dhillon, J. Rode, I. N. Day, R. J. Thompson, and J. M. Polak. 1988. The immunolocalization of protein gene product 9.5 using rabbit polyclonal and mouse monoclonal antibodies. *Br J Exp Pathol* 69 (1):91-104.
- Wolak, M., G. Stochel, M. Hamza, and R. van Eldik. 2000. Aquacobalamin (vitamin B12a) does not bind NO in aqueous solution. Nitrite impurities account for observed reaction. *Inorg Chem* 39 (10):2018-9.
- Wolak, M., G. Stochel, and R. van Eldik. 2006. Reactivity of Aquacobalamin and Reduced Cobalamin toward S-Nitrosoglutathione and S-Nitroso-N-acetylpenicillamine. *Inorg Chem* 45 (3):1367-79.
- Wolak, M., A. Zahl, T. Schnepfensieper, G. Stochel, and R. van Eldik. 2001. Kinetics and mechanism of the reversible binding of nitric oxide to reduced cobalamin B(12r) (Cob(II)alamin). *J Am Chem Soc* 123 (40):9780-91.
- Wu, W. W., G. Wang, S. J. Baek, and R. F. Shen. 2006. Comparative study of three proteomic quantitative methods, DIGE, cICAT, and iTRAQ, using 2D gel- or LC-MALDI TOF/TOF. *J Proteome Res* 5 (3):651-8.

- Wuerges, J., G. Garau, S. Geremia, S. N. Fedosov, T. E. Petersen, and L. Randaccio. 2006. Structural basis for mammalian vitamin B12 transport by transcobalamin. *Proc Natl Acad Sci U S A* 103 (12):4386-91.
- Wuerges, J., S. Geremia, S. N. Fedosov, and L. Randaccio. 2007. Vitamin B12 transport proteins: crystallographic analysis of beta-axial ligand substitutions in cobalamin bound to transcobalamin. *IUBMB Life* 59 (11):722-9.
- Xia, L., A. G. Cregan, L. A. Berben, and N. E. Brasch. 2004. Studies on the formation of glutathionylcobalamin: any free intracellular aquacobalamin is likely to be rapidly and irreversibly converted to glutathionylcobalamin. *Inorg Chem* 43 (21):6848-57.
- Xin, X., M. Pache, B. Zieger, I. Bartsch, C. Prunte, J. Flammer, and P. Meyer. 2007. Septin expression in proliferative retinal membranes. *J Histochem Cytochem* 55 (11):1089-94.
- Xu, C., P. Zheng, S. Shen, Y. Xu, L. Wei, H. Gao, S. Wang, C. Zhu, Y. Tang, J. Wu, Q. Zhang, and Y. Shi. 2005. NMR structure and regulated expression in APL cell of human SH3BGRL3. *FEBS Lett* 579 (13):2788-94.
- Yamada, K., T. Kawata, M. Wada, T. Isshiki, J. Onoda, T. Kawanishi, A. Kunou, T. Todokoro, T. Tobimatsu, A. Maekawa, and T. Toraya. 2000. Extremely low activity of methionine synthase in vitamin B-12-deficient rats may be related to effects on coenzyme stabilization rather than to changes in coenzyme induction. *J Nutr* 130:1894-1900.
- Yamada, K., S. Yamada, T. Tobimatsu, and T. Toraya. 1999. Heterologous high level expression, purification, and enzymological properties of recombinant rat cobalamin-dependent methionine synthase. *J Biol Chem* 274:35571-35576.

- Yoshio, T., T. Morita, Y. Kimura, M. Tsujii, N. Hayashi, and K. Sobue. 2007. Caldesmon suppresses cancer cell invasion by regulating podosome/invadopodium formation. *FEBS Lett* 581 (20):3777-82.
- Zheng, D., and R.L. Birke. 2002. The reaction of nitric oxide with glutathionylcobalamin. *J Am Chem Soc* 124:9066-9067.
- Zheng, D., and R.L. Birke. 2001. Spectroscopic evidence for nitric oxide binding with Cob(II)alamin. *J Am Chem Soc* 123:4637-4638.
- Zheng, D., L. Yan, and R.L. Birke. 2002. Electrochemical and spectral studies of the reactions of aquocobalamin with nitric oxide and nitrite ion. *Inorg Chem* 41:2548-2555.
- Zimmermann, A. G., J. Sychala, and B. S. Mitchell. 1995. Characterization of the human inosine-5'-monophosphate dehydrogenase type II gene. *J Biol Chem* 270 (12):6808-14.
- Zou, X., and K. L. Brown. 1998. The crystal structure of trifluoromethylcobalamin, a coenzyme B<sub>12</sub> analog. *Inorg Chim Acta* 267:305-308.

**Copyright © 2009**

By

Luciana Hannibal

All Rights Reserved